

# Estimation Using Cross-correlation in a Communications Network

**Author:**

Anower, Md. Shamim

**Publication Date:**

2012

**DOI:**

<https://doi.org/10.26190/unsworks/15726>

**License:**

<https://creativecommons.org/licenses/by-nc-nd/3.0/au/>

Link to license to see what you are allowed to do with this resource.

Downloaded from <http://hdl.handle.net/1959.4/52168> in <https://unsworks.unsw.edu.au> on 2024-04-19

# **Estimation Using Cross-correlation in a Communications Network**

by

**MD. SHAMIM ANOWER**



**A thesis submitted for the degree of PhD in Electrical Engineering at the  
School of Engineering & Information Technology  
University of New South Wales  
Australian Defence Force Academy**

**© Copyright 2011 by Md. Shamim Anower**

**Thesis Supervisor: Prof. Michael R. Frater  
Co-Supervisor: Dr. Michael J. Ryan**



# Abstract

In a large-scale wireless sensor network, it is often desirable to count the number of nodes in the network, or the number of nodes that are within communications range of a particular node. In such networks, nodes are deployed for a wide variety of military and civilian applications. These applications require a balance among the number of operating nodes, energy efficiency, and the lifetime of the network. The number of operating nodes is a very crucial factor for the networks. However, the number of operating nodes can vary with time due to various artificial as well as natural reasons (for example, some nodes might fail and some could be damaged because of fouling and corrosion, or batteries might fail). It is therefore a matter of great interest for a communication network to know how many operating nodes or transmitters are available in the region at any point in time to ensure proper network operation (such as routing), as well as to obtain optimum performance or to prevent failure of the mission by network maintenance (such as replacement of faulty nodes). Similarly, a concurrent estimation of the dimensionality of the network might also be important for localising the nodes and estimating their number in a deployed network. To date, techniques employed to estimate the number of nodes and dimensionality have been based on some aspect of the communications protocol(s) in use. The protocol technique can be very hard to implement in harsh environment (e.g. underwater) due to the unavoidable capture effect, poor efficiency due to long propagation delay, high path loss, etc. In this thesis, we propose a novel estimation technique based on cross-correlation of random signals, in which the ratio of the mean of the cross-correlation function to its standard deviation determines the number of nodes. Within the limited scope of this thesis, we have provided some estimation techniques to estimate the number of nodes and network dimensionality. The proposed number of node estimation techniques also addresses a number of practical issues in a digital receiver and channel, including fractional-sample delays, multipath reception, noise etc. An error analysis is provided with comparison to conventional protocol techniques that demonstrates the superior performance of this technique to protocol-based methods. The thesis includes an initial verification of the performance of the proposed techniques and suggests other issues for future verification.



# Acknowledgements

I would like to express profound gratitude to my supervisor, Prof. Michael Frater, whose support and guidance from the initial to the final level enabled me to develop an understanding of the research work. Without his assistance this thesis would not have been possible.

I am indebted to my co-supervisor, Dr. Mike Ryan, for his help and support throughout my research during the last three and half years.

I would also like to thank Denise Russel, for her time and effort for helping me with the thesis writings.

I am expressing my deep appreciation and gratitude to all underwater group (UNSW@ADFA, Australia) members for their kind co-operation and constant encouragement throughout this research work.

Finally, I would like to thank very much my parents and my wife, Jesmin, for their continuous encouragement, support and love during this endeavour.

Md. Shamim Anower

Canberra, 2011



*Dedicated to*  
*My respected parents, beloved wife, Jesmin, daughter, Sadika,*  
*and*  
*my son, Jawad*





# Originality Statement

I hereby declare that this submission is my own work and to the best of my knowledge it contains no materials previously published or written by another person, or substantial proportions of material which have been accepted for the award of any other degree or diploma at UNSW or any other educational institution, except where due acknowledgement is made in the thesis. Any contribution made to the research by others, with whom I have worked at UNSW or elsewhere, is explicitly acknowledged in the thesis.

I also declare that the intellectual content of this thesis is the product of my own work, except to the extent that assistance from others in the project's design and conception or in style, presentation and linguistic expression is acknowledged.

Signed.....

Date.....



# Table of Contents

<b>Chapter 1</b>	<b>Introduction.....</b>	<b>1</b>
1.1	Background.....	3
1.1.1	Mobile wireless telephone network (MWTN).....	4
1.1.2	Terrestrial wireless sensor network (TWSN).....	4
1.1.3	Radio frequency identification (RFID) system.....	6
1.1.4	Space wireless communication network (SWCN).....	7
1.1.5	Underground wireless communication network (UGWCN).....	7
1.1.6	Underwater wireless communication network (UWCN).....	8
1.2	Practical issues regarding estimation.....	10
1.2.1	Signal propagation underwater .....	10
1.2.2	Propagation delay in underwater acoustic network (UANs).....	11
1.2.3	Path loss .....	12
1.2.4	Background noise.....	14
1.2.5	Multipath effects .....	15
1.2.6	Other issues .....	16
1.3	Importance of the proposed estimation .....	16
1.4	Objectives .....	20
1.4.1	Estimation of the number of nodes .....	20
1.4.2	Estimation of networks' dimensionality .....	21
1.4.3	Analysis of error in estimation.....	21
1.5	Robustness of the estimation process .....	21
1.6	Contributions and novelty .....	22
1.7	Thesis organisation .....	24
1.8	Publications.....	25
<b>Chapter 2</b>	<b>Literature review.....</b>	<b>27</b>
2.1	Introduction.....	27
2.2	Existing estimation techniques using protocols.....	28
2.2.1	Using identification protocols in RFID systems .....	29
2.2.2	Estimation without identification in RFID systems.....	32
2.2.3	Protocols in TCN .....	42

2.2.4	Protocols in UCN .....	45
2.3	Limitations of conventional techniques.....	51
2.4	Use of cross-correlation.....	53
2.4.1	Cross-correlation for travel-time and direction of arrival estimations. ....	53
2.4.2	Cross-correlation for weak signal detection.....	54
2.5	Motivation for using cross-correlation .....	55
2.6	Formation of CCF.....	57
2.7	Statistical signal processing.....	57
2.7.1	Occupancy problem.....	57
2.7.2	Use of binomial distribution.....	58
2.8	Coefficient of variation (CV).....	59
2.9	Conclusion .....	59

### **Chapter 3 Estimation of the number of nodes in wireless**

<b>communication networks.....</b>	<b>61</b>
3.1 Introduction.....	61
3.2 Formulation of random signal cross-correlation.....	65
3.3 CCF for infinite long signal.....	68
3.4 Mean, $\mu$ and standard deviation, $\sigma$ , of CCF.....	73
3.5 Reframing cross-correlation as a probability problem.....	74
3.6 Some simulated results and selection of estimation tool.....	76
3.7 Estimation process - equal received power (ERP) case.....	79
3.7.1 Theoretical estimation.....	80
3.7.2 Estimation from simulation.....	82
3.7.3 Conclusion.....	93
3.8 Estimation process - equal transmitted power (ETP) case.....	94
3.8.1 Fitting of simulation results with theory.....	96
3.8.2 Results and discussion after scaling.....	101
3.8.3 Direct scaling of theoretical $R$ of CCF to follow simulated results ...	103
3.8.4 Results and discussion after direct scaling.....	104
3.8.5 Conclusion.....	105
3.9 Selection of signal length, $N_s$ .....	105

3.10	Effect of fractional-samples delays on estimation.....	108
3.11	Effect of noise on estimation .....	109
3.11.1	Estimation considering internal noise of the receivers .....	113
3.11.2	Conclusion .....	119
3.12	Effects of multipath propagation on estimation .....	119
3.12.1	Estimation of $N$ in multipath environment.....	120
3.12.2	Explanation of multipath effects in deep ocean .....	128
3.12.3	Near-field range to neglect multipath effect .....	129
3.12.4	Robust estimation technique in multipath environment.....	130
3.12.5	Conclusion .....	150
3.12.6	Multipath effects in protocols .....	150
3.13	Conclusion .....	150
<b>Chapter 4 Estimations of the dimensionality and numbers of</b>		
<b>nodes in different dimensions in a communication network .....</b>		<b>153</b>
4.1	Introduction.....	153
4.2	Estimation using CCF of dimensionality.....	154
4.2.1	Shapes of CCFs.....	155
4.2.2	Estimation of dimensionality of communication network.....	162
4.2.3	Effect of fractional-samples delays on dimensionality estimation ....	164
4.2.4	Conclusion .....	165
4.3	Estimation using $R$ of CCF of dimensionality.....	165
4.3.1	Theoretical estimation.....	166
4.3.2	Estimation from simulation.....	170
4.3.3	Effect of fractional-samples delays on dimensionality .....	174
4.3.4	Conclusion .....	175
4.4	Estimation of the numbers of nodes in different dimensions .....	176
4.4.1	Effect of fractional-samples delays.....	177
4.5	Estimation of the numbers of nodes for different dimensions: another approach.....	180
4.5.1	Effect of fractional-samples delays.....	186
4.6	Conclusion .....	187

<b>Chapter 5</b>	<b>Analysis of error in estimation.....</b>	<b>189</b>
5.1	Introduction.....	189
5.2	Error in estimation .....	190
5.2.1	Theory regarding error in estimation in ERP case .....	191
5.2.2	Obtaining CV from theoretical CCF .....	193
5.2.3	Obtaining CV from simulated CCF in ERP case .....	195
5.2.4	Theory regarding error in estimation in ETP case .....	198
5.2.5	Effect of fractional-samples delays .....	206
5.2.6	Deriving generalised expression for CV .....	208
5.2.7	Conclusion.....	210
5.3	Selection of signal length from OCV .....	210
5.4	Selection of sampling rate, $S_R$ , and distance between sensors, $d_{DBS}$ ..	213
5.5	Effect of noise on CV .....	216
5.6	Required estimation time in the proposed method .....	221
5.7	Required energy in terms of the product of SNR and $N_s$ .....	226
5.8	Comparison with conventional protocol-based techniques .....	230
5.8.1	Performance comparisons in terms of CV .....	239
5.8.2	Performance comparisons in terms of required estimation time.....	248
5.8.3	Performance comparisons in terms of required transmit energy.....	253
5.8.4	Results and discussion.....	266
5.9	Conclusion .....	269
<b>Chapter 6.....</b>	<b>.....</b>	<b>271</b>
<b>Conclusions .....</b>	<b>.....</b>	<b>271</b>
6.1	Introduction.....	271
6.2	Future directions .....	272
6.2.1	Method can be used in any environment networks .....	272
6.2.2	Random transmitted and received power (RTRP) case .....	273
6.2.3	Estimation using more than 2 sensors .....	275
6.2.4	Practical implementation.....	277
6.2.5	Effect of Doppler shift.....	277
6.2.6	Sensors not being at centre of the network .....	278
6.2.7	Distribution of nodes being sufficiently non-random .....	278

6.2.8	Non-Gaussian signals.....	278
6.2.9	Effect of bandwidth.....	280
6.2.10	Effect of shape of the network .....	282
6.2.11	Non-Gaussian noise .....	282
6.2.12	Effect of more than two reflected path.....	282
6.2.13	Effect of variable propagation delays .....	283
6.2.14	Effect of $N$ on CV of estimation. ....	283
6.2.15	Further works on dimensionality estimation.....	284
6.3	Conclusion .....	284
<b>Appendix A Obtaining receiver internal noise and channel</b>		
	<b>background noise .....</b>	<b>287</b>
<b>Appendix B List of Symbols.....</b>		
	<b>Appendix C Used Abbreviations .....</b>	<b>293</b>
<b>References .....</b>		
		<b>295</b>





# Chapter 1

## Introduction

---

It is often useful to know the number of operating nodes in a wireless communication network (WCN), in which the nodes are deployed in different forms to cover small or large areas of interest for a wide variety of personal and commercial applications. In such a network, the number of operating nodes can vary with time due to the ad hoc nature of the network, power failure of the nodes, or natural disasters. But, as a network's proper operation (including maintenance), optimal performance, useful data collection depends on the number of operational nodes; it is a matter of great interest to know that number at any point in time.

Similarly, a concurrent estimation of the dimensionality of the network might also be important for localising the nodes and estimating their number in a deployed network. Although there are several estimation techniques in the literature, they are only suitable for some defined communication-friendly networks, such as ground-based networks like radio frequency identification systems (RFIDs). Many existing protocols cannot be used in networks in harsh environments (underwater, underground, etc.) because very few of those investigated take into account the non-negligible capture effect in these types of networks and, therefore, suffer from poor performance due to long propagation delays and high path losses. Moreover, protocols for estimating the numbers of nodes in WCNs also suffer from time complexity, i.e., they take a long time for just a single estimation and, in most cases, the estimation time increases with an increase in the number of nodes.

This thesis investigates estimation using cross-correlation, a signal processing technique, to estimate the number of nodes in, and the dimensionality of, a WCN. The cross-correlation of signals collected from two sensors contains information about the number of nodes which is used as the estimation parameter. This proposed signal processing approach greatly improves estimation performance and reduces

time requirements and protocol complexity. The fact that the required time is independent of the number of nodes makes this approach very efficient for a dense network.

The methods presented in this thesis may be applied to estimations in a large variety of the networks. It might be applied in voice or data communication networks which can be subdivided into: space communication networks (SCNs) such as the space wireless sensor network (SWSN); terrestrial communication networks (TCNs), for example, the terrestrial WSN (TWSN), the RFID system and the mobile ad hoc network (MANET); underground communication networks (UGCNs) such as the underground WSN (UGWSN); and underwater communication networks (UWCNs), for example, the underwater WSN (UWSN).

The proposed method can be used to estimate the number of nodes in, and the dimensionality of, a network in which the nodes (terminal equipment of WCNs) can transmit any kind of signal, for example, sensors in WSNs, tags in RFID systems. It might even be able to be used to estimate the number of fish in a school, based on their acoustic signatures. Although the proposed signal processing technique is equally applicable to any type of voice or data communication network, the UWCN is emphasised because it presents many technical challenges and is of practical importance due to the large underwater area (about 71% of the earth's surface). Basically, this estimation process will be the same for all types of networks as it takes into account the appropriate signal characteristics (propagation speed, signal length, sampling rate, propagation delay, path loss, etc.) required for networks in different environments to reach their sensors.

Three possible cases of the transmission and reception of signals in a transmitter/receiver system which might occur in the practical environment are: 1) equal received power (ERP) in which a network protocol ensures by probing that the signals received at each node will be equal in strength from all other nodes; 2) equal transmitted power (ETP) in which the transmitted signal strength from all nodes will be equal but the received signals strength will be different due to distance-dependent attenuations; and 3) random transmitted and received power (RTRP) in which both

signals are of random strengths. As our technique has major application in WSNs, RFIDs, etc., in which the probing technique is easily applicable, the first case would be sufficient for estimation. However, to make the estimation process robust, the second case is also investigated while the third is beyond the scope of this thesis. Although it is expected that experimental results will follow, as no field experiment has yet been undertaken, we provide only theory and simulation. The results presented in this thesis comprise a mix of theory and simulation. They represent a starting point for the investigation of correlation-based estimation techniques, but it is recognised that much further work is required before these techniques can be applied in real networks.

This chapter briefly outlines the background to the proposed work (a brief description of major WCNs and their importance), some practical signal propagation issues regarding estimation in the applied field, the importance of the problem of estimation, and the contributions of the proposed work. As the proposed method is effective in all types of networks, the following section briefly outlines the significance of different WCNs.

## **1.1 Background**

Recent advances in communications technology have produced WCNs in which information exchange occurs among nodes without wires. WCNs may be roughly classified by their geographical coverage area as: terrestrial (TWCN), space (SWCN), underground (UGWCN) and underwater (UWCN). Of these, the TWCN is the most dominant and covers almost the whole land area of the earth's surface; for example, wireless mobile phone networks are widely used for personal communication and internet access. RFID systems have received much attention in both academia and industry for applications such as monitoring and tracking objects. Also, MANETs, which are self-configuring networks of wirelessly linked mobile nodes, have gained significant attention for establishing survivable, efficient and dynamic communications for emergency rescue operations, disaster relief efforts and military networks.

Apart from TWCNs, SWCNs are another major application of a WCN. The main goals of the SWCN are earth observation (EO), telecommunication with space vehicles, and missions of localisation from space. WSN technology can also be deployed underground where applications might be voice communication within underground environments (e.g., in caves or mines), or monitoring of soil conditions. Moreover, nodes are deployed underwater in the forms of MANETs or WSNs. The major applications of UWCNs are voice communication among divers, AUVs, etc., information collection from oceans, lakes, and rivers to observe and predict the characteristics of the underwater environment which can help in pollution monitoring, disaster prevention, undersea exploration, tactical surveillance. In this section, some of the most important WCNs are briefly discussed.

#### **1.1.1 Mobile wireless telephone network (MWTN)**

The last two decades have been the most dynamic in the history of TWCNs. Most notably, cellular systems have experienced huge growth over the last decade and there are currently about two billion users worldwide. Many people use wireless cellular radio telephones, also known as cell phones, to stay in contact with colleagues and clients. In such systems, wireless communications allow people greater flexibility while communicating because they do not need to remain at a fixed location, such as a home or office but, instead, can travel in a car or walk along a street. Increasingly, people are using wireless devices for a variety of everyday purposes, such as scheduling appointments, arranging meeting places, shopping for food and agreeing on home video selections while in a video store. Wireless communication devices are useful in places where communication services are only temporarily needed, such as at outdoor festivals or large sporting events. These technologies are also useful for communicating in remote locations, such as mountains, jungles and deserts where a wire-based telephone service might not exist.

#### **1.1.2 Terrestrial wireless sensor network (TWSN)**

Recent advances in embedded system and communication technologies have pushed a higher level of functionality into ever-smaller devices capable of sensing and

providing wireless communication. Networks formed by these devices, known as WSNs, have attracted a tremendous amount of research effort due to their huge potential in both the military and civil domains. A TWSN consists of a large number of sensor nodes, often in the order of thousands, placed close to each other and spread across a geographical area. Each sensor node has a wireless communication capability and some level of intelligence for signal processing and networking of the data. WSNs may be ad hoc in nature, which implies that each sensor supports a multi-hop routing algorithm so that several nodes may forward data packets to the base station.

There are different types of TWSNs (for example, seismic, low sampling rate magnetic, thermal, visual, infrared, acoustic, radar, optical and electromagnetic) deployed for a variety of applications by observing the relevant decision-making parameters (for example, temperature, humidity, vehicular movement, lightning conditions, pressure, soil makeup, noise levels, presence or absence of certain types of objects, mechanical stress levels on attached objects, speed, direction and size of an object).

To date, TWSNs have been used to perform collaborative tasks in areas such as the military, environmental research, the health sector, smart home appliances, industrial processing and disaster relief. In military applications, sensor networks are used to sense and obtain information about enemy movements, to characterise types of attacks as nuclear, biological or chemical, to monitor friendly forces and equipment, and for battlefield surveillance and targeting, etc.

Sensor networks are also employed to detect and monitor environmental changes in plains, forests, etc. Some environmental monitoring applications are: investigating conditions that affect different types of life in the earth; studying pollution and precision agriculture; and for flood and bush fire detection. The Great Barrier Reef Ocean Observing System (GBROOS) (Bainbridge 2009; Kininmonth 2004; Freitas 2009) uses a TWSN to monitor the environment near the Great Barrier Reef (GBR). Habitat monitoring is another application of a TWSN; for example, researchers in

UNSW, Australia, proposed a sensor network to detect the existence of cane toads (Shukla 2004; Hu 2009).

In the health sector, integrated patient monitoring, diagnostics, telemonitoring of human physiological data, and the tracking and monitoring of doctors and patients inside a hospital are major applications. Disaster (bush fire, earthquake, tsunami, etc.) prediction is a very important application of a TWSN as it can provide prior information about such events. The integration of electronics, sensors and wireless communications has enabled the easy installation of TWSNs in industrial motor's condition monitoring, which saves the cost of deploying large numbers of traditional wired monitoring systems (Lu 2005). The low cost, flexible, and rapid deployment characteristics of these sensor networks form an ideal platform for industrial condition monitoring systems (Lee 2008) .

Some other applications are: wireless traffic sensor networks for monitoring vehicular traffic on highways or in congested parts of a city and detecting accidents; wireless surveillance sensor networks for providing security in shopping malls, parking garages and other facilities; and wireless parking lot sensor networks for determining occupied and unoccupied spots. Other applications are the monitoring of product quality, the construction of smart homes and offices, the monitoring of disaster areas, automatic meter reading and facility management.

### **1.1.3 Radio frequency identification (RFID) system**

An application of wireless communication is the RFID, a system that transmits the identity of an object or person (in the form of a unique serial number) wirelessly using radio waves. In recent years, RFID systems have received much attention both in academia and industry for monitoring and tracking applications. They also offer a promisingly affordable, cheap and flexible solution for object identification. Among their applications, the localisation of objects and people, animal identification, ensuring secure operations in dangerous environments, and facilitating electronic payments and production control can be cited. Researchers believe that this technology can be used to save money and lives, and even the environment. In a

RFID system, there are two main parts: tags and readers. As the tags are most important for proper information exchange, knowledge of their number is important because of tag failure could render the whole identification process useless.

#### **1.1.4 Space wireless communication network (SWCN)**

Apart from TWCNs, space communications and commercial satellites are other major applications of wireless communication infrastructure (Vladimirova 2008; Colitti 2008). The main goals of a satellite are earth observation (EO), telecommunication with space vehicles and positioning missions. There are three different satellite systems which are positioned in accordance with the earth's orbit: LEO at roughly 2000 km, MEO at roughly 9000 km and GEO at 40,000 km. The most common EO applications are: monitoring the environment and agriculture regarding pollution, land, ocean surface and crop conditions, etc.; hazard and disaster predictions of events such as floods, earthquakes and urban disasters; and observations of borders, vehicles and activities for security and crisis management.

Traditional satellite missions using large satellite units are extremely expensive and difficult to design, build, launch, operate and maintain. For that reason, groups of smaller satellites (nano and/or pico) are scattered around the earth (Colitti 2008) to achieve global coverage in order to achieve success in different applications; this is the concept of a satellite sensor network (Krishnamurthy 2005). Although recent advances in TWSN technology limit the use of commercial satellites, some are still used due to their compelling features, for example, ubiquitous worldwide coverage, especially in remote areas, entertainment broadcasts using hundreds of TV channels, and high-quality digital radio offering audio transmission at near-CD quality.

#### **1.1.5 Underground wireless communication network (UGWCN)**

WCN technology can also be deployed underground where applications might be voice communication (Sicignano 2010) within underground environments (e.g., caves and mines), or the monitoring of soil conditions by observing the parameters of water content, mineral content, salinity, temperature, etc. UGWCN can be deployed



for a number of applications (Akyildiz 2006). This can be helpful in both agriculture and the construction of buildings. Wireless sensors that operate independently using a single-hop link to a base station are already being used for the monitoring of soil conditions in sports fields (Akyildiz 2006). Another application is for security purposes where sensors buried at a shallow depth can be used to detect movement via pressure, vibration and/or sound. This may be useful for business and home security as well as military applications. Although aboveground WSNs can be used for this purpose, it is desirable for security applications that sensors are hidden. Also, as a significant amount of infrastructure, including plumbing as well as electrical and communications wiring, exists underground, sensors can be used to monitor underground activity, for example, a plumbing leakage. With many miles of pipes to monitor, wireless sensors allow for the quick and cost-efficient deployment of a leakage detection system. UGWCNs can also be used to monitor the soil around underground storage tanks such as those at a fuel station. Although it is challenging, some researchers (Stuntebeck 2006; Akyildiz 2009; Bogen 2009) have tried wireless communications underground to develop efficient UGWCN.

### **1.1.6 Underwater wireless communication network (UWCN)**

Geographically, almost three-quarters of our planet is covered by water, of which oceans account for almost 71% with the remainder being water reservoirs such as rivers, lakes, dams and ponds. As nearly all the world's habitation is encompassed by water, if it is possible to use it as an efficient and reliable information communication medium, this would be a very valuable achievement for the communications industry. However, to date, very little communication coverage has been achieved by researchers due to the lack of means rather than limited human curiosity. Although underwater areas are naturally harsh to human exploration, in recent years, with technological advancements in the communications industry and increased knowledge of the reserves of natural resources underwater, research on UWCNs has been attracting attention for military and commercial purposes. UWCNs include, but are not limited to, UWSNs using acoustic waves (Quazi 1982; Sozer 2000) and electromagnetic waves (Frater 2006). As underwater personal communication is very limited and sensory application dominant, an underwater wireless acoustic sensor

network (UWASN), which is a more flexible form of communication in that environment, is the main use of a UWCN.

The major applications of UWASNs include, but are not limited to, the following (Jiang 2008):

- ❖ information exchange among nodes within the communication range of the network, or outside the network with the help of a switch centre; for example, underwater internet and voice communication among submarines;
- ❖ information collection from oceans, lakes and rivers which could improve the human ability to observe and predict the characteristics of the underwater environment;
- ❖ surveillance, including reconnaissance, targeting and intrusion detection;
- ❖ environmental monitoring: a UWASNs can monitor different types of pollution, for example, chemical, biological, nuclear and oil leakage in bays, lakes and/or rivers (Yang 2002), and might also be useful for monitoring ocean currents and temperature changes in terms of global warming;
- ❖ underwater exploration: without any appropriate technological tool, this is very difficult due to the high water pressure, unpredictable water activities and vast size of an unknown area but an UWASNs could be such a tool;
- ❖ disaster alleviation: remote UWASNs can be helpful in the prediction of, and preparation for, the results of undersea disasters, such as tsunamis and ocean-bottom earthquakes, by issuing real-time warnings (Soreide 2004); and
- ❖ underwater mine detection in which optical sensors are employed (Freitag 2005).

There exist a number of research groups who have used oceanic WSNs to study underwater environments. One research group involved randomly distributed WSN involving magneto-elastic sensors over a lake to measures the pH-values of the water

in order to determine whether the water is safe to drink (Ong 2004). Another group have proposed a cost effective WSN for marine research to monitor water temperature and salinity (Dunkels 2004) and the proposed theoretical model is intended to be applied in an area where freshwater movements significantly affect temperature and salinity of the sea water. Potential research works are also available addressing several points of interests such as the development of middleware, routing, security and localization of underwater nodes in WSNs (Blumenthal 2004a; Blumenthal 2004b).

However, while terrestrial networks, in particular “smart dust” (Buettner 2008; Shwe 2009), emphasize low-cost nodes, dense deployments, and multi-hop and short-range communications, today’s typical underwater wireless networks are expensive and sparsely deployed (a few nodes placed kilometers apart). They communicate directly with a base station and sometimes use underwater manned or unmanned vehicles. In comparison with this common strategy, a nature-inspired approach, such as smart dust in a TWCN, smart plankton (Anguita 2008a; Anguita 2008b) can address the challenges and provide a roadmap for future generations of UWCNs.

## **1.2 Practical issues regarding estimation**

As the approach proposed in this thesis is based on the cross-correlation of signals received by two digital receivers from random signal sources, the estimation process can be affected by some practical issues of digital receiver and signal propagation through the channel such as propagation delay, path loss, background noise, multipath propagation, internal noise of the receiver and fractional-sample delays.

Some dominant practical issues are discussed in this section. As in this thesis UWCNs are emphasized, signal propagation issues are for the underwater environment.

### **1.2.1 Signal propagation underwater**

There are three possible physical waves (electromagnetic (EM), acoustic and optical) used to carry communication signals in a UWCN, all of which have their advantages

and limitations. Optical systems which use lasers are limited to very short distances as the light is rapidly attenuated in water due to backscattering (Akyildiz 2005). While an EM wave is a promising signal used in terrestrial communication, due to its very high absorption rate in water because of its high frequency, EM waves can only propagate over extremely short distances underwater (Che 2010). Instead, acoustic waves, which can propagate over long distances (Sozer 2000), are used in practice. Thus, although sound waves are of great interest for the transmission of information in water, and acoustic communication is a promising underwater technique, there are some limitations which require further work. Underwater acoustic communication poses the limitations of long and variable propagation delays (Akyildiz 2005), high path losses, strong background noises and multipath of signal propagation.

The following section briefly describes the fundamental physical characteristics and critical issues for EM and acoustic wave propagation underwater.

### **1.2.2 Propagation delay in underwater acoustic network (UANs)**

An EM wave's propagation speed in air is considered to be the speed of light but, in water, it is affected by the factor  $\sqrt{\epsilon_r \mu_r}$ , where  $\epsilon_r$  is the relative permittivity and  $\mu_r$  the relative permeability. As, for the reasonable EM frequencies underwater,  $\epsilon_r \approx 81$  and  $\mu_r = 1$ , the speed of an EM wave underwater is  $c_{water} \approx 3.33 \times 10^7$  m/s (Goh 2009). Although this speed is lower than that in air, as it is still very high, the propagation delay of a signal from a transmitter to a receiver is negligible for an EM signal.

On the other hand, acoustic signals travel underwater much more slowly than EM waves. The typical value used for an acoustic transmission is 1500 m/s (Preisig 2006; Lucani 2007; Wenli 2008). Limited bandwidth often leads to data delivery rate of merely a few kbps. Moreover, the deployed area for UAWSNs is much larger than that for TWSNs which results in its propagation delay becoming significant. Thus, the low data rate and long propagation delay in a UAWSN provide significant

challenges for networking concepts using RF radios with negligible propagation delay developed for TWSNs.

### 1.2.3 Path loss

To design feasible communication schemes for efficient application in UWSNs, it is important to understand the characteristics of the underwater channel, one of the most representatives being the high path loss which becomes severe as the carrier frequency of the signal increases. Thus, an EM signal has much greater path loss than an acoustic signal.

There are three possible causes of path loss in a channel: absorption, geometrical dispersion and scattering. When propagated, wave energy can be transformed into other forms, such as heat, and be absorbed by the medium; this is known as absorption loss and is due to particular properties of a communication channel. The relevant property for acoustic waves is inelasticity whereas, for EM waves, it is electrical conductivity. In underwater communication, the cause of absorption loss is the inelastic property of water for acoustic waves, and the conductivity of salty water for EM waves.

Dispersion loss, also known as spreading loss, is due to the geometrical dispersion of the signal in the communication medium. When an acoustic signal propagates further away from its source, the wave front occupies an ever-increasing surface area. Hence, the energy per unit surface area (i.e., the energy flow) consistently decreases. For a spherical wave generated by a point source, the dispersion loss is proportional to the square of the distance whereas, for a cylindrical wave, the loss is proportional only to the distance.

Path loss is defined as (Howlader 2009):

$$L_p = d^{-k} a^{-d} \quad (1.1)$$

where

$L_p$  is the path loss which is a function of the distance between the transmitter and receiver,  $d$ , and the signal frequency,  $f$ ;  
 $k$  is the dispersion factor; and  
 $a$  is the frequency-dependent absorption coefficient.

The dispersion component typically depends only on distance, while absorption depends both on operating frequency and distance.

The expression of path loss in dB is (Howlader 2009):

$$10\log L_p = -10k\log d - 10d\log a \quad (1.2)$$

On the right-hand side, the distance-dependent first term with the dispersion factor represents the dispersion loss whereas the frequency-dependent second term represents the absorption loss. It is shown in (1.2) that for a particular operating frequency the absorption loss in dB is also a linear function of distance.

The expression (1.1) implies that the dispersion loss results from energy decay due to propagation, with the decay proportional to  $d^{-k}$  and the absorption loss proportional to  $a^{-d}$ , where  $a$  is an increasing function of frequency. Due to this frequency dependency, an underwater acoustic channel is effectively considered as bandwidth-limited (and not, like an RF channel, power-limited). This limitation occurs because, in general, the low cutoff of the available bandwidth is determined by ambient noise levels and the high point by absorption. Due to its distance dependency, the absorption loss becomes more significant at longer distances and the effective bandwidth decreases as the range increases.

The dispersion factor,  $k$ , describes the geometry of propagation, and its commonly used values are  $k = 2$  for spherical spreading,  $k = 1$  for cylindrical spreading and  $k = 1.5$  for so-called practical spreading (Stojanovic 2006a). (The counterpart of  $k$  in a radio channel is the path loss exponent, the value of which is usually between 2 and 4, the former representing the free-space line-of-sight propagation and the latter the

two-ray ground-reflection model.) Thorp's formula is used to express absorption coefficient as (Berkhovskikh 1982):

$$10 \log a = 0.11 \frac{f^2}{1 + f^2} + 44 \frac{f^2}{4100 + f} + 2.75 \times 10^{-4} f^2 + 0.003$$

where  $10 \log a$  in dB/km and  $f$  in kHz.

The absorption coefficient is plotted in Figure 1.1 (Stojanovic 2006a).

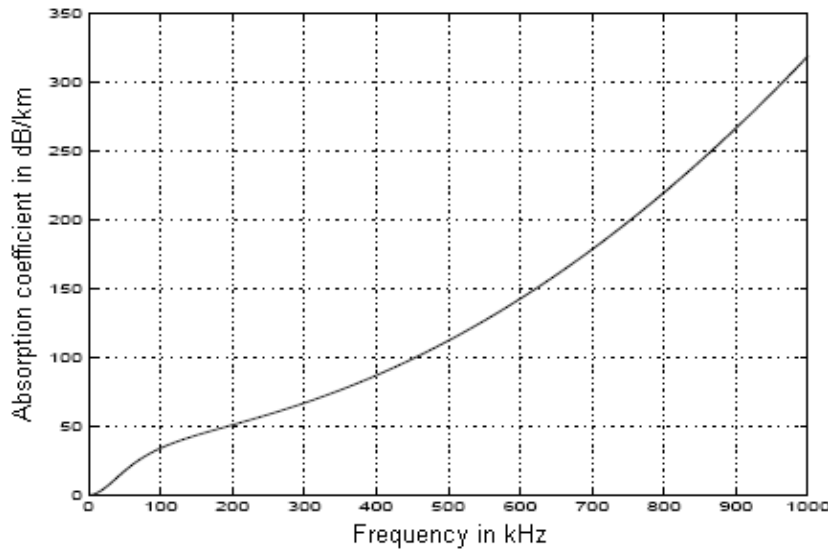


**Figure 1.1 Absorption coefficient,  $a(f)$**

#### 1.2.4 Background noise

Another major factor of disturbance is background noise, also known as ambient noise, which can be defined as the unwanted signal from unidentified sources in the medium. Its distinguishing features are: it is due to multiple sources; individual sources cannot be identified; and no one source dominates the received field. Common sea surface noise sources include ships' radiated noises, breaking waves associated with ensuing bubble production, etc., and deep water noises, mainly from marine mammals.

The ambient noise in the ocean comes from a number of sources as: turbulence, shipping, waves and thermal noise, most of which can be described by Gaussian statistics and a continuous power spectral density (Stojanovic 2006a). Due to the

frequency dependence nature of the ocean ambient acoustic noise (Urlick 1986), the power spectral densities of the above four major noise components are expressed by the frequency dependent empirical relations in (Coates 1989) as:

$$\begin{aligned}
10 \log U_t(f) &= 17 - 30 \log f; \text{ for } f < 10 \text{ Hz} \\
10 \log U_s(f) &= 40 + 20(s_a - 0.5) + 26 \log f \\
&\quad - 60 \log(f + 0.03); \text{ for } 10 \text{ Hz} < f < 100 \text{ Hz} \\
10 \log U_w(f) &= 50 + 7.5w^{1/2} + 20 \log f \\
&\quad - 40 \log(f + 0.4); \text{ for } 100 \text{ Hz} < f < 100 \text{ kHz} \\
10 \log U_{th}(f) &= -15 + 20 \log f; \text{ for } f > 100 \text{ kHz}
\end{aligned} \tag{1.3}$$

where

$U_t(f)$  is the power spectral density of ambient noise due to turbulence in dB re  $\mu\text{Pa}$  per Hz and  $f$  in kHz.

$U_s(f)$  is the power spectral density of ambient noise due to shipping in dB re  $\mu\text{Pa}$  per Hz and  $f$  in kHz.

$U_w(f)$  is the power spectral density of ambient noise due to wind in dB re  $\mu\text{Pa}$  per Hz and  $f$  in kHz.

$U_{th}(f)$  is the power spectral density of thermal ambient noise in dB re  $\mu\text{Pa}$  per Hz and  $f$  in kHz.

$s_a$  is shipping activity factor, whose value ranges between 0 and 1 (Stojanovic 2006a) for low and high activity, respectively.

$w$  is the wind speed in m/s

### 1.2.5 Multipath effects

Multipath propagation is the type of wave propagation in which a wave reaches a receiver through multiple paths. An acoustic channel underwater is subject to multipath propagation. In a shallow water channel, the acoustic waves travel through a direct path and also bounce from the surface and the bottom which results in multipath propagation. Although not as severe as in shallow water, there is still multipath propagation in deep water. Multipath propagation creates signal echoes which result in inter-symbol interference (ISI) in a communication system and its effects are more severe underwater than in a ground-based system; for instance, in a



cellular radio-based system, multipath spans only a few symbol intervals whereas, in an underwater acoustic channel, it can span tens, or even hundreds, of symbol intervals (Stojanovic 2006b). Although a solution to avoiding ISI is to use a guard time between successively transmitted symbols, this reduces the overall data rate and can cause higher error probability. One way of keeping the symbol rate high is to design receivers to counteract very long ISI. Although multipath effects might be neglected, the estimation process developed here analyses the negligible and non-negligible multipath effects.

### **1.2.6 Other issues**

Signal length, which might be a vital factor in the estimation process, is discussed later in this thesis. However, some other practical issues, such as the Doppler spread, refraction, which affect the performance of underwater acoustic propagation, are not considered.

## **1.3 Importance of the proposed estimation**

Although there is no particular literature to summarize the importance of node estimation, some literature (Akyildiz 2005; Proakis 2003; Partan 2006; Roux 2005; Swamy 2007; Chen 2008) demonstrate the importance directly or indirectly. This section summarises the importance of node estimation in wireless communication systems.

### A. Estimation in WSN

#### *1. Maintain coverage area*

The coverage area of a WSN depends mainly on the number of nodes present. There should be an area-node ratio in a network to be deployed in order to obtain sufficient data of interest. However, in a harsh remote environment, network nodes are often failure-prone and have limited power. It is thus a matter of great interest to know the number of nodes at any point in time after the deployment of a network to ensure that the predefined coverage area is achieved.

## *2. Assist proper network operation*

To optimise the use of energy (which is very important in a WSN where the nodes are unattended, remote and have a limited non-rechargeable power supply), it is necessary to utilise the variable numbers of nodes in a whole network according to the tasks to be performed. Thus, the network's deployment topology will vary from time to time. But, as real operations, such as routing, medium access and the protocols of the network, depend on the number of nodes, to achieve the proper operation of a network with a varying number of nodes, it is equally important to know the number of active nodes at any point in time. This might also help other processes such as localisation and direction finding.

## *3. Provide useful data collection*

The traditional approach (Proakis 2003) for ocean-bottom or ocean-column monitoring is to deploy underwater sensors that record data during the monitoring mission and then recover the instruments. As there is no interaction between the onshore control systems and monitoring instruments; real-time monitoring is not possible. This is critical, especially in surveillance or environmental monitoring applications, such as seismic monitoring. The recorded data cannot be accessed until the instruments are recovered, which may happen several months after the beginning of the monitoring mission. Also, if failures or misconfigurations have occurred, it may not be possible to detect them before the instruments are recovered. Thus, the data recorded during a monitoring mission will be useless if one or more nodes fail and this can easily lead to the complete failure of the mission (Akyildiz 2005).

## *4. Achieve cost-efficient missions*

The failure of a mission leads to high financial loss as the cost of manufacturing, deployment, maintenance and recovery of underwater equipment is much higher than that of its ground-based counterpart; for example, an acoustic modem with a rugged pressure housing costs roughly \$3000 (Partan 2006), an underwater sensor can be even more expensive, and supporting hardware, e.g., an underwater cable connector, is often more than \$100 (Partan 2006). Deployment

costs are also very high. An oceanographic research vessel typically costs \$5000 - \$25,000/day depending on its size (Partan 2006) and the operation being weather dependent exacerbates the situation. Recovery can also be expensive. Increasing its number of nodes is one way of improving the robustness of a network. However, the number of operating nodes can vary with time due to various artificial, as well as natural, reasons (for example, some nodes might fail, some can be damaged because of fouling and corrosion, or batteries might fail).

#### *5. Regain network topology*

The deployment of a WSN follows some geometrical topology which changes if any node fails. However, this can be overcome by knowing the number of active nodes as well as their locations.

### B. Estimation in mobile ad hoc network

#### *6. Assist traffic management and knowledge of community's lifestyle*

Accurately determining the number of operating nodes, i.e., mobile phones, could provide a complete picture of a community's demand which would be helpful for the proper operation and planning of a communications company which could, based on that information, decide to extend or reduce a facility, for example, install another base transceiver station. Also, knowing the number of mobile phones used in a community can provide an indication of that community's lifestyle.

### C. Estimation in RFID system

#### *7. Provide proper identification of tagged body in RFID system*

In an RFID system, the failure of any tag means that its body is untagged, i.e., it will not be identified by the reader. This failure of any tag could be identified by knowing the accurate number of active tags. If all tags are sound, this process will help to count the number of tagged bodies which is the main goal of an identification process. Thus, to know the number of faulty tags, for their

replacement, and also to identify the number of tagged bodies, estimation of the number of tags is necessary.

#### D. Estimation of other nodes

##### *8. Count speakers in multi-speaker teleconferencing system*

In the case of multi-speaker data, the problem is determining the number of speakers, and then localising and tracking them from the signals collected using a number of spatially distributed microphones (Swamy 2007). It is also necessary to separate the speech of each individual speaker from the multi-speaker signals which again requires prior knowledge of the number of speakers.

##### *9. Obtain idea of ambient environmental noise*

Studies of unwanted signal, especially underwater ambient noise in the ocean, are of both scientific and applied interest as they provide information on processes in the ocean and oceanic fauna; for example, the depth estimation of an ocean is possible using the ocean's ambient noise cross-correlation (Siderius 2006). Again, as underwater ambient noises interfere with the operation of underwater acoustic systems such as UWASNs (Alam 2010), knowledge of their characteristics (number, strength, etc.) are necessary for the development of methods to suppress them. Thus, knowing the number of ambient noise sources is of interest.

##### *10. Count natural nodes, such as fish underwater and vehicles in street*

In this work, any signal-creating animals, materials, etc. can be also considered nodes. Natural underwater sources of sound, such as fish, and vehicles in the street are taken as examples. Estimating the number of fish is a very important achievement in the fisheries field as its management depends mostly on knowing the number of fish underwater, such as in hatcheries, ponds, lakes and even the ocean. This knowledge might assist a country's government to establish a fish-catching quota. Also, as vehicles in the street make sounds, they can be considered nodes. Estimating their number in a certain area will be helpful for a traffic management system. Also, as vehicles in the street make sounds, they can

be considered nodes. Estimating their number in a certain area will be helpful for a traffic management system. Although there are other more reliable ways (manual/automatic) to count the number of vehicles in a street, this approach would be a useful addition to them.

In a communication network, the nodes may be placed in 1D, 2D and, for a wide range of applications, 3D. Most terrestrial networks are 2D and most underwater are 3D. Dimensionality estimations of the nodes after deployment are essential in order to establish a practical network's dimension. The connectivity of the network might alter due to a harsh environment, especially in an underwater network in which the network nodes are sparsely placed. Also, a network will lose its deployment dimensionality after deployment if one or more nodes are damaged; this will lead to the loss of the project for which the network is deployed. Thus the estimation of the deployed networks' dimensionality is very important.

## **1.4 Objectives**

The objectives of this thesis are to: estimate the number of nodes in different WCNs (using in an underwater network as an example); estimate network's dimensionality; and propose a novel technique, instead of conventional protocols, for overcoming the inefficiency of protocols for estimating the number of nodes and dimensionality of an underwater network.

### **1.4.1 Estimation of the number of nodes**

To date, conventional techniques employed to estimate the number of nodes in a communication network have been based on protocols already in use. Those in a TWCN are well established whereas the harsh underwater environment poses several difficulties. In this study, a cross-correlation technique for estimating the number of nodes, which will be equally usable in all environments, is proposed. As underwater networks represent the worst cases in communication, all simulations are conducted for that environment.

### **1.4.2 Estimation of networks' dimensionality**

The dimensionality of a communication network is important for various purposes, such as localisation, direction finding and estimation. As estimation of the number of nodes using cross-correlation might depend on the dimensionalities of the networks, it is better to first estimate the later, that is, whether the nodes are oriented in 1D, 2D or 3D in space. The dimensionality of a network affects the cross-correlation function (CCF). Based on this effect, a concurrent cross-correlation method for estimating dimensionality is proposed.

### **1.4.3 Analysis of error in estimation**

Errors are mirrors of estimates and are divided into two categories: mathematical and statistical. As the method of cross-correlation has statistical properties, it is better to analyse the error of such a technique statistically rather than mathematically which is carried out in this work. The ratio of the standard deviation to the mean of estimation, also known as the coefficient of variation (CV), is investigated and analysed as a statistical error in estimation.

## **1.5 Robustness of the estimation process**

To ensure the estimation process is robust, the following practical issues are considered in the simulation.

- 1) Background noise
- 2) Internal receiver noise
- 3) Fractional-sample delays
- 4) Propagation delays
- 5) Multipath effects

Different performance analyses are conducted and the system's performance is compared with that of conventional protocol techniques. It is noted that there are many other possible channel properties and components, but investigation of these is left for further work.

## 1.6 Contributions and novelty

The major contributions of this thesis are as follows.

### ❶ *Estimation of the number of nodes in WCN: ERP case*

This work formalises a novel process for the estimation of the number of nodes in a communication network using cross-correlation. The impact of large propagation delays on the performances of protocol techniques is most significant. The technique developed here performs better than the protocol methods. A number of practical issues are investigated, which are listed below.

- i. Estimation is performed with integer and fractional-sample delays, and compares them to show the effect on estimation of the fractional part of the sample delay. This helps to design a practical estimation system.
- ii. Theoretical estimation is proposed for infinite signal length, which is an energy-related term in a practical system and is therefore not possible to attain. So the effect of finite signal length and its proper selection is investigated.
- iii. To make the estimation process robust, the effects of noise are investigated and proposed solutions are provided.
- iv. Realistic deployment environments might have multipath effects which in turn might affect the estimation process. The effects of multipath are analysed and a solution provided to obtain estimation.

### ❷ *Estimation of the number of nodes in WCN: ETP case*

The first contribution is investigated in the ERP case, in which the signals received at each node will be equal in strength from all other nodes, and is possible with a simple network protocol using a probing technique. Direct use of this technique is not suitable for the ETP case, in which the transmitted signal strength from all nodes will be equal but the received signals strength will be different due to distance-dependent attenuations. The modified estimation technique is investigated for the ETP case, in which we provide a concise treatment of the fundamental concept of ERP case. This extension

might be helpful in estimating the number of network nodes even if the nodes are uncontrolled, i.e., the nodes of enemy sensor networks and those in the natural underwater networks, such as fish. The effects on estimation are provided for practical issues as fractional-samples delay, signal length, and noise.

③ *Error formulation and analysis*

The process of cross-correlation has statistical properties. So, the coefficient of variation (CV), a statistical error in estimation, is formulated and analysed. The analyses are provided in terms of the following investigations.

- i. Theoretical and simulated investigations are provided for CV in the ERP case.
- ii. Theoretical and simulated investigations are provided for CV in the ETP case.
- iii. Required energy estimation and comparison in the proposed techniques.
- iv. Required time estimation and comparison in the proposed techniques.
- v. Comparison with conventional protocols in terms of CV and required time.

④ *Dimensionality (i.e. a network is 1D, 2D, or 3D) estimation: Method 1*

A dimensionality estimation of communication networks using the shape of the cross-correlation function (CCF) is undertaken.

⑤ *Dimensionality (i.e. a network is 1D, 2D, or 3D) estimation: Method 2*

A dimensionality estimation of communication networks using the ratio of standard deviation to the mean of the CCF is conducted, where the ratio is obtained from the individual bin probabilities.

⑥ *Estimation of the number of nodes in WCN for all dimensions: Method 1*

An estimation process of the number of nodes for all network dimensions (1D, 2D, and 3D) using the ratio of the standard deviation to the mean of the CCF is undertaken, where the ratio is obtained from the entire CCF at a time.



⑦ *Estimation of the number of nodes in WCN for all dimensions: Method 2*

An estimation process of the number of nodes for all network dimensions (1D, 2D, and 3D) using the basic approach (as in the first contribution) is conducted.

## **1.7 Thesis organisation**

The remaining chapters of this thesis are organised as follows.

Chapter 2 - a detailed review of the literature pertaining to the topic; this chapter describes the scope of the estimation technique. Important literature pertaining to estimation of the number of nodes and network dimensionality have been summarized based on their estimation process, advantages and limitations. The chapter also describes the cross-correlation applications which lead to the motivation using cross-correlation to estimate the number of nodes. Moreover some statistical signal processing terms relevant to the estimation process are discussed.

Chapter 3 - estimation of the number of nodes; this chapter describes the details estimation process using cross-correlation. Theory is developed for the basic estimation in ERP case with some assumptions. Most of the assumptions are analysed later in the thesis. Theories are supported by simulations. The estimation technique is analysed with practical issues such as fractional-samples delays, noise, and multipath effects.

Chapter 4 - estimations of dimensionality and the number of nodes in different dimensions; this chapter analyses the theory and simulation of network dimensionality estimation for three basic dimensional (1D, 2D, and 3D) networks. Moreover, the estimation of the number of nodes for all dimensions is investigated in this chapter.

Chapter 5 - a detailed error analysis of estimations of the number of nodes using investigations of comparative performances, the energy required for estimation, the effects of practical issues; and

Chapter 6 - the conclusion of the whole thesis. Important future work has also been suggested with possible direction for research.

## 1.8 Publications

Major publications resulting from this work are:

- [1] “Estimation by Cross-correlation of the Number of Nodes in Underwater Networks”, In *Proc. Australasian Telecommunications and Applications Conference (ATNAC) 2009*, Canberra, 10–12 November 2009.
- [2] “A Novel Signal Processing Approach of Network Size Estimation in an Underwater Environment”, Submitted to *IEEE Transaction on Signal Processing*, 2012.
- [3] “Estimation using cross-correlation of the dimensionality and corresponding size of wireless communication networks”, Draft to be submitted to *IEEE Journal of Oceanic Engineering*.
- [4] “Estimation using cross-correlation of the number of nodes in ocean wireless sensor networks”, journal to be submitted to *Ocean Engineering*, Elsevier.



# Chapter 2

## Literature review

---

### 2.1 Introduction

There are several artificial forms of wireless communication using different forms of signals (i.e., electromagnetic, acoustic and optical) and their combinations; for example, wireless communications in terrestrial communication systems, e.g., RFID, mobile wireless telephone and internet, in WSN systems in different media, i.e., air (TWSN), underwater (UWSN) and underground (UGWSN), and in space communication systems, e.g., satellite communication networks. In these forms of wireless communication systems, the terminal equipment (i.e., the user handset in a mobile phone system and sensors in a WSN) are taken as the nodes. Strictly speaking, the parts of a wireless communication system which transmit signals of any kind are the nodes of interest.

Accurately determining the number of nodes in a communication network is an important issue for both practical network operations (such as routing and medium access) and networked applications (such as information retrieval and processing) as they depend upon the number of transmitting nodes present. Moreover, estimation of the number of nodes, i.e., the number of transmitters, has recently received much attention in the field of WSNs. In underwater networks, there may be a large number of nodes deployed over a large area for a practical purpose, such as oceanographic data collection or pollution monitoring. In other applications, underwater vehicles in a UWSN, using electromagnetic waves (Frater 2006) and acoustic waves (Quazi 1982; Sozer 2000) equipped with a sufficient fraction of operating nodes that can communicate with each other, travel underwater for the purposes of climatic data collection, environmental monitoring, seismic and acoustic monitoring, surveillance and national security, military purposes and health care, discovery of natural resources, location of man-made artefacts and extraction of information for scientific analysis. As optimal performance requires a balance among the number of operating

nodes, the energy efficiency and the lifetime of the network, the number of operating nodes is a crucial factor for networks.

However, this balance can vary over time due to various artificial, as well as natural, causes (for example, some nodes might fail or become damaged, or batteries might fail). So, it is a matter of great interest for a communication network to know how many operating nodes or transmitters are available in the region at any point in time to ensure proper network operation (such as routing) as well as network maintenance (such as replacement of faulty nodes).

Again, precisely determining the number of ambient noise sources, i.e., the natural nodes, might be an important issue for WCNs as, in a communication network, issues such as communication quality, and information retrieval and processing capabilities, depend on the number of ambient noise sources present. It is also important in, for example, fisheries, animal and vehicle management systems, where the estimation of the number of ambient signal sources is itself interesting.

Moreover, the dimensionality of a network is very important for ensuring its appropriate coverage area, proper network operation, such as routing, and design of network protocols, as well as for processes of localisation and direction finding. In such cases, although the dimensionality is assumed, in practice, it might be totally different. Again, as estimating the number of nodes using cross-correlation depends on dimensionality, in order to create a robust estimation technique, the dimensionality of the network has to be estimated first.

## **2.2 Existing estimation techniques using protocols**

Protocols are widely used in WCNs for different purposes, such as routing purposes in WSNs, and identification of tags in RFID systems. Existing protocols can also be used for the estimation of the number of nodes in those networks. Identification is the process to identify the ID of the tags in an RFID network whereas estimation of the tags is the process of estimating their number. The following sections contain a brief literature review of network protocols to estimate the number of tags i.e. nodes.

### **2.2.1 Using identification protocols in RFID systems**

There have been many investigations into identifying the number of tags in RFID systems which is a similar problem to the estimation of the number of nodes in WCNs. A RFID system consists of one (or more) networked electromagnetic readers and a number of radio frequency tags, as shown in Figure 2.1 (Burdet 2004). The tags contain limited computation power and memory whereas the reader is powerful and has abundant memory. There is a single communication channel for exchanging messages between the reader and the tags but the tags are unable to do this among themselves. Initially, the tags are totally unknown to the reader. The reader can broadcast a message to which each tag has the option of sending a response to the reader. The reader receives responses from the tags and tries to identify them. If only one tag responds at a time, it is correctly identified. But, if more than one tag responds at a time, the reader detects only a collision on the channel. A RFID protocol specifies the algorithms for the reader and the tags so that the reader can properly collect all the tag IDs. Knowing the numbers of tags in large-scale RFID systems is an important task. Their estimation is possible by using the existing protocol to identify individual tags and then computing the cardinality of the system.

There have been many tag identification protocols, probabilistic, deterministic and hybrid, proposed in the literature. Probabilistic algorithms decrease the possibility of tag collisions by allowing the tags to transmit their own serial numbers at a distinct time (Myung 2007) whereas, using deterministic algorithms, the reader sends its ID-based requests to tags to obtain responses (Alotaibi 2009). ALOHA-based protocols (Vogt 2002a; EPC-Global 2005; Lee 2005; Bonuccelli 2006; Cha 2006; Kodialam 2006; Peng 2007) are probabilistic whereas tree-based protocols (Choi 2005; Chiang 2006; Choi 2006; Myung 2006a; Myung 2006b; Myung 2007) are deterministic. Some hybrid approaches, in which randomisation is applied in a tree scheme, are discussed in (Micic 2005; Simplot-Ryl 2006; Ryu 2007). In (Kodialam 2006), a framed slotted ALOHA protocol, in which each tag transmits its serial number to the reader in a randomly selected slot of a frame (a time interval between the requests of a reader consisting of a number of slots) and the reader identifies tags when a time

slot is used by only one tag, is proposed. This process is repeated until all tags are identified.

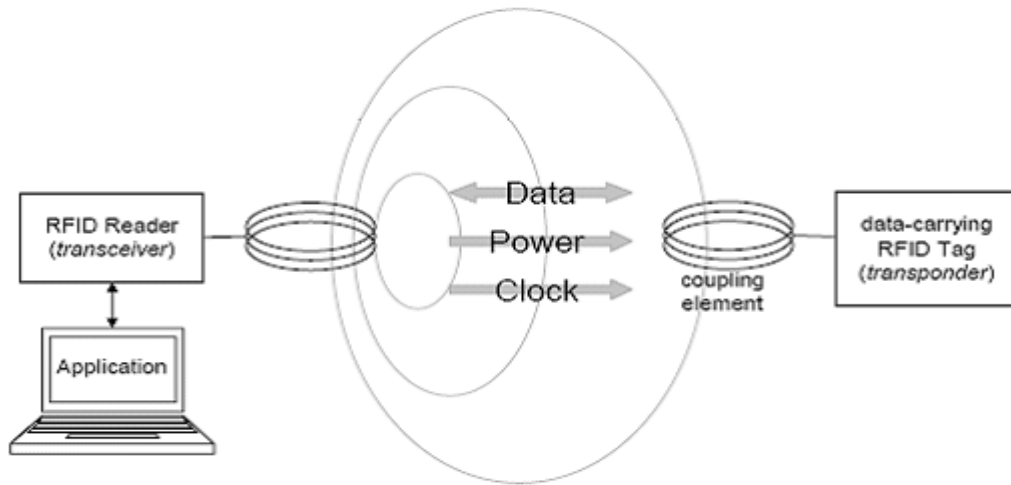


**Figure 2.1 Basic RFID system (Alotaibi 2009)**

There might be some collisions in the basic ALOHA-based protocols, which affect the identification process by degrading the performance. To significantly reduce the number of transmission collisions, a new probabilistic protocol, based on a modified version of the slotted ALOHA protocol (called the tree-slotted ALOHA protocol), is proposed in (Bonuccelli 2006). In this scheme, each tag selects a slot into which to transmit its ID by generating a random number. When a collision occurs in a slot, only the tags that generate such a collision are queried in the next read cycle. Thus, a transmission frame can be viewed as a node in a tree where the root is the initial frame and the leaves represent frames in which no collision has occurred.

However, collisions (which may cause a serious problem of tag starvation, i.e., a specific tag may not be identified for an unlimited time) are not completely removed by ALOHA-based protocols. To remove this tag starvation problem, tree-based tag anti-collision protocols, such as binary search protocols (MIT-Auto-ID-Center 2003) and query tree (QT) protocols (Law 2000), have been proposed. A splitting mechanism for tag identification is used in tree-based protocols in which colliding tags are split into two subsets which are identified one after another by the reader. In this method, all the tags can be identified by continuing the mechanism until the reader receives tag signals without collisions.

In the QT protocol (Law 2000; Feng 2004), the reader sends a prefix and asks the tags to answer if their IDs match it. If a collision occurs, the reader queries for a prefix that is one bit longer and this process continues until no collision occurs. Thus, once a tag is identified, the reader starts a new round of queries with another prefix until all tags are identified. However, since readers use prefixes, their performances are sensitive to the distributions of the tag IDs they have to identify. Further improvements are proposed in (Law 2000; Chiang 2006). In binary search protocols (Capetanakis 1979; ISO-Standard 2003; MIT-Auto-ID-Center 2003), the processes are similar to those of query tree protocols except that they use random binary numbers to split the tag set.

Although tree-based protocols do not suffer from the tag starvation problem, they have relatively long identification delays caused by the splitting procedure. To reduce this effect, Myung et al. (Myung 2006a; Myung 2006b; Myung 2007) propose two adaptive tag anti-collision protocols: the adaptive query-splitting protocol, an improvement on the QT protocol, and the adaptive binary-splitting protocol which is based on the binary tree protocol. Also, an improvement on the adaptive binary-splitting protocol is proposed in (Chen 2007).

All the protocols proposed to date exhibit average performance well below 50% of maximum throughput (in terms of both messages and transmitted bits). To improve on this, another protocol, in which the reader asks all tags to transmit their own complete IDs, is proposed in (Bonuccelli 2008). From the answer, which is the sum of all the IDs, the reader divides the set of tags in a recursive way until all tags are identified.

However, these estimation processes based on tag identification protocols suffer from the shortcoming of a long processing latency; for example, the deterministic protocol in (Myung 2006c) requires more than 1000 seconds (Chen 2008) for the identification of 3000 tags while an even longer time is required for the probabilistic protocol proposed in (Lee 2004). Due to this long processing delay, tag identification-based estimations are often impractical, especially when a tag is attached to a moving object in which case it may go outside the reader's range before



being identified. In some instances, for security purposes, readers may not be allowed to query the tags for their identification. In other cases, a tag set may undergo a quick change of their location and shape which makes identification by the reader of all the tags impossible.

## 2.2.2 Estimation without identification in RFID systems

In order to overcome the effect of the long processing time required for identification when estimating the number of tags and to obtain proper estimations of all tags in cases with some non-identifiable tags, some estimation processes without identification are proposed in (Vogt 2002b; Floerkemeier 2006; Kodialam 2006).

### 2.2.2.1 Estimation process proposed by Kodialam (2006)

In this work (Kodialam 2006), the authors propose two estimation algorithms based on the framed slotted ALOHA (FSA) and probabilistic framed slotted ALOHA (PFSA) protocols for a static tag set using analysis and simulated verifications. In their FSA method, all tags respond in a randomly selected slot within a frame, whereas only a portion of the total tags determined by a probability factor respond in the randomly selected slot within the frame in their PFSA method.

In a respondent frame of size  $F$  in the FSA method, the reader measures some empty slots,  $m_0$ , some singleton slots,  $m_1$ , and some collision slots,  $m_c$ . For these slots, the authors propose three tag estimators as shown in the following table.

Estimator	Expression
Empty estimator	$e^{-\rho} = \frac{m_0}{F}$
Singleton estimator	$\rho e^{-\rho} = \frac{m_1}{F}$
Collision estimator	$1 - (1 + \rho)e^{-\rho} = \frac{m_c}{F}$

where,  $\rho$  is the normalised offered load and is defined as

$$\rho = \frac{\text{Number of tags to be estimated}}{\text{Frame size}} = \frac{N}{F}$$

So, the replacement of  $\rho$  gives the following estimator expressions.

Estimator	Expression
Empty estimator	$e^{-\frac{N}{F}} = \frac{m_0}{F}$
Singleton estimator	$\frac{N}{F} e^{-\frac{N}{F}} = \frac{m_1}{F}$
Collision estimator	$1 - \left(1 + \frac{N}{F}\right) e^{-\frac{N}{F}} = \frac{m_c}{F}$

In their PFSA method with total probability  $M$ , only the  $M$  portion of the tags responds in the frame of size  $F$ . Thus, the estimator expressions are as follows.

Estimator	Expression
Empty estimator	$e^{-\frac{MN}{F}} = \frac{m_0}{F}$
Singleton estimator	$\frac{MN}{F} e^{-\frac{MN}{F}} = \frac{m_1}{F}$
Collision estimator	$1 - \left(1 + \frac{MN}{F}\right) e^{-\frac{MN}{F}} = \frac{m_c}{F}$

It is shown that the empty estimator expressions can be solved easily for  $\hat{N}$  (denoting the estimated  $N$  as  $\hat{N}$ ) in the closed form but, as the other two non-linear expressions require numerical techniques, the authors solve them using the bisectional search method.

Of the estimators, it is shown that the singleton is non-monotonic in nature with respect to  $\rho$ , and the solution of the estimator equation for  $\hat{N}$  is not unique, i.e., for a certain number of singleton slots, there exist two different  $\rho$  (except  $\rho = 1$ ) and, thus, two different  $\hat{N}$ . So, the singleton estimator alone is not suitable for the estimation of the number of tags. Again, as it is shown in the above tag estimation

process that the collision estimator is better than the empty estimator, they prefer it for estimation. It can estimate the number of tags of any size within a near-constant time for a certain accuracy of estimation. However, although it might provide comparatively quick, accurate estimations in RFID systems with collision slots in which the capture effect can be neglected, in environments such as UCNs, in which the capture effect cannot be neglected, it is not suitable for estimation.

#### **2.2.2.2 Estimation process proposed by Chen (2008)**

The approaches proposed by Kodialam (2006) are designed for only a single reader and no information is provided for multiple readers. But, due to the terrain and coverage limitations of their readers, large-scale RFID systems often require multiple readers. It has been shown through analysis that, although the method proposed by Kodialam and Nondogopal is efficient and effective, it has a problem with multiple reading, i.e., the reading of a tag by more than one reader in a multi-reader system. To overcome this problem, a replicate insensitive Lottery Frame (LoF) estimation protocol is proposed by Chen (2008). In this process, the elimination of replicates can be achieved by hashing and a logical OR operation, as discussed below (Chen 2008).

In its initial phase, each reader constructs an ALOHA frame of size  $F$  with  $\eta$  time slots, and then broadcasts the length,  $\eta$ , to probe the tags within its communication range. When a tag receives the probe request from the reader, it applies a particular hash function to its ID,  $i$ , whose values are uniformly distributed. Upon obtaining the result of a particular hash function, the respondent tag normalises the hash function to a value within the range of  $[0, \eta - 1]$  and denotes the normalised value as the slot number in the frame in which it will respond.

In this way, every tag hashes itself to a time slot of a frame with size  $\eta$  in the reader which keeps a bitmap with the tag hashes. After hearing the whole frame, the reader knows that some slots have no transmission, with a bit value of 0 denoted by  $h_0$ , and some have one or multiple transmissions, with a bit value of 1 denoted by  $h_1$ . If the

estimated number of tags is again denoted by  $\hat{N}$ , the estimation expression will, for a single reader (Chen 2008), be

$$\hat{N} = -\eta \ln\left(\frac{h_0}{\eta}\right) \quad (2.1)$$

The property of hashing is suitable for eliminating replications in a multi-reader case since datum with the same value will have the same hash value. In this process,  $h_0$  and  $h_1$  are no longer individual computations. Instead, all readers report their bitmaps to a central server which obtains a merged bitmap using the logical OR to those individual bitmaps. Then, the server estimates  $\hat{N}$  from the merged bitmap using the expression (2.1) above.

### **2.2.2.3 Methods proposed by Vogt (2002b)**

Two FSA processes for estimating the number of tags around a reader in a RFID system have been proposed by Vogt. In the first, a reader with a frame of size  $F$  sends probe requests to the tags. Being energised by the probes from the reader, the tags reply to that frame in which there will be some singleton,  $m_1$ , some collision,  $m_c$ , and some empty,  $m_0$ , slots. In singleton slots, only one tag, in collision slots more than one and in empty slots no tag will have responded. In this estimation method, the author of Vogt (2002b) provides a lower bound on the value of the estimated number of tags which is obtained through the assumption that, to get a collision slot, at least two different tags must have responded in a slot. Thus, from the respondent frame, the estimated number of tags,  $\hat{N}$ , is obtained using the numbers of singleton and collision slots by

$$\hat{N} = m_1 + 2m_c \quad (2.2)$$

It is shown in Wang (2007) that estimation using this lower bound is suitable for small numbers of tags and large frame sizes with respect to the numbers of tags. As a system with a large number of tags increases the offered load and, if the frame size is not large enough to accommodate them properly, there will be a high probability of

collision slots occurring with responses from more than two tags and the estimation using (2.2) will be error prone.

To obtain an improved lower bound, another proposed approach uses Chebyshev's inequality which states that the outcome of a random experiment involving a random variable is most likely somewhere near the expected value of the random variable. From this statement, an alternate estimation function, using the deviations between the observed values and expected values of singleton, collision and empty slots, is proposed as:

$$\varepsilon(F, m_0, m_1, m_c) = \left| \begin{pmatrix} E(M_0) \\ E(M_1) \\ E(M_c) \end{pmatrix} - \begin{pmatrix} m_0 \\ m_1 \\ m_c \end{pmatrix} \right|$$

The estimated number of tags is that for which the estimation function is the minimum. Thus, the Chebyshev's inequality improved lower bound estimation algorithm of Vogt (2002b) can be described by (2.3).

$$\hat{N} = \min_N (\varepsilon(F, m_0, m_1, m_c)) = \min_N \left| \begin{pmatrix} E(M_0) \\ E(M_1) \\ E(M_c) \end{pmatrix} - \begin{pmatrix} m_0 \\ m_1 \\ m_c \end{pmatrix} \right| \quad (2.3)$$

To obtain the proper estimation using (2.3), an exhaustive search of  $N$  is required in which  $N$  varies from the lower bound proposed in the first method to an unlimited upper bound. However, as no upper bound is mentioned in this process, its estimation suffers from time complexity.

To overcome this, a similar expression is used to estimate the number of tags in Bonuccelli (2006) by varying  $N$  in the range of  $[m_1 + 2m_c, \dots, 2(m_1 + 2m_c)]$ . Bonuccelli (2006) proposes an upper bound of the search equal to  $2(m_1 + 2m_c)$  to reduce the time complexity as it is clear from their simulation that no further accuracy in the estimation can be achieved beyond this value.

#### 2.2.2.4 Method of binomial distribution estimation (BDE)

To shorten the identification time and gain maximum throughput, a BDE algorithm, based on a combinatorial model of the communication mechanism between tags and reader, for estimating the number of tags is proposed in (Cha 2005; Wang 2007). Simulation results show that the method using LB proposed by Vogt (2002a) is quite accurate when the number of tags is less than twice the number of slots but that the estimation error increases rapidly with increases in the number of tags. In (Vogt 2002b), Vogt improves the estimation algorithm in (Vogt 2002a) using Chebyshev's inequality and obtains a lower estimation error when the object number is more than twice the slot number; however, when the object number is small, the estimation error is much larger.

The method in (Cha 2005; Wang 2007) estimates  $N$  tags by comparing the expected value of the collision percentage in  $F$  slots with the observed collision percentage obtained after the end of an identification round. For the tags, the binomial slot allocation process, in which the probability  $p$  out of  $N$  tags transferring their IDs into a particular slot is used, is given by:

$$M(X = p) = \binom{N}{p} \left(\frac{1}{F}\right)^p \left(1 - \frac{1}{F}\right)^{N-p} \quad (2.4)$$

where  $p$  is also known as the occupancy number of the slots (Vogt 2002b). Then, the expected value of the number of slots with  $p$  is given by:

$$E(X = p) = F \binom{N}{p} \left(\frac{1}{F}\right)^p \left(1 - \frac{1}{F}\right)^{N-p}$$

Using the above expression, the expected number of slots can be obtained as follows.

The expected number of empty slots is:

$$E(X = 0) = F \binom{N}{0} \left(\frac{1}{F}\right)^0 \left(1 - \frac{1}{F}\right)^{N-0} = F \left(1 - \frac{1}{F}\right)^N$$

The expected number of singleton slots is:

$$\begin{aligned}
E(X=1) &= F \binom{N}{1} \left(\frac{1}{F}\right)^1 \left(1 - \frac{1}{F}\right)^{N-1} \\
&= F \binom{N}{F} \left(1 - \frac{1}{F}\right)^{N-1} \\
&= F \binom{N}{F} \left(\frac{F}{F-1}\right) \left(1 - \frac{1}{F}\right)^N \\
&= F \binom{N}{F-1} \left(1 - \frac{1}{F}\right)^N
\end{aligned}$$

So, the expected number of collision slots is:

$$\begin{aligned}
E(X > 1) &= F - E(X=0) - E(X=1) \\
&= F - F \left(1 - \frac{1}{F}\right)^N - F \binom{N}{F-1} \left(1 - \frac{1}{F}\right)^N \\
&= F \left\{ 1 - \left(1 - \frac{1}{F}\right)^N \left(1 + \frac{N}{F-1}\right) \right\}
\end{aligned}$$

Thus, the expected ratio of collision to total slots, termed the collision ratio or collision percentage,  $C_{\text{ratio}}$  is:

$$E(C_{\text{ratio}}) = 1 - \left(1 - \frac{1}{F}\right)^N \left(1 + \frac{N}{F-1}\right)$$

After the end of an identification round, the observed collision ratio or collision percentage can be obtained from the known number of collision slots and the frame size by:

$$C_{\text{ratio}} = \frac{\text{Number of collision slots}}{\text{Frame size}} = \frac{m_c}{F}$$

Then,

$$C_{\text{ratio}} = 1 - \left(1 - \frac{1}{F}\right)^N \left(1 + \frac{N}{F-1}\right) \quad (2.5)$$

From this expression, as  $C_{\text{ratio}}$  and  $F$  are known, it is easy to obtain only the unknown parameter,  $N$ , can be obtained as the estimation of the number of tags.

The proposed estimation parameter in (2.5) can also be expressed figuratively for different frame sizes of the reader (Cha 2005), as shown in Figure 2.2. Thus, estimation of the number of tags is possible from the obtained  $C_{ratio}$  using the plot for the corresponding frame size.

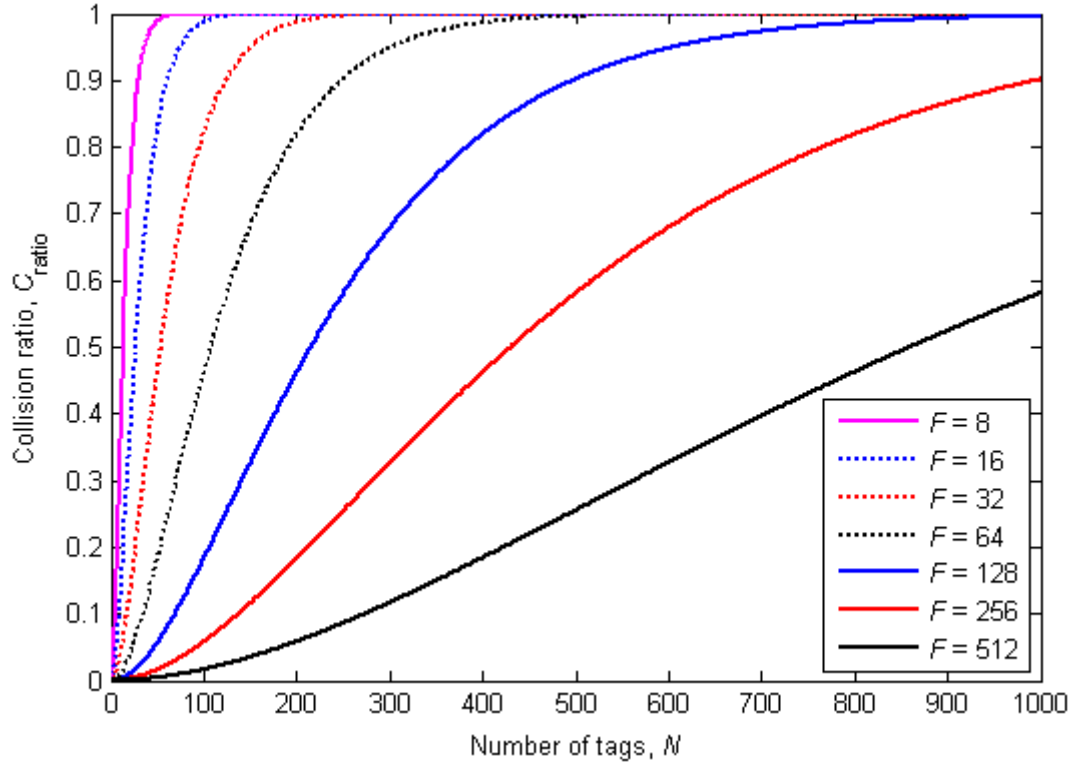


**Figure 2.2 Collision ratio versus number of tags (Cha 2005).**

### 2.2.2.5 Method using maximum throughput conditions proposed by (Cha 2005)

As the proposed scheme in (Cha 2005) is similar to the BDE technique, by using (2.4) the probability of obtaining empty, singleton and collision slots is as follows.

The total probability of empty slots is:

$$M(X=0) = \binom{N}{0} \left(\frac{1}{F}\right)^0 \left(1 - \frac{1}{F}\right)^{N-0} = \left(1 - \frac{1}{F}\right)^N$$

The total probability of singleton slots is:



$$M(X=1) = \binom{N}{1} \left(\frac{1}{F}\right)^1 \left(1 - \frac{1}{F}\right)^{N-1} = \frac{N}{F} \left(1 - \frac{1}{F}\right)^{N-1}$$

The total probability of collision slots is:

$$\begin{aligned} M(X > 1) &= 1 - M(X=0) - M(X=1) \\ &= 1 - \left(1 - \frac{1}{F}\right)^N - \left(\frac{N}{F-1}\right) \left(1 - \frac{1}{F}\right)^N \\ &= 1 - \left(1 - \frac{1}{F}\right)^N \left(1 + \frac{N}{F-1}\right) \end{aligned}$$

So, the throughput is:

$$\psi = \frac{M(X=1)}{M(X=0) + M(X=1) + M(X > 1)} = \frac{N}{F} \left(1 - \frac{1}{F}\right)^{N-1}$$

The condition for maximum throughput is obtained by:

$$\frac{d}{dF}(\psi) = 0 \text{ which gives us the condition } N = F.$$

Upon obtaining this condition, the optimum collision rate,  $C_{\text{rate}}$ , is obtained for maximum throughput from (Cha 2005) by:

$$C_{\text{rate}} = \lim_{N \rightarrow \infty} \left( \frac{M(X > 1)}{1 - M(X=1)} \right) \approx 0.418$$

So, the number of tags in a collided slot,  $N_{\text{coll}}$ , is (Cha 2005):

$$N_{\text{coll}} = \frac{1}{C_{\text{rate}}} = 2.3922$$

If the total number of collided slots is  $\eta_c$ , the estimated number of tags,  $\hat{N}$ , after a round is obtained using:

$$N = N_{\text{coll}} \times \eta_c = 2.3922 \times \eta_c$$

### 2.2.2.6 Method using received signal strength properties (Alotaibi 2009)

In this method, received signal strengths are used to estimate the number of tags where the tags are situated in an area around the tag reader, as shown in Figure 2.3. There is an interrogation zone with the minimum and maximum ranges,  $d_{\min}$  and  $d_{\max}$ , respectively in which the separation between the tags and reader are evenly distributed. The signal strength at the reader is obtained by the Friis transmission formula (Barclay 2003):

$$Q_r = Q_t G_t G_r \left( \frac{\lambda}{4\pi d} \right)^2 \quad (2.6)$$

where  $Q_t$  and  $Q_r$  respectively are the transmitted and received signal powers at the reader,  $G_t$  and  $G_r$  respectively are the gains of the transmitting and receiving antenna,  $\lambda$  the signal wavelength and  $d$  the effective radial distance (which is twice (Alotaibi 2009) the distance between the tag and reader) between the tags and reader.

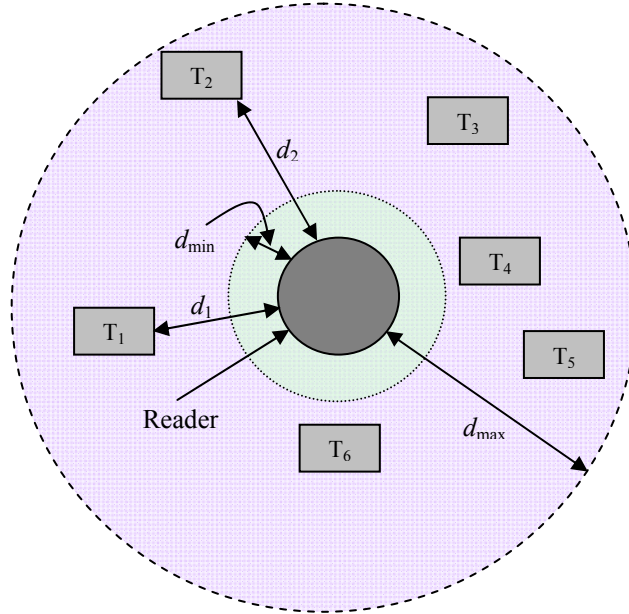


**Figure 2.3 Sample RFID system for method proposed in (Alotaibi 2009)**

In this method, the estimation of the number of tags is obtained from the cumulative distributions of the received signal strengths which are provided in (Alotaibi 2009) for 1000 scenarios with different numbers of tags responding simultaneously; where significant differences are evidenced. When there are two tags in the system, the

signal strength distribution curve is small and, for each additional tag, becomes smoother with a larger distribution of signal strengths.

### 2.2.3 Protocols in TCN

Before discussing the estimation protocols in a TCN, a brief description of a WSN's node and its functionality is provided because the estimation techniques are often applied in a WSN. A WSN is one of the most important applications of a wireless communication system. It consists of a large number of nodes for sensing different physical quantities and converts them into signals readable by other neighbouring nodes and a central node is known as a sink node or base station. One or more sensor(s), an ADC, a processor, a transceiver, memory and a battery are the major parts of a typical sensor node's architecture, as shown in Figure 2.4 (Akyildiz 2002).

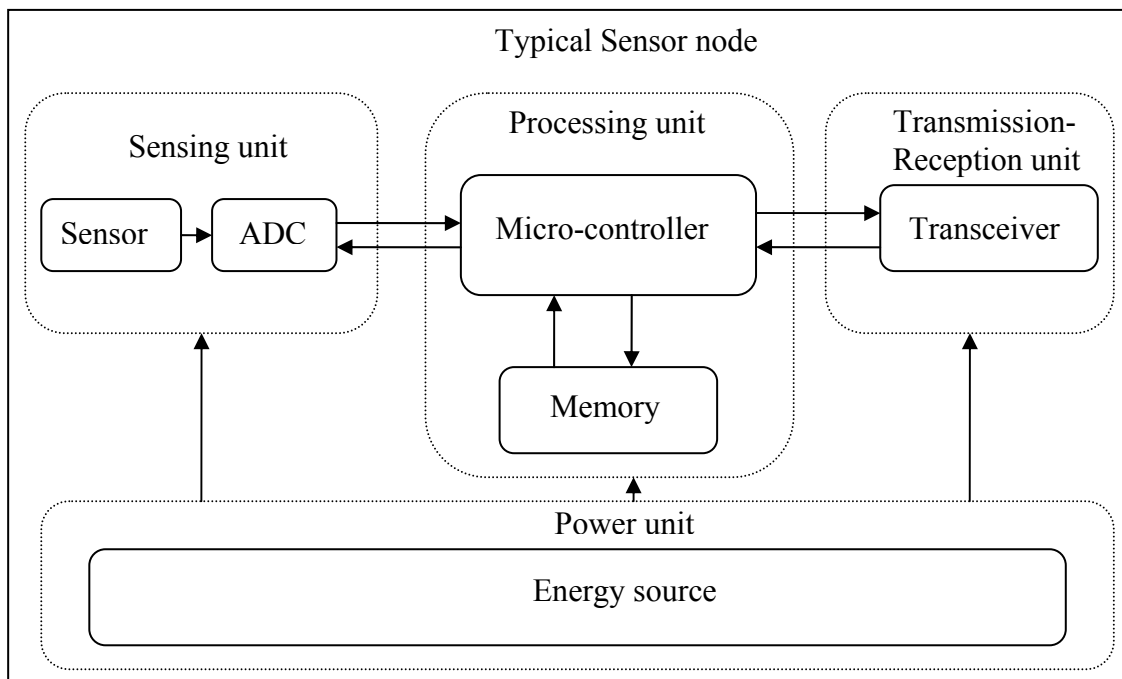


**Figure 2.4 Typical sensor node architecture**

The sensor(s) in a sensor node is/are the hardware component(s) for sensing environmental changes, such as pressure and temperature, in a monitoring area or sending probe requests to the other node(s) and collecting their response(s). They are

classified as passive and active. The former sense the data without actually manipulating the environment by active probing and are self-powered, i.e., energy is needed only to amplify their analogue signals. On the other hand, active sensors actively probe the environment or other neighbouring nodes and sense the responses and there is an ADC to digitise the analogue signals received by the sensor(s). Some sources of power consumption in sensors are: a) signal sampling and conversion of physical signals to electrical ones; b) signal conditioning; and c) analogue-to-digital conversion. The digitised signal from the ADC is sent to the micro-controller which processes the data and performs tasks accordingly while also controlling the functionality of other components of the node. A single device with the functionality of both a transmitter and a receiver, known as a transceiver, is used in sensor nodes to connect them to the network.

Another important component of the sensor node is the power unit which needs to supply electrical energy to the electronic circuitry of the other components. Sometimes, a sensor node contains some sort of location-finding system to gather accurate knowledge of its location, a mobiliser to move the sensor nodes and a power generator to recharge the power unit.

One technique for estimating the number of TWCN nodes is proposed in (Budianu 2003; Budianu 2004; Budianu 2006). It involves an estimator based on the Good-Turing (GT) estimator (Good 1953) of the missing mass which was invented by Turing. This is investigated in (Budianu 2003; Budianu 2004; Budianu 2006) for a terrestrial sensor network with mobile access (SENMA) architecture in which there is a mobile access point (MAP) which acts as a base station for the nodes. Each node can transmit its ID to the MAP with the data packet in which packet transmission follows the slotted ALOHA protocol. Practically, as the MAP wants to know the number of operating nodes, it broadcasts probe requests using a frame with some slots and the operating nodes respond by transmitting information in the form of packets with their IDs by choosing the slots randomly with the same transmission and reception probabilities. This estimation of the number of operating nodes is based on the nodes' IDs embedded in the observed packets in the MAP. Packet

collection by the MAP is modelled as an independent, identically distributed (i.i.d.) sampling with uniform distribution.

In SENMA, the missing mass is the conditional probability that, given a frame with already observed packets (called a vector sample in their process) from some nodes, the newly received packet comes from a new node. More conveniently, consider a network of size  $N$  in which the MAP collects  $N_p$  packets from the nodes in which  $N_{p_1}$  packets appear exactly once in the vector sample of  $N_p$  packets. Then, the estimated missing mass is defined as:

$$\hat{H}_0 = \frac{N_{p_1}}{N_p} \quad (2.7)$$

In this process, another expression of the missing mass for the packets that do not appear in the MAP is used. If all nodes transmit packets and, among them, the  $N_{p_d}$  number of packets is distinct, then  $N_{p_0} = N - N_{p_d}$  will be the packets that do not appear in the MAP.

Thus, the missing mass in the case of i.i.d. sampling with a uniform distribution, i.e., with equal probability of packets to slots, is:

$$H_0 = \frac{N_{p_0}}{N} = 1 - \frac{N_{p_d}}{N}$$

Substituting the estimated value of  $H_0$  from (2.7), the following expression for estimating the number of nodes is obtained:

$$\hat{N} = \frac{N_{p_d}}{1 - \frac{N_{p_1}}{N_p}}$$

It is again observed in (Budianu 2006), with a certain confidence interval, the total number of slots needed for estimation using the Good-Turing estimator is dependent on the number of operating nodes and is  $O(\sqrt{N})$  (Howlader 2009). The order depends on the certain confidence level and the interval. With a confidence level of

$(1 - \phi)$ , where  $\phi$  is the probability of error in estimation, and an accuracy estimation of  $\beta$  (confidence level  $[N(1 - \beta), N(1 + \beta)]$ ), the total number of slots,  $\eta$ , needed is (Howlader 2009):

$$\eta = \left( \sqrt{\frac{-2(1 + \beta) \log\left(\frac{\phi}{2}\right)}{\beta - \log(1 + \beta)}} \right) \sqrt{N}$$

## 2.2.4 Protocols in UCN

Although the abovementioned methods are easy to apply in RFID and in terrestrial systems, they do not take into account the capture effect. This means that they are difficult to apply in UWSNs because of the unavoidable capture effect. One solution, which uses a node estimation technique using a protocol that takes the capture effect into account, is proposed by Howlader (2007, 2008). The procedure is very similar to that of the probabilistic framed ALOHA (Kodialam 2006) in that the probing node sends a probe request with a frame size,  $F$  (the number of slots in the frame), and a probability,  $p$ .

### 2.2.4.1 Estimation of number of nodes in UCN using Probabilistic Framed Slotted ALOHA (PFSA) protocol (Howlader 2007)

In this estimation process, there is a probing node in the centre of the network which wants to know the number of neighbouring nodes within its communication range as shown in Figure 2.5 (a). In the Figure 2.5 (b) the typical slotted frame structure is also shown (from Klair, 2007).

The probing node broadcasts some probe requests with frames towards the neighbours which, upon receipt of the requests, reply to the probing node into the frames with pre-defined packets. Consider such a probe request with a frame of  $F$  slots and a probability,  $p$ . To respond, each neighbour generates a uniform random number between  $[0, 1]$  and compares it with  $p$ . Only the neighbours with random numbers less than or equal to  $p$  transmit into that frame.

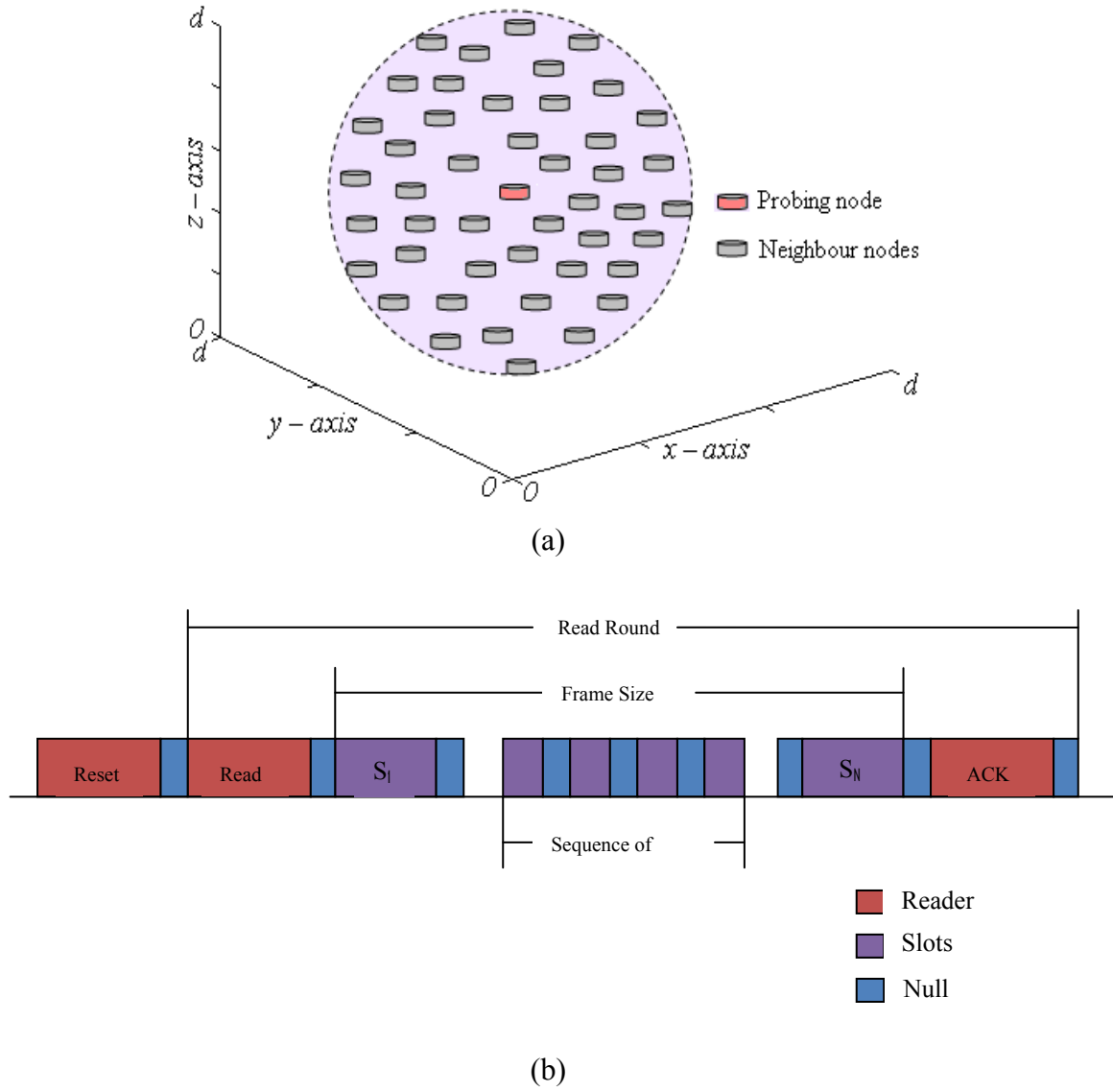


**Figure 2.5 (a) Distribution of nodes (b) Frame structure in PFSA technique**

Thus, only  $N \times p$  neighbours will transmit into that particular frame in the case of  $N$  neighbours. To obtain the optimum performance (by making the variance minimum), Howlader et al. assume the value of  $p$  such that the number of transmitting nodes in a frame has the following relationship (Howlader 2007) with the frame size:

$$N \times p = 1.59 \times F \quad (2.8)$$

Now, to transmit to the slots in the frame, each transmitting node generates a random integer between  $[1, F]$  and transmits to the slot according to the number. In the respondent frame, there will be some singleton slots,  $m_1$ , with only one packet, some

collided slots,  $m_c$ , where two or more packets collide and some empty slots,  $m_0$ , without any packet. Due to the capture effect, some collided slots might appear to the probing node as singleton slots. So, as the singleton and collided slots are dependent on the capture effect, they are not used for the estimation parameter. On the other hand, the number of empty slots is independent of the capture effect and follows the normal distribution as investigated in (Feller 1968; Kodialam 2006).

With this finding, the estimation of the number of nodes in their work is obtained from the observed number of empty slots in every probe,  $m_0$ , by obtaining the mean of the numbers of empty slots for all probes as:

$$\mu_0 \approx Fe^{-\rho_\xi} \quad (2.9)$$

where  $\rho_\xi$  is the effective normalised load, i.e., the actual number of transmitting nodes per slot and is obtained by:

$$\rho_\xi = \frac{N \times p}{F} \quad (2.10)$$

As, in a normal distribution, the expected value might be replaced by the observed value, we can write:

$$Fe^{-\rho_\xi} = m_0 \quad (2.11)$$

After some manipulation of (2.10) and (2.11), the estimation of the number of nodes is obtained as:

$$\hat{N} = -\frac{F}{p} \ln\left(\frac{m_0}{F}\right)$$

To achieve better performance, the probing and replies using a fixed frame size continue.

#### 2.2.4.2 Dimensionality estimation using protocol

It has already been mentioned that, in a response frame (Howlader 2008), there are some singleton, some collided and some empty slots. Of them, the number of empty



slots is independent of the capture effect whereas those of the singleton and collided slots are dependent on the capture effect. As the capture effect depends on the dimensionality of a network, this same relationship is followed by the parameters, as shown in their results. Although the estimation of the number of nodes is based on the number of empty slots, this method is not suitable for the dimensionality estimation as the number of empty slots is independent of dimensionality. Thus, they propose an algorithm based on the other two parameters,  $m_1$  and  $m_c$ , to roughly estimate the network's dimensionality.

It is assumed that the nodes are uniformly distributed along a straight line in 1D, inside a circle in 2D and inside a sphere in 3D where the probing node will be the centre node. If, in those spaces, the maximum possible range of the probing node is  $d$  and the dimension of network  $D$ , the CDF of the neighbouring nodes will be:

$$g(d) = d^D$$

Using the numbers of singleton and collision slots,  $D$  is estimated to obtain the dimensionality of the network.

Due to the capture effect, some of the collision slots will be received by the probing node as singleton slots. The transmitting node for which a collision occurs is called the interfering node. In their process for receiving a packet with the capture effect, there is a relationship between the interfering and transmitting nodes' ranges which is obtained from the capture model with the help of the received power model in TCNs:

$$C_R \leq \frac{Q_{tc}}{Q_{jc}} \text{ or } C_R \leq \left( \frac{d_t}{d_j} \right)^{-k}, \quad d_j \geq \left( C_R^{\left( \frac{1}{k} \right)} \right) d_t$$

where  $C_R$  is the capture ratio,  $Q_{tc}$  the received power from the transmitting node in a capture,  $Q_{jc}$  the received power from the interfering node in a capture,  $d_t$  the path length of the transmitting node from the receiver,  $d_j$  the path length of the interfering node from the receiver.

This means that, to obtain a collided slot as a singleton slot, the interfering node range should be greater than or equal to a constant multiple of the transmitting node range. Where, the capture constant is defined from the above expression as

$$\gamma(\geq 1) = C_R \left( \frac{1}{k} \right)$$

There is also a limiting range within which the capture effect may occur. All the ranges in their process are shown in Figure 2.5.

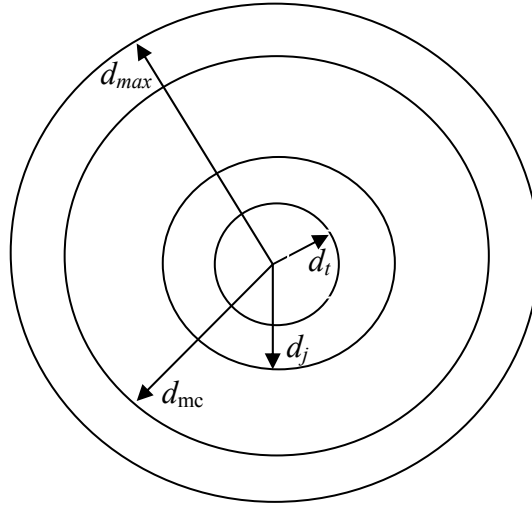


**Figure 2.6 Distances of transmitting and interfering nodes with capture effect (Howlader 2009)**

In this figure,  $d_{mc}$  is the maximum range beyond which no capture effect occurs, i.e., collision slots appear as collision slots and, within this range due to the capture effect, collision slots appear as singleton slots following the relationship between the interfering and transmitting nodes' ranges. (Howlader 2009) provides the following statistical expressions for obtaining the dimensionality parameter.

The expected numbers of singleton slots within and outside the range,  $d_{mc}$ , are:

$$E[M_{lc} : d \leq d_{mc}] = F\gamma^{-D} (1 - e^{-\rho_\xi})$$

and

$$E[M_{lc} : d \geq d_{mc}] = F\rho_\xi e^{-\rho_\xi} (1 - \gamma^{-D}),$$

respectively.

Thus, the total expected number of singleton slots with and without the capture effect is:

$$E[M_{1c}] = F\gamma^{-D}(1 - e^{-\rho_\xi}) + F\rho_\xi e^{-\rho_\xi}(1 - \gamma^{-D}) \quad (2.12)$$

Substituting the observed number of singleton slots with and without the capture effect, i.e.,  $m_{1c}$  instead of  $E[M_{1c}]$ , and the value of  $\gamma$  in (2.12), they propose an expression for the estimation of the spatial dimensionality of a network as:

$$\hat{D} = \left( \frac{-k}{\log(C_R)} \right) \log \left( \frac{m_{1c} - F\rho_\xi e^{-\rho_\xi}}{F(1 - (1 + \rho_\xi)e^{-\rho_\xi})} \right) \quad (2.13)$$

In the terms  $F\rho_\xi e^{-\rho_\xi} \approx E[M_1]$  and  $F(1 - (1 + \rho_\xi)e^{-\rho_\xi}) \approx E[M_c]$ ,  $E[M_1]$  and  $E[M_c]$  are the expected number of singleton and collision slots without capture respectively.

Thus, (2.13) will become:

$$\hat{D} = \left( \frac{-k}{\log(C_R)} \right) \log \left( \frac{m_{1c} - E[M_1]}{E[M_c]} \right) \quad (2.14)$$

By defining the probability of capture,  $p_c$ , as  $p_c = \frac{m_{1c} - E[M_1]}{E[M_c]}$  and substituting into (2.14), they provide the following closed-form formula for estimating the dimensionality parameter:

$$\hat{D} = \frac{-k \log(p_c)}{\log(C_R)}$$

In a UWCN, the capture ratio is defined as:

$$C_R = \frac{a^{-d_i} d_i^{-k}}{a^{-d_j} d_j^{-k}}$$

$$\text{or } d_j \approx \left( 1 + \frac{\log(C_R)}{k + d_i \log(a)} \right) d_i.$$

Thus, as in the previous case:

$$\gamma(d_i) = 1 + \frac{\log(C_R)}{k + d_i \log(a)}$$

Again, the expected number of singleton slots with and without the capture effect in a UWCN is:

$$E(M_{1c}) = F\rho_\xi \left( \int_0^{d_{mc}} De^{\{(D-1)\log d - (d_j)^D \rho_\xi\}} dd + e^{-\rho_\xi} (1 - d_{mc}^D) \right)$$

As they do not obtain any closed-form formula, they use Chebyshev's inequality to estimate the dimensionality parameter for which the proposed algorithm is:

$$\hat{D} = \arg \min_{D=1:3} |E[M_{1c}] - \text{mean}(m_{1c})|$$

## 2.3 Limitations of conventional techniques

It is obvious from the literature discussed in the previous section that most of the proposed estimation techniques have been designed for RFID systems which are different from ad hoc networks. RFID systems are very simple forms of wireless networks in which only the reader(s) acts as a base station(s) and wants to know the number of nodes (tags) within its communication range while the tags have no such ability. In contrast, nodes are self-reconfigurable in ad hoc networks in which every node needs to know the number of surrounding nodes within its communication range. Thus, although the proposed conventional techniques are suitable for RFID systems, in ad hoc networks, their direct use faces some limitations which require some adjustment. One such adjustment is proposed for a TWSN by Budianu in (Budianu 2006) (as discussed previously).

However, the techniques for RFID systems and TWSNs are similar in that they do not consider the capture effect because it is not so severe and can be neglected in a TCN. However, the direct use of the existing protocols (in which the capture effect is not considered) in harsh environmental networks (e.g., UWASNs) is mostly impossible due to this non-negligible capture effect. In addition, protocols designed

for TCNs ignore the signal propagation delay (Elson 2002; Maroti 2004) because they assume the use of high-speed EM waves. Sometimes, industry standard terrestrial protocols provide solutions for typically small (20 microseconds (Syed 2009) for IEEE 802.11) delays but do not perform satisfactorily under a long-delay regime (Ganeriwal 2003). Very few protocols (Howlader 2007; Howlader 2008) which take the capture effect into account have been investigated in such networks, but still they suffer from poor performance in a harsh environmental network due to the abovementioned signal propagation characteristics (Lanbo 2008) in such environments.

In addition, to date, most research studies regarding dimensionality have investigated the design of a network before deployment (Akyildiz 2005; Pompili 2006; Pompili 2009). Only one protocol technique has been investigated after deployment (Howlader 2008).

Moreover, all the abovementioned procedures for estimating the number of nodes in RFID and UWSN systems are similar in that they are based on protocol designs. However, underwater acoustic propagation characteristics (Lanbo 2008), such as propagation delay, high absorption and dispersion may make their use difficult.

Besides, protocols for estimating the number of nodes in every type of WCN also suffer from time complexity, i.e., they need a long time for even a single estimation which, in most cases, increases with increasing numbers of nodes. Also, the implementation of these conventional techniques based on network protocols to obtain precise measurements is often expensive and inefficient.

Being aware of these limitations, new techniques using cross-correlation as a replacement for the existing protocol techniques are being searched for in the literature presented in Section 2.4. As cross-correlation is a statistical signal-processing technique which possesses different characteristics of the signal and signal sources, it may well be a suitable replacement for the existing protocols.

## **2.4 Use of cross-correlation**

The impulse response of a communication channel, i.e., the Green's function (GF) retrieval of cross-correlating the waves excited by randomly generated ambient noise sources recorded by sensors at two locations, is currently a very important issue. There have been many investigations regarding the use of the ambient noise cross-correlation to extract the time-domain GF in various environments and frequency ranges of interest, for example, underwater acoustics (Roux 2004; Sabra 2005b; Sabra 2005d), crustal seismology (Shapiro 2004; Wapenaar 2004; Sabra 2005a; Shapiro 2005; Snieder 2004), helioseismology (Rickett 1999) and ultrasonics (Weaver 2001; Weaver 2002; Weaver 2003; Larose 2004; Malcolm 2004; Weaver 2004). The procedural steps for determining the noise CCF are similar for all the abovementioned environments. In brief, the procedure is as follows: firstly, the signals from a number of different noise sources are collected by two sensors separated by a certain distance in the region of interest; secondly, the received signals are summed at each of the two sensor locations; and, finally, these two noise signals are cross-correlated.

Most researchers have only tried to retrieve an estimate of the GF; for example, it has been shown theoretically that the GF can be obtained with ambient noise cross-correlation in the simple case of a homogeneous medium with attenuation (Roux 2005). Similarly, Snieder (Snieder 2007) and Godin (Godin 2006) show the extraction of the GF in the case of a heterogeneous medium. Some researchers (Weaver 2001; Weaver 2002; Sabra 2005c) have given their attention to the emergence rate of the time-domain GF (TDGF). Moreover, Ward (Weaver 2008) identities, fluctuations (Weaver 2005a) and means and variances (Weaver 2005b) have been performed in diffuse field-field correlations. However, none of these investigations indicate the estimation of the number of noise sources.

### **2.4.1 Cross-correlation for travel-time and direction of arrival estimations**

Cross-correlation is used for time delay of arrival (TDOA) estimation in (Ianniello 1982; Kumar 1993; Cheng 2007). Sensor arrays are often used in many fields of

science and engineering, particularly when the goal is to collect the signals and study their characteristics by processing them in order to take collaborative decisions. Cross-correlation between two received signals is widely used for these estimations due to its simplicity and efficiency. In (Varma 2002), two estimations are investigated concurrently. First, the TDOA estimate is performed between pairs of sensors using the CCF of the two signals in those sensors and then combining them with the knowledge of array geometry to obtain the DOA estimate. In (Knapp 1976; Azaria 1984), the DOA is investigated using the generalised cross-correlation (GCC) technique. Another approach for determining the number of speakers from the multi-speaker speech signals at two spatially separated microphones, in which cross-correlation is used to detect the TDOA, is proposed in (Swamy 2007).

#### **2.4.2 Cross-correlation for weak signal detection**

Radio weak-signal detection, i.e., the detection of signals with low signal to noise ratios (SNRs) is of wide concern in satellite communication systems. For proper management and monitoring of radio waves, expanding their coverage areas and improving the sensitivity of the monitoring system, this detection technique becomes increasingly important. Conventional methods, such as the low-frequency and phase-sensitive filtering techniques, firstly need some information about the signal which is difficult to achieve in a monitoring mission. In (Jian-fei 2009), a method of cross-correlation (Kay 2003; Moore 2006) for detecting a radio's weak signals, which does not require prior knowledge of the signal, is investigated. The proposed cross-correlation algorithm effectively detects whether the unknown signal exists.

The method of cross-correlation has application in blood-flow sonography (Bonnetfous 1986; Gao 1998) for which the conventional ultrasonic Pulsed Wave (PW) Doppler blood-flow analysers are widely used in clinical examinations. However, it has the limitation of spectrum aliasing when the velocities exceed the Nyquist rate. A cross-correlation-PW method proposed in (Gao 1998) provides sonogram output without aliasing. In this technique, the delay times of the received RF echoes from pulse to pulse are estimated by the cross-correlation method. The

series of delay times with their related maximum values in the CCF are then used to form a time sequence which is sent to a spectrum analyser to produce the sonogram.

## 2.5 Motivation for using cross-correlation

As discussed previously, there are several properties of signal sources and signals that can be estimated through cross-correlation. In this work we investigate the use of cross-correlation for estimation of the number of nodes in a communication network. To understand the motivation for using cross-correlation for a number of nodes' estimation, we provide a simple example from (Callaghan 2010). Consider that a node in a line-of-sight environment emits a pulse,  $S_1(t) = \delta(\tau)$ , while two receivers record the signals,  $S_{r_{11}}(t)$  and  $S_{r_{12}}(t)$ , where  $\tau$  denotes the delay position of the Dirac delta function  $\delta(\cdot)$ . The positions of the node and receivers are unknown. The signal emitted from the node is received by both receivers with certain delays. Thus, the received signals become  $S_{r_{11}}(t) = \alpha_{11}\delta(\tau - \tau_{11})$  and  $S_{r_{12}}(t) = \alpha_{12}\delta(\tau - \tau_{12})$ , where  $\tau_{ij}$  denotes the delay lag from the  $i^{\text{th}}$  node to the  $j^{\text{th}}$  receiver, and  $\alpha_{ij}$  the corresponding path loss of the signal. By cross-correlating the two received signals

$$C(\tau') = \int S_{r_{11}}(t)S_{r_{12}}(t - \tau')d\tau' = \alpha_{11}\alpha_{12}\delta(\tau - (\tau_{11} - \tau_{12})) \quad (2.15)$$

It is seen in the above expression that the resulting cross-correlation is a Dirac delta at the delay difference,  $\Delta\tau = \tau_{11} - \tau_{12}$ . If the process is extended for more than one node, we will obtain a delta function for each node. Although the above explanation is for a delta signal, this also holds true for nodes with arbitrary signals as long as they have certain auto-correlation properties, such as Gaussian signals.

To provide another reason for cross-correlations being used for a number of nodes' estimation, we briefly review results for cross-correlations in a homogeneous environment (Roux 2005; Garnier 2009; Snieder 2004). Let us consider two sensors in an environment designed to record the time-dependent wave fields from the nodes present in that environment. Consider that  $S_{r_{11}}(t)$  and  $S_{r_{12}}(t)$  denote the received signals from a transmitter. Their CCF with the time lag,  $\tau$ , is given by:



$$C(\tau) = \lim_{T \rightarrow \infty} \frac{1}{T} \int_{-T}^T S_{r_{i1}}(t) S_{r_{i2}}(t - \tau) d\tau$$

In the case of a 3D homogeneous medium with a spatially uniform node distribution, the field at each receiver can be decomposed as a superposition of the uncorrelated plane waves from various directions (Callaghan 2010). It has been established (Cox 1973; Callaghan 2010) that the normalised cross-spectral density,  $I(\omega)$ , at frequency  $\omega$  between two sensors separated by  $d_{DBS}$  is:

$$I(\omega) = \text{sinc}\left(\frac{\omega \times d_{DBS}}{S_p}\right).$$

where,  $S_p$  is the speed of sound propagation.

In the time domain, the normalised correlation function is (Roux 2005):

$$C(\tau) = \frac{1}{2\pi} \int_{-\infty}^{\infty} I(\omega) \exp(i\omega\tau) d\omega$$

which can be written as (Roux 2005):

$$C(\tau) = \frac{1}{4\pi} \int_{-\infty}^{\infty} \frac{\exp[i\omega(t + d_{DBS}/S_p)]}{i\omega(d_{DBS}/S_p)} d\omega - \frac{1}{4\pi} \int_{-\infty}^{\infty} \frac{\exp[i\omega(t - d_{DBS}/S_p)]}{i\omega(d_{DBS}/S_p)} d\omega.$$

It is well known (Roux 2005; Garnier 2009) that, if there is an infinite number of nodes, the resulting equation of the CCF will form a rectangular shape centred at zero and have a width of  $2d_{DBS}/S_p$ . Actually, this rectangular pattern is formed from the delta functions of the individual cross-correlations for each node and its height depends on the number of signal sources and strengths.

From this rectangular CCF, one can deduce the estimation of the number of nodes by finding the standard deviation or mean, or its ratio, of the CCF. These problems have a statistical character, and it is therefore more convenient to solve them by statistical rather than deterministic methods.

## 2.6 Formation of CCF

If we cross-correlate signals in two sensors which are the summation of several Gaussian signals inside a boundary, for every signal we get a Dirac delta which occupies a place inside a space of a width twice the distance between the sensors (we divide that space equally into several bins) and that place is determined by the delay difference of the signal coming to the sensors. The deltas of delay differences equal to a bin distance from the origin are placed in that particular bin. It is shown in (Roux 2005) that the deployment of nodes (which determines the placement of deltas) of equal delay differences follows a hyperbola. Thus, the number of deltas in a certain bin is the number of transmitting nodes inside two hyperbolas placed in the edges of that bin. As the transmitting nodes are distributed randomly, the number of nodes is proportional to the area inside those hyperbolas.

## 2.7 Statistical signal processing

Direct manipulation of the CCF is a complex problem. To make it simpler in this research, the cross-correlation technique is reframed to a probability problem using the well-known occupancy problem which follows the binomial probability distribution from which a parameter is chosen to estimate the number of nodes and dimensionality of a network.

### 2.7.1 Occupancy problem

Occupancy problems deal with the pairings of objects and have a wide range of applications in different fields containing probabilistic and statistical properties. The basic occupancy problem is about placing  $m$  marbles into  $b$  bins (Feller 1968). If one threw some marbles randomly towards several bins, the bins would be randomly filled by the marbles, resulting in some bins being occupied by more than one marble, some by one while some may have none. In his thesis (Howlader 2009), Howlader reframes the framed slotted ALOHA protocol of the number of nodes' estimation in terms of this occupancy problem. He describes the reframing process as follows.

1. In FSA,  $N$  nodes transmit to  $F$  slots in a frame.
2. Some slots will get no packet; some will one and others more than one.

Thus, by defining the slots with only one packet as singleton slots, those with more than one packet collision slots and those with no packet empty slots, Howlader uses the classical occupancy problem to determine the probabilities of empty, singleton and collision slots. This helps him to determine the number of neighbouring nodes in a communication network.

### 2.7.2 Use of binomial distribution

The binomial distribution is the distribution of the counts of the number of successes in a certain number of trials. Another definition is the probability of obtaining the result of interest  $p$  (where  $p$  is a discrete integer-valued variable) times out of  $n$  independent observations if the overall probability of the result is  $M$ .

If an experiment satisfies the following characteristics, one can use the binomial distribution:

- the number of trials is fixed;
- each trial is independent;
- there exist only two possible outcomes for every trial: success or failure; and
- each trial has the same probability of success.

For example, a coin-tossing experiment might be binomially distributed if:

- one tosses the coin  $n$  (a fixed number) times;
- one decides on which side (heads or tails) it will land, i.e., only two possible outcomes: success or failure;
- one makes the coin ‘fair’, meaning that the probability of its landing on either a head or tail is 50%; and
- the result of a previous toss does not affect the present toss (i.e., trials are independent).

The binomial distribution has an enormous number of uses. One major application is in stochastic processes which have statistical properties and can be completely, or mostly, usefully reframed to a binomial process in order to resolve a problem in an easier manner. Also, it has applications in simply modelling binomial processes.

## **2.8 Coefficient of variation (CV)**

The CV is a probabilistic and statistical error tool. It is defined by the ratio of the standard deviation,  $\sigma$ , to the mean,  $\mu$ , of a probability distribution (Smith 1999), as:

$$CV = \frac{\sigma}{\mu}$$

The cross-correlation has significant statistical properties and CV may be used to obtain the error in estimation.

## **2.9 Conclusion**

Existing estimation methods relating to protocol design have significant problem for estimating the number of nodes in an underwater network. This is caused by a range of issues, including long propagation delays between nodes. In Chapter 3, the cross-correlation of random signals is investigated as an alternative tool. Reframing the cross-correlation problem as a probability problem provides a simple way of conducting this type of estimation.



# Chapter 3

## Estimation of the number of nodes in wireless communication networks

---

### 3.1 Introduction

The technique of cross-correlation is an essential statistical tool in various fields of interest. It has been used in communication networks to identify and localise nodes, and for angle of arrival (AOA) estimations of signals from the nodes in a WSN. Some researchers have used it for the detection of weak signals in the field of cardiology. In this chapter, the use of the cross-correlation function to estimate the number of signal sources (nodes in WCN) is described. The chapter begins with the formulation of the cross-correlation of random signals, which is the starting material and method for estimating the number of nodes in a network. In adhoc networks where a node needs to know the number of neighbours, cross-correlation is performed by a computer associated with the node. In other networks, cross-correlation is performed by a remote computer controlled by testing personnel. All the signals transmitted are received by the receiving node and recorded in the associated computer, in which the cross-correlation is performed. Transmission and reception of the signals are performed for a time frame which is called signal length throughout this thesis. The received signals are the delayed copy of the transmitted signals. The proposed method does not require any time synchronisation and thus the time stamp is not a performance factor. The signal length or the recording time is a major performance factor and is discussed with its selection in Chapter 3 and 5. The communication requirement that need to be satisfied is that the transmitters and the receivers need to be capable of transmitting and receiving signals for the specified recorded time without becoming overheated.

In this chapter, it is shown that the cross-correlation problem can be reframed as a probability problem from which it is possible to develop a theoretical formulation for

the estimation of the number of nodes, which can be verified by simulations. This estimation technique is analysed for two broad cases: Case 1 – equal received power (ERP); and Case 2 – equal transmitted power (ETP). In the first case, using a simple probe-requesting technique, all the powers of the signals received by the receiving nodes from the transmitting nodes are made equal. This can be achieved by sending probe requests from each receiving node to the transmitting nodes and the transmitting nodes transmit their responses with setting their transmit power inverse proportion to the received power from the original probing signal. Thus, the powers of the received signals are compensated for distance-dependent attenuations. On the other hand, in the ETP case, the transmitted powers from the nodes are equal but the received powers are different due to the distance-dependent attenuations for the signals to reach the receivers. It is shown that estimation parameter (from simulation) follows the theory in the ERP case, but in the ETP case, it deviates. Thus, it requires modification in theory either using proper statistical property (which is very complex as the formation of CCF in ETP case is not uniform) of the CCF, or by proper scaling (which is useful and easy to obtain). So, to avoid complexity, proper scaling is provided and analysed.

Though the theory is developed for an infinitely long signal, practically the signal length will be finite. So, the effect and proper selection of signal length is investigated. Some other factors such as fractional-samples delays, noise, and multipath propagation might affect the estimation performance, so their effects are investigated as well.

Before detailing the estimation process, it is necessary to point out some initial assumptions in order to clarify the experimental setup. These assumptions are listed in Table 3.1 and most are investigated later.

**Table 3.1 Initial assumptions on the parameters**

<b>Parameter</b>	<b>Initial assumption</b>	<b>Explanation and further investigation required to remove assumption</b>
Network dimension	3D spherical	The nodes are uniformly distributed inside a sphere in order to produce equal numbers of signals from all

		directions. This assumption is possible in the case of a 3D WCN (such as a 3D UWSN, 3D SWSN, 3D UGWSN, etc.). Because the other dimensions (1D and 2D) might be different, this assumption is analysed in the following chapter.
Propagation delays	Integer valued	All delay durations are assumed to be integer valued in the first instance. A simulation with real (fractional-sample) delays is investigated later in this chapter.
Signal length	Infinitely long	Initially, to ensure better performance, a very long (considered infinitely long) signal length is considered. Any possible significant effects of the signal length on estimation using the proposed signal processing technique are investigated later.
Channel property	Ideal	The channel is assumed ideal so that there is no background noise present in it. In practice, as there will be some background noise, the assumption might be realisable by simply using the sufficient signal strength with respect to the noise power. This effect is discussed later.
Receiver property	Ideal	The receivers are assumed to be ideal, i.e., there is no internal noise present in them. It is also possible to neglect any internal noise by using high-precision receivers and making the received signal sufficiently strong; this is discussed later.
Signal power	Equal received powers from all nodes	The signals received from different transmitted nodes are of equal power. This can be achieved by sending probe requests from the sensors with each node setting its transmitted power in accordance with the received power from the probe such that all received signals are of equal power. This probing technique requires extra care, and in the case of natural and/or uncontrolled nodes, it is impossible to achieve this assumption. So,



		the case of ETP is also analysed later in this chapter. In this case, the received power will be different due to the distance-dependent attenuations.
Multipath effect	No multipath	No multipath effect is considered. In the case of an electromagnetic wave, because of the high absorption in an underwater channel, this effect can be neglected. However, acoustic underwater communication will be affected by multipath; this is discussed in a separate section of this chapter.
Doppler effect	No Doppler shift	No Doppler effect, which might occur due to the movement of a network's nodes, is considered. In many WCNs, as the nodes of interest are deployed in fixed locations (e.g., in a WSN, the nodes are fixed in a region to monitor the observed area), there is no Doppler effect as signal taking a direct path. In the case of a movable network (e.g., swarms of AUVs or UUVs in which the nodes move around a region to monitor it), the Doppler shift can be neglected by using a high-speed wave (e.g., electromagnetic). Due to the Doppler effect, there will be a slight variation in the propagation wavelength and, thus, in propagation delay which can affect the placing of balls in the bins of the cross-correlation process and might lead to fractional-sample delays being created. However, the effect of fractional samples has no significant effect on estimation; this is discussed later in this chapter.
Transmitted Signal	White Gaussian	The white Gaussian nature of the signals ensures the delta function in the bins of CCF. Similar delta functions are possible from delta signal as well as from the signal which fulfils the Gaussian property. If the signals are non-Gaussian we will not get only the desired peaks, we will get some undesired peaks as well in the CCF and the investigations are left for

		<p>future work. If the nodes transmit Gaussian signal normally then the signals are the part of the normal transmission, otherwise they require transmitting signals specifically for the purpose of node estimation. The transmission time relates with the estimation error and is discussed with the error analysis in Chapter 5 of this thesis.</p>
--	--	---

### 3.2 Formulation of random signal cross-correlation

Consider two receiving nodes surrounded by  $N$  transmitting nodes in a 3D space, as shown in Figure 3.1 (a). Assume that the transmitting nodes are the sources of white Gaussian signals and are uniformly distributed over the volume of a large sphere, the centre of which lies halfway between the receiving nodes, because only a sphere provides equal amounts of signals from every direction. The propagation velocity is assumed to be constant which, in our case, is the sound velocity,  $S_p$ , in the medium. To make the distinction between the receiving and transmitting nodes easily understandable, we call them the *sensor/receiver* and *node*, respectively.

To formulate the random signal cross-correlation problem in this analysis, the two sensors,  $H_1$  and  $H_2$ , and a node,  $N_1$ , are taken at locations  $(x_1, y_1, z_1)$ ,  $(x_2, y_2, z_2)$  and  $(x_3, y_3, z_3)$ , respectively (using rectangular coordinate system), somewhere inside the sphere, as shown in Figure 3.1 (b). The distance between the sensors,  $d_{DBS}$  is then

$$d_{DBS} = \sqrt{(x_1 - x_2)^2 + (y_1 - y_2)^2 + (z_1 - z_2)^2} .$$

Consider that  $N_1$  emits a signal,  $S_1(t)$ , which is infinitely long. Then, the signals received by  $H_1$  and  $H_2$  are, respectively:

$$S_{r_{11}}(t) = \alpha_{11} S_1(t - \tau_{11}) \quad (3.1)$$

and

$$S_{n_2}(t) = \alpha_{12} S_1(t - \tau_{12}) \quad (3.2)$$

where,  $\alpha_{11}$  and  $\alpha_{12}$  are the respective attenuations due to the absorption and dispersion present in the medium,  $\tau_{11} = \frac{d_{11}}{S_p}$  and  $\tau_{12} = \frac{d_{12}}{S_p}$  the respective time delays for the signal to reach the sensors, and  $S_p$  is the speed of wave propagation.

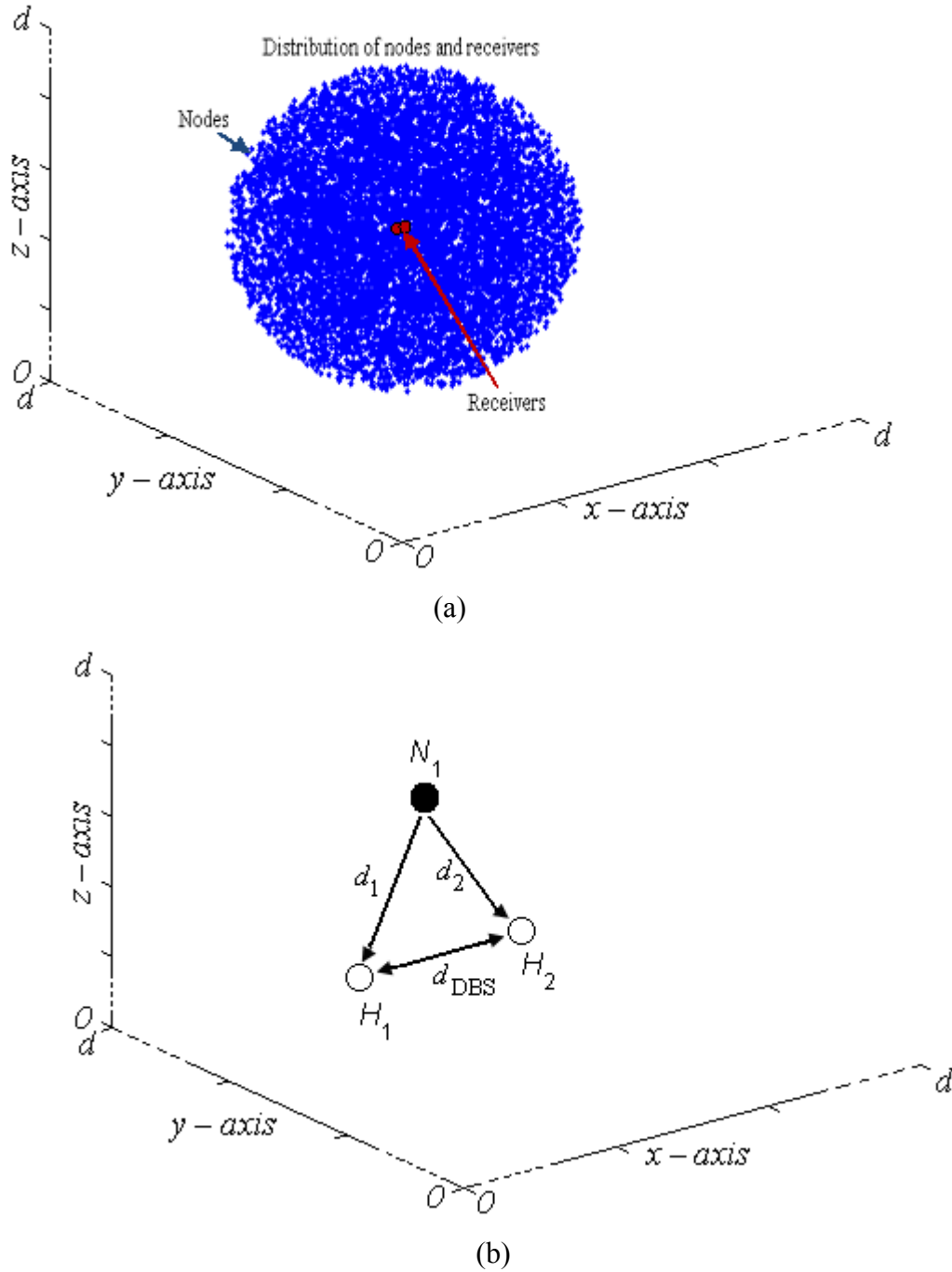


**Figure 3.1 Distributions of underwater network nodes in 3D space:**

**(a)  $N$  nodes; and (b) only one node**

Assuming  $\tau$  is the time shift in the cross-correlation, and then the CCF is:

$$C_1(\tau) = \int_{-\infty}^{+\infty} S_{r_{11}}(t) S_{r_{12}}(t - \tau) d\tau, \quad (3.3)$$

which takes the form of a delta function as it is a cross-correlation of two white Gaussian signals where one signal essentially is a delayed copy of the other..

To find the CCF for  $N$  nodes, we have to take the total signal received by the sensors from the nodes which involves collecting all the signals from the nodes and summing them. Now, the received signals from the second node are:

$$S_{r_{21}}(t) = \alpha_{21} S_2(t - \tau_{21}) \quad (3.4)$$

and

$$S_{r_{22}}(t) = \alpha_{22} S_2(t - \tau_{22}) \quad (3.5)$$

Then, for the third node:

$$S_{r_{31}}(t) = \alpha_{31} S_3(t - \tau_{31}) \quad (3.6)$$

and

$$S_{r_{32}}(t) = \alpha_{32} S_3(t - \tau_{32}) \quad (3.7)$$

Thus, for the  $N^{th}$  node, they are:

$$S_{r_{N1}}(t) = \alpha_{N1} S_N(t - \tau_{N1}) \quad (3.8)$$

and

$$S_{r_{N2}}(t) = \alpha_{N2} S_N(t - \tau_{N2}) \quad (3.9)$$

Summing (3.1), (3.4), (3.6), and (3.8), the total signal at sensor  $H_1$  is:

$$\begin{aligned} S_{r_{11}}(t) + S_{r_{21}}(t) + S_{r_{31}}(t) + \dots + S_{r_{N1}}(t) \\ = \alpha_{11} S_1(t - \tau_{11}) + \alpha_{21} S_2(t - \tau_{21}) + \alpha_{31} S_3(t - \tau_{31}) + \dots + \alpha_{N1} S_N(t - \tau_{N1}) \\ = \sum_{j=1}^N \alpha_{j1} S_j(t - \tau_{j1}) \end{aligned}$$

Denoting the total signal at sensor  $H_1$  by  $S_{r_{11}}(t)$  gives:

$$S_{r_{i1}}(t) = \sum_{j=1}^N \alpha_{j1} S_j(t - \tau_{j1}) \quad (3.10)$$

Similarly, summing (3.2), (3.5), (3.7), and (3.9), the total signal at sensor  $H_2$  is:

$$\begin{aligned} S_{r_{i2}}(t) + S_{r_{22}}(t) + S_{r_{32}}(t) + \dots + S_{r_{N2}}(t) \\ = \alpha_{12} S_1(t - \tau_{12}) + \alpha_{22} S_2(t - \tau_{22}) + \alpha_{32} S_3(t - \tau_{32}) + \dots + \alpha_{N2} S_N(t - \tau_{N2}) \\ = \sum_{j=1}^N \alpha_{j2} S_j(t - \tau_{j2}) \end{aligned}$$

Denoting the total signal at sensor  $H_2$  by  $S_{r_{i2}}(t)$  gives:

$$S_{r_{i2}}(t) = \sum_{j=1}^N \alpha_{j2} S_j(t - \tau_{j2}) \quad (3.11)$$

Thus, the final CCF between the signals at the sensors is:

$$\begin{aligned} C(\tau) &= \int_{-\infty}^{+\infty} S_{r_{i1}}(t) S_{r_{i2}}(t - \tau) d\tau \\ &= \int_{-\infty}^{+\infty} \sum_{j=1}^N \alpha_{j1} S_j(t - \tau_{j1}) \sum_{j=1}^N \alpha_{j2} S_j(t - \tau_{j2} - \tau) d\tau \end{aligned} \quad (3.12)$$

which takes the form of a series of delta functions as it is a cross-correlation of two signals which are the summations of several white Gaussian signals.

### 3.3 CCF for infinitely long signal

It is already discussed in Sections 2.5 and 3.2 that if a source emits an infinitely long unity strength Gaussian signal, which is recorded at two sensors with the corresponding time delays and attenuations, the cross-correlation function of these two signals can be expressed by a delta function, whose amplitude depends on the attenuations and position will be the delay difference of the signals from the centre of the CCF.

Thus, the CCF for such a source is

$$C_1(\tau) = \alpha_{11} \alpha_{12} \delta \left( \tau - \left[ \frac{d_{11} - d_{12}}{s_p} \right] \right) \quad (3.13)$$

In the proposed ERP case, the strength of the signal will be such that it overcomes the corresponding attenuations. So, there will be no attenuation term in the CCF expression (3.13) Thus the CCF in the ERP case for a source will be

$$C_1(\tau) = \delta \left( \tau - \left[ \frac{d_{11} - d_{12}}{s_p} \right] \right)$$

Similarly for 2<sup>nd</sup>, 3<sup>rd</sup>, ...,  $N^{\text{th}}$  node is

$$C_2(\tau) = \delta \left( \tau - \left[ \frac{d_{21} - d_{22}}{s_p} \right] \right)$$

.

.

.

$$C_N(\tau) = \delta \left( \tau - \left[ \frac{d_{N1} - d_{N2}}{s_p} \right] \right)$$

Thus the CCF will be for  $N$  number of nodes

$$\begin{aligned} C(\tau) &= C_1(\tau) + C_2(\tau) + \dots + C_N(\tau) \\ &= \delta \left( \tau - \left[ \frac{d_{11} - d_{12}}{s_p} \right] \right) + \delta \left( \tau - \left[ \frac{d_{21} - d_{22}}{s_p} \right] \right) + \dots + \delta \left( \tau - \left[ \frac{d_{N1} - d_{N2}}{s_p} \right] \right) \end{aligned} \quad (3.14)$$

It can be seen from the above expression that the CCF for  $N$  source is summation of  $N$  numbers of deltas with their corresponding positions which are determined by the delay differences of the signals in the sensors.

So the expression (3.14) can be further expressed as

$$C(\tau) = \sum_{j=1}^N \delta \left( \tau - \left[ \frac{d_{j1} - d_{j2}}{s_p} \right] \right) \quad (3.15)$$

It is intuitive that if  $N$  is larger than the number of bins,  $b$ , which is usually the case, the bins are occupied by more than one delta due to the same delay differences. This increases the amplitude of the deltas in the bins, and thus the CCF is expressed in terms of bins as

$$C(\tau) = \sum_{i=1}^b P_i \delta_i \quad (3.16)$$

where,  $P_i$  is the amplitude or peak of the dirac delta,  $\delta_i$  in the  $i^{\text{th}}$  bin.

The above analytical expression is verified by simulation in the following Figure 3.2. Here we use 32 nodes and 19 bins. The nodes are the sources of equal unity power signal. It is shown that some bins are occupied by only one, some of them by more than one, and rest of them are empty due to the delay differences in the cross-correlation process. The results follow the expression (3.16) where the  $P_i$  values are as follows.

$P_1 = P_{19} = 4, P_4 = P_{10} = P_{13} = 3, \dots$  and so on.

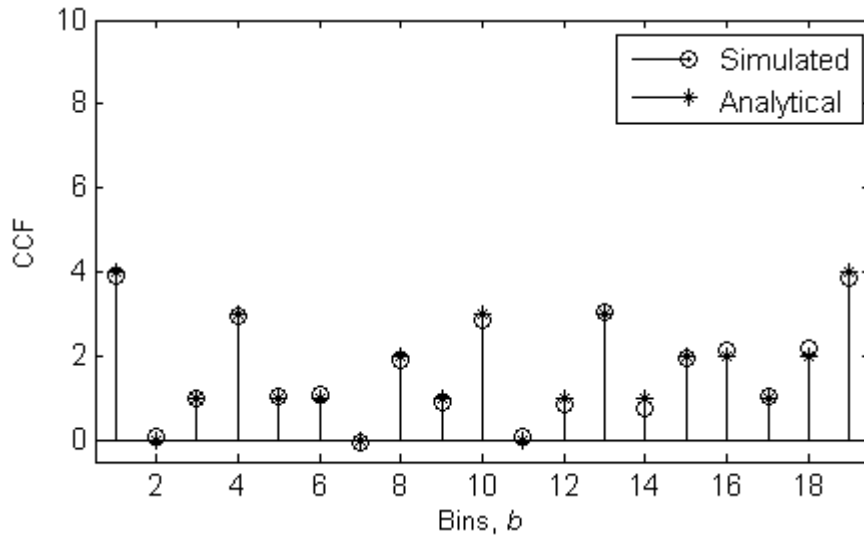


**Figure 3.2 CCF in ERP case:  $N=32$ , and  $b=19$**

In the ETP case, the transmitted signal strengths will be same for all sources and which will have to be such that all signals can overcome the attenuations to reach the sensors properly. Thus to get appropriate peaks of the CCF bins signal power, a factor will have to be multiplied in right hand side of (3.13) which is selected from the largest communication distance in the network as

$$\chi = d_{\max}^k \quad (3.17)$$

Thus the expression of CCF can be represented from (3.13) and (3.17) for a source as

$$C_1(\tau) = (d_{\max}^k) \alpha_{11} \alpha_{12} \delta \left( \tau - \left[ \frac{d_{11} - d_{12}}{s_p} \right] \right)$$

Similarly for 2<sup>nd</sup>, 3<sup>rd</sup>, ...,  $N^{\text{th}}$  node is

$$\begin{aligned} C_2(\tau) &= \left(d_{\max}^k\right) \alpha_{21} \alpha_{22} \delta\left(\tau - \left[\frac{d_{21} - d_{22}}{s_p}\right]\right) \\ &\vdots \\ C_N(\tau) &= \left(d_{\max}^k\right) \alpha_{N1} \alpha_{N2} \delta\left(\tau - \left[\frac{d_{N1} - d_{N2}}{s_p}\right]\right) \end{aligned}$$

Thus the CCF will be for  $N$  number of nodes

$$\begin{aligned} C(\tau) &= C_1(\tau) + C_2(\tau) + \dots + C_N(\tau) \\ &= \left(d_{\max}^k\right) \alpha_{11} \alpha_{12} \delta\left(\tau - \left[\frac{d_{11} - d_{12}}{s_p}\right]\right) + \left(d_{\max}^k\right) \alpha_{21} \alpha_{22} \delta\left(\tau - \left[\frac{d_{21} - d_{22}}{s_p}\right]\right) + \dots \\ &\quad + \left(d_{\max}^k\right) \alpha_{N1} \alpha_{N2} \delta\left(\tau - \left[\frac{d_{N1} - d_{N2}}{s_p}\right]\right) \end{aligned} \quad (3.18)$$

It can be seen from the above expression that the CCF for  $N$  source is summation of  $N$  numbers of deltas as the ERP case but the amplitude will be different by the distance dependent attenuations.

So the expression (3.18) can be further expressed as

$$C(\tau) = \sum_{j=1}^N P_j \delta\left(\tau - \left[\frac{d_{j1} - d_{j2}}{s_p}\right]\right) \quad (3.19)$$

where,  $P_j = \left(d_{\max}^k\right) \alpha_{j1} \alpha_{j2}$  is the amplitude of the delta due to  $j^{\text{th}}$  node.

It is intuitive that if  $N$  is larger than the number of bins,  $b$ , which is usually the case, the bins are occupied by more than one delta due to the same delay differences. This increases the amplitude of the deltas in the bins, and thus again the CCF is expressed in terms of bins as

$$C(\tau) = \sum_{i=1}^b P_i \delta_i \quad (3.20)$$

where,  $P_i$  is the amplitude of the dirac delta,  $\delta_i$  in the  $i^{\text{th}}$  bin.



The above analytical expression is verified by simulation in the following Figure 3.3.

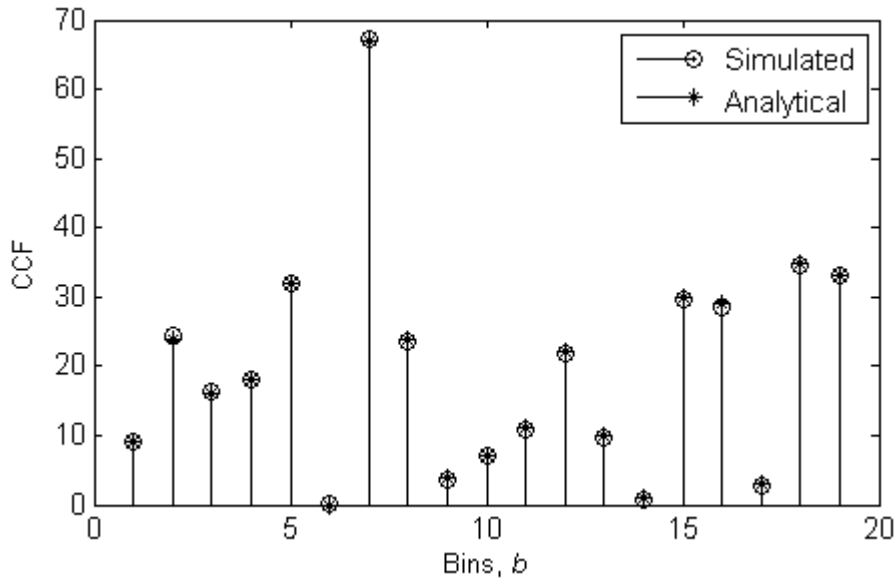


**Figure 3.3 CCF in ETP case;  $N=32$ , and  $b=19$**

Thus (3.16) is the generalized expression for any CCF in this thesis. In some cases (where the signal length is very small, noise is severe etc.), obtaining the peak of the CCF is difficult from the above process and might be obtained from the moving average technique of cross-correlation.

The CCF, using the moving average technique of cross-correlation can be represented generally by the following expression (Hanson 2008a; Hanson 2008b).

$$C(\tau) = \frac{1}{N_s - \tau} \sum_{i=1}^{N_s - \tau} x_i y_{i+\tau} - \left( \frac{1}{N_s} \sum_{i=1}^{N_s} x_i \right) \left( \frac{1}{N_s} \sum_{i=1}^{N_s} y_i \right)$$

where  $N_s$  is the signal length in number of samples,  $\tau$  the time delay of cross-correlation,  $x_i$  and  $y_i$  are  $i^{\text{th}}$  samples of the two sensors' signals.

As we are using zero mean Gaussian signal so the product of their means is zero. So, the CCF will be reduced to

$$C(\tau) = \frac{1}{N_s - \tau} \sum_{i=1}^{N_s - \tau} x_i y_{i+\tau}$$

This gives the peaks for the desired bins as follows:

$$\frac{1}{N_s + \tau} \sum_{i=1}^{N_s + \tau} x_i y_{i-\tau}, \dots, \frac{1}{N_s + 1} \sum_{i=1}^{N_s + 1} x_i y_{i-1}, \frac{1}{N_s - 0} \sum_{i=1}^{N_s - 0} x_i y_{i+0}, \frac{1}{N_s - 1} \sum_{i=1}^{N_s - 1} x_i y_{i+1}, \dots, \frac{1}{N_s - \tau} \sum_{i=1}^{N_s - \tau} x_i y_{i+\tau}$$

where the peaks are the strengths of the deltas of (3.16), which are

$$\begin{aligned} P_1 &= \frac{1}{N_s + \tau} \sum_{i=1}^{N_s + \tau} x_i y_{i-\tau}, \\ P_2 &= \frac{1}{N_s + (\tau - 1)} \sum_{i=1}^{N_s + (\tau - 1)} x_i y_{i-(\tau - 1)}, \\ &\vdots \\ P_b &= \frac{1}{N_s - \tau} \sum_{i=1}^{N_s - \tau} x_i y_{i+\tau} \end{aligned}$$

Putting these values in (3.16), we get the desired CCF which is called here the theoretical CCF.

### 3.4 Mean, $\mu$ and standard deviation, $\sigma$ , of CCF

The ensemble average of the signal cross-correlation is expressed analytically in (Roux 2005) as

$$\langle C(t) \rangle = Q_T T_r \nu \int_{-\infty}^{+\infty} d\vec{r}_s \frac{1}{|\vec{r}_b - \vec{r}_s| |\vec{r}_a - \vec{r}_s|} \times \delta \left( t + \frac{|\vec{r}_a - \vec{r}_s|}{S_p} - \frac{|\vec{r}_b - \vec{r}_s|}{S_p} \right). \quad (3.21)$$

where  $Q_T$  represents the acoustic power of the received signals from the nodes taken to be constant over time and space, and  $\nu$  the creation rate of the random nodes whose unit is unit time per unit volume,  $T_r$  total recording time,  $\vec{r}_s$  path length of node  $s$  from the origin,  $\vec{r}_a$  path length of first receiver from the origin, and  $\vec{r}_b$  the path length of second receiver from the origin.

Again, the variance of the CCF (i.e., the square of the mean level of the fluctuations) is defined in (Sabra 2005c) as

$$Var(C(t)) = \langle C^2(t) \rangle - \langle C(t) \rangle^2 \quad (3.22)$$

where the value  $\langle C_{1,2}(t) \rangle^2$  and  $\langle C^2(t) \rangle$  are defined, respectively, in (Sabra 2005c) as

$$\begin{aligned} \langle C(t) \rangle^2 = Q_T^2 v^2 & \left( \int_{-T_r/2}^{+T_r/2} dt \int_{-\infty}^{+\infty} d\vec{r}_1 \int_{-\infty}^{+t} d\tau_1 G(\vec{r}_1, \vec{r}_a; t - \tau_1) \times G(\vec{r}_1, \vec{r}_b; \tau + t - \tau_1) \right) \\ & \times \left( \int_{-T_r/2}^{+T_r/2} d\tilde{t} \int_{-\infty}^{+\infty} d\vec{r}_3 \int_{-\infty}^{+\tilde{t}} d\tau_3 G(\vec{r}_3, \vec{r}_a; t - \tau_3) \times G(\vec{r}_3, \vec{r}_b; \tau + \tilde{t} - \tau_3) \right) \end{aligned} \quad (3.23)$$

and

$$\begin{aligned} \langle C^2(t) \rangle = Q_T v^2 & \left( \int_{-T_r/2}^{+T_r/2} dt \int_{-\infty}^{+\infty} d\vec{r}_1 \int_{-\infty}^{+t} d\tau_1 G(\vec{r}_1, \vec{r}_a; t - \tau_1) \times G(\vec{r}_1, \vec{r}_b; \tau + t - \tau_1) \right) \\ & \left( \int_{-T_r/2}^{+T_r/2} d\tilde{t} \int_{-\infty}^{+\infty} d\vec{r}_3 \int_{-\infty}^{+\tilde{t}} d\tau_3 G(\vec{r}_3, \vec{r}_a; t - \tau_3) \times G(\vec{r}_3, \vec{r}_b; \tau + \tilde{t} - \tau_3) \right) \\ & + Q_T v^2 \int_{-T_r/2}^{+T_r/2} dt \int_{-T_r/2}^{+T_r/2} d\tilde{t} \left( \int_{-\infty}^{+\infty} d\vec{r}_1 \int_{-\infty}^{+t} d\tau_1 G(\vec{r}_1, \vec{r}_a; t - \tau_1) \times G(\vec{r}_1, \vec{r}_a; \tilde{t} - \tau_1) \right) \\ & \left( \int_{-\infty}^{+\infty} d\vec{r}_1 \int_{-\infty}^{+t} d\tau_1 G(\vec{r}_1, \vec{r}_a; t - \tau_1) \times G(\vec{r}_1, \vec{r}_a; \tilde{t} - \tau_1) \right) \\ & + Q_T v^2 \int_{-T_r/2}^{+T_r/2} dt \int_{-T_r/2}^{+T_r/2} d\tilde{t} \left( \int_{-\infty}^{+\infty} d\vec{r}_1 \int_{-\infty}^{+t} d\tau_1 G(\vec{r}_1, \vec{r}_a; t - \tau_1) \times G(\vec{r}_1, \vec{r}_b; \tau + \tilde{t} - \tau_1) \right) \\ & \left( \int_{-\infty}^{+\infty} d\vec{r}_2 \int_{-\infty}^{+\tilde{t}} d\tau_2 G(\vec{r}_2, \vec{r}_a; \tilde{t} - \tau_2) \times G(\vec{r}_2, \vec{r}_b; \tau + t - \tau_2) \right) \end{aligned} \quad (3.24)$$

where  $G(\cdot)$  is the Green's function, and the other parameters indicate their usual meanings.

We can then obtain the standard deviation,  $\sigma$ , of the CCF which is the square root of the variance by:

$$\sigma = \sqrt{\text{Var}(C(t))} = \sqrt{\langle C^2(t) \rangle - \langle C(t) \rangle^2} \quad (3.25)$$

As it is quite difficult to analyse the random signal cross-correlation problem to estimate the standard deviation and mean in the above way, the problem can be reframed as a probability problem which makes the analysis much simpler. This process is discussed in the following section.

### 3.5 Reframing cross-correlation as a probability problem

It has been shown in the previous section that the cross-correlation of random signals takes the form of a delta function and occupies the space between the sensors where

the space is divided by several samples, as shown in Figure 3.4. Thus, for every node, after cross-correlation we obtain a delta function which occupies any position in the sample space between the sensors. We can now consider each delta function as a ball and the samples between the sensors as bins into which the balls may fall. So, we can simply model the random signal cross-correlation problem as a probability problem based on the well-known occupancy problem, i.e., the problem of placing  $B$  balls in  $b$  bins.

To demonstrate the problem of random signal cross-correlation as a probability problem, consider an experiment of the repetitive type in which only the occurrence or non-occurrence of an event is recorded. Suppose the probability that the event occurs when the experiment is performed is  $p$ . Let  $q = 1 - p$  denote the probability that it fails to occur. If the event occurs in a given trial of the experiment, it is called a success, otherwise a failure. Let  $n$  independent trials be conducted and denote the number of successes obtained in the  $n$  trials by  $X$ . In our case, the number of trials,  $n$ , is equivalent to the number of nodes,  $N$ , and the probability of success,  $p$ , is equivalent to  $1/b$ , where  $b$  is the number of bins.

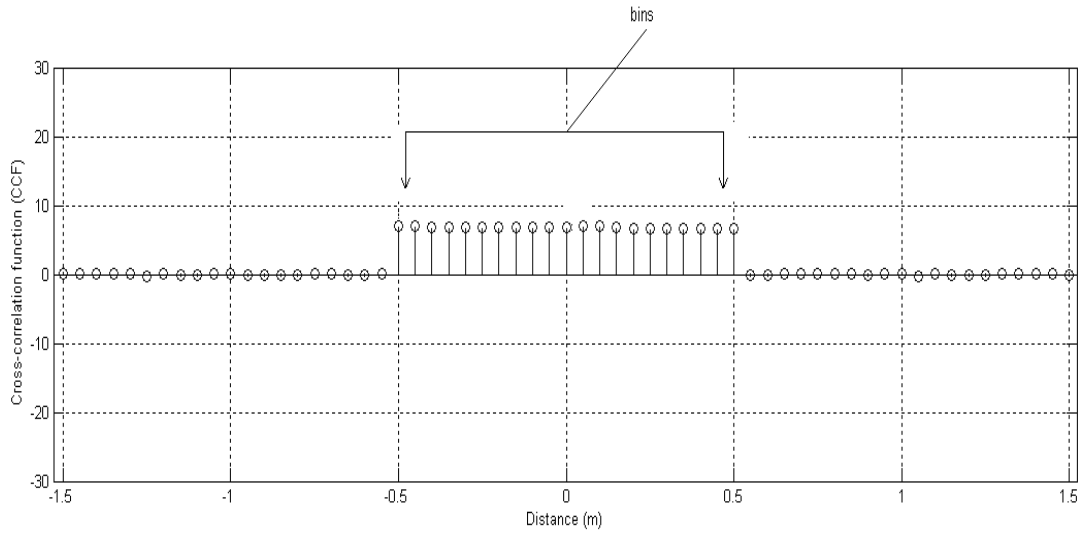


**Figure 3.4 Bins,  $b$ , in cross-correlation process**

In this case, we need to consider the discrete probability distribution because we use the sampled signal in the cross-correlation process. The binomial distribution is also appropriate because the experiment fulfils the conditions of binomial probabilities.

### 3.6 Some simulated results and selection of estimation tool

By reframing the cross-correlation problem as a probability problem, it is easy to obtain the proper estimation tool, as shown by some simulated results in Matlab programming environment presented in Figures 3.5, 3.6 and 3.7 and Tables 3.2, 3.3 and 3.4. Figure 3.5 and Table 3.2 show the means, Figure 3.6 and Table 3.3 the standard deviations, and Figure 3.7 and Table 3.4 the ratios of the standard deviation to the mean of the CCF. All figures and tables are for three distinct simulation setups: (a) unity signal strength; (b) double signal strength; and (c) half signal strength.

It can be seen from Figures 3.5 and 3.6 and Tables 3.2 and 3.3 that the means and standard deviations increase by the same factor with increases in the signal strength and decrease by the same factor with decreases in the signal strength. For that reason, their ratios are constant, as shown in Figure 3.7 and Table 3.4.

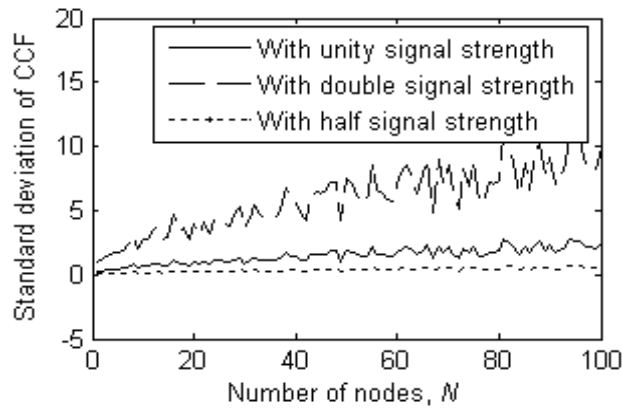


**Figure 3.5 Standard deviations of CCF versus  $N$  with: unity signal strength; signal strength doubled; and signal strength halved.**

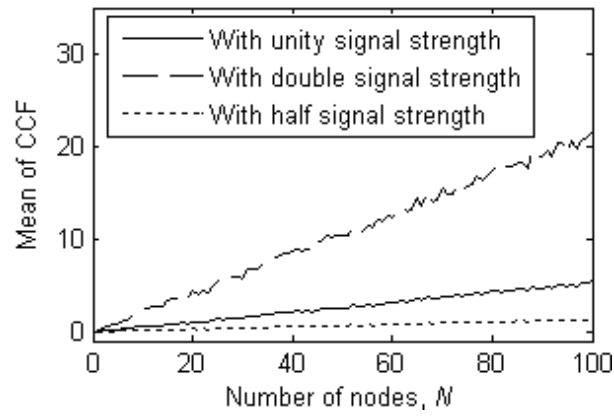


**Figure 3.6 Means of CCF versus  $N$  with: unity signal strength; signal strength doubled; and signal strength halved.**

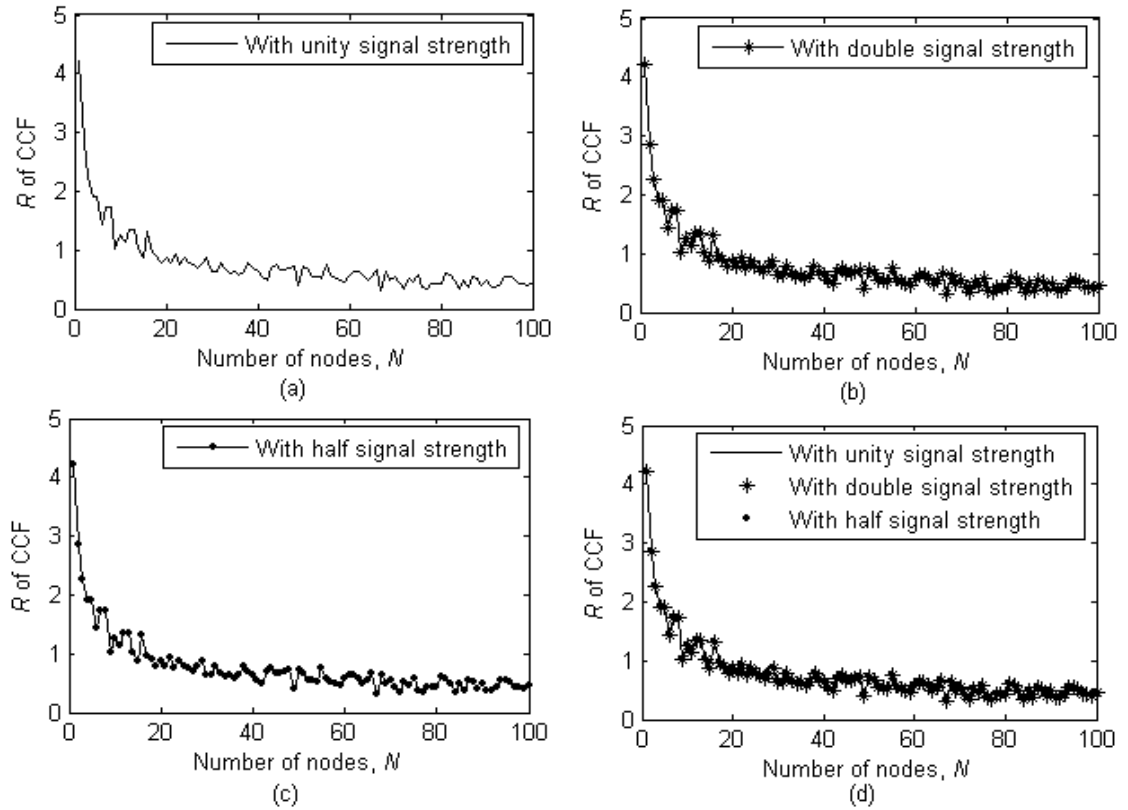


**Figure 3.7 Ratios of standard deviation to mean,  $R$ , of CCF versus  $N$  with: (a) unity signal strength; (b) signal strength doubled; (c) signal strength halved; and (d) their comparison.**

**Table 3.2 Standard deviations of CCF for different numbers of nodes  
with three distinct signal powers**

<b>Number of nodes, <math>N</math></b>	<b>Standard deviation of CCF with unity signal strength</b>	<b>Standard deviation of CCF with double signal strength</b>	<b>Standard deviation of CCF with half signal strength</b>
1	0.2299	0.9196	0.0575
10	0.6961	2.7844	0.174
20	0.9763	3.9052	0.2441
30	0.9025	3.61	0.2256
40	1.3942	5.5768	0.3486
50	1.8568	7.4272	0.4642
60	1.7564	7.0256	0.4391
70	2.1391	8.5564	0.5348
80	1.8327	7.3308	0.4582
90	2.2864	9.1456	0.5716
100	2.4605	9.842	0.6151

**Table 3.3 Means of CCF for different numbers of nodes  
with three distinct signal powers**

<b>Number of nodes, <math>N</math></b>	<b>Mean of CCF with unity signal strength</b>	<b>Mean of CCF with double signal strength</b>	<b>Mean of CCF with half signal strength</b>
1	0.0546	0.2185	0.0137
10	0.5544	2.2177	0.1386
20	1.1189	4.4758	0.2797
30	1.4474	5.7895	0.3618
40	2.1668	8.6674	0.5417
50	2.5841	10.3364	0.646
60	3.0811	12.3242	0.7703
70	3.8854	15.5415	0.9713
80	4.3332	17.3326	1.0833
90	4.7348	18.9394	1.1837
100	5.4279	21.7116	1.357

**Table 3.4 Ratios of standard deviation to mean,  $R$ , of CCF for different numbers of nodes with three distinct signal powers**

Number of nodes, $N$	$R$ of CCF with unity signal strength	$R$ of CCF with double signal strength	$R$ of CCF with half signal strength
1	4.2082	4.2082	4.2082
10	1.2555	1.2555	1.2555
20	0.8725	0.8725	0.8725
30	0.6235	0.6235	0.6235
40	0.6434	0.6434	0.6434
50	0.7185	0.7185	0.7185
60	0.5701	0.5701	0.5701
70	0.5506	0.5506	0.5506
80	0.4229	0.4229	0.4229
90	0.4829	0.4829	0.4829
100	0.4533	0.4533	0.4533

It is also clear from the results that, as the mean and standard deviation of the CCF and its ratio are all related to the number of nodes,  $N$ , it is possible to use any of them to estimate  $N$ . However, as the mean and standard deviation are also dependent on the signal strength, we can only use them as the estimation tool if the exact signal strengths are known, which is not usual. On the contrary, as the ratio,  $R$ , is not dependent on the signal strength, we choose it as the estimation tool in this thesis as it requires no prior knowledge of the signal strengths from the nodes. Thus, having obtained the estimation tool, the estimation process is discussed in the following section.

### **3.7 Estimation process - equal received power (ERP) case**

The basic approach for estimation using the cross-correlation of the number of nodes is discussed in this section. Formation of the CCF from the mixture of signals in two spatially separated sensors within a number of nodes has been explained in the previous section. It has also been shown that the standard deviation and mean of the CCF and its ratio are related to the number of nodes from which the signals originate. The ratio,  $R$ , is independent of the signals' power, is chosen as the tool for estimating the number of nodes. The following subsections discuss the process. Firstly, the



analytical relationship between  $N$  and  $R$  is established and then it is verified by simulation.

### 3.7.1 Theoretical estimation

The cross-correlation problem has been reframed into a probability problem in Section 3.5 where it is shown that it follows the binomial probability distribution in which the parameters are the number of nodes,  $N$ , and the inverse of the number of bins,  $b$ .

The expected value of the first moment (the mean) of the CCF is:

$$\begin{aligned} E(X) &= \text{mean}, \mu = \langle C(\tau) \rangle = np \\ &= N \div b \end{aligned} \quad (3.26)$$

where  $b$  is twice the number of samples between the sensors (NSBS),  $m$  minus one, as we cross-correlate two vectors of length  $m \times 1$ ; and the second moment is:

$$\begin{aligned} E(X^2) &= \text{second moment} = \langle C^2(\tau) \rangle \\ &= (np)^2 + npq \end{aligned} \quad (3.27)$$

From (3.26) and (3.27), we can obtain the variance:

$$\begin{aligned} \sigma^2 &= E(X^2) - E(X)^2 = npq \\ &= N \times (1/b) \times (1 - 1/b) \end{aligned} \quad (3.28)$$

Then, the standard deviation is:

$$\begin{aligned} \sigma &= \sqrt{E(X^2) - E(X)^2} \\ &= \sqrt{N \times (1/b) \times (1 - 1/b)} \end{aligned} \quad (3.29)$$

Thus, the ratio of the standard deviation to the mean,  $R$ , is:

$$R = \sigma \div \mu = \sqrt{\frac{q}{np}} = \sqrt{\frac{(1 - 1/b)}{N \times (1/b)}} = \sqrt{\frac{(b-1)}{N}} \quad (3.30)$$

This is the relationship between the number of nodes,  $N$ , and the ratio of the standard deviation to the mean,  $R$ , of the CCF. Since we know  $b$  and can measure  $\sigma$  and  $\mu$  (and, therefore, determine  $R$ ) from the CCF, we can readily determine the number of

nodes,  $N$ . Figure 3.8 shows the theoretical results derived from (3.30) for different  $b$  (Figure 3.8 (a) for 19, Figure 3.8 (b) for 99 and Figure 3.8 (c) for 179 bins).

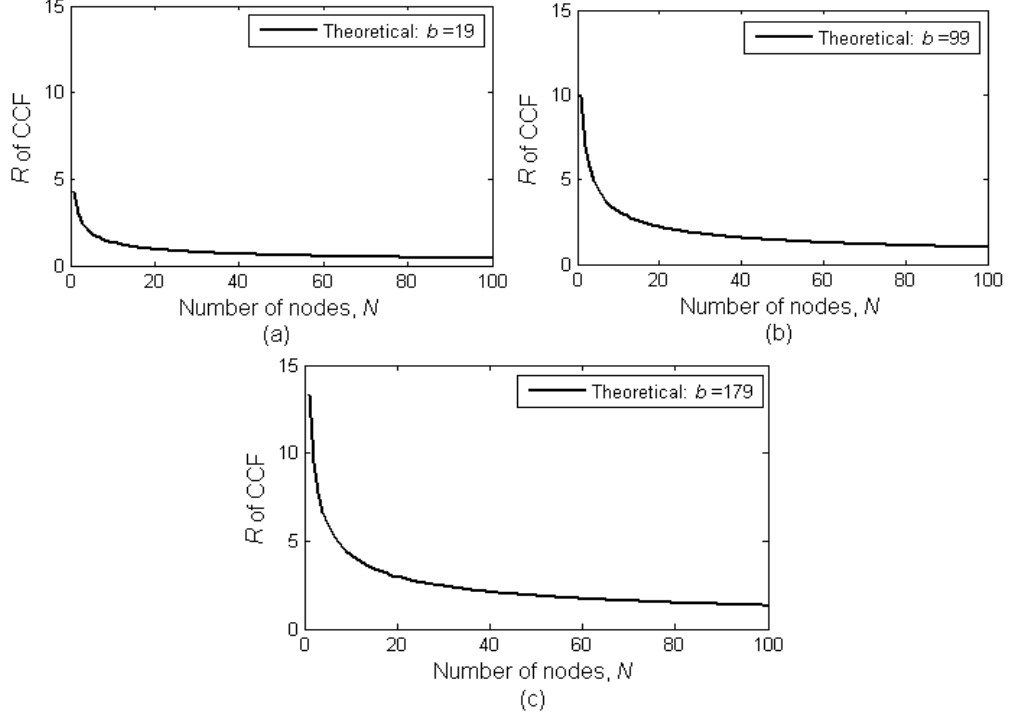


**Figure 3.8 Theoretical  $R$  versus  $N$ : for (a)  $b = 19$ ; (b)  $b = 99$ ; and (c)  $b = 179$**

It is clear from (3.30) that the ratio,  $R$ , is also dependent on  $b$ . Recalling (3.30),

$R = \sqrt{\frac{b-1}{N}}$  and, assuming  $b \gg 1$ , i.e.,  $b-1 \approx b$ :

$$R = \sqrt{\frac{b}{N}} \quad (3.31)$$

Figure 3.9 shows the original and approximated values of  $R$  with respect to  $b$ , demonstrating that using the approximations is sufficient for estimating the number of nodes.

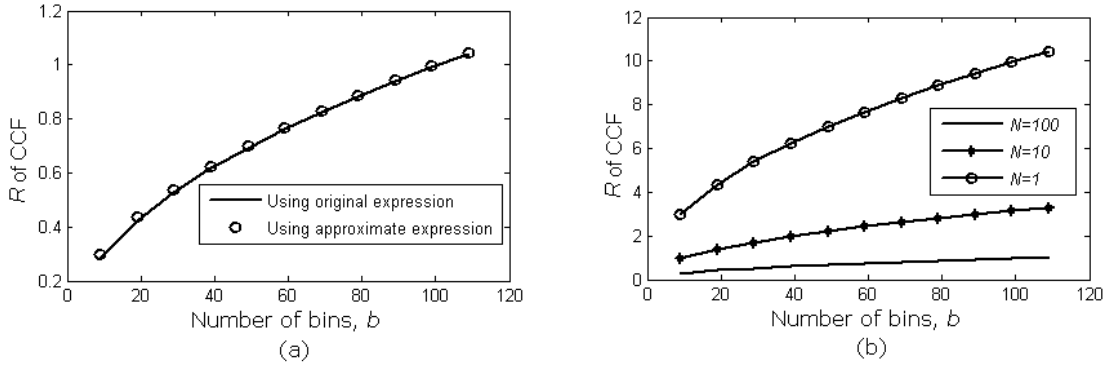


**Figure 3.9 Theoretical results for  $R$  versus  $b$ : (a) original and approximated,  $N = 100$ ; and (b) approximated,  $N = 1, 10$  and  $100$**

### 3.7.2 Estimation from simulation

As discussed in Section 3.2, after cross-correlating signals received at two sensors from a number of random Gaussian signal sources, the CCF, which is a rectangular pulse over the space between the sensors, can be obtained. Then, it is easy to estimate the mean and standard deviation of this CCF and, therefore, the ratio,  $R$ , as the sampling rate and  $d_{\text{DBS}}$  are known. In the particular case in which the sampling rate, speed of propagation and  $d_{\text{DBS}}$  are fixed, (3.30) tells us that the ratio,  $R$ , is inversely proportional to the square root of the number of nodes,  $N$ . Thus, (3.30) becomes:

$$R \propto \frac{1}{\sqrt{N}}$$

or,

$$R = \frac{c}{\sqrt{N}} \quad (3.32)$$

where  $c(=\sqrt{b-1})$  is a known constant. Thus, from the simulation, we can readily estimate the number of nodes by knowing only the ratio of the standard deviation to the mean of the CCF.

### 3.7.2.1 Verification of theoretical results

This subsection discusses the estimation setup and simulation parameters used, and verification of the theoretical results by those from the simulations. A similar setup to that discussed in the previous section is employed to perform the simulations, i.e., two spatially separated sensors are placed somewhere in the middle of a sphere inside a cube such that the diameter of the sphere is equal to the dimension of the cube, and the sphere is filled with a number of uniformly distributed nodes. The signals (responses to probe requests from the sensors or autonomous) emitted from the nodes are collected by the sensors. By cross-correlating these two signals at the sensors, the CCF is obtained. Using this CCF, the estimation tool, i.e., the ratio of the standard deviation to the mean of the CCF, is obtained.

The following parameters are used in the simulations.

- Dimension of the cube, 2000 m, for simplicity of calculation; however, it does not matter what the dimension of the cube is within the direct communication range. The maximum distance between the two nodes will be 2000 m as the nodes are uniformly distributed within a 3D sphere inside the cube.
- Exact number of transmitting nodes taken are,  $N = 1, 2, 3, \dots, 100$ , to reduce the simulation time, however, the estimation process is equally suitable for any  $N$ .
- Signal length,  $N_S = 10^6$  samples, to approximate infinitely long signals. The effect of signal length on the estimation process is investigated later in this section. The range of the signal length is selected in order to perform useful estimations.
- Sampling rate,  $S_R = 30$  kSa/s; as underwater acoustic communications currently operate within the bandwidth (BW) of 1-15 kHz, we arbitrarily choose this value without violating the sampling theorem. The effect of sampling rate on the estimation process is discussed later in this chapter.
- Speed of propagation,  $S_P = 1500$  m/s; this is the propagation speed of a sound wave as we use the acoustic signal in an UAWSN. Although this might vary

due to the channel's property and the Doppler effect, any effect of a variation is negligible in the estimation process, as discussed earlier.

- Distance between sensors,  $d_{\text{DBS}} = 0.5$  m; this can be varied. In this chapter, it is shown that the estimation performance depends on  $b$ , a function of  $d_{\text{DBS}}$  and  $S_{\text{R}}$ , thus they can vary oppositely to have a certain  $b$ .
- Absorption coefficient,  $a = 1$  and dispersion factor,  $k = 0$ ; but, as we receive the signals with equal power from the appropriate probe request, the estimation process is not affected by path loss i.e. the estimation is independent of  $k$ .

Figure 3.10 shows the simulation results in normal (Figure 3.10 (a)) and log-log (Figure 3.10 (b)) scales. Figure 3.10 (b) shows that the log-log plot of the simulated result can be approximated by a straight line whose slope can be derived as

$$s_1 = \frac{\log\left(\frac{c}{d}\right)}{\log\left(\frac{b}{a}\right)} \approx -\frac{1}{2}$$

So, the simulated ratio,  $R$ , is:

$$\begin{aligned} \log_{10}(R) &= -\frac{1}{2} \log_{10}(N) + c_1 \\ &= \log_{10}(N \times c_{11})^{-\frac{1}{2}} \end{aligned}$$

Thus,

$$R = c_{12} \times N^{-\frac{1}{2}}$$

i.e.,

$$R \propto \frac{1}{\sqrt{N}} \quad (3.33)$$

where  $c_1$ ,  $c_{11}$ , and  $c_{12}$  are the constants and are related as  $c_1 = \log_{10}(c_{11}^{-\frac{1}{2}}) = \log_{10}(c_{12})$ .

The value of  $c_{12}$  can be obtained by substituting particular values (the first point with  $b = 19$ , where  $N = 1$ ,  $R \approx 4.25$ ) of  $R$  and  $N$  from Figure 3.10 (a) so that:

$$c_{12} = 4.25 \approx \sqrt{b} \text{ for } N=1.$$

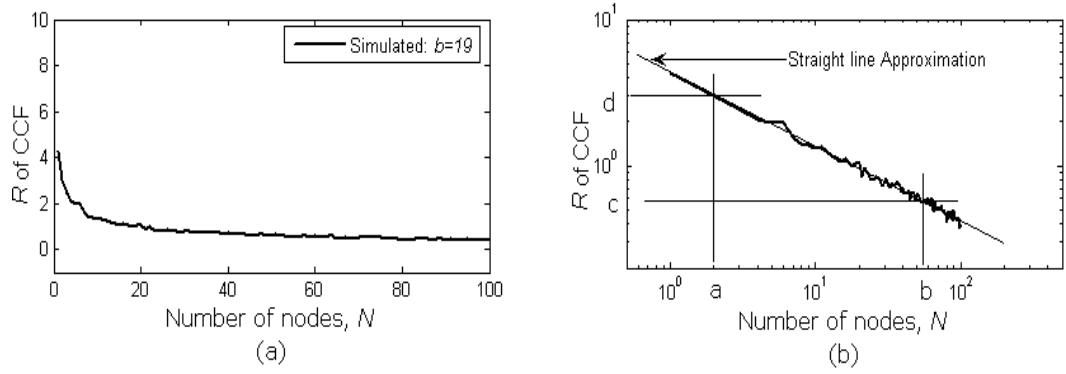


**Figure 3.10 Simulated results for  $R$  versus  $N$ : (a) normal plot; and (b) log-log plot**

Now, to show the relationship between  $R$  and  $b$ , the estimation process is simulated with different  $b$ . Variations in  $b$  can be obtained by changing  $d_{\text{DBS}}$  and/or  $S_R$ . Figure 3.11 shows the variations in  $R$  with the number of bins,  $b$ , plotted in normal (Figure 3.11 (a)) and log-log (Figure 3.11 (b)) scales. Again, it is obvious from Figure 3.11 (b) that the log-log plot of the simulated results can be approximated by a straight line whose slope is obtained as

$$s_2 \approx \frac{1}{2}$$

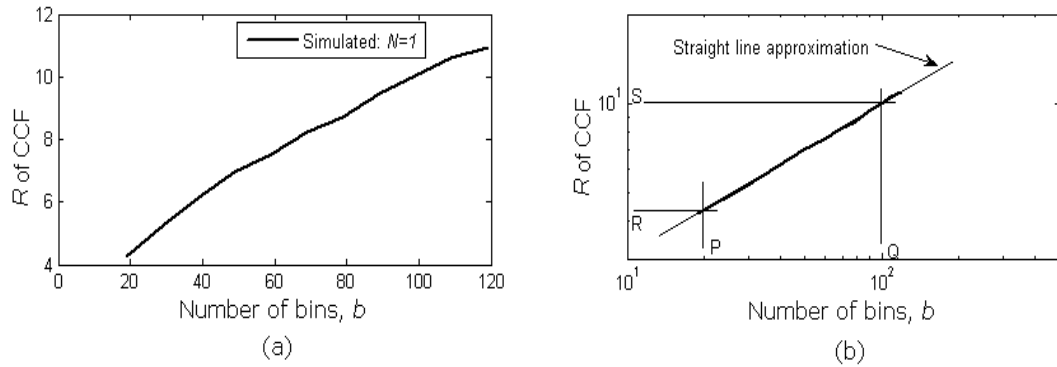


**Figure 3.11 Simulated results for  $R$  versus  $b$ : (a) normal plot; and (b) log-log plot**

So the estimated ratio,  $R$ , is:

$$\begin{aligned} \log_{10}(R) &= \frac{1}{2} \log_{10}(b) + c_2 \\ &= \log_{10}(b \times c_{21})^{\frac{1}{2}} \end{aligned}$$

Thus,

$$R = c_{22} \times b^{\frac{1}{2}}$$

i.e.,

$$R \propto \sqrt{b} \quad (3.34)$$

where  $c_2$ ,  $c_{21}$ , and  $c_{22}$  are the constants and are related as  $c_2 = \log_{10}(c_{21}^{-\frac{1}{2}}) = \log_{10}(c_{22})$

The value of  $c_{22}$  can be obtained by substituting particular values (the first point with  $N = 1$ , where  $R \approx 4.25$ ,  $b = 19$ ) of  $R$  and  $b$  from Figure 3.11 (a) so that:

$$c_{22} = 1 \approx \frac{1}{\sqrt{N}} \text{ for } b = 19.$$

Thus, from the above two relationships, it can be concluded that

$$R \approx \sqrt{\frac{b}{N}} \approx \sqrt{\frac{b-1}{N}} \text{ which agrees with the theoretical results obtained earlier.}$$

### 3.7.2.2 Results and discussion: estimation parameter, $R$ , of CCF

Several simulations are performed and some useful results are compared with the theoretical results to verify the effectiveness of the estimation process. Figure 3.12 shows the simulated results with error bars. It can be seen that the error bars are very small in size, i.e. the variations of the results are very small and the error bars can be neglected. Thus error bars are omitted from the simulation results later.

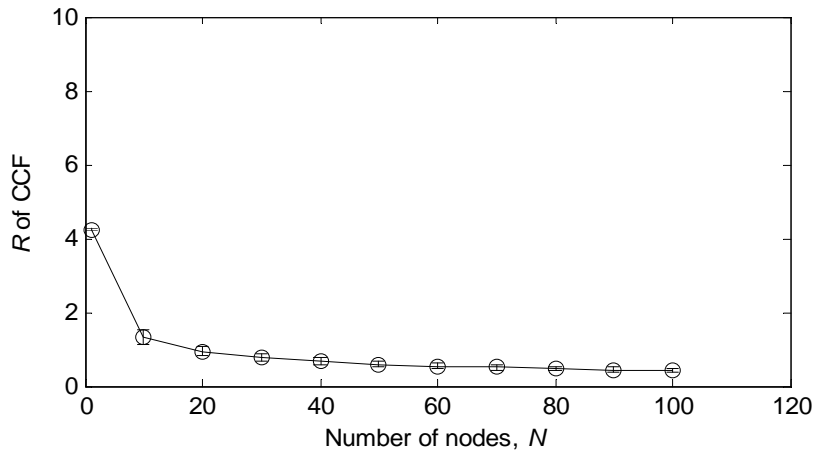


**Figure 3.12 Simulation results with error bar**

Figure 3.13 shows the theoretical and corresponding simulated results for the estimation of the number of nodes in a network. The solid lines indicate the theoretical results and the circles the corresponding simulated results. The variations of  $b$  in the three different figures are as a result of varying  $d_{\text{DBS}}$ . The distances between the sensors are: 0.5 m in Figure 3.13 (a), 1m in Figure 3.13 (b) and 2m in Figure 3.13 (c). The other parameters remain the same as in the first simulation, i.e., with  $S_R = 30 \text{ kSa/s}$ .

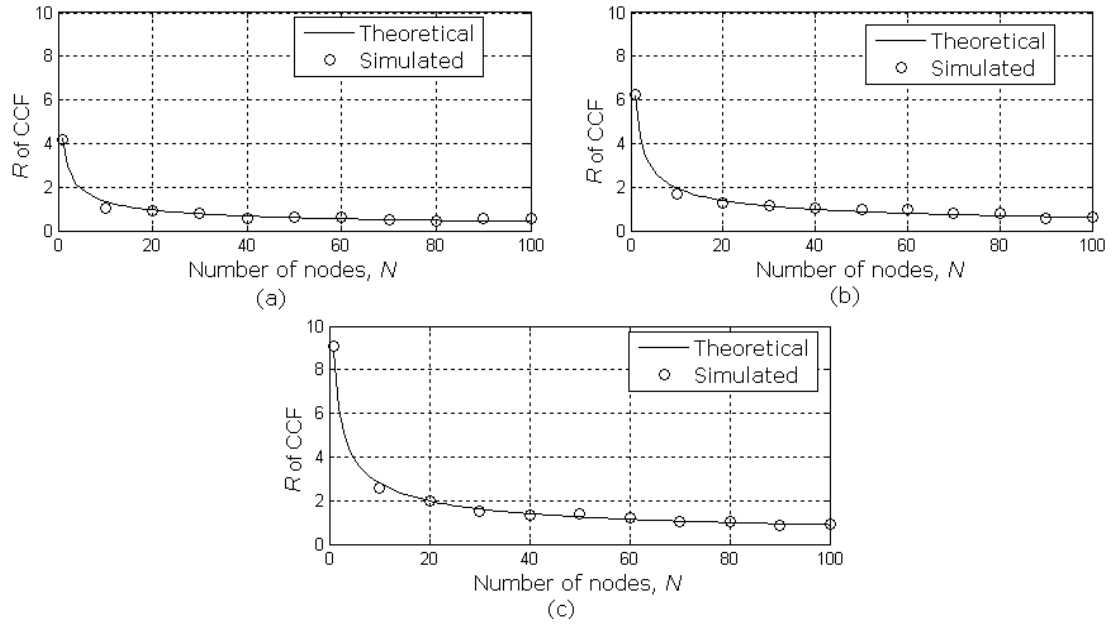


**Figure 3.13  $R$  versus  $N$  for  $b = 19, 39$  and  $79$  using fixed  $S_R$  and variable  $d_{\text{DBS}}$ :**

**(a)  $d_{\text{DBS}} = 0.5\text{m}$ ; (b)  $d_{\text{DBS}} = 1\text{m}$ ; and (c)  $d_{\text{DBS}} = 2\text{m}$  [ $S_R = 30 \text{ kHz}$ ]**

Then, the results of  $R$  for different  $b$  are plotted in Figure 3.14.

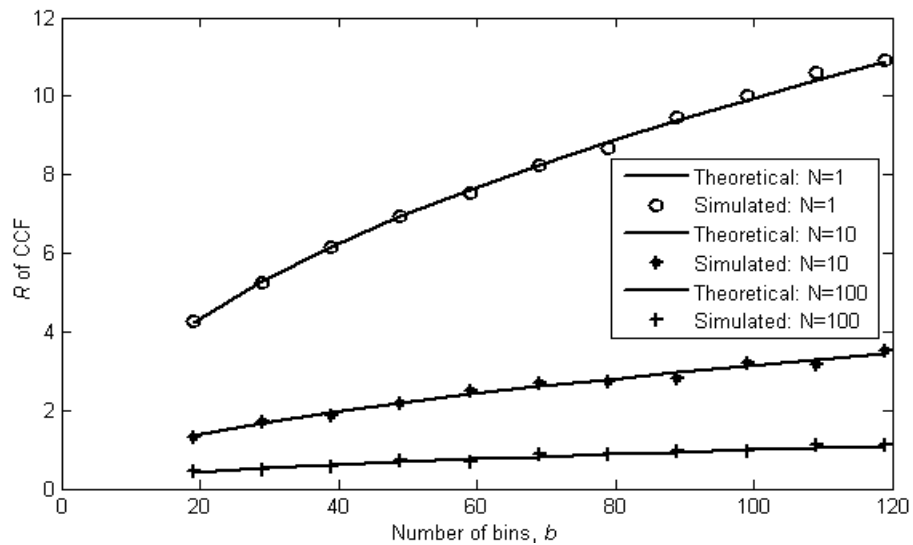


**Figure 3.14 Comparisons of theoretical and simulated results:  $R$  versus  $b$**



The simulations are performed in the MATLAB® programming environment. In the results depicted in the above figures, the theoretical and simulated lines are very close to each other, i.e., the theoretical and simulation results match which indicates that the process is satisfactory for estimation. In the figures, the solid and differently marked lines indicate the theoretical (from the mathematical relationships shown in Section 3.7.1) and simulated (from the simulation discussed in Section 3.7.2) results, respectively.

Again, it is obvious that  $b$  will be larger if  $d_{DBS}$  increases and has an effect on the estimation process, as discussed in Section 3.7.1. It is shown that large values of  $d_{DBS}$  result in large values of  $R$  and the closer the simulated lines are to the theoretical lines the greater the degree of accuracy. However, there might be some limitations on this relationship, as discussed later.

### 3.7.2.3 Dependency of $R$ on $b$ , $S_R$ and $d_{DBS}$

It is possible to vary the number of bins,  $b$  by also varying the sampling rate,  $S_R$ . The number of bins,  $b$ , in samples is related to the distance between the sensors,  $d_{DBS}$ , and the sampling rate,  $S_R$ , as follows:

$$b = \frac{2 \times d_{DBS} \times S_R}{S_p} - 1, \quad (3.35)$$

where the symbols have their defined meanings.

The effects of varying the sampling rate and the distance between the sensors are shown in Figures 3.15 to 3.17. In Figure 3.15, there are three different figures for different  $b$ , as there are in Figure 3.13, but the variations occur due to varying  $S_R$ . The values used for the sampling rates are: 30 kSa/s for Figure 3.15 (a), 60 kSa/s for Figure 3.15 (b) and 120 kSa/s for Figure 3.15 (c). The other parameters remain the same as in the first simulation with  $d_{DBS} = 0.5$  m.

In Figure 3.16, there are three different figures for different  $b$ , as in Figures 3.13 and 3.15, but the variations occur due to varying both  $d_{DBS}$  and  $S_R$ . The values used are: 0.25 m and 60 kSa/s for Figure 3.16 (a), 0.75 m and 40 kSa/s for Figure 3.16 (b) and

1.2 m and 50 kSa/s for Figure 3.16 (c). The other parameters remain the same as in the first simulation.

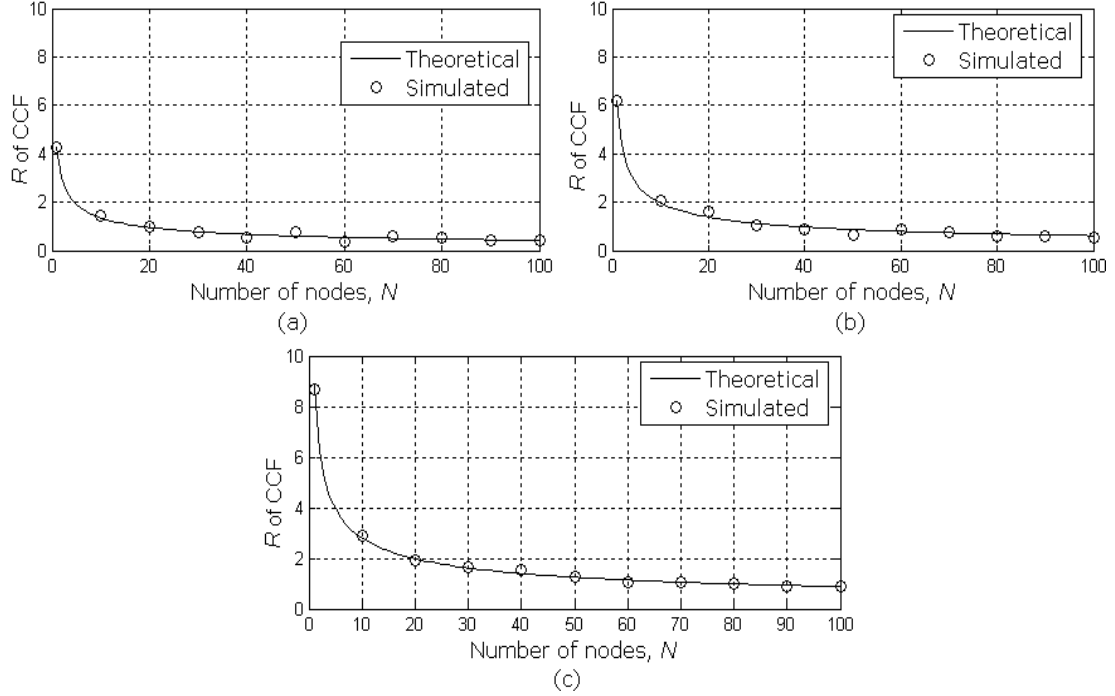


**Figure 3.15  $R$  versus  $N$  for  $b = 19, 39$  and  $79$  using fixed  $d_{DBS}$  and variable  $S_R$ :  
 (a)  $S_R = 30$  kSa/s; (b)  $S_R = 60$  kSa/s; and (c)  $S_R = 120$  kSa/s [ $d_{DBS} = 0.5$  m]**

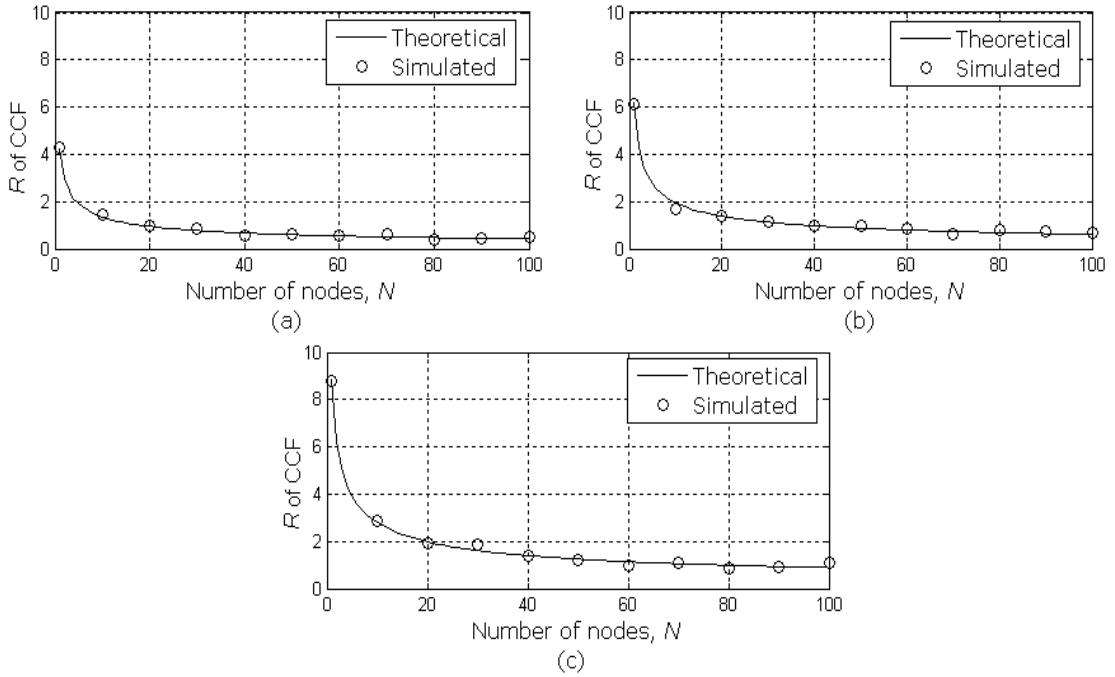


**Figure 3.16  $R$  versus  $N$  for  $b = 19, 39$  and  $79$  using both  $d_{DBS}$  and  $S_R$  as variables:  
 (a)  $d_{DBS} = 0.25$  m,  $S_R = 60$  kSa/s; (b)  $d_{DBS} = 0.75$  m,  $S_R = 40$  kSa/s;  
 and (c)  $d_{DBS} = 1.2$  m,  $S_R = 50$  kSa/s**

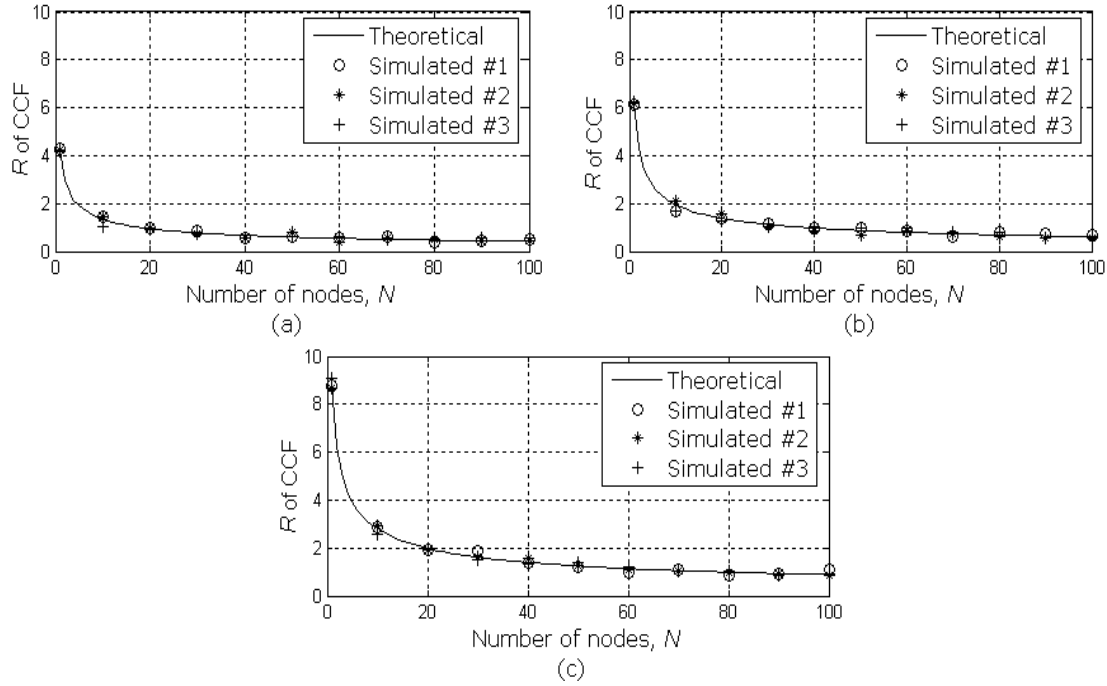


**Figure 3.17  $R$  versus  $N$ : (a)  $b = 19$ ; (b)  $b = 39$ ; and (c)  $b = 79$**

**[Simulated#1 -  $d_{DBS}$  variable and  $S_R$  fixed; simulated#2 -  $d_{DBS}$  fixed and  $S_R$  variable; and simulated#3 - both  $d_{DBS}$  and  $S_R$  variable]**

The results shown in Figures 3.13, 3.15 and 3.16 are compared in Figure 3.17 in which there are three different plots, each comparing four different results with the same  $b$ . This figure shows comparisons of three different simulated  $R$ s for  $b = 19$  (Figure 3.17 (a)),  $b = 39$  (Figure 3.17 (b)) and  $b = 79$  (Figure 3.17 (c)) using a variable  $d_{DBS}$  and a fixed  $S_R$  in simulated#1, a fixed  $d_{DBS}$  and a variable  $S_R$  in simulated#2 and both  $d_{DBS}$  and  $S_R$  variable in simulated#3 with theoretical  $R$ . The results in Figure 3.17 demonstrate that, whatever the value of  $d_{DBS}$  and  $S_R$ , the estimation parameter,  $R$ , will only vary when  $b$  is varied. To make the matter clearer, further simulation results are shown in the Figures 3.18 and 3.19.

Figure 3.18 shows the three different theoretical with corresponding simulated results for  $R$  for three different numbers of nodes. The circles and associated line are for  $N = 1$ , the stars and associated line for  $N = 10$ , and the plus signs and associated line for  $N = 100$ . It is shown that  $R$  is constant for a certain number of nodes when  $b$  remains unchanged (although  $S_R$  and  $d_{DBS}$  change).

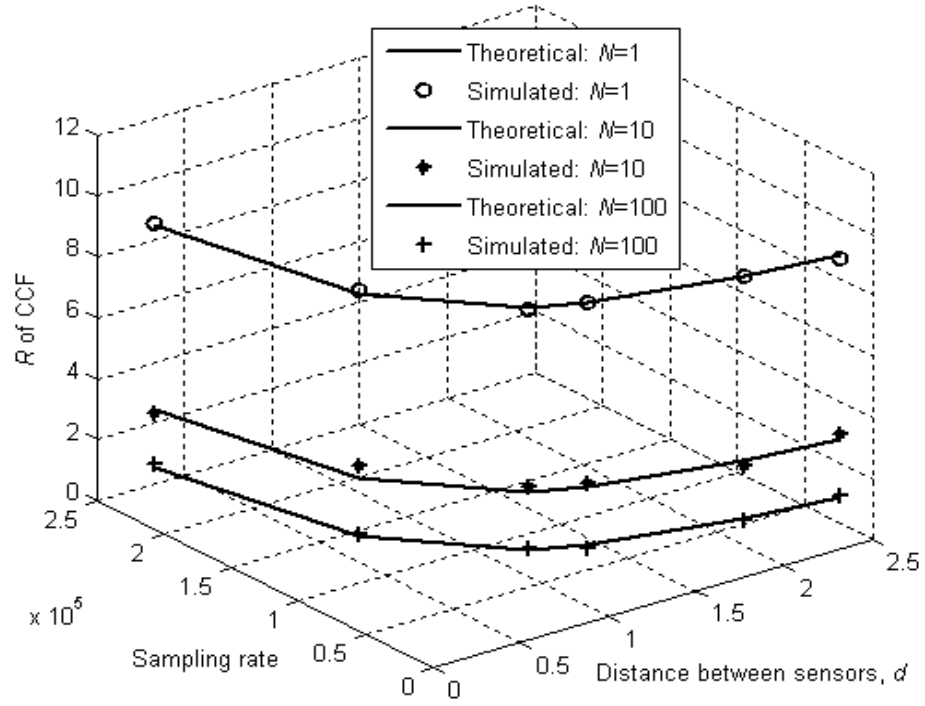


Figure 3.18 3D plots of  $R$ ,  $S_R$  and  $d_{DBS}$

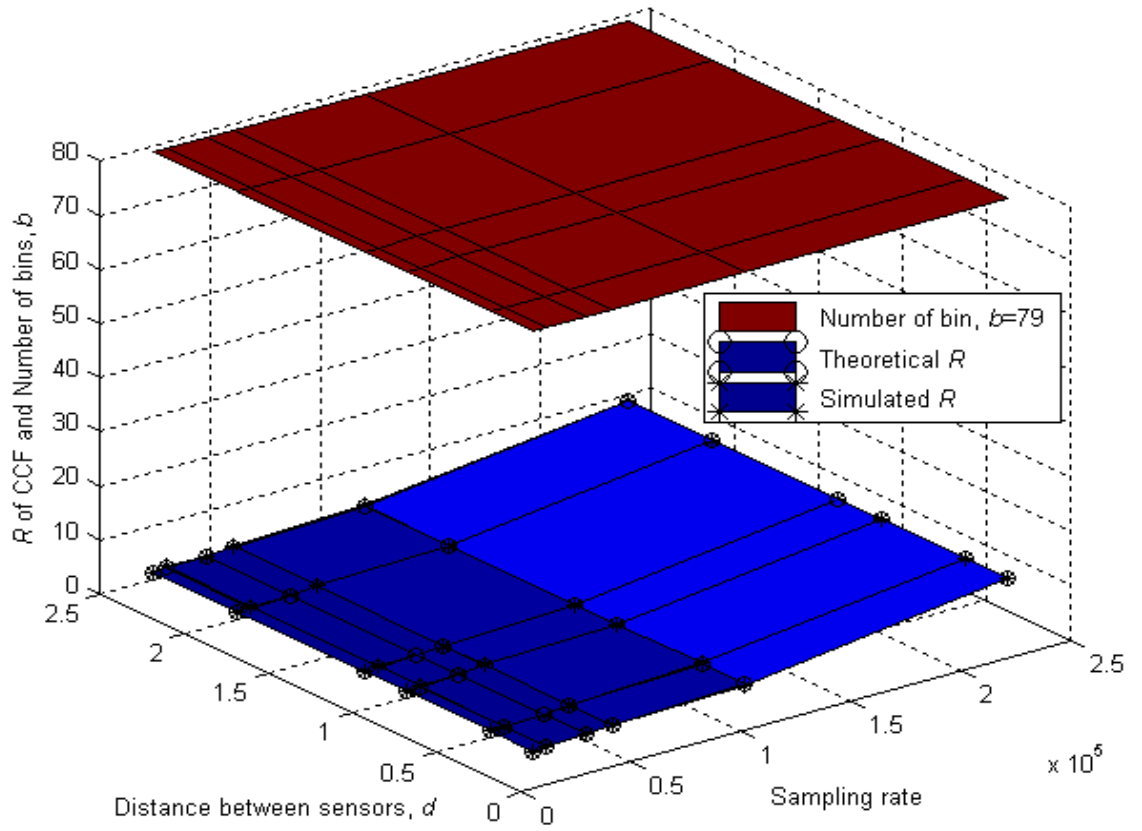


Figure 3.19 Surface plots of  $R/b$ ,  $S_R$  and  $d_{DBS}$

Figure 3.19 shows similar effects of  $S_R$  and  $d_{DBS}$ , and thus  $b$ , as shown in Figure 3.18 using the surface plots for six different values of  $N$ . In Figure 3.19,  $b$  remains fixed at 79 by taking six different pairs of values of  $S_R$  and  $d_{DBS}$ , as shown in the top surface plot. In the bottom of the figure, the surface plot marked by circles is for the theoretical results and that marked by stars is for the simulation results; they show that the theory matches the simulation.

It is shown from the above results that, although the values of  $S_R$  and  $d_{DBS}$  change (keeping  $b$  fixed), the values of  $R$  for a particular  $N$  remain unchanged due to the unchanged  $b$ . Thus, it is possible to set suitable values for  $S_R$  and  $d_{DBS}$  by varying them oppositely to estimate  $N$  with a certain  $b$ .

#### 3.7.2.4 Results and discussion: estimation of $N$

After some manipulation, from the expression in (3.30) we have:

$$N = \frac{b-1}{R^2}$$

So, if the ratio,  $R$ , is available from the simulation, an estimate of the number of nodes  $N$  is readily available using the above equation as  $b$  is known from the experimental setup. Several simulations are investigated in this respect and the results obtained from the average of 1000 estimated  $\hat{N}$  are shown in Figure 3.20.

Figure 3.20 also demonstrate that a good approximation of the number of nodes,  $N$ , can be obtained from the ratio,  $R$ , of the CCF even when the distance between sensors is small; if a distance of 0.25 m is sufficient, the two sensors can be collocated with the same node, thereby removing the requirement to transmit data between them.

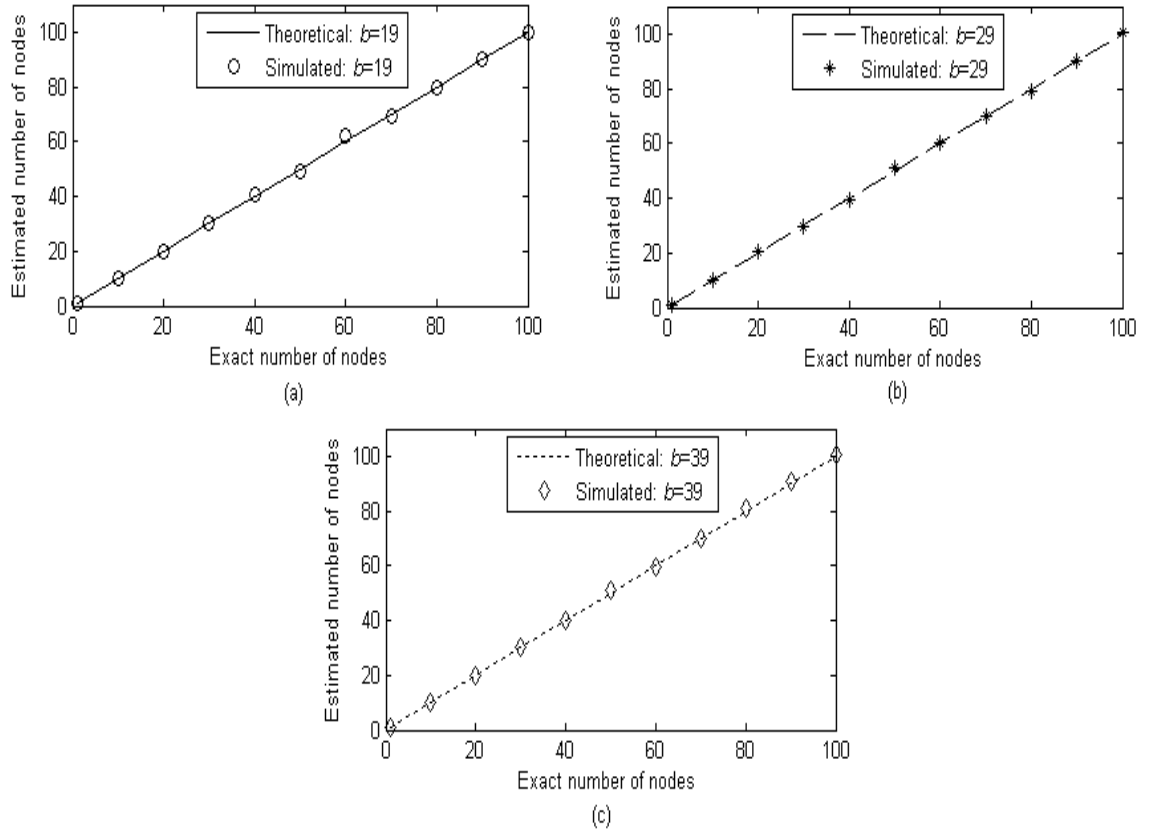


**Figure 3.20 Comparisons of theoretical and simulated numbers of nodes:**  
**(a)  $b = 19$  ( $d_{\text{DBS}}=0.25$  m and  $S_{\text{R}}=60$  kSa/s); (b)  $b = 29$  ( $d_{\text{DBS}}=0.25$  m and  $S_{\text{R}}=90$  kSa/s); and (c)  $b = 39$  ( $d_{\text{DBS}}=0.25$  m and  $S_{\text{R}}=120$  kSa/s).**

### 3.7.3 Conclusion

Estimation of the number of nodes is investigated here with theory (obtained from statistical property of CCF) and simulation. It can be seen from the results that the proposed technique is good enough for estimation. Although error bars are required for simulated results (as they are random in nature with a standard deviation), it is shown that the error bar is sufficiently small to neglect and so simulation results are provided without error bars. There are some assumptions in this basic technique which are investigated later in this chapter, starting with the estimation in ETP case.

### 3.8 Estimation process - equal transmitted power (ETP)

#### case

The estimation process discussed in the previous section is applied to the ERP case in which the powers of all the received signals are the same. It can be achieved by proper probe requests emanating from the receivers, and the transmitters replying with signal powers which are inverse proportions of the received probes. In this section, the ETP case, in which the nodes transmit signals of equal power but the received powers are different due to the distance-dependent attenuations, which also depend on the dispersion coefficient,  $k$ , is discussed. Several simulations are performed using a similar procedure to that discussed earlier for the ERP case. The results for the ratios of the standard deviations to the means of the CCF are presented in Figure 3.21 for different dispersion coefficients,  $k$  (0, 1, 1.5, and 2). Simulated results shown are obtained from the average of 100 iterations to get the better results and this is followed always for the ETP case. Although the simulated results in the ERP (i.e., where  $k = 0$ ) case follow the basic theory, they are different in the ETP cases as shown in Figure 3.21.

To verify the simulations, the estimation parameter,  $R$  is also obtained from the theoretical CCF using (3.16) and (3.20) and compared with the simulation as shown in Figure 3.22. It can be seen that the two results coincide each other which ensure the correctness of the simulation results.

However, as in the practical environment both cases may arise. In order to make the process robust, we should design it for the ETP case as well. Although the results do not exactly match those of the theory, their well-behaved shapes suggest that we derive a scaling factor which follows the theory. To do this, we take the results for  $k = 1.5$  from Figure 3.21, as shown in Figure 3.23 (a), and re-plot them in a log scale, as shown in Figure 3.23 (b), from which it is clear that the log-log plot completely follows a straight line as it does in the case of equal received power and theoretical discussed earlier. Now, assume straight line approximations of both results in Figure 3.23 (b) to fit the simulation results with the theory and vice versa.

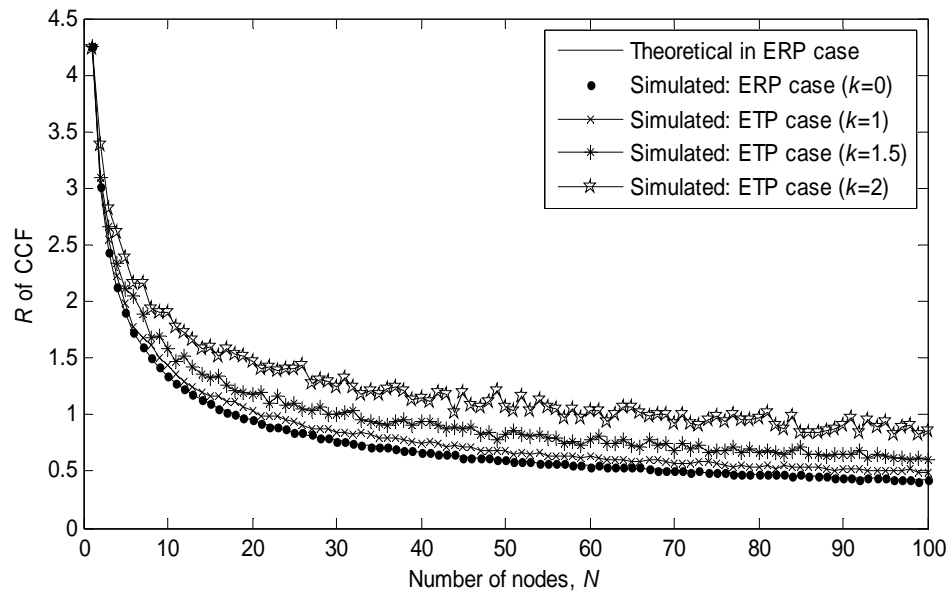


**Figure 3.21 Ratios of standard deviation to mean of CCF,  $R$  versus  $N$ : comparison of theoretical and different  $k$  results**

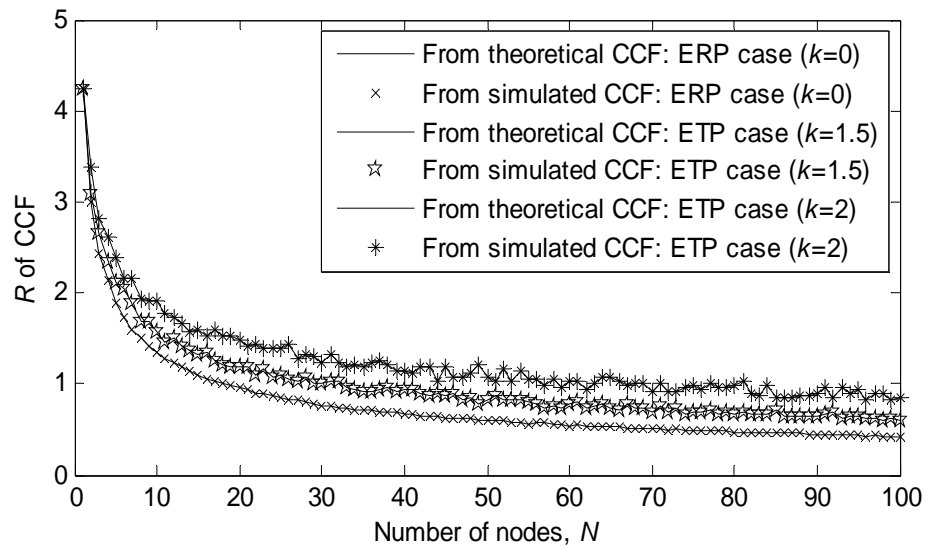


**Figure 3.22 Ratios of standard deviation to mean of CCF,  $R$  versus  $N$ : comparison of  $R$  obtained from theoretical and simulated CCF**



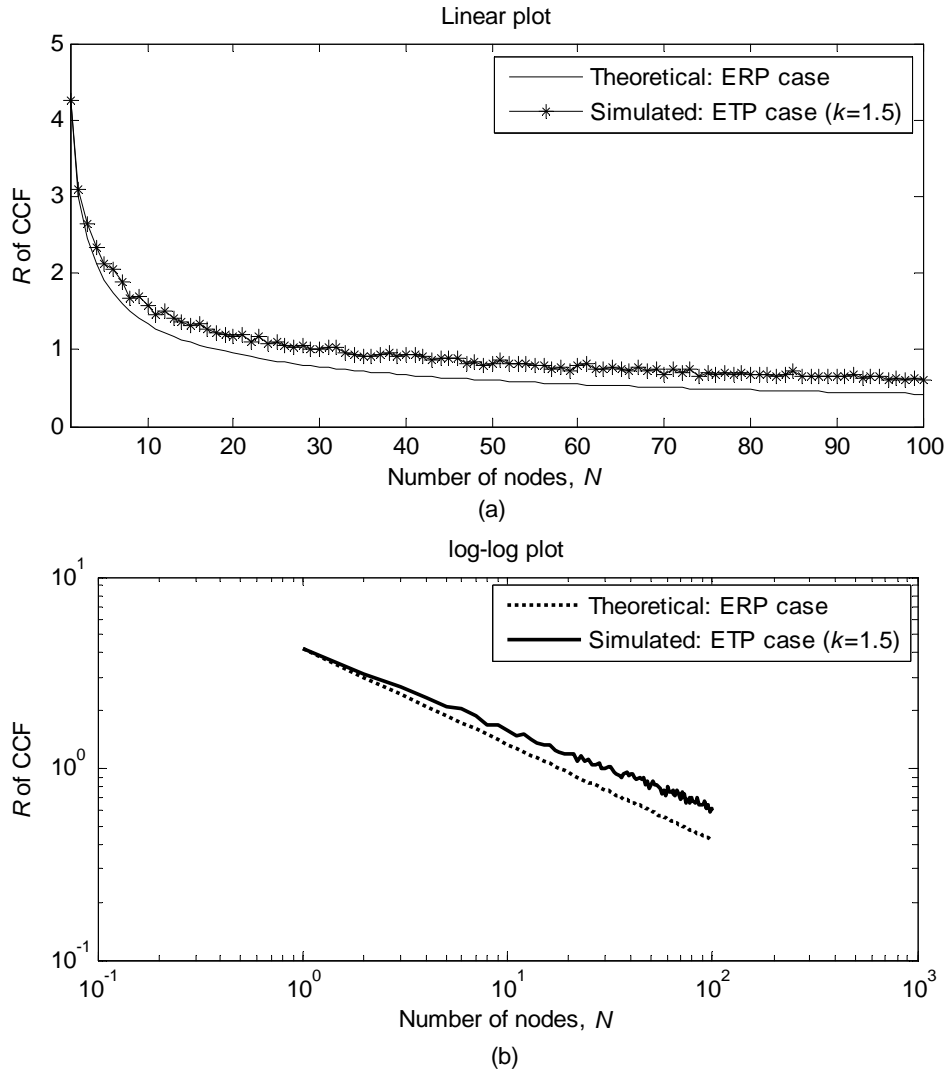


**Figure 3.23 Ratios of standard deviation to mean of CCF,  $R$  versus  $N$ : (a) comparison with  $k = 1.5$  and theoretical; (b) re-plotting of (a) in log scale**

### 3.8.1 Fitting of simulation results with theory

It is shown that the theoretical value of the estimation parameter  $R$  is expressed in (3.30) as

$$R = \sqrt{\frac{b-1}{N}}$$

It can be written as

$$R = (b-1)^{\frac{1}{2}} N^{-\frac{1}{2}}$$

This expression is also verified by the simulation results in ERP case, where the value of dispersion coefficient is considered as  $k=0$ . Thus, for  $k=0$ , denoting simulated estimation parameter by  $R_0$ , power of  $(b-1)$  by  $\varphi_0$ , and power of  $N$  by  $s_0$ , the simulated estimation parameter in ERP case can be expressed as

$$R_0 = (b-1)^{\varphi_0} N^{s_0} \quad (3.36)$$

Letting the slopes of the straight line approximation from Figure 3.23 (b) be  $s_{1.5}$  for the simulated line and for  $k=1.5$ , denoting simulated estimation parameter by  $R_{1.5}$ ,

$$\begin{aligned} \log_{10}(R_{1.5}) &= (s_{1.5})\log_{10}(N) + c_s \\ \Rightarrow \log_{10}(R_{1.5}) &= (s_{1.5})\log_{10}(N) + (s_{1.5})\log_{10}(c_{ss}) \\ \Rightarrow \log_{10}(R_{1.5}) &= (s_{1.5})\log_{10}(c_{ss}N) \\ \Rightarrow \log_{10}(R_{1.5}) &= \ln(c_{ss}N)^{(s_{1.5})} \\ \Rightarrow R_{1.5} &= c_{ss} \times N^{s_{1.5}} \end{aligned} \quad (3.37)$$

where  $c_s$  and  $c_{ss}$  are constants and are related as  $c_s = s_{1.5} \log_{10}(c_{ss})$ .

To make the (3.37) as (3.36), defining  $c_{ss}$  as  $c_{ss} = (b-1)^{\varphi_{1.5}}$ , the expression (3.37) can be written as

$$R_{1.5} = (b-1)^{\varphi_{1.5}} N^{s_{1.5}} \quad (3.38)$$

Thus, for any  $k$ , simulated estimation parameter  $R_k$  can be expressed by a generalised expression as

$$R_k = (b-1)^{\varphi_k} N^{s_k} \quad (3.39)$$

It is already known the value of  $s_0 = -0.5$  and the value  $\varphi_0 = 0.5$ . The value of  $s_{1.5}$  is obtained from Figure 3.22 (b) as  $s_{1.5} \approx -0.418$  and substituting this value and a  $R_{1.5}$  for a particular  $N$  from Figure 3.22 (a) in (3.37), the value of  $c_{ss}$  is obtained as  $c_{ss} \approx 4.25 \approx (19-1)^{\frac{1}{2}}$  i.e., as  $c_{ss} \approx (b-1)^{\frac{1}{2}}$  (as the simulation was conducted for  $b=19$ ). This gives the value of  $\varphi_{1.5} = 0.5$ .

It has already been mentioned that the value of  $k$  for underwater acoustic communication can vary from 1 to 2. So, to find the generalised expressions for the  $\varphi_k$  and the slopes,  $s_k$ , of the simulated results, several are obtained for different  $k$  (0, 0.5, 1, 1.5, and 2) with the  $b=19$ . The results are shown in Table 3.5.

**Table 3.5 Parameters  $p_k$  and  $s_k$  of expression (3.39)**

Parameters	Values				
	$k=0$	$k=0.5$	$k=1$	$k=1.5$	$k=2$
$\varphi_k$	0.5	0.5	0.5	0.5	0.5
$s_k$	-0.5	-0.495	-0.468	-0.418	-0.346

It is shown that the values of  $s_k$  is always negative, thus the (3.39) can be expressed as

$$R_k = (b-1)^{\varphi_k} N^{-|s_k|} \quad (3.40)$$

It is again shown that for the suitable  $s_k$  the  $\varphi_k$  is always 0.5. Thus for  $b=19$ , it requires scaling only the powers of  $N$ , i.e. the  $s_k$ . Whether it is valid or not for the  $b$  other than 19, to confirm and to make the scaling sufficiently robust that the simulated results follow the theory, more demonstration is provided with following Figure 3.24.

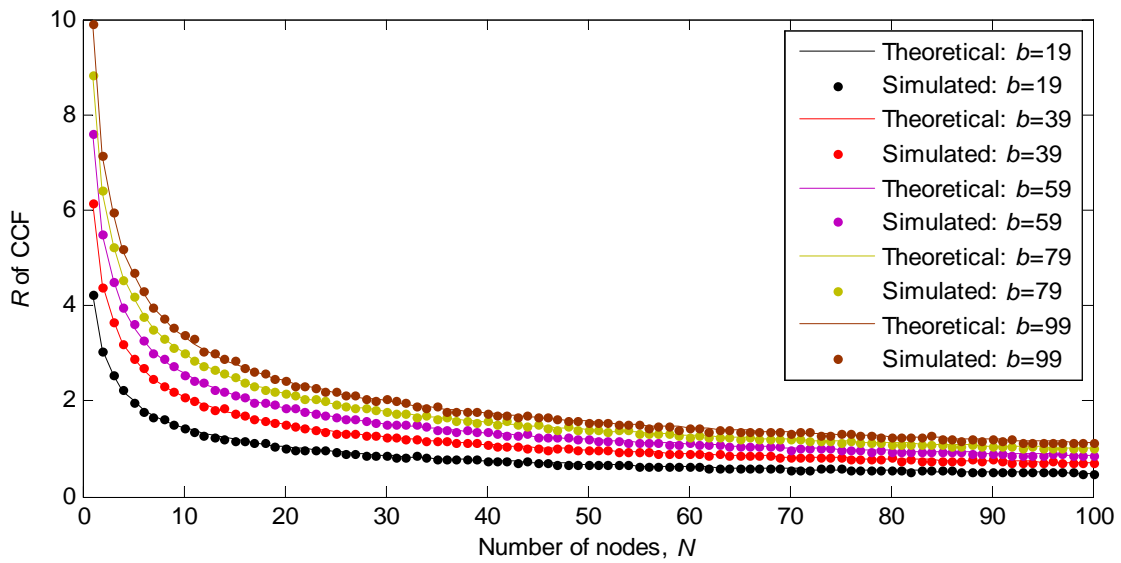


**Figure 3.24 Ratios of standard deviation to mean of CCF,  $R$  versus  $N$ :  $k = 1$**

Theoretical and corresponding simulated results are plotted in the figure, where theoretical means the corresponding theoretical results using (3.39) or (3.40) with corresponding  $b$  for  $k=1$ . The theoretical expressions are as follows.

$$R_{19}(k=1) = (19-1)^{\frac{1}{2}}(N^{-0.468})$$

$$R_{39}(k=1) = (39-1)^{\frac{1}{2}}(N^{-0.468})$$

$$\vdots$$

$$R_b(k=1) = (b-1)^{\frac{1}{2}}(N^{-0.468})$$

It is already evidenced that similar expressions are applicable in ERP case (where  $k=0$ ) with  $s_k = -0.5$ .

Similarly, to get a robust scaling of the simulation results, we express the ratio of the standard deviation to the mean of the CCF for all dispersion coefficients with  $b=19$  as:

$$R_{19}(k=0) = (19-1)^{\frac{1}{2}}(N^{-0.5})$$

$$R_{19}(k=0.5) = (19-1)^{\frac{1}{2}}(N^{-0.495})$$

$$\vdots$$

$$R_{19}(k=2) = (19-1)^{\frac{1}{2}}(N^{-0.346})$$

For 39 bins, the expressions are:

$$R_{39}(k=0) = (39-1)^{\frac{1}{2}}(N^{-0.5})$$

$$R_{39}(k=0.5) = (39-1)^{\frac{1}{2}}(N^{-0.495})$$

$$\vdots$$

$$R_{39}(k=2) = (39-1)^{\frac{1}{2}}(N^{-0.346})$$

And so for the  $b$  bins:

$$\begin{aligned} R_b(k=0) &= (b-1)^{1/2} (N^{-0.5}) \\ R_b(k=0.5) &= (b-1)^{1/2} (N^{-0.495}) \\ &\vdots \\ R_b(k=2) &= (b-1)^{1/2} (N^{-0.346}) \end{aligned}$$

It can be seen from the all expressions that the constant term is dependent on only the number of bins,  $b$ . Also, the powers of the number of nodes only vary with a varying  $k$ .

Thus, from these series of expressions, we obtain the generalised expression of scaled theoretical  $R$  for ETP case as in (3.41)

$$R_b(k) = (b-1)^{1/2} (N^{s_k}) \quad (3.41)$$

where the  $s_k$  values are those presented in Table 3.5.

In (3.41) replacement of  $s_k$  gives the theoretical values of estimation parameter, where the appropriate value of  $s_k$  can be obtained from the following quadratic expression as shown in Figure 3.25.

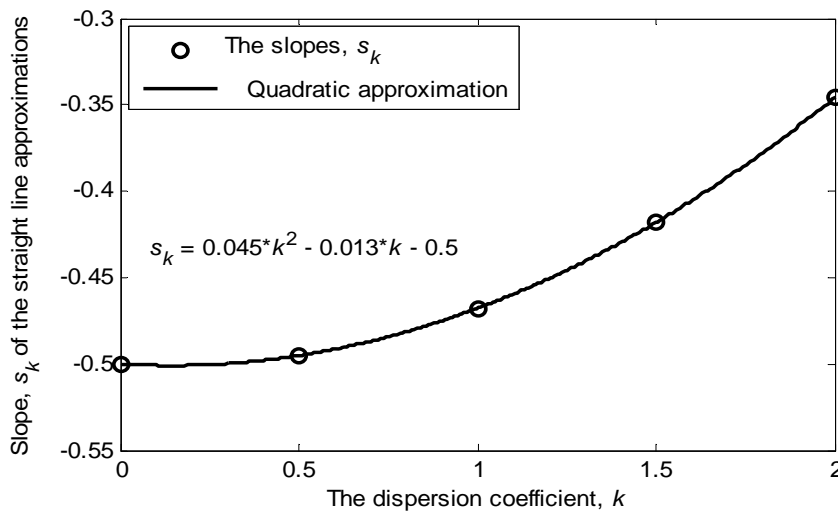


**Figure 3.25** The powers,  $s_k$  of  $N$  in the expression of estimation parameter

Now from (3.41), for  $k=0$ , the expression is

$$R = R_b(0) = (b-1)^{\frac{1}{2}}(N^{-0.5}) \quad (3.42)$$

Again, the expression (3.41) can be solved for  $N$  as

$$N = \left\{ \frac{R_b(k)}{(b-1)^{\frac{1}{2}}} \right\}^{\frac{1}{s_k}}$$

Inputting this  $N$  in (3.42), we have the expression of  $R_b(0)$  from  $R_b(k)$  as:

$$R_b(0) = (b-1)^{\frac{1}{2}} \left\{ \frac{R_b(k)}{(b-1)^{\frac{1}{2}}} \right\}^{\frac{-1}{2s_k}}$$

i.e.,

$$R_b(0) = (b-1)^{\left(\frac{1}{2} + \frac{1}{4s_k}\right)} (R_b(k))^{\frac{-1}{2s_k}}$$

Thus, using (3.41) and (3.42), the expression to make the simulations (for any  $k$ ) compatible with the theory will be:

$$R_{tb}(k) = (b-1)^{\left(\frac{1}{2} + \frac{1}{4s_k}\right)} (R_b(k))^{\frac{-1}{2s_k}} \quad (3.43)$$

where  $R_{tb}(k)$  is the scaled value of  $R_b(k)$ , which matches the theory in ERP case.

### 3.8.2 Results and discussion after scaling

Several simulations are investigated and their results compared with the theoretical results. It is shown that, after scaling of the original simulation results, the process is satisfactory for estimating the number of nodes. All results are plotted in Figure 3.26 and 3.27, and it can be seen that, for any  $k$ , the estimation is satisfactory.

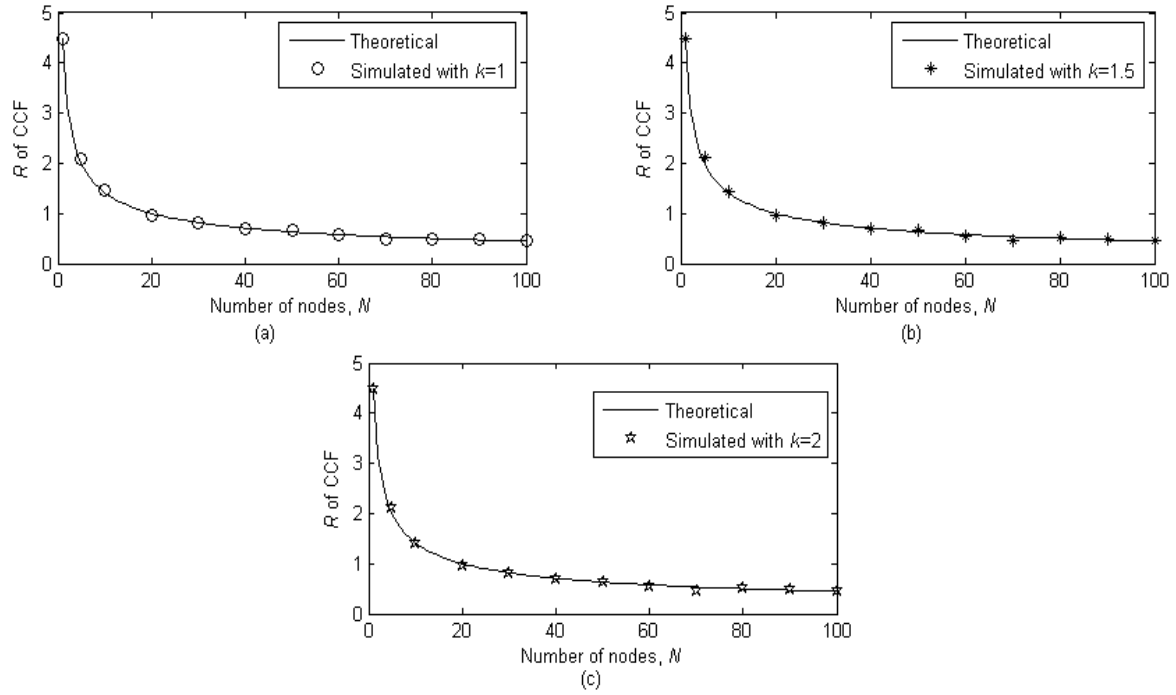


**Figure 3.26  $R$  versus  $N$ : (a)  $k = 1$ ; (b)  $k = 1.5$ ; and (c)  $k = 2$  [ $b = 19$ ]**

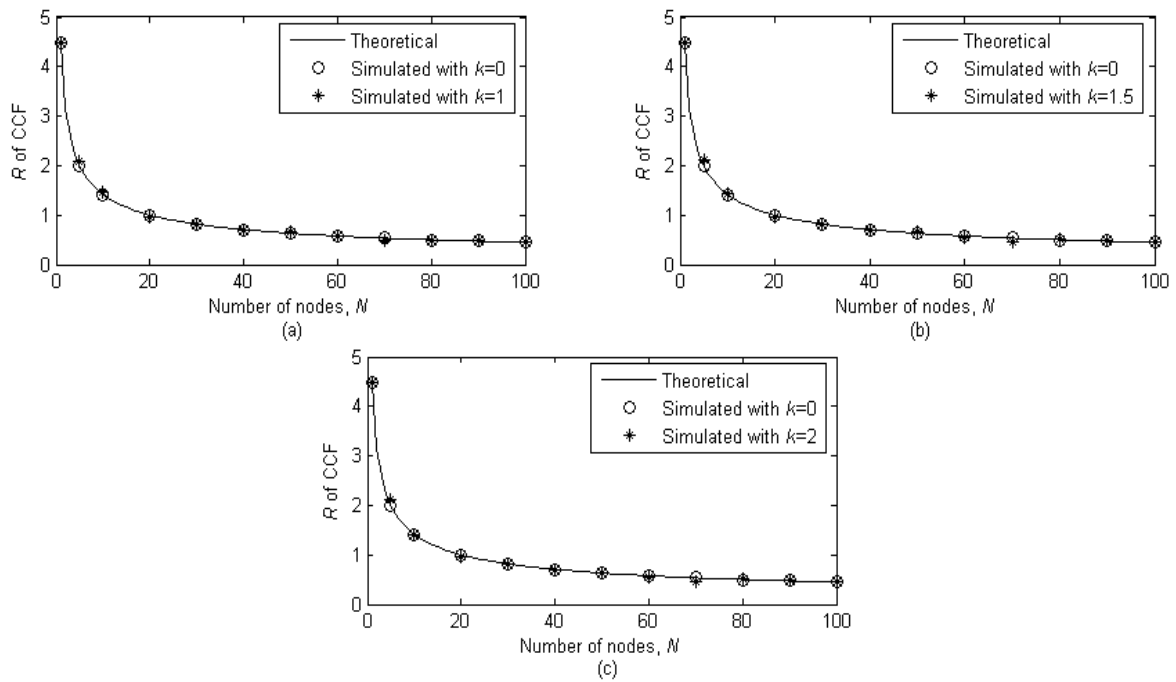


**Figure 3.27  $R$  versus  $N$  comparisons: (a)  $k = 1$ ; (b)  $k = 1.5$ ; and (c)  $k = 2$  [ $b = 19$ ]**

### 3.8.3 Direct scaling of theoretical $R$ of CCF to follow simulated results

The ratio of the standard deviation to the mean of the CCF has already been expressed as:

$$R_b(k) = (b-1)^{1/2} (N^{s_k})$$

Thus, for  $k = 0$ , we have:

$$R_b(0) = (b-1)^{1/2} (N^{-0.5})$$

and, then:

$$\frac{R_b(k)}{R_b(0)} = N^{s_k + 0.5}$$

So,

$$R_b(k) = N^{s_k + 0.5} R_b(0)$$

The above scaling expression shows that it does not depend on the number of bins,  $b$ , but on the number of nodes,  $N$ . Thus, for 32 nodes, we show the scaling factors for different dispersion coefficients,  $k$ , in Table 3.6 and Figure 3.28.

**Table 3.6 Direct scaling factors for a particular  $N (=32)$**

Parameters	Values				
	$k=0$	$k=0.5$	$k=1$	$k=1.5$	$k=2$
$f(k)$	1	1.0175	1.1173	1.3287	1.7053

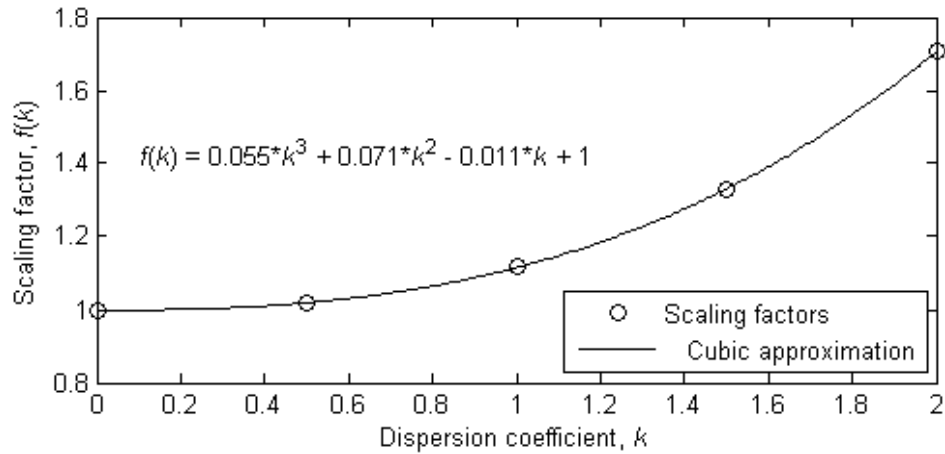


**Figure 3.28 Direct scaling factors for theoretical ratio of standard deviation to mean of CCF,  $R$  versus dispersion coefficient,  $k$ .**



Thus, the expression for the direct scaling factors for the theoretical ratio of the standard deviation to the mean of the CCF to follow the simulated results is:

$$f(k) = 0.055k^3 + 0.071k^2 - 0.011k + 1$$

### 3.8.4 Results and discussion after direct scaling

Several simulations after using direct scaling are investigated and the results compared with the theoretical results. It is shown in Figure 3.29 that, after direct scaling of the original simulation results, the process is adequate for estimating the number of nodes. All values are plotted in Figure 3.29 in which it can again be seen that, for any  $k$ , the use of scaling is sufficient for estimation.

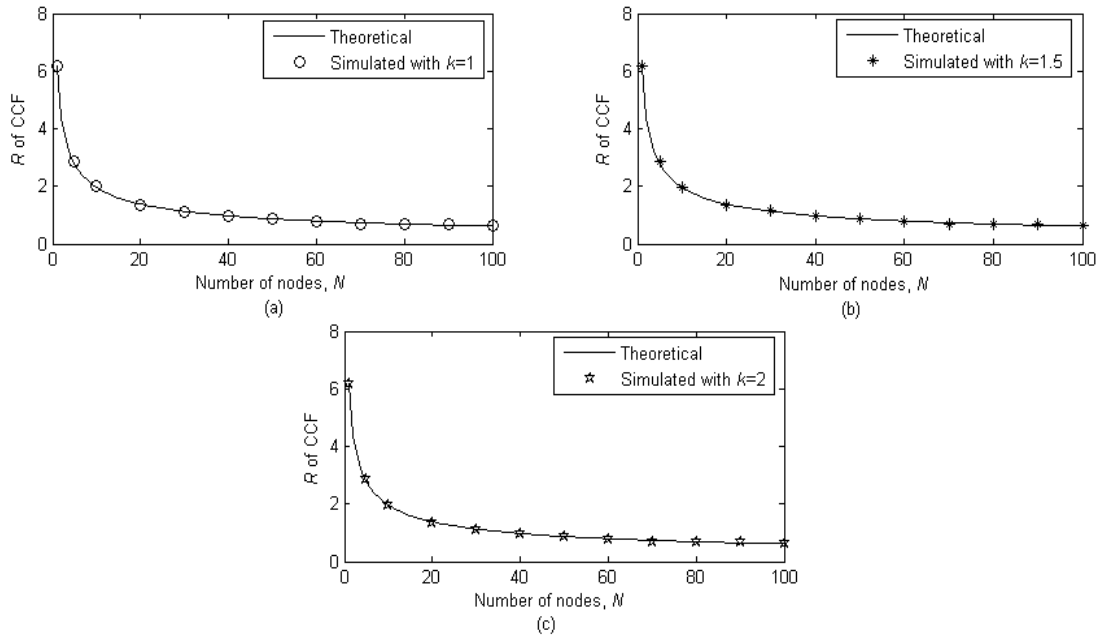


**Figure 3.29  $R$  versus  $N$ : (a)  $k = 1$ ; (b)  $k = 1.5$ ; and (c)  $k = 2$  [ $b = 39$ ]**

Thus in ETP case, it is again possible to obtain estimations using this scaled  $R$  by the following relationship (as it is in the ERP case):

$$\hat{N} = \frac{b-1}{R^2}$$

Several simulations are investigated in this way and the results shown in Figure 3.30.

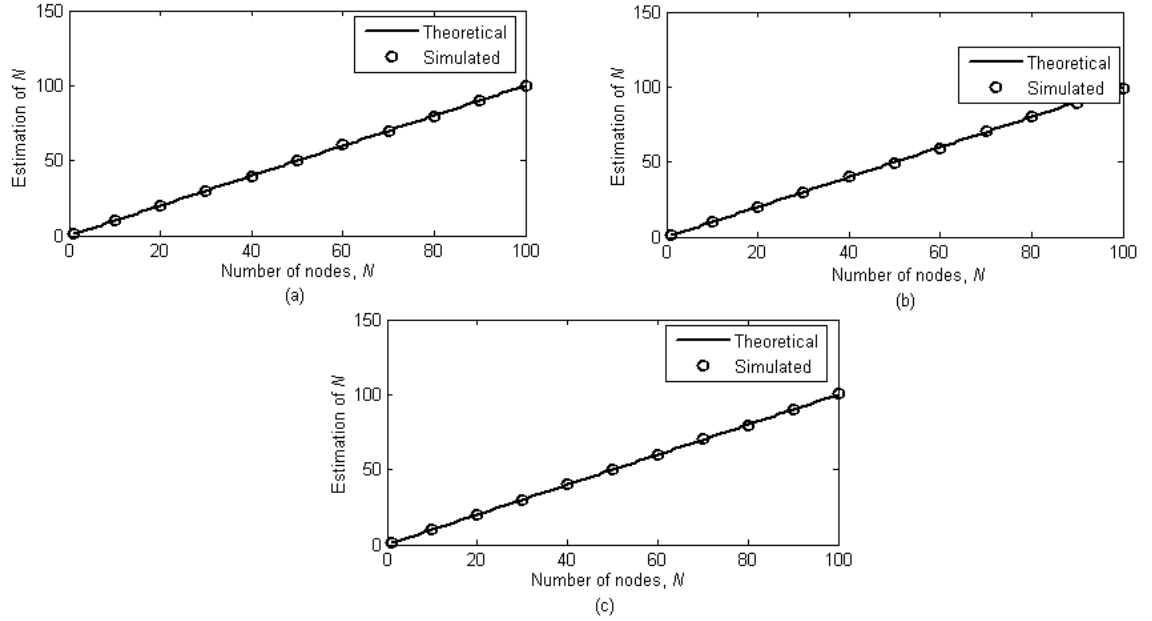


**Figure 3.30 Estimated  $N$  versus exact  $N$ : (a)  $k = 1$ ; (b)  $k = 1.5$ ; and (c)  $k = 2$**   
 (The values of estimation of  $N$  are from average of 1000 estimations)

### 3.8.5 Conclusion

It can be seen from these results that proper estimations are possible in both the ETP and ERP cases. Although there are differences in the initial results of  $R$ , its proper scaling in the ETP case provides as good an estimation as it does in the ERP case. As the results from all iterations are not sufficiently informative to obtain estimations, in the ETP case, the number of nodes is estimated with  $R$  from 100 iterations.

## 3.9 Selection of signal length, $N_S$

The ideal signal length is ideally infinitely long (considered as  $10^6$  samples in all of the above simulations). Unfortunately, this length is an energy-related term in the estimation process. The greater the signal length, the more energy is required to perform the estimation. The exact signal length for a particular estimation is therefore of interest and has been investigated in the following section.

Figures 3.31 and 3.32 show the number of nodes,  $N$  for different signal lengths,  $N_S$ . Figures 3.31 (a), (b), (c) and (d) show the same results but use different scales (normal, semi-log, semi-logx and log-log, respectively) for clarity of understanding.

Figure 3.31 (d) is re-plotted in Figure 3.32 with the exact number of nodes in order to discuss and select the appropriate signal length. It can be seen that the estimations are similar for 32 and 64 nodes up to the signal length of 1000 samples. But, beyond this point, i.e., if the signal length involves more than 1000 samples, the results are different for different numbers of nodes which implies that this is the effective lower limit of the signal length for estimating the number of nodes. This is indicated by large errors occurring at smaller signal lengths and the results only improve with increases in the signal length, as shown in the figure. At around 10,000 samples, the estimated numbers of nodes are about 22 and 35 instead of the exact numbers of 32 and 64 and about 30 and 60 at around 80,000 samples whereas, at around 300,000 samples, the process starts to estimate the exact numbers of nodes.

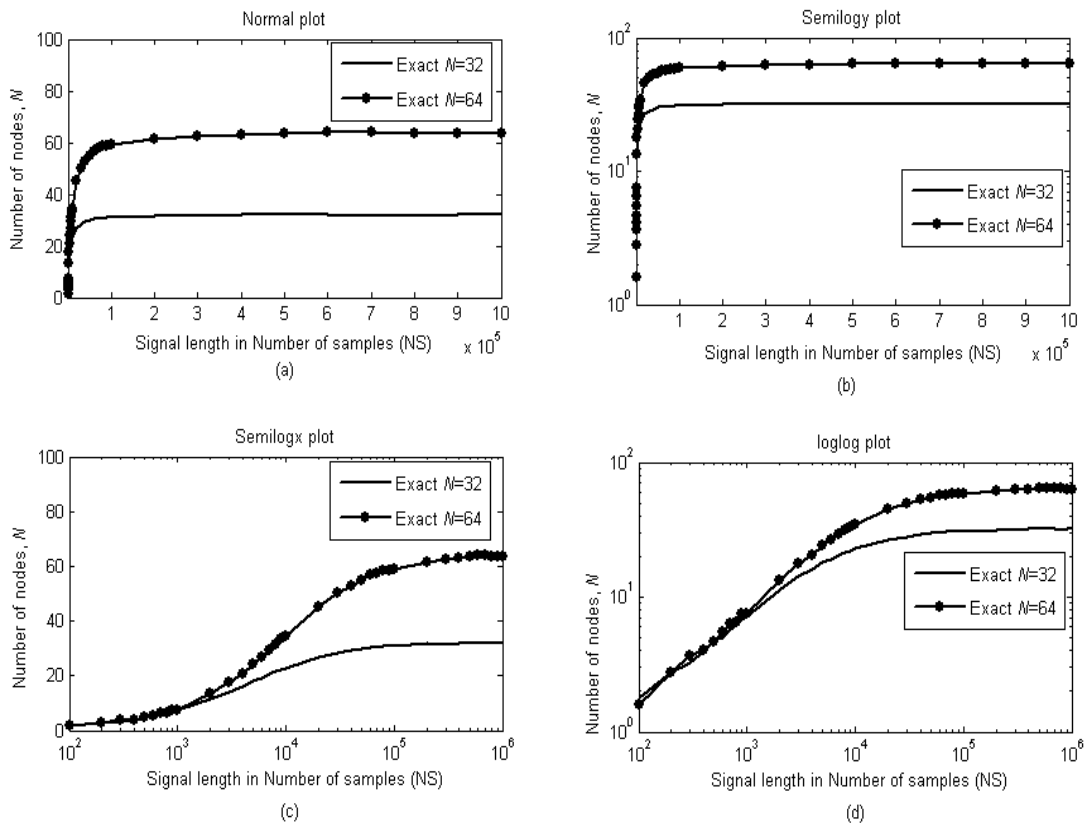


**Figure 3.31 Estimated  $N$  versus  $N_s$  plot: (a) normal scale; (b) x-normal, y-log scale; (c) x-log, y-normal scale; and (d) x-log, y-log scale (all values taken from 1 iteration and average of 1000 estimations with fixed  $b$  of 139 in ERP case)**

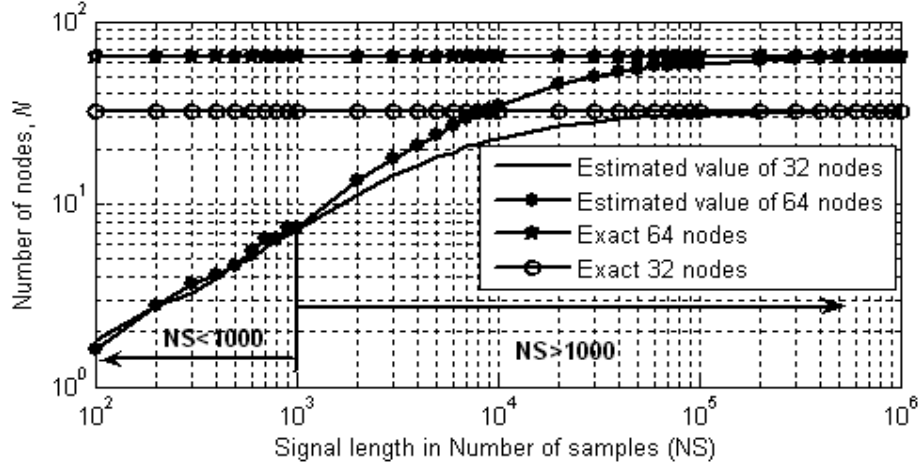


**Figure 3.32 Re-plotting of Figure 3.31 (d) with exact numbers of nodes**

In the above discussion, it is shown in the ERP case that the estimation of the number of nodes is dependent on the transmitted signal length. Similar effects in the ETP case are shown in Figure 3.33 in which it can be seen that, if the signal length is low, the estimation is poor but an increased signal length improves it. In the case of 32 original nodes with 1000 samples, the estimation process gives only about 5 nodes but the estimated number increases with increases in the signal length and, beyond about 300,000 samples, it estimates almost 32 nodes and is almost constant beyond this signal length.

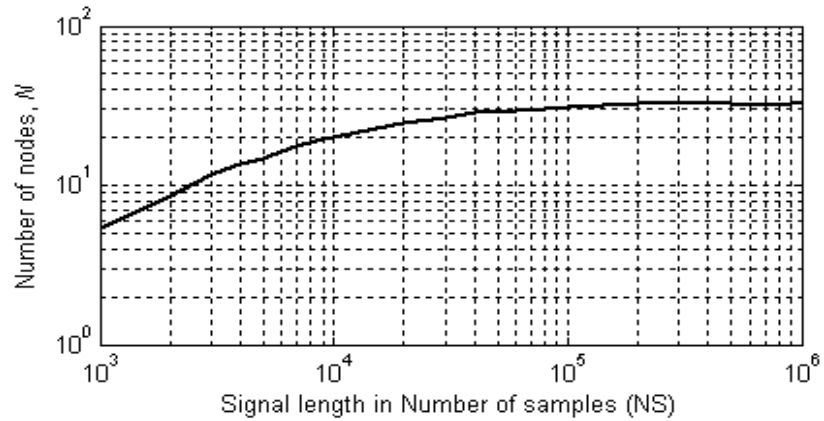


**Figure 3.33 Estimated  $N$  versus  $N_s$  plot with 32 original nodes  
(all values taken from 100 iterations and average of 1000 estimations  
with fixed  $b$  of 139 in ETP case)**

Thus, one can choose the signal length from 100,000 samples or more to estimate the number of nodes without compromising the estimation's performance. This is

discussed again in terms of the error analysis in Chapter 5 where it will be more easily understandable how the performance of the estimation system improves with increases in the signal length.

### 3.10 Effect of fractional-samples delays on estimation

In the previous section, the delays take integer values implemented in the simulation by rounding them to their nearest integers. This is an ideal case but, in practice, delays might have the fractional part which could affect the estimation process. To show the effect of the fractional parts of the delays, i.e., the fractional parts of the samples, simulations are performed using the original values and the results are plotted in Figure 3.34 and 3.35.

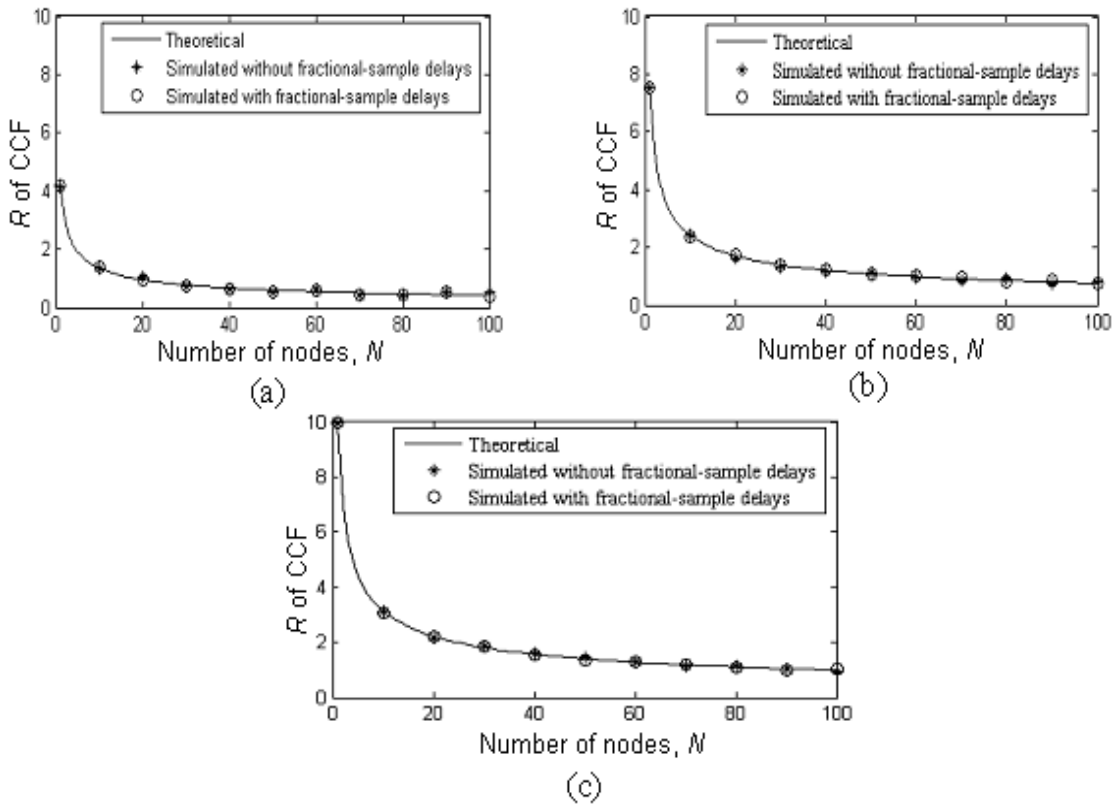


**Figure 3.34  $R$  versus  $N$  plot in ERP case: comparisons of results for theoretical, and simulated with and without fractional-sample delays:**  
(a)  $b = 19$ ; (b)  $b = 59$ ; and (c)  $b = 99$

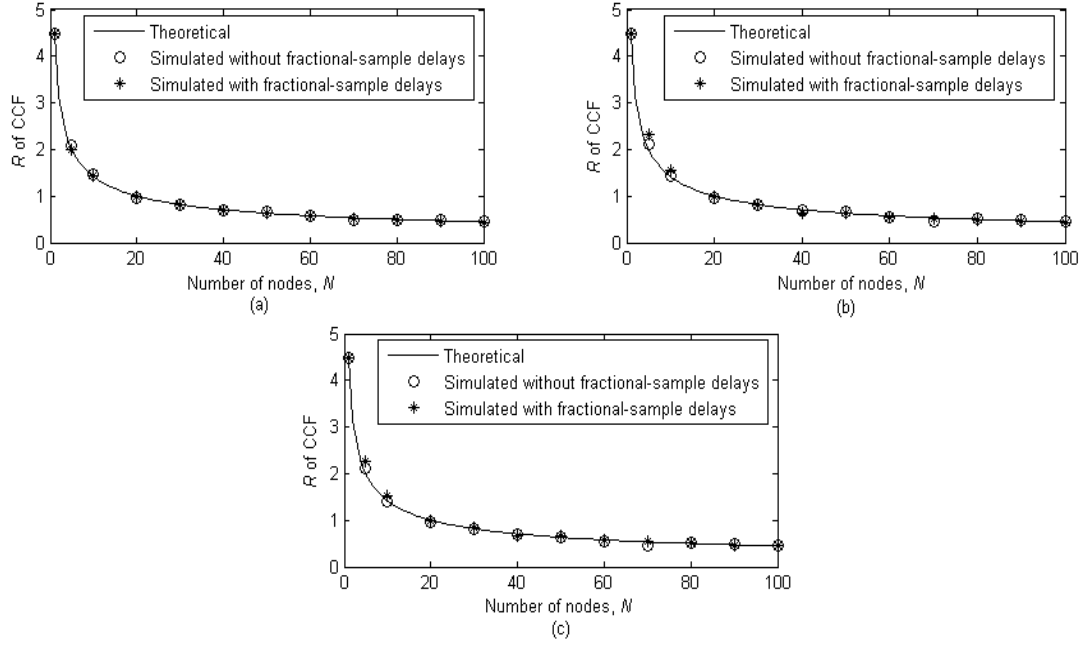


**Figure 3.35  $R$  versus  $N$  in ETP case: comparisons of results for theoretical, and simulated with and without fractional-sample delays:**  
**(a)  $k = 1$ ; (b)  $k = 1.5$ ; and (c)  $k = 2$**

Figures 3.34 and 3.35 compare the performance of the proposed technique for estimating the number of nodes considering the fractional parts of the sample delays with that of the theoretical and simulated with integer samples-delays. As can be seen from the figures the simulated results, both with and without the fractional parts of the sample delays, shows similar performance and follows the theoretical results, it does not matter whether the fractional part is considered. Thus, it is not necessary to explicitly model fractional sample delays in the theoretical analysis.

### 3.11 Effect of noise on estimation

It has already been discussed that wireless communication channels are subject to background noise and, in practice, the transmitters and receivers themselves have some internal noise which may affect the estimation process. It is important to know these effects in the proposed technique for estimating the number of nodes because, in order for the signals from the transmitter to be useful, they will have to be stronger than the noise and the range of their strengths could be decided from this analysis. In all type of noise cases, the added noises in the signals will take place in the cross-correlation i.e., if the signals are received with noise, the CCF will be due to both

noise and signal. Thus, although the effect of noise in the proposed estimation process will be similar for all types of noise (assuming AWGN), the noise strengths might be different. Here, the effect of noise is discussed for the internal noise of a receiver. Let us consider a signal received by two noisy receivers as:

$$f_1(t) = S_1(t) + S_{n_1}(t) \quad (3.44)$$

$$f_2(t) = S_2(t) + S_{n_2}(t) \quad (3.45)$$

where  $S_1(t)$  is the delayed version of the signal transmitted from the source 1 transmitter to receiver 1,  $S_2(t)$  the delayed version of the signal transmitted from the source 1 transmitter to receiver 2,  $S_{n_1}(t)$  the internal noise received in receiver 1 and  $S_{n_2}(t)$  the internal noise received in receiver 2.

Then, the CCF,  $C(\tau)$ , is (Jian-fei 2009):

$$\begin{aligned} C(\tau) &= \lim_{T \rightarrow \infty} \frac{1}{2T} \int_{-T}^T f_1(t) f_2(t - \tau) dt \\ &= \lim_{T \rightarrow \infty} \left[ \frac{1}{2T} \int_{-T}^T S_1(t) S_2(t - \tau) dt + \frac{1}{2T} \int_{-T}^T S_1(t) S_{n_2}(t - \tau) dt \right. \\ &\quad \left. + \frac{1}{2T} \int_{-T}^T S_{n_1}(t) S_2(t - \tau) dt + \frac{1}{2T} \int_{-T}^T S_{n_1}(t) S_{n_2}(t - \tau) dt \right] \\ &= C_{S_1 S_2}(\tau) + C_{S_1 S_{n_2}}(\tau) + C_{S_{n_1} S_2}(\tau) + C_{S_{n_1} S_{n_2}}(\tau) \end{aligned} \quad (3.46)$$

where  $C_{S_1 S_2}(\tau)$  is the CCF of  $S_1(t)$  with  $S_2(t)$

$C_{S_1 S_{n_2}}(\tau)$  is the CCF of  $S_1(t)$  with  $S_{n_2}(t)$

$C_{S_{n_1} S_2}(\tau)$  is the CCF of  $S_{n_1}(t)$  with  $S_2(t)$

$C_{S_{n_1} S_{n_2}}(\tau)$  is the CCF of  $S_{n_1}(t)$  with  $S_{n_2}(t)$

$\tau$  is the time delay in the cross-correlation process.

As  $S_1(t)$  and  $S_{n_2}(t)$ ,  $S_{n_1}(t)$  and  $S_2(t)$ , and  $S_{n_1}(t)$  and  $S_{n_2}(t)$  are independent random processes, their CCFs tend to be zero with the integration time extension and zero when the integration time is infinity. Thus, (3.46) becomes  $C(\tau) \approx C_{S_1 S_2}(\tau)$ . But, as in real-world problems it is not possible to take an infinite time interval, it is interesting how the cross-correlation works with finite time

integration. Details regarding these effects are discussed in this section using simulation.

To show the effect of noise in the number of nodes' estimation technique, the simulations are investigated by adding white Gaussian noise to the signals in the receivers. In the proposed node estimation technique SNR is used as the ratio of voltage levels of signal and noise unless otherwise mentioned. Sometimes it is converted to dB as for example, SNR=1 indicates 0dB, SNR=10 indicates 20dB, and so on. Figure 3.36 (a) and (b) show the results for SNR = 10 and SNR = 1 with  $N_S = 100,000$  samples for the cases with and without noise, and the theoretical. The solid line indicates those without noise, the dash-dot line those with noise and the dashed line the theoretical results. To determine whether there any difference between the results for the internal noise of the receivers and for background noise, simulation with background and internal noise is performed and the results shown in Figure 3.37. The simulation parameters are the same as those used in the basic estimation with the noise taken into account.

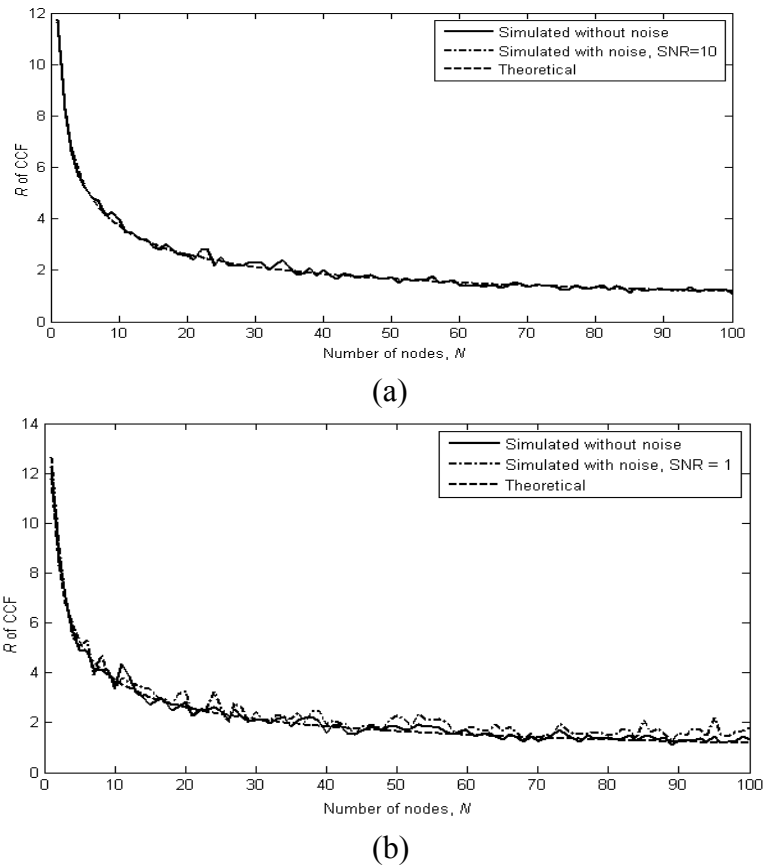


**Figure 3.36  $R$  versus  $N$  considering noise: (a) SNR = 10; and (b) SNR = 1**



The theoretical results are presented using a solid line while the three simulated results are marked by stars, circles and diamonds for without noise, receivers' internal noises and background noise, respectively. It can be seen in Figure 3.37 that simulated results for both types of noise follow similar patterns which indicates that both have similar effects on the estimation process.

From the results in Figures 3.36 and 3.37, it can be concluded that noise has an effect on estimation in which the SNR plays a vital role. Both results are taken with 100,000 samples of signal length. But, according to the noise theory of cross-correlation, the signal length also has a significant effect on estimates with noise. The significance of signal length in estimation considering the internal noises of the receivers is investigated in the following section.

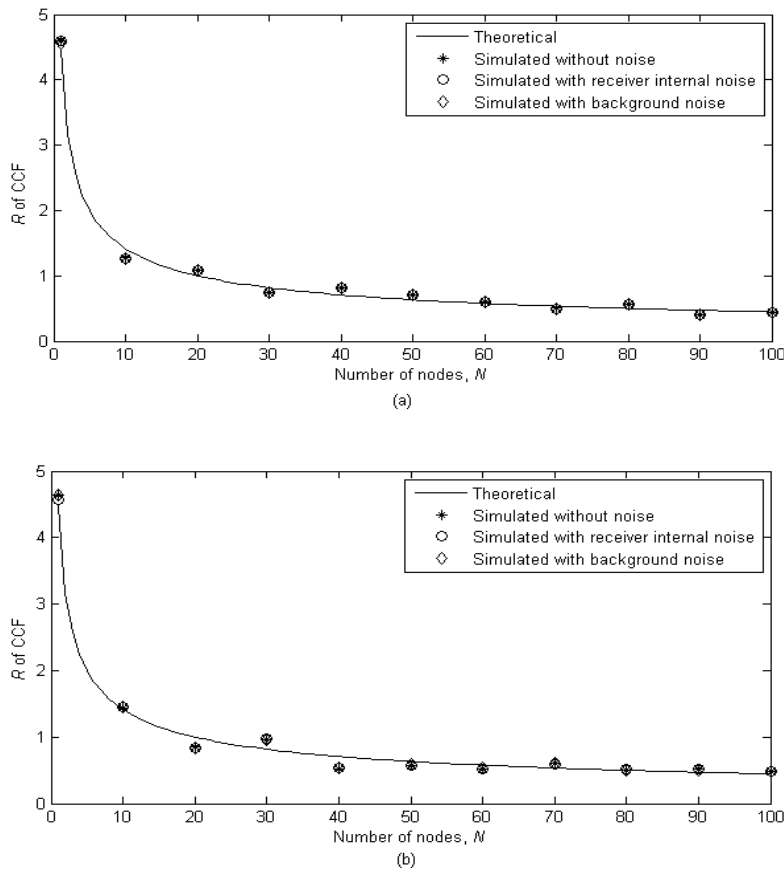


**Figure 3.37  $R$  versus  $N$  plot comparisons of results for theoretical, simulated without noise, simulated with receiver internal noise, and simulated with background noise: (a) SNR = 10; and (b) SNR = 1**

### 3.11.1 Estimation considering internal noise of the receivers

To show the effect of noise, the internal noise of the receivers is added to the estimation process. Simulations are conducted, with varying signal lengths and SNRs of the receivers for a certain number (32) of nodes. Results are given in Table 3.7 and plotted in Figures 3.38, 3.39 and 3.40 for both the ERP and ETP cases. Figure 3.38 shows the estimated  $N$  versus SNR plot for a certain signal length of 100,000 samples whereas Figure 3.39 presents the surface plots of the CV, SNR and  $N_s$ .

**Table 3.7 SNRs and corresponding estimations [ $N_s = 10^5$ ]**

SNR	Estimated $N$ : ERP case	Rounded value: ERP case	Estimated $N$ : ETP case	Rounded value: ETP case
0.001	1.1088	1	1.0308	1
0.01	1.1714	1	1.0582	1
0.05	2.5783	3	2.1923	2
0.1	5.9214	6	5.0564	5
0.5	23.1471	23	21.7998	22
1	29.5006	30	27.516	28
2	30.0510	30	29.5916	30
10	30.7269	31	30.5512	31
20	30.6989	31	30.5455	31
100	30.9369	31	30.5791	31
1000	30.922	31	30.5326	31
Without noise	31.1343	31	30.5571	31

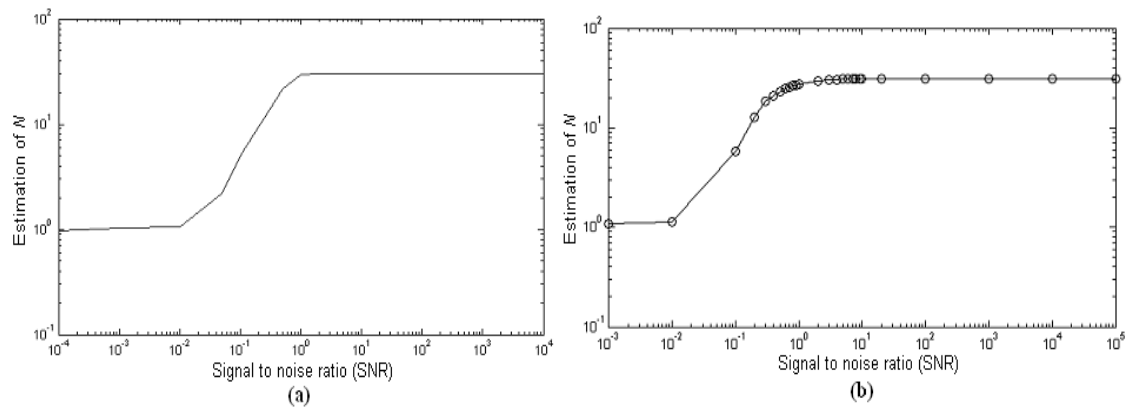
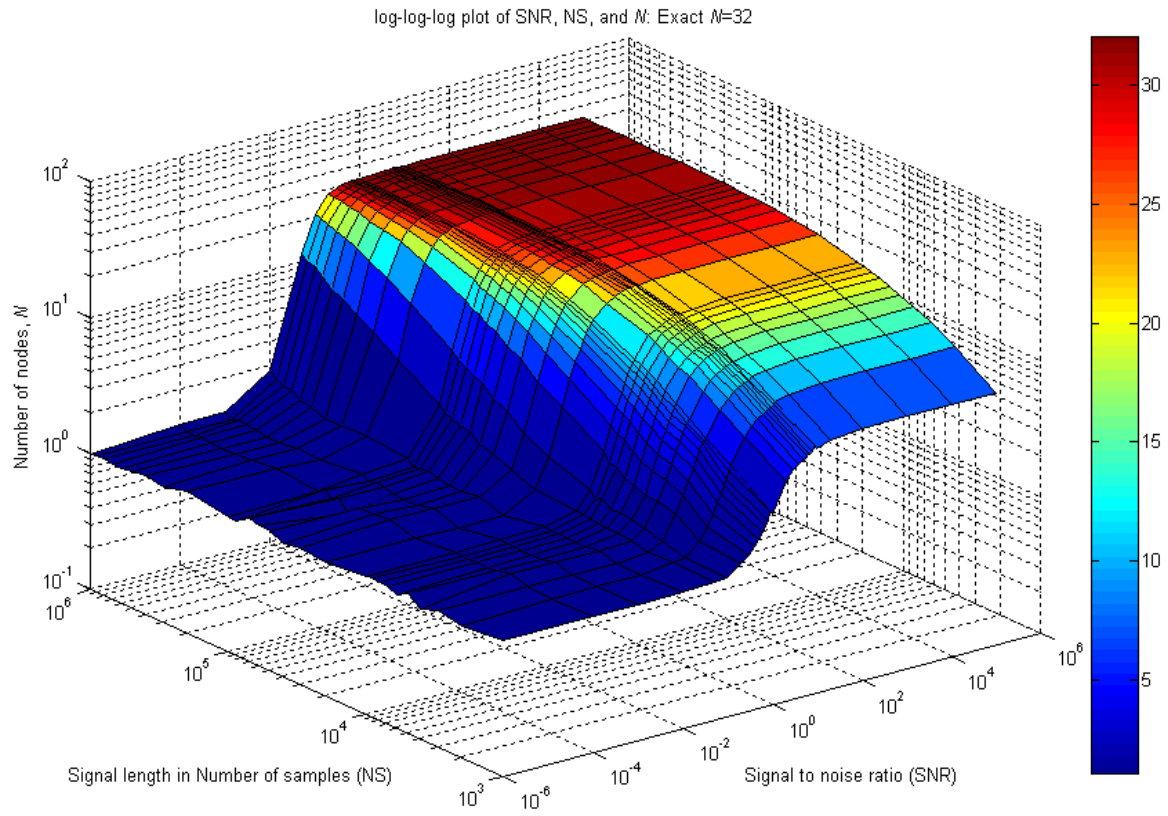
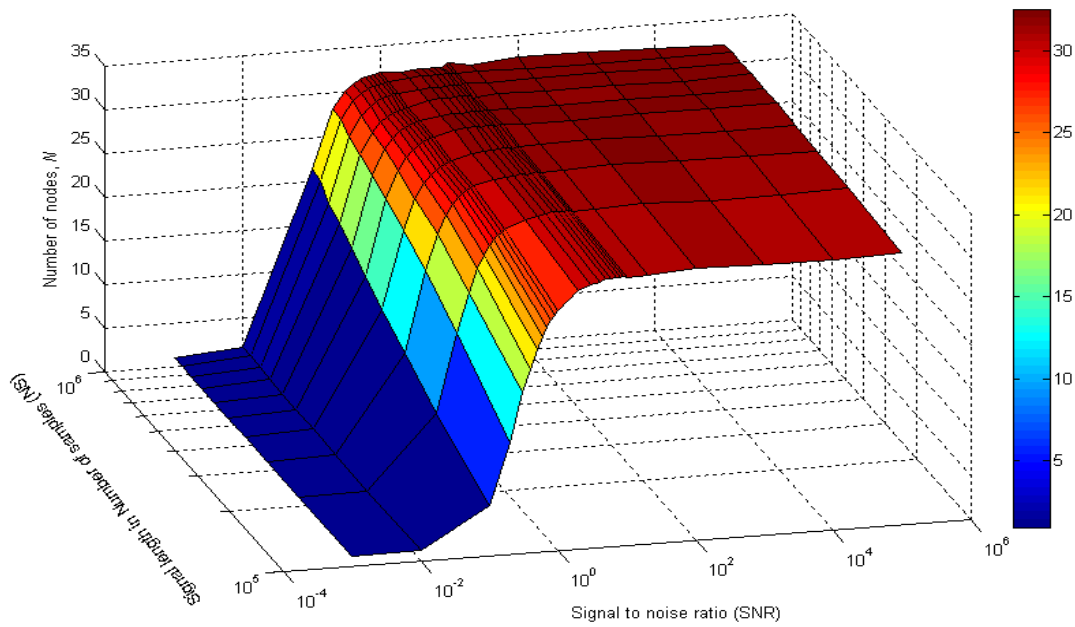


**Figure 3.38 Estimated  $N$  versus SNR: (a) ERP case; and (b) ETP case**  
( $N_s = 100,000$  samples)



(a)

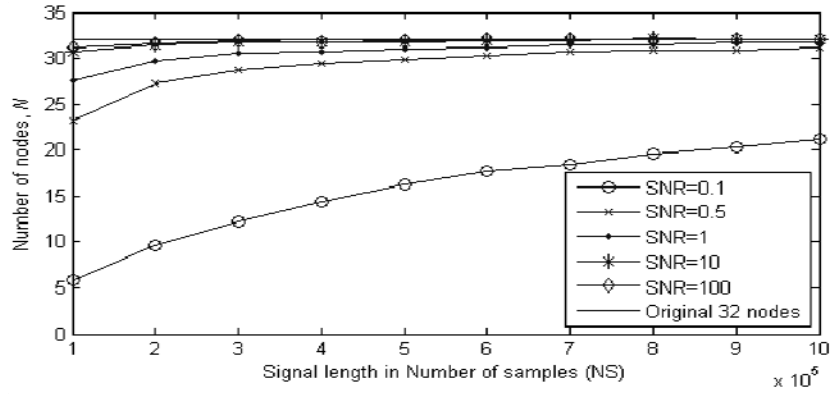


(b)

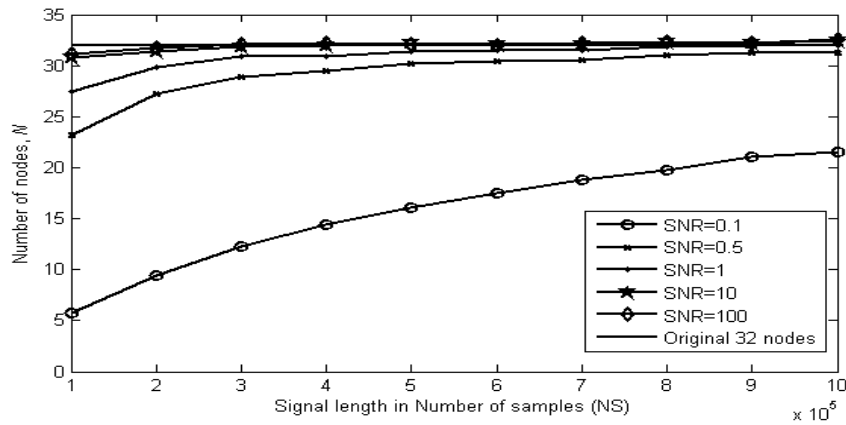
**Figure 3.39 Log-log-log plots of SNR,  $N_s$  and estimated  $N$  for  $N_s = 1000$  to 1,000,000: (a) ERP case; and (b) ETP case**

It can be seen in Figure 3.38 that, for a particular signal length of 100,000 samples and up to a certain SNR ( $\leq 0.05$ ), the estimation is constant at the worst possible value but then improves with increases in the SNR (up to SNR = 1). Finally, it becomes constant again at the best possible value as shown for the case without noise. It can also be seen from Figure 3.39 that the worst possible values will continue longer and the best possible values start later if the signal length is lower, with the opposite occurring for higher signal lengths. In other words, there is a transition zone between the worst and best possible values in which the estimation is varied with the SNR whose starting and ending points are varied with the signal length, i.e., it will start earlier with a higher signal length and later with a lower signal length. In Figure 3.40, estimations are plotted with respect to  $N_s$  (values from  $10^5$  to  $10^6$  samples) for different SNRs of 0.1, 0.2, 0.5, 1, 10 and 100, and original 32 nodes. From these results, it can be seen from the results that, for a particular SNR, the estimation performance improves with higher  $N_s$ . It needs to be mentioned that all results regarding the effect of noise on estimation are from investigations using 32 nodes. It has already been shown that the estimation process is equally suitable for any number of nodes in a ‘without noise’ case. However, to confirm, similar results for 64 nodes have been provided for ERP case in Figure 3.41. Comparisons of the results obtained for the 64 and the 32 nodes in the ERP case are shown in Figures 3.42 and 3.43. Figure 3.42 shows the surface plots and Figure 3.43 the corresponding contour plots of the SNR,  $N_s$  and estimated  $N$  for both the 64- and 32-node cases. It is clear that effect of noise is similar for any number of nodes,  $N$ , and if the SNR is sufficiently large, the method can properly estimate any  $N$  as without noise case.

From the figures, it is clear that, for SNRs greater than a certain value, the estimated  $N_s$  are almost the same (with small variations due to the randomness of the experiments). For lower SNRs the estimation is more erroneous, the performances improve with increase in SNRs and finally achieve the best possible values. That is: when the SNR is less than 1, although the noise dominates over the signal, there will be some signals which are strong enough to count; and, although we do not obtain the appropriate number, we receive a reduced number of the signal sources, i.e., nodes.



(a)



(b)

**Figure 3.40 CV versus signal length for different SNRs:**

**(a) ERP case; and (b) ETP case**

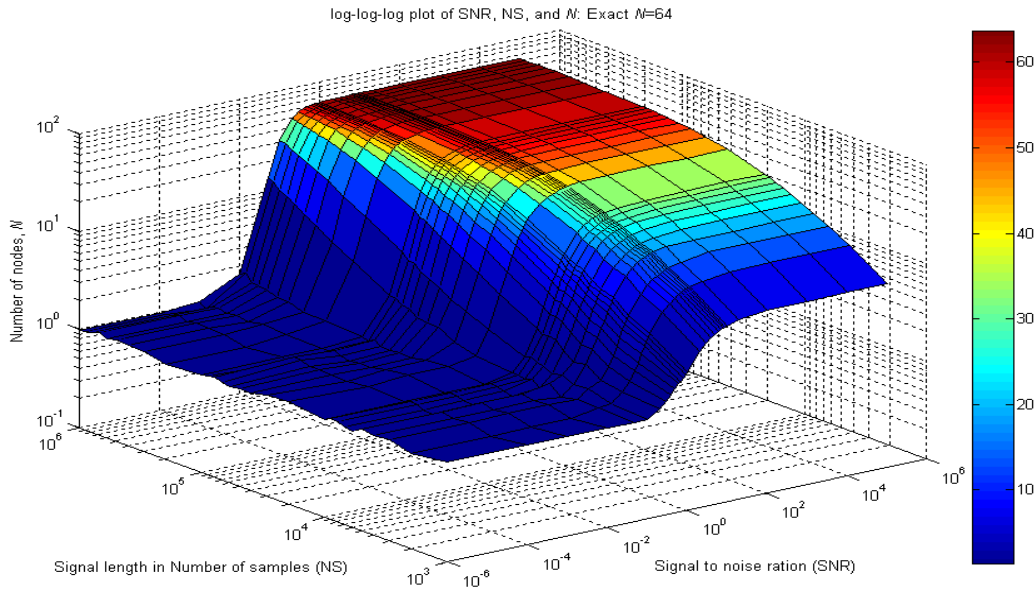


**Figure 3.41 Log-log-log plots of SNR,  $N_s$  and  $N$ : original  $N= 64$ ;  
and  $N_s = 1000$  to  $1,000,000$**

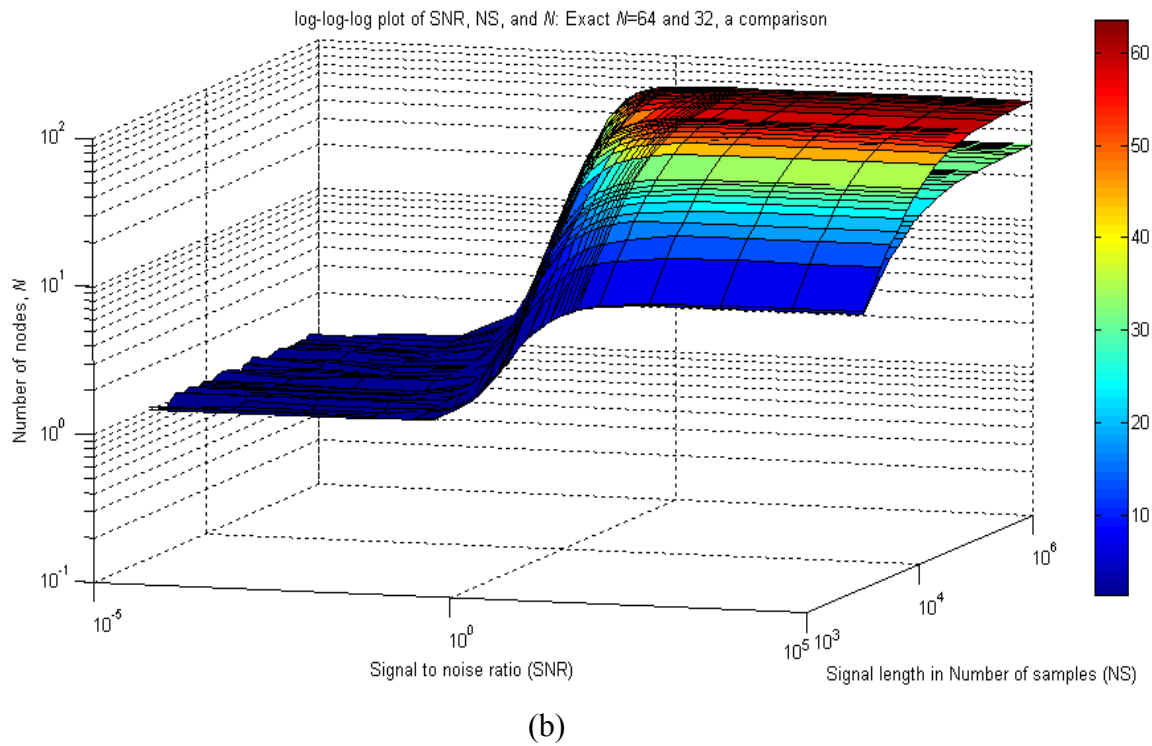
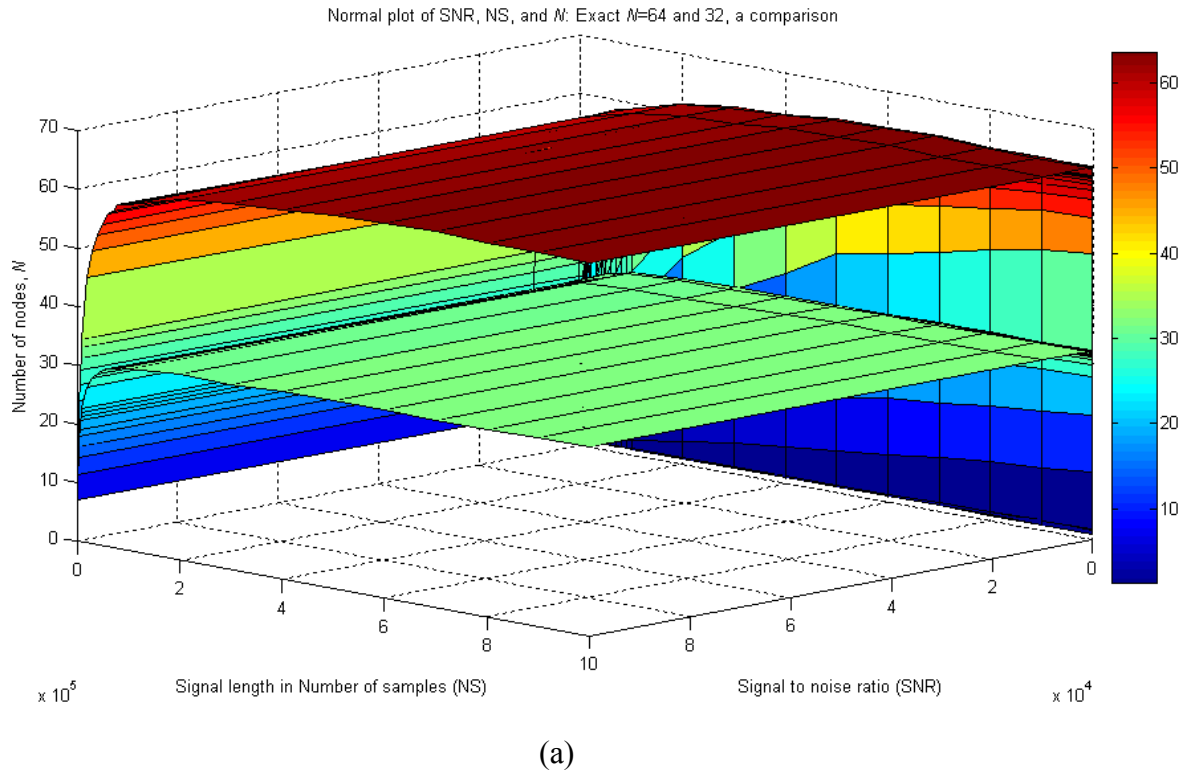
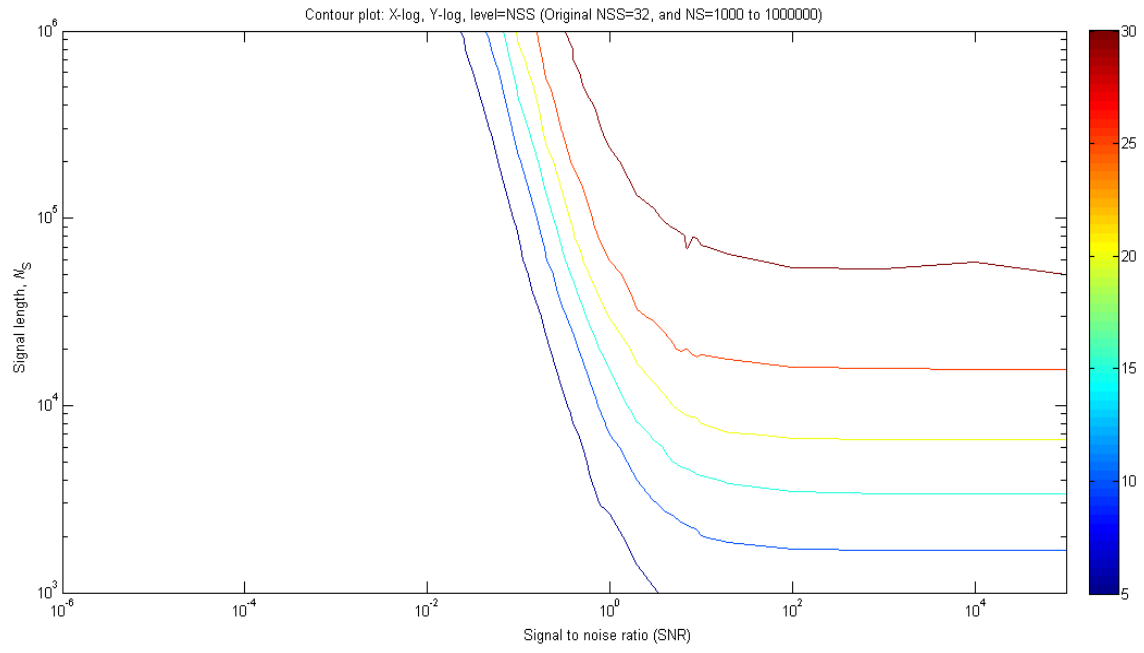
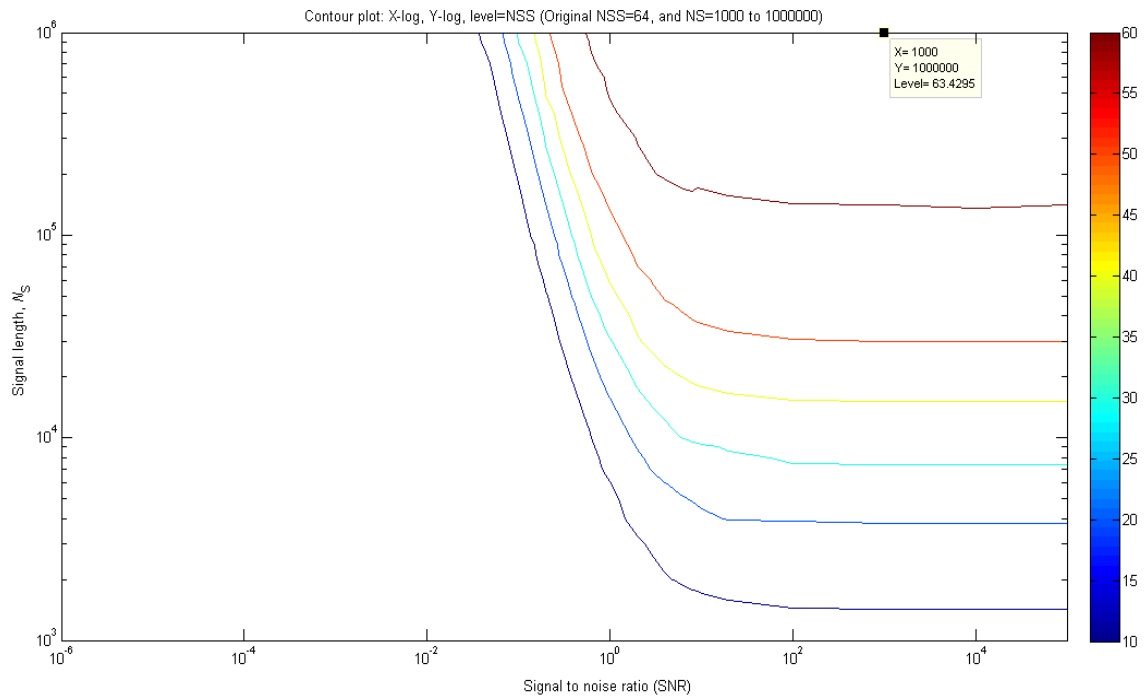


**Figure 3.42 Log-log-log plots of SNR,  $N_s$  and CV for  $N_s = 1000$  to 1,000,000:**

**(a) original  $N = 64$ ; and (b) comparison for  $N = 32$  and 64**



(a)



(b)

**Figure 3.43 Contour plots of SNR,  $N_s$  and CV for  $N_s = 1000$  to 1,000,000:**

**(a) original  $N = 32$ ; and (b) original  $N = 64$**

### **3.11.2 Conclusion**

The consideration of noise is very important in the proposed signal processing technique of estimation, especially for use in real networks. In the ideal noise free environment, the receiver will receive the desired transmitted signal successfully without noise. But in a noisy environment, the signal received will usually be corrupted by noise. Thus in a practical environment, where noise always exists, the transmitted signal will have to be with sufficient power that it overcomes the noise sufficiently (that is, there is a sufficient SNR). The effect of noise also varies with the variation in signal length (which determines the integration time of the cross-correlation process), the longer the signal length the lower the effect and vice-versa.

This section properly investigates the estimation process with taking the noise into consideration. It is shown that proper selection of signal strength gives the estimation performance similar to the ideal (without noise) case. It is clear from the investigations that an SNR of 20dB (signal is 10 times stronger than noise) is sufficient to neglect the noise effect in the proposed estimation process.

Although protocol techniques to estimate the number of nodes are different in some aspects, they face similar problems in the presence of noise. In fact, in the protocol technique, the transmitter transmits a number of bits with the carrier signal using a modulation technique through the channel in a manner similar to that of the CC technique. Although there is no literature to show the effect of noise in the number of nodes estimation process using the protocol technique, it is shown in at least one work (Heinzelman 2000) that a protocol requires an SNR of at least 30dB to receive the signal without error.

### **3.12 Effects of multipath propagation on estimation**

In the previous sections, in order to obtain the CCF in the simulation process, only the line-of-sight signals are considered. This is an ideal case but, in practice, signals might be a mixture of the line-of-sight and some reflected signals due to the reflector present in the medium and the dispersive nature of the wave. So, to make the



estimation process robust, an analysis of multipath effects on estimation is required. In the underwater environment with an acoustic wave, the seabed and sea surface will be the two major reflectors. To show the effect of this multipath on estimation, simulations are performed, firstly using only the bottom reflection, and then using both the bottom and surface reflections.

### 3.12.1 Estimation of $N$ in multipath environment

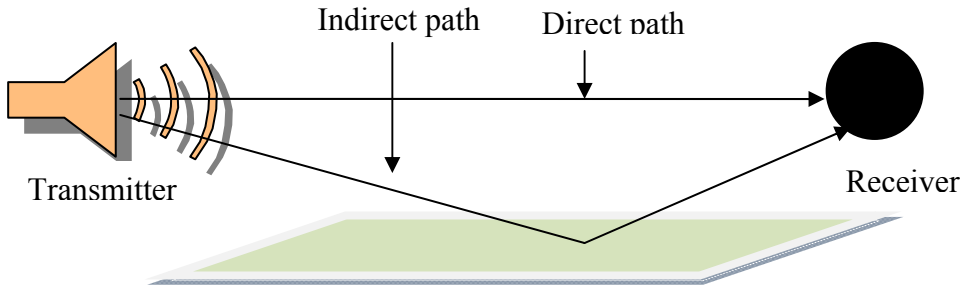


**Figure 3.44 Concept of typical multipath**

Consider that a transmitter emits a Gaussian signal,  $S_1(t)$ , which is infinitely long. If the signal propagates in two (one direct and one reflected) paths, as shown in Figure 3.44, the signal received by the receiver will be:

$$S_{r_{11}}(t) = \alpha_{11}S_1(t - \tau_{11}) + \alpha_{m11}S_1(t - \tau_{m11}) \quad (3.47)$$

Similarly, if there is another receiver in the communication range as is in the proposed technique, then the signal received by that receiver will be:

$$S_{r_{12}}(t) = \alpha_{12}S_1(t - \tau_{12}) + \alpha_{m12}S_1(t - \tau_{m12}) \quad (3.48)$$

In (3.47) and (3.48),  $\alpha$ 's are the attenuations due to absorption and dispersion present in the medium and  $\tau$ 's the time delays for the signal to reach the sensors. Attenuations  $\alpha_{11}$  and  $\alpha_{12}$  are for the direct paths, and  $\alpha_{m11}$  and  $\alpha_{m12}$  for the indirect paths whereas the delays,  $\tau_{11} = d_{11}/S_p$  and  $\tau_{12} = d_{12}/S_p$ , are for the direct paths and  $\tau_{m11} = d_{m11}/S_p$  and  $\tau_{m12} = d_{m12}/S_p$  for the indirect paths.

Assuming  $\tau = d_{DBS} / S_p$  is the time shift in the cross-correlation, the CCF is:

$$\begin{aligned}
C(\tau) &= \int_{-\infty}^{+\infty} S_{r_{11}}(t) S_{r_{12}}(t - \tau) d\tau \\
&= \alpha_{11} \alpha_{12} \int_{-\infty}^{+\infty} S_1(t - \tau_{11}) S_1(t - \tau_{12} - \tau) d\tau + \\
&\quad \alpha_{m11} \alpha_{m12} \int_{-\infty}^{+\infty} S_1(t - \tau_{m11}) S_1(t - \tau_{m12} - \tau) d\tau + \\
&\quad \alpha_{11} \alpha_{m12} \int_{-\infty}^{+\infty} S_1(t - \tau_{11}) S_1(t - \tau_{m12} - \tau) d\tau + \\
&\quad \alpha_{m11} \alpha_{12} \int_{-\infty}^{+\infty} S_1(t - \tau_{m11}) S_1(t - \tau_{12} - \tau) d\tau \\
&= C_{dd}(\tau_{dd}) + C_{ii}(\tau) + C_{di}(\tau) + C_{id}(\tau)
\end{aligned} \tag{3.49}$$

where  $C_{dd}(\tau)$  is the CCF due to the direct paths

$C_{ii}(\tau)$  is the CCF due to the indirect paths

$C_{di}(\tau)$  is the CCF due to the direct and indirect paths

$C_{id}(\tau)$  is the CCF due to the indirect and direct paths

and  $\tau$ 's are the delay differences between the signals in the cross-correlation process.

It can be seen that all signals in this cross-correlation process are correlated as they are generated from the same transmitter but they will differ in strength and delay in reaching the receivers. So, the four terms in the right-hand side of (3.49), as they are Gaussian, produce four delta functions which are placed according to their delay differences. Of them, the deltas due to similar paths occupy positions between the receivers whereas those due to opposite paths occupy positions outside the place between the receivers. In the proposed method of estimating the number of nodes, the place between the receivers is the region of interest. Thus, for a particular transmitter with two paths (one direct and one indirect), there will be two deltas in the region of interest. This is equivalent to the cross-correlation with two transmitters just considering the indirect path is coming from an image transmitter as shown in Figure 3.45.

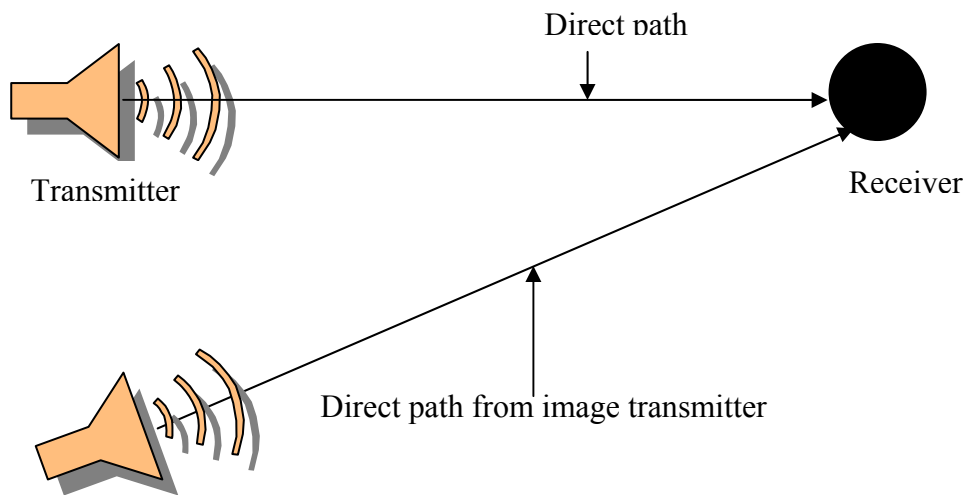


**Figure 3.45 Concept of image transmitter**

Now, if more than one transmitter exists, as shown in Figure 3.46, the CCF will be formed by the number of deltas equal to twice the number of transmitters. The strengths of the deltas will be equal if the direct and reflected signals are of equal power, as shown by the simulated results in Figure 3.47. Figure 3.47 (a), (b), and (c) show the CCF due to both the direct and reflected, only the reflected, and only the direct signals, respectively.

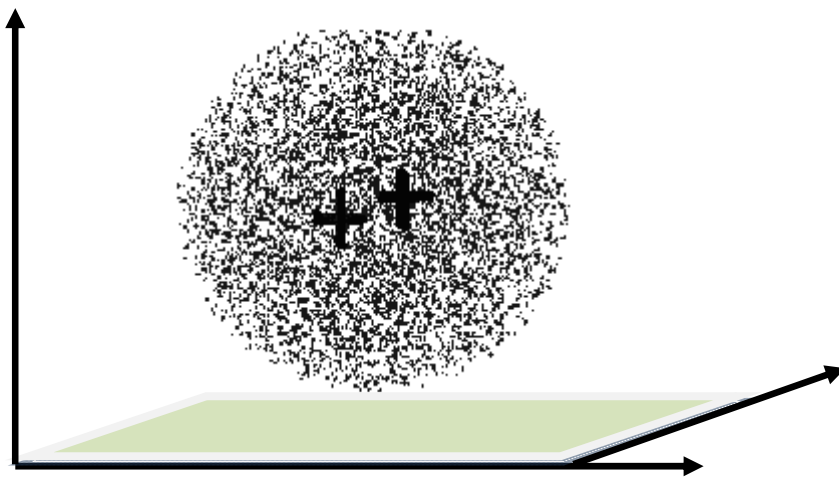


**Figure 3.46 Distributions of transmitters and receivers with one reflector**

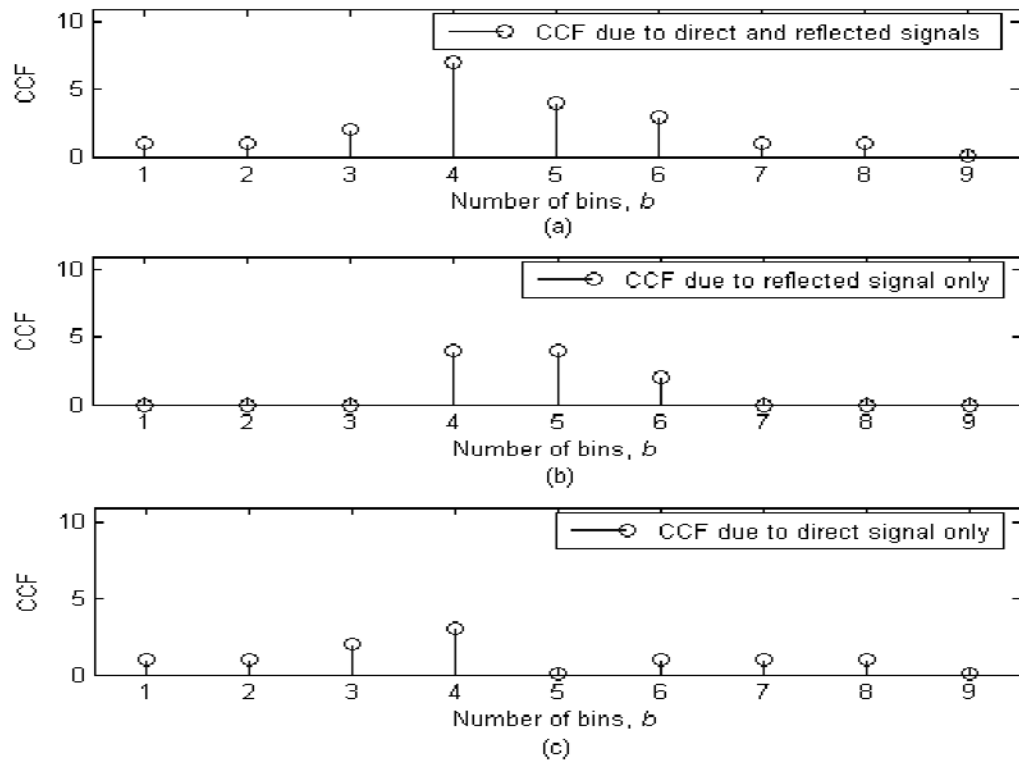


**Figure 3.47 CCFs due to: (a) both direct & reflected signals; (b) only reflected signal; and (c) only direct signal [using 1 iteration with  $k = 0$ ]**

However, in reality, the powers will be different in the direct and reflected paths depending on the dispersion coefficient,  $k$ , and the estimation process. Here, we consider the ERP case for the investigation of multipath effects. In this case, the emitted power from each node will have to be such that the powers received at the sensors will be the same. This is possible by employing a proper probing technique for line-of-sight communication, i.e., direct path signals. In the case of reflection, there will be an indirect path(s) signal to reach the sensors whose powers will depend on attenuation in the medium which, in turn, depends on  $k$ . As the direct path is always less than the indirect path and their powers are inversely proportional to the path length, the powers of the direct path signals will be stronger than those of the indirect path signals. It is also known that the signals' strengths are responsible for the strengths of the deltas in the CCF. Thus, the deltas due to the direct path will be dominant and contribute more to form the CCF, as shown in the simulated results in Figure 3.48 for a certain case of the dispersion coefficient,  $k = 3$ , 9 number of bins and 10 nodes.

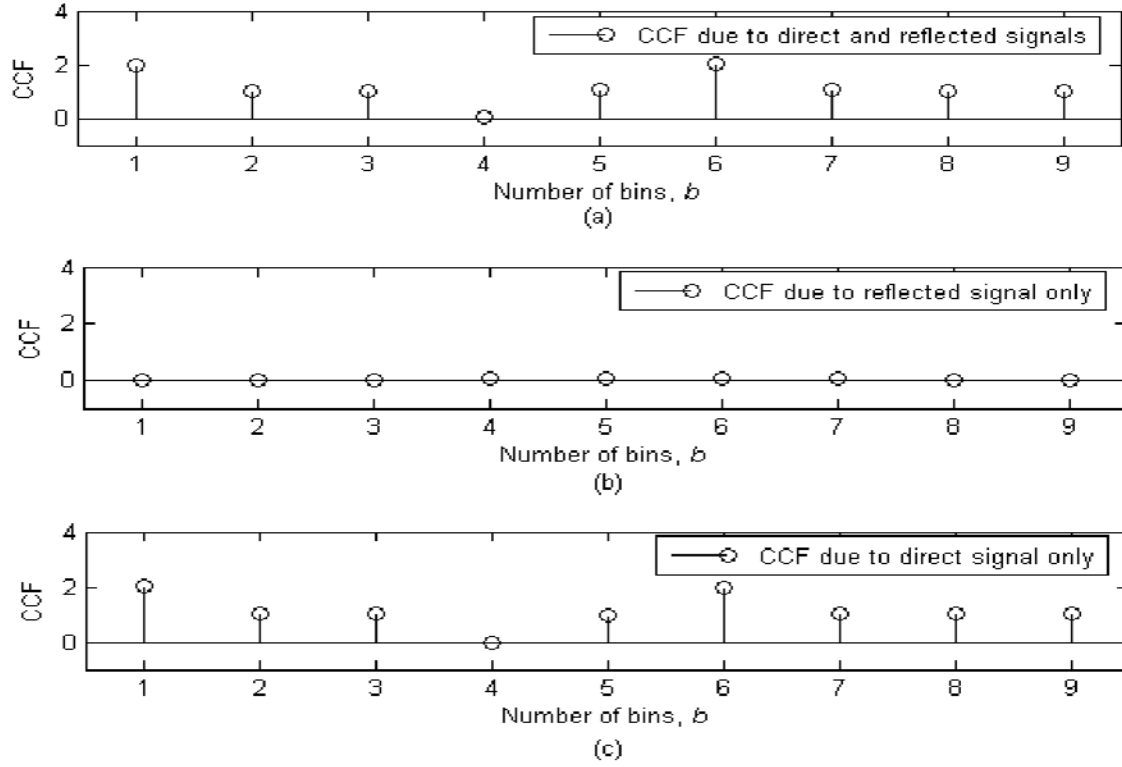


**Figure 3.48 CCFs due to: (a) both direct & reflected signals; (b) only reflected signal; and (c) only direct signal [using 1 iteration with  $k = 3$ ]**

It has been demonstrated that deltas without multipath, i.e., with only direct paths, follow a random distribution to form the CCF. This will also be true for deltas with indirect paths. Thus, the CCF with a multipath is the summation of two random variables. To estimate the number of nodes using the ratio of the standard deviation to the mean of the CCF considering the multipath, the following demonstration is necessary.

Considering two random variables (two CCF),  $X$  (CCF from direct path signals cross-correlation) and  $Y$  (CCF from indirect path signals cross-correlation), it is well known that the variance in their summation,  $X+Y$ , can be defined as:

$$\text{Var}(X + Y) = \text{Var}(X) + \text{Var}(Y) + 2 \times \text{Covariance}(X, Y) \quad (3.50)$$

Denoting the variance of  $X+Y$ ,  $X$  and  $Y$  as  $\sigma_{X+Y}^2$ ,  $\sigma_X^2$ , and  $\sigma_Y^2$ , respectively, and the covariance between  $X$  and  $Y$  as  $\sigma_{XY}^2$ , the expression (3.50) will become:

$$\sigma_{X+Y}^2 = \sigma_X^2 + \sigma_Y^2 + 2\sigma_{XY}^2 \quad (3.51)$$

Using the correlation coefficient,  $\rho_{XY}$ , instead of the covariance, the expression (3.51) might be written as:

$$\sigma_{X+Y}^2 = \sigma_X^2 + \sigma_Y^2 + 2\rho_{XY}\sigma_X\sigma_Y \quad (3.52)$$

Thus, the standard deviation of the summation of two random variables from (3.52) will be:

$$\sigma_{X+Y} = \sqrt{\sigma_X^2 + \sigma_Y^2 + 2\rho_{XY}\sigma_X\sigma_Y} \quad (3.53)$$

If the variables (two CCF) are independent or weakly dependent, i.e.,  $\rho_{XY} \cong 0$ , the above expression can be reduced to:

$$\sigma_{X+Y} = \sqrt{\sigma_X^2 + \sigma_Y^2} \quad (3.54)$$

In addition, the expectation of the sum of two random variables is expressed as:

$$\mu_{X+Y} = \mu_X + \mu_Y \quad (3.55)$$

Thus, the ratio of the standard deviation to the mean of the CCF is:

$$R_{X+Y} = \frac{\sigma_{X+Y}}{\mu_{X+Y}} = \frac{\sqrt{\sigma_X^2 + \sigma_Y^2}}{\mu_X + \mu_Y} \quad (3.56)$$

Again, in the case of different scaling of the variables, one standard deviation will be greater than the other, which will also be true for the expectation and, if the variables' scaling are sufficiently different, e.g., if  $\sigma_X \gg \sigma_Y$  and  $\mu_X \gg \mu_Y$ , the expression of  $R_{X+Y}$  can be written as:

$$R_{X+Y} = \frac{\sigma_X}{\mu_X} \quad (3.57)$$

Now, in the proposed method of estimation of the number of nodes considering the multipath (taking into account only two paths, one direct and one indirect), the CCF can be considered to be the summation of two random variables. Then, as the scaling of the direct path will be sufficiently dominant, according to expression (3.57),  $R_{X+Y}$  can be approximated by the ratio,  $R$  of the standard deviation to the mean of the part of the CCF due to the direct path. It was discussed earlier that the CCF with only the direct path follows the binomial distribution. Thus, using the binomial distribution, the estimation parameter,  $R$ , is presented in Figure 3.49.

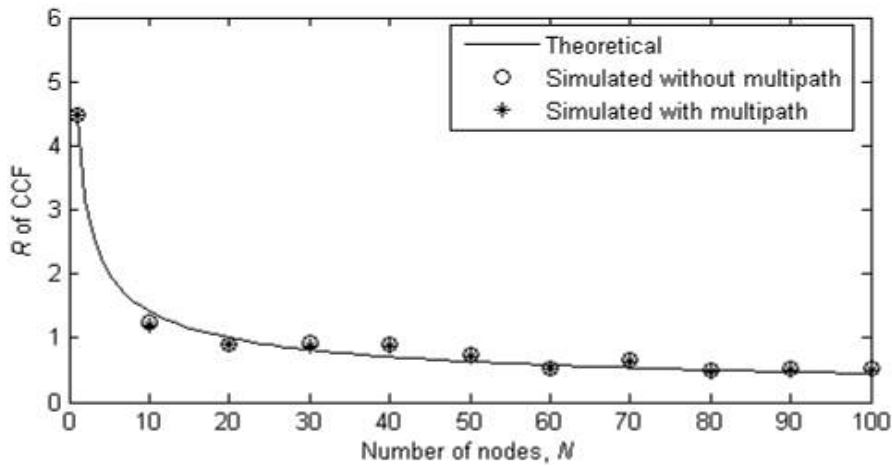


**Figure 3.49  $R$ s of CCF:  $k=3$**

The results in Figure 3.49 show the effectiveness of the proposed method in case of multipath reception of signals by the sensors. The solid line indicates the theoretical results and the stars and circles the simulated results with and without a multipath, respectively. It can be seen that the two simulated results are sufficiently close to each other and both follow the theoretical results.

Now, if we consider that one direct and two indirect paths are present in the signals, as shown in Figures 3.50 and 3.51, the CCF will be the summation of three random variables and the random variable due to the direct path will still be sufficiently dominant to form the CCF. Thus, expression (3.57) of the ratio of the standard deviation to the mean of the CCF will still be valid. The results for the estimation parameter,  $R$ , are provided in Figure 3.52 for both the surface and bottom reflections.

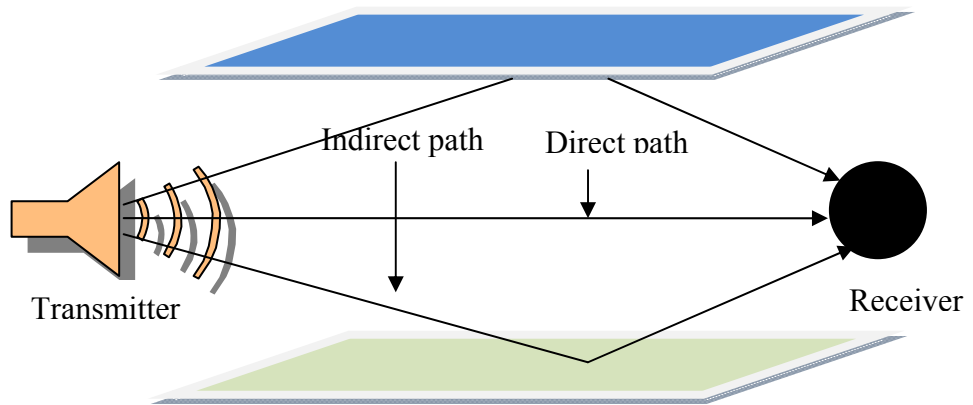


**Figure 3.50 Concept of multipath: one direct and two indirect paths**

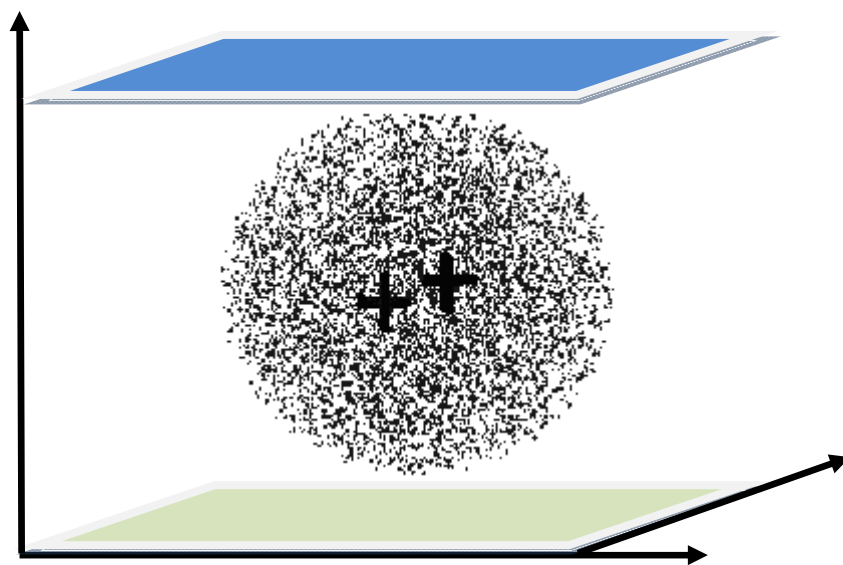


**Figure 3.51 Distributions of transmitters and receivers with two reflectors**

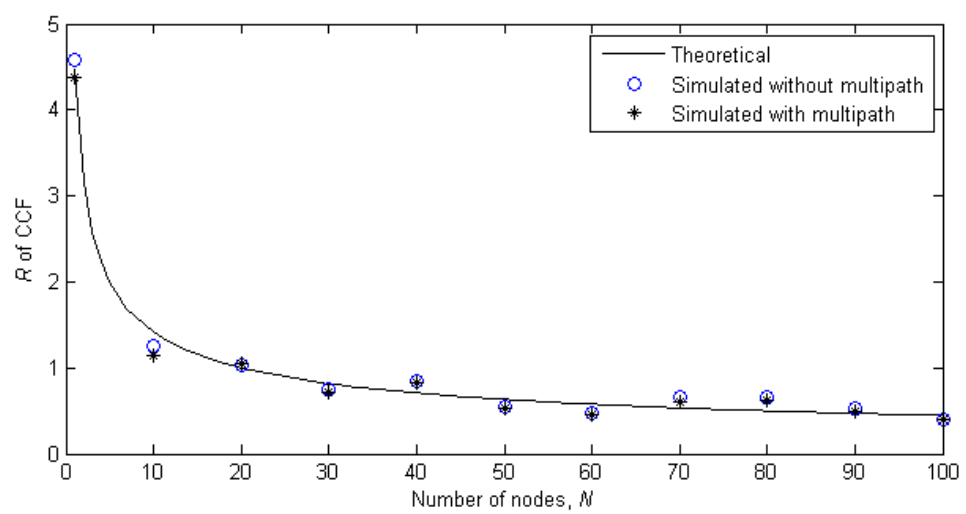


**Figure 3.52  $R$  of CCF:  $k=3$**



### 3.12.2 Explanation of multipath effects in Deep Ocean

If we consider a refraction-free absorptionless medium,  $\alpha_{11}, \alpha_{12}$  depend on only the spreading loss and  $\alpha_{m11}, \alpha_{m12}$  on the spreading loss as well as the reflection coefficient. Medwin (2005) tells us that the largest possible value of the reflection coefficient for any type of interface (i.e., soft or hard) will be 1. So, assuming that value, attenuation in the indirect path is also dependent on only the spreading loss.

Generally, the spreading loss can be expressed as  $L_p = d^{-k}$ , where  $d$  is the range and  $k$  the spreading factor. Spreading factor,  $k$  varies between 1 to 6, depending on the communication signals and environments. In this discussion, the value of  $k$  is again taken as 3 to show the negligible effect of multipath propagation. The robust multipath effect will have been discussed for all  $k$  in the next section.

So, the attenuation factors of the direct and indirect paths can be expressed as:

$$\begin{aligned}\alpha_{11} &= d_{11}^{-k/2} \\ \alpha_{12} &= d_{12}^{-k/2}\end{aligned}\tag{3.58}$$

and

$$\begin{aligned}\alpha_{m11} &= d_{m11}^{-k/2} \\ \alpha_{m12} &= d_{m12}^{-k/2}\end{aligned}\tag{3.59}$$

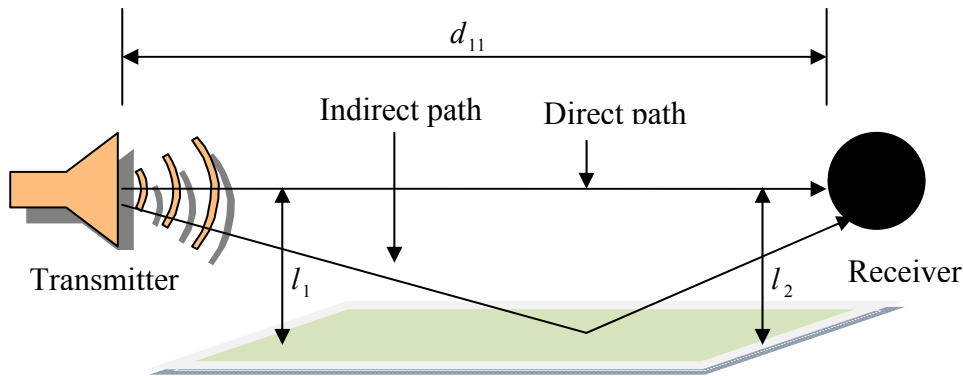


**Figure 3.53 Explanation of single reflection**

If the ranges of the direct paths are sufficiently smaller than those of the indirect paths, i.e., if  $d_{m11} \gg d_{11}$  and  $d_{m12} \gg d_{12}$ , the attenuation factors of the indirect paths will be sufficiently small compared with those of the direct paths, i.e.,  $\alpha_{m11} \ll \alpha_{11}$  and  $\alpha_{m12} \ll \alpha_{12}$ .

It is discussed in the literature (Urlick 1983) that, if a transmitter is sufficiently close to its receiver, the above assumption will be true. The possible distance ranges are expressed in (Urlick 1983) as  $d_{11} \leq 2(l_1 l_2)^{\frac{1}{2}}$ , where the symbols indicating the lengths are shown in Figure 3.53, and are defined as the near field. Distances beyond these ranges are defined as, firstly, interference and then far field. In the interference field, the indirect path's distance becomes closer to that of the direct path and, after a certain distance; their lengths are almost equal which is the start of the far field. In the case of the near field having some portion of the interference field close to it (with higher  $k$  values), the term  $\alpha_{m11} \times \alpha_{m12}$  in the cross-correlation will be far less than the term  $\alpha_{11} \times \alpha_{12}$ .

Thus, if the transmitters fall within the near field and some portion of the interference field is close to the near field, the contribution of the indirect path to the CCF will be negligible and could be assumed by the CCF of the direct path only. Similarly, if a transmitter falls in the interference field close to the far field, the contribution of the indirect path to the CCF starts to become significant and will be similar to that of the direct path when the transmitter falls in the far field. In our simulation, the dimension of the cube is 2000 m and the receivers are placed at the middle of the cube. Assuming the surface and bottom reflectors are placed at the boundaries of the cube, the simulation setup mostly fulfils the criteria of neglecting the effect of the indirect paths on the CCF with higher values of  $k$ .

### 3.12.3 Near-field range to neglect multipath effect

After some manipulation, it can be shown from the expression  $d_{11} \leq 2(l_1 l_2)^{\frac{1}{2}}$  that, in the proposed simulation setup, the CCF will follow the near field placement of the

transmitter if the radial distance of the reflector plane i.e. surface or bottom from the receiver follows the relationship:

$$l_2 \geq \frac{d_{11}^2}{4l_1}$$

where  $l_2$  is the radial distance of the receiver from the reflector plane,  $d_{11}$  the radial distance of the receiver from the source, and  $l_1$  the radial distance of the source from the reflector plane. Placement of the network following the above relation will be helpful to neglect the multipath effect in the proposed estimation process.

### 3.12.4 Robust estimation technique in multipath environment

Previous sections demonstrate how multipath effects can be neglected in the estimation process as is possible in the case of a high dispersion factor. In this section, a robust estimation approach, which can estimate using any dispersion factor, is provided.

#### 3.12.4.1 Considering a direct and a reflected path

Now, to properly demonstrate the estimation with multipath effects, let us consider a similar experimental setup to that for the ERP case with a 3D spherical distribution of the nodes underwater. Two sensors have to be placed at the centre of the sphere and their orientations will have to be parallel to the seabed which is considered to be the only reflector, i.e., the cause of the multipath. The theoretical & simulated results for the CCF from such a setup for 100 nodes with 9 bins, 100 iterations, and for different  $k$  values are shown in Figures 3.54 to 3.57. These four figures have different dispersion coefficient,  $k$ , values of 0, 1, 1.5 and 2, respectively. In each figure, there are three separate plots: the top for the CCFs with multipath, i.e., both direct and indirect path signals are responsible for forming the CCF; the middle the CCFs due to only the reflected (bottom) signal; and the bottom the CCFs due to only the direct signal, i.e., without a multipath as in the earlier ERP case. It has already been demonstrated that a delta without a multipath, i.e., with only a direct path, follows a random distribution to form the CCF. This is also true for the deltas with indirect

paths. Thus, the CCF with a multipath will be the summation of two random variables.

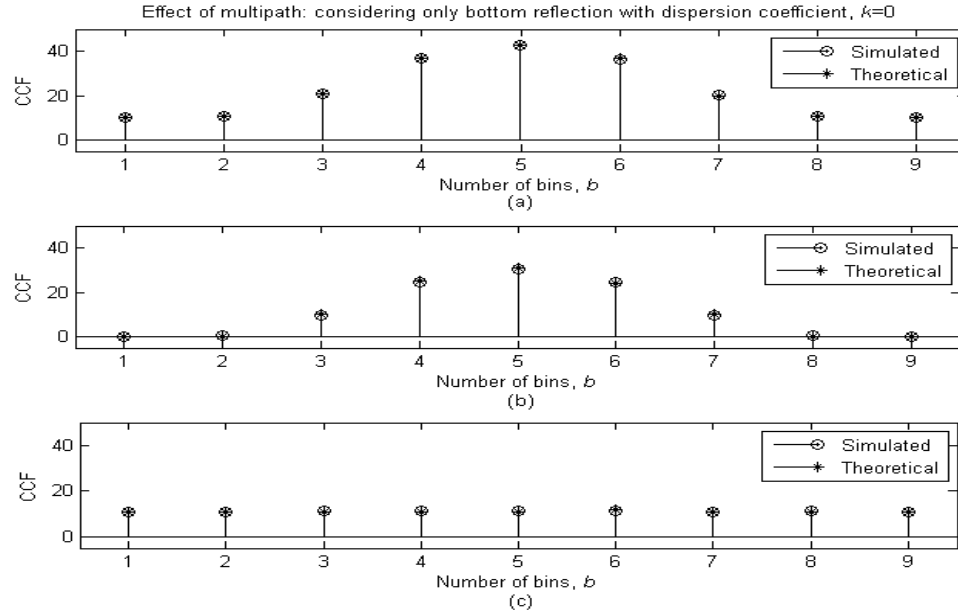


**Figure 3.54 CCF with  $k = 0$  from: (a) direct and bottom reflected signals; (b) only bottom reflected signal; and (c) only direct signal**

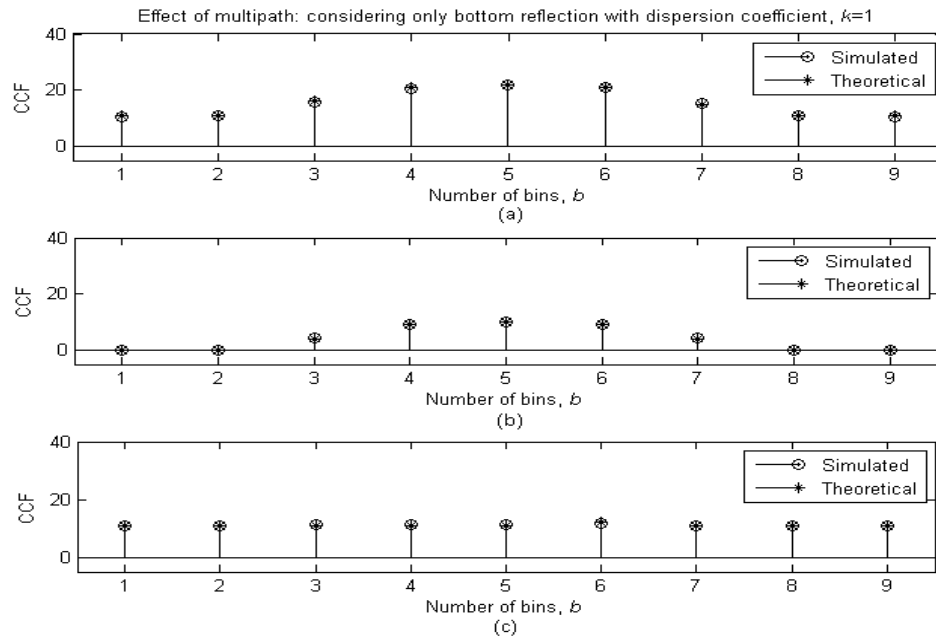


**Figure 3.55 CCFs with  $k = 1$  from: (a) direct and bottom reflected signals; (b) only bottom reflected signal; and (c) only direct signal**

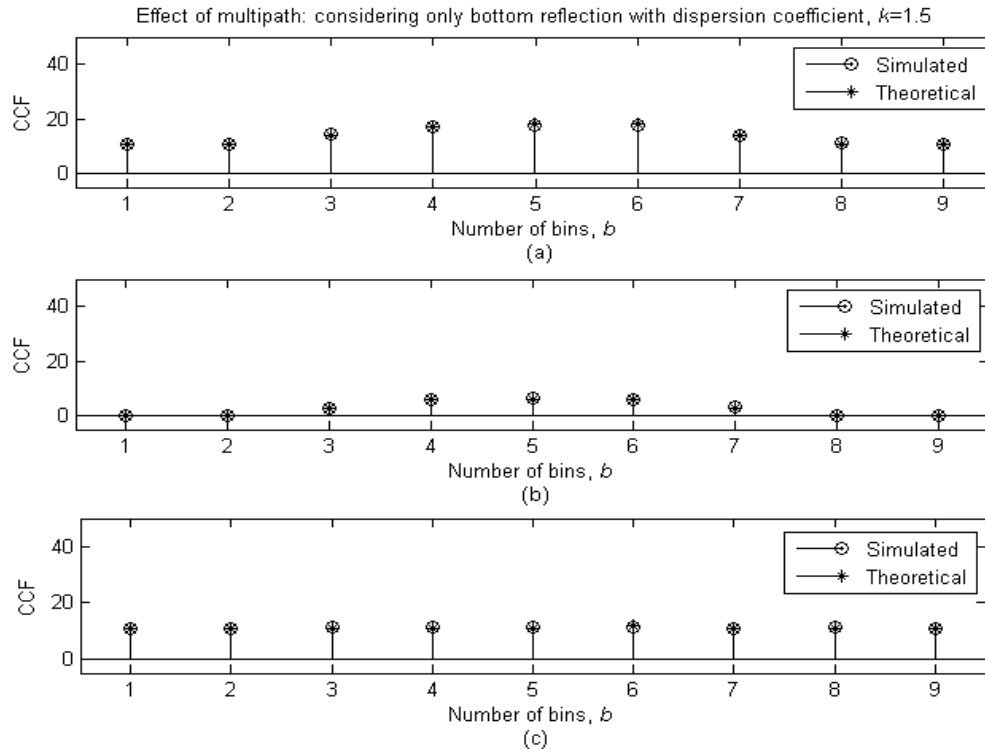


**Figure 3.56 CCFs with  $k = 1.5$  from: (a) direct and bottom reflected signals; (b) only bottom reflected signal; and (c) only direct signal**

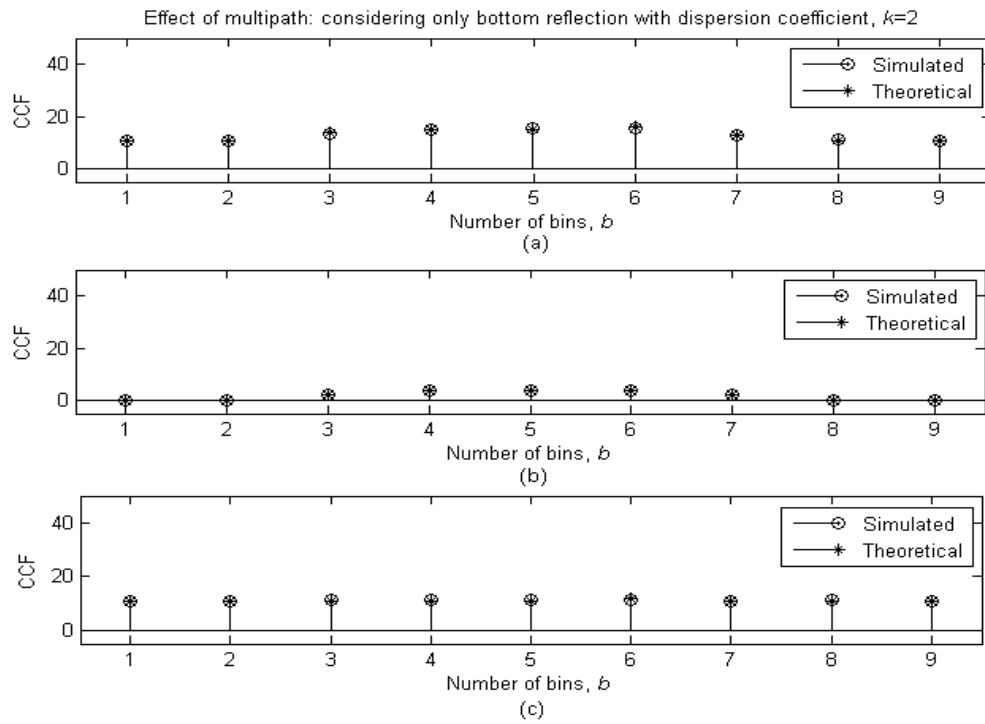


**Figure 3.57 CCFs with  $k = 2$  from: (a) direct and bottom reflected signals; (b) only bottom reflected signal; and (c) only direct signal**

To clarify the above discussion, Figures 3.58 to Figure 3.60 are plotted.

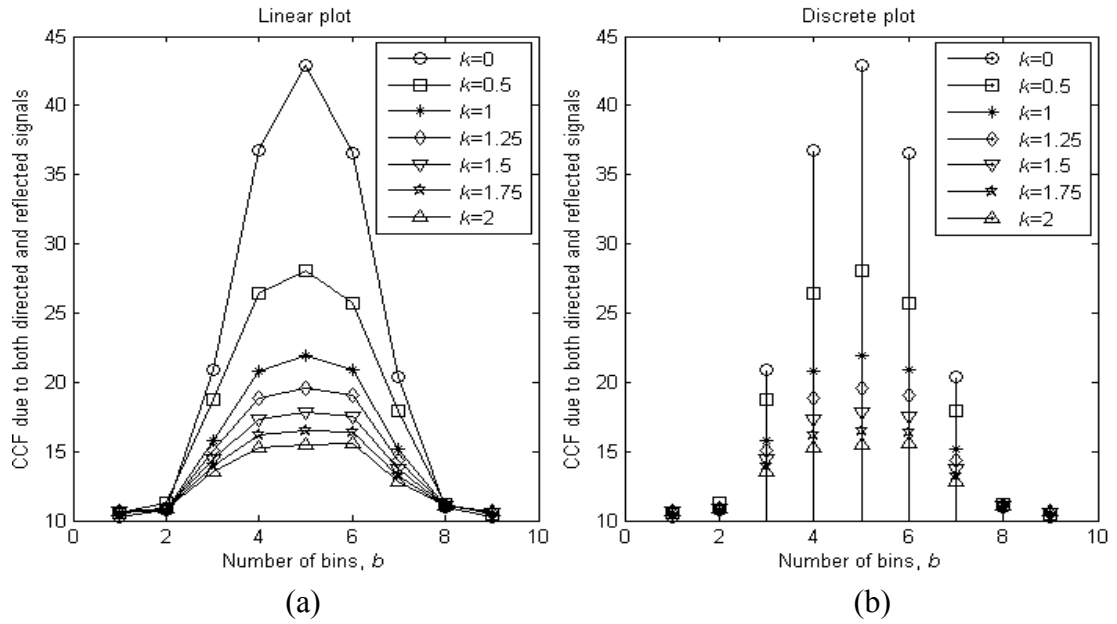


**Figure 3.58 CCFs with different  $k$  (0, 0.5, 1, 1.25, 1.5, 1.75 and 2) from direct and bottom reflected signals: (a) linear plot; and (b) discrete plot**

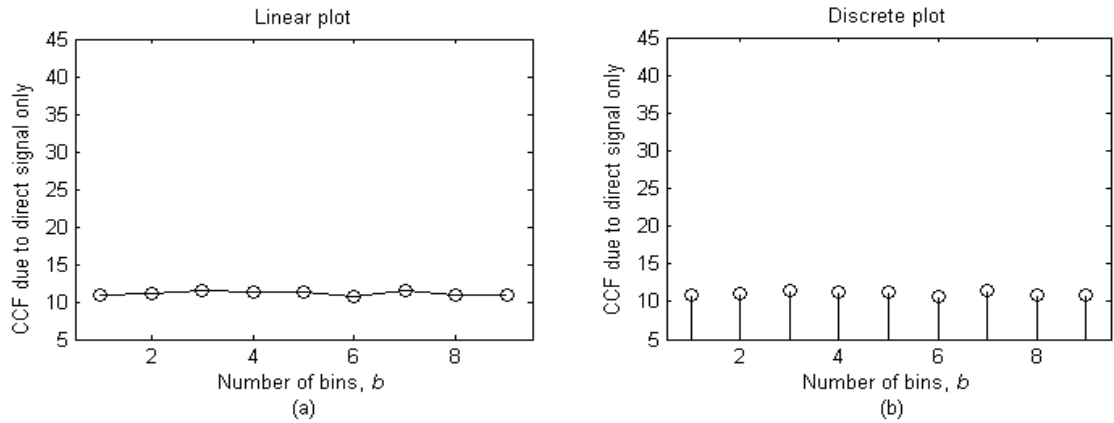


**Figure 3.59 CCFs due to only direct signal: (a) linear plot; and (b) discrete plot**

It can be seen from the results that the multipath effects decrease with increasing  $k$  and, in practice, can be neglected because of the higher values of  $k$  in a real underwater environment. The process of neglecting the multipath has already been provided in Section 3.12.

However, to obtain a generalised estimation of the number of nodes using the ratio of the standard deviation to the mean of the CCF considering a multipath with any possible values of  $k$ , the following example is provided.

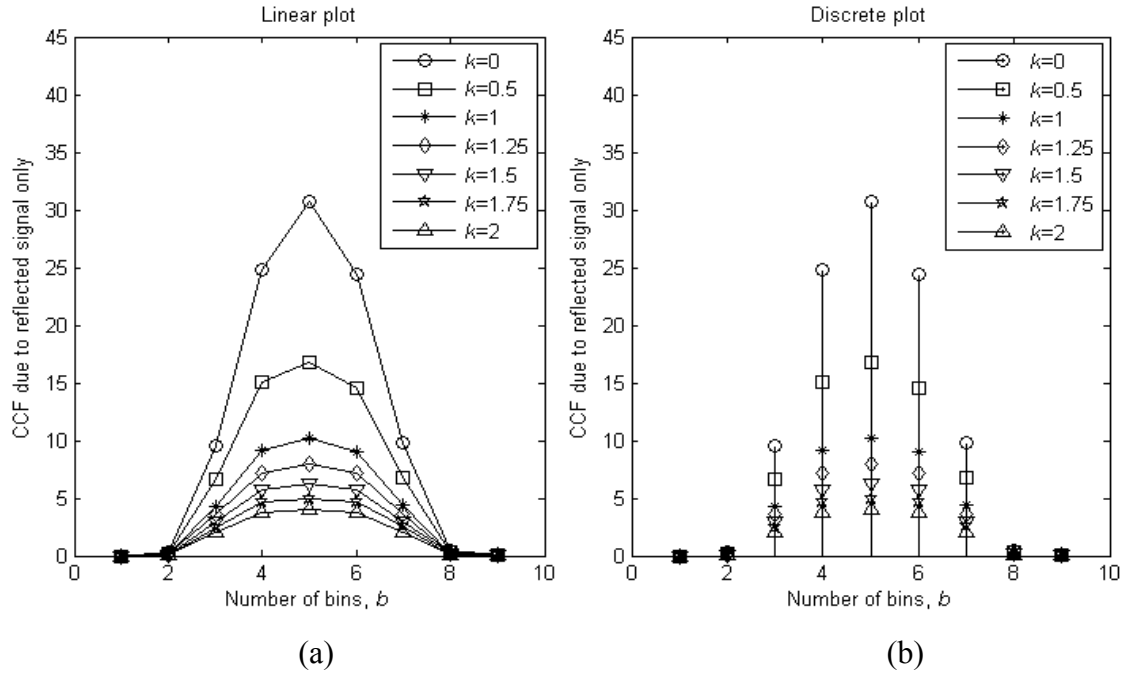


**Figure 3.60 CCFs with different  $k$  (0, 0.5, 1, 1.25, 1.5, 1.75 and 2) from only bottom reflected signal: (a) linear plot; and (b) discrete plot**

Let us consider a CCF with a multipath (one direct and one indirect path) for a 9-bin setup in which the delta peaks in the bins are  $P_1, P_2, P_3, P_4, P_5, P_6, P_7, P_8$  and  $P_9$ , as shown in Figure 3.61, and the corresponding delta peaks for the direct and reflected paths are  $P_{1d}, P_{2d}, P_{3d}, P_{4d}, P_{5d}, P_{6d}, P_{7d}, P_{8d}$  and  $P_{9d}$ , and  $P_{1r}, P_{2r}, P_{3r}, P_{4r}, P_{5r}, P_{6r}, P_{7r}, P_{8r}$  and  $P_{9r}$ , respectively, as shown in Figure 3.62,

where  $P_1 = P_{1d} + P_{1r}$ ,  $P_2 = P_{2d} + P_{2r}$ ,  $P_3 = P_{3d} + P_{3r}$ ,  $P_4 = P_{4d} + P_{4r}$ ,  
 $P_5 = P_{5d} + P_{5r}$ ,  $P_6 = P_{6d} + P_{6r}$ ,  $P_7 = P_{7d} + P_{7r}$ ,  $P_8 = P_{8d} + P_{8r}$  and  
 $P_9 = P_{9d} + P_{9r}$ .

It is shown in the above figures that all bins are not affected by the reflected signal and there is a mirror effect with respect to the middle bin. In the case of 9 bins, the affected bins are 2 to 8 and, due to the mirror effect, the peaks of the 2<sup>nd</sup> & 8<sup>th</sup>, 3<sup>rd</sup> & 7<sup>th</sup>, 4<sup>th</sup> & 6<sup>th</sup> bins are similar. As only the CCF with a multipath obtained from the experiment is available, it will have to suffice for the estimation. However, using a similar process to that for finding the ratio of the standard deviation to the mean of the CCF to estimate the number of nodes for a case without a multipath is not appropriate because of the extended peaks due to the reflected path signal. But, if we

can deduct the extended peaks from the CCF with a multipath, it will be exactly the same as the CCF without a multipath and the process will be appropriate for estimation.

To do this, we represent the peaks due to reflected signals (Figure 3.61) as percentages of the peaks due to both direct and reflected signals (Figure 3.62). The process of obtaining the percentages is:

$$\text{Percentage at 2}^{\text{nd}} \text{ bin, } p_{m2} = \frac{\text{Peak at 2}^{\text{nd}} \text{ bin due to reflected signal only}}{\text{Peak at 2}^{\text{nd}} \text{ bin due to both direct and reflected signals}} \times 100\%$$

$$\text{i.e., } p_{m2} = \frac{P_{2r}}{P_2} \times 100\%$$

Similarly, for other affected bins, the percentages are obtained using the following expressions:

$$p_{m3} = \frac{P_{3r}}{P_3} \times 100\%, \quad p_{m4} = \frac{P_{4r}}{P_4} \times 100\%, \quad p_{m5} = \frac{P_{5r}}{P_5} \times 100\%, \quad p_{m6} = \frac{P_{6r}}{P_6} \times 100\%,$$

$$p_{m7} = \frac{P_{7r}}{P_7} \times 100\%, \text{ and } p_{m8} = \frac{P_{8r}}{P_8} \times 100\%.$$

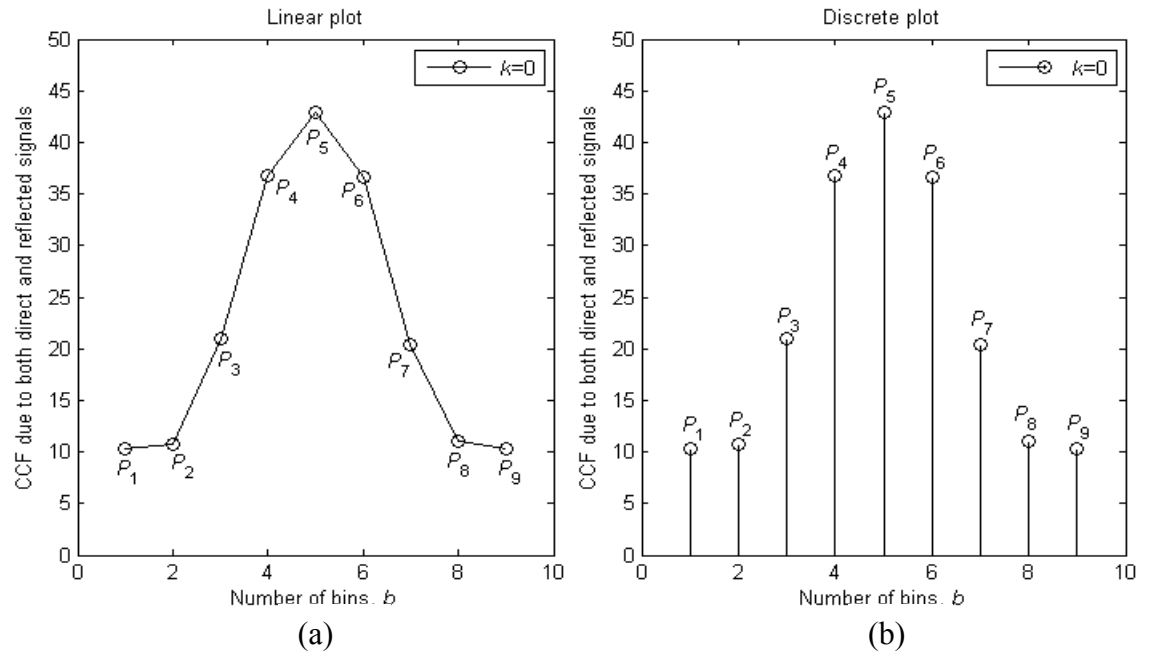


**Figure 3.61 Peaks of deltas in bins of CCF due to both direct and reflected signals with  $k = 0$**



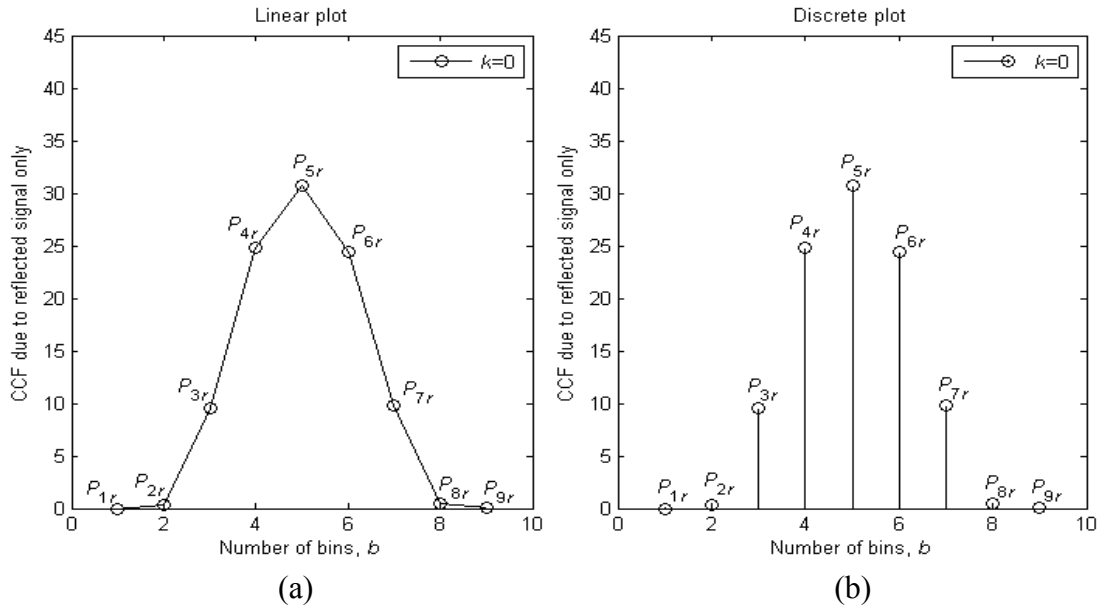


**Figure 3.62 Peaks of deltas in bins of CCF due to only reflected signal with  $k = 0$**

The percentages are independent of the number of nodes but dependent on the dispersion coefficient,  $k$ , and the number of bins,  $b$ . We investigate them for different values of  $k$  in 9 bins. Figure 3.63 shows the percentages of deltas due to only the reflected signal in each affected bin of the CCF in terms of deltas due to both direct and reflected signals. Percentages in the different affected bins for different  $k$  are presented in Figure 3.64.

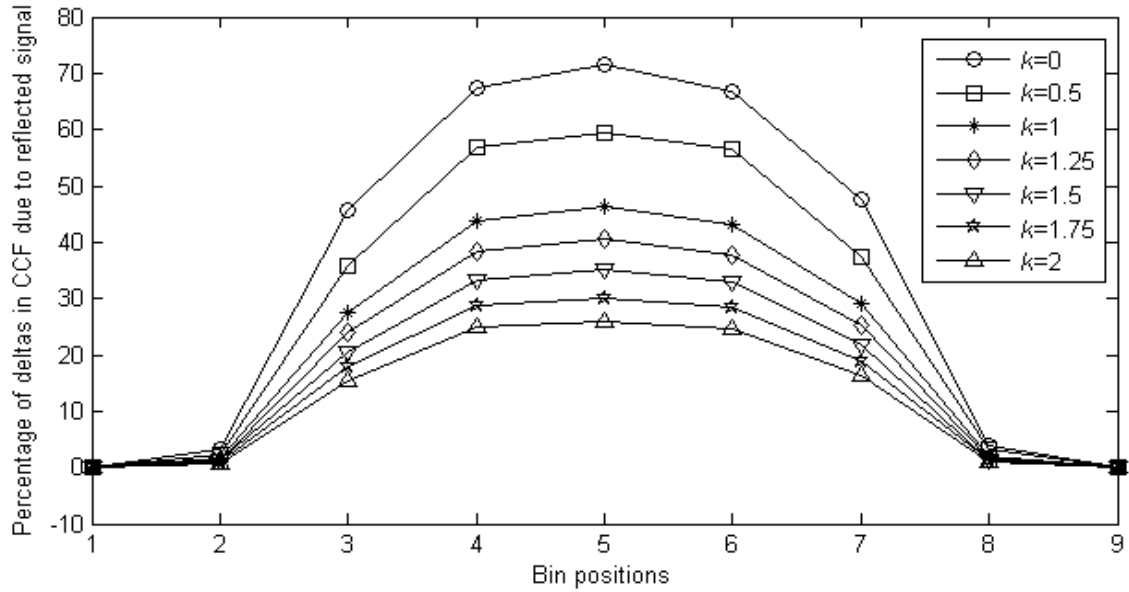


**Figure 3.63 Percentages of deltas in affected bins of CCF due to only reflected signal with different  $k$  (0, 0.5, 1, 1.25, 1.5, 1.75 and 2)**

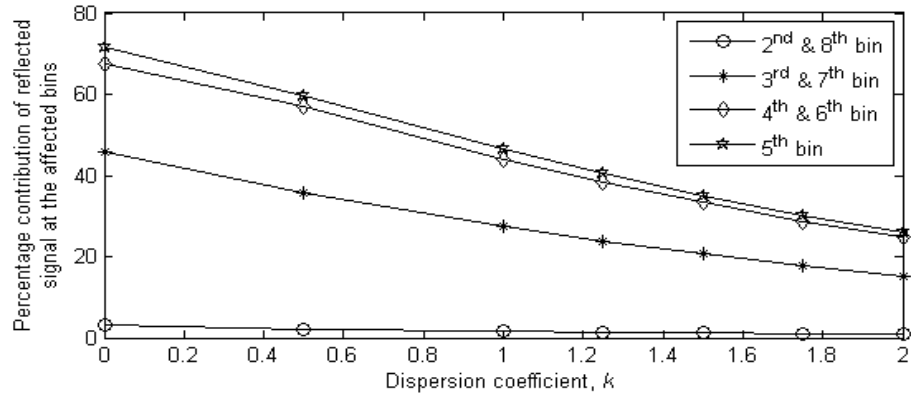


**Figure 3.64 Percentage contributions of reflected signal in affected bins for different  $k$  (0, 0.5, 1, 1.25, 1.5, 1.75 and 2)**

To obtain information on the percentage contributions for any  $k$ , those in all bins are expressed by the 4<sup>th</sup> degree approximation, as shown in Figure 3.65.

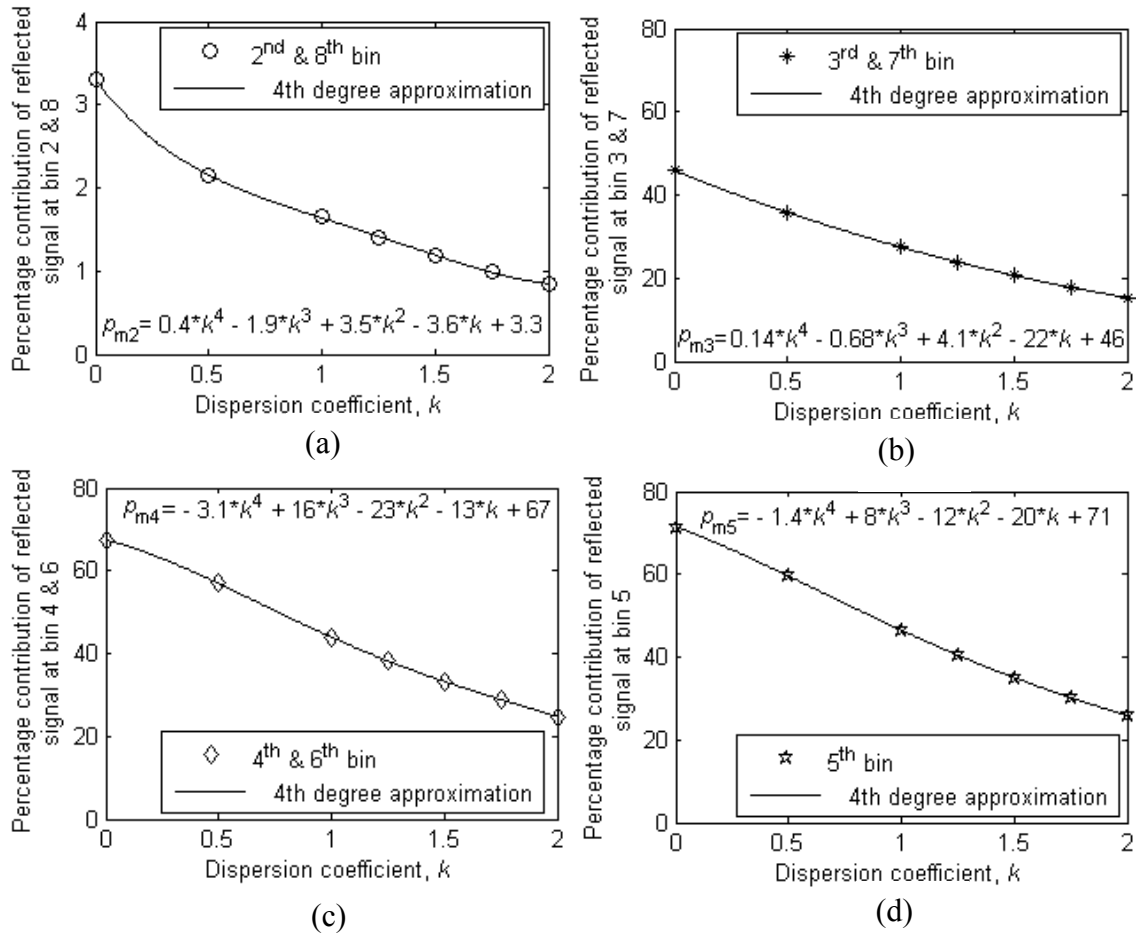


**Figure 3.65 Percentage contributions of reflected signal for different  $k$  (0, 0.5, 1, 1.25, 1.5, 1.75 and 2) in: (a) bin 2 and 8, (b) bin 3 and 7, (c) bin 4 and 6, and (d) bin 5**

The approximated expressions are:

$$p_{m2} \approx p_{m8} = 0.4k^4 - 1.9k^3 + 3.5k^2 - 3.6k + 3.3 \quad (3.60)$$

$$p_{m3} \approx p_{m7} = 0.14k^4 - 0.68k^3 + 4.1k^2 - 22k + 46 \quad (3.61)$$

$$p_{m4} \approx p_{m6} = -3.1k^4 + 16k^3 - 23k^2 - 13k + 67 \quad (3.62)$$

$$P_{m5} = -1.4k^4 + 8k^3 - 12k^2 - 20k + 71 \quad (3.63)$$

Now, to obtain the estimation parameter, i.e., the ratio of the standard deviation to the mean of the CCF, deductions of the extended peaks of the corresponding bins are obtained as follows (in the case of  $k = 0$ ).

In bin 2, the deducted peak is:

$$P_{2ds} = P_2 - p_{m2} \% \text{ of } P_2$$

Similarly, for the other affected bins 3 to 8, the deducted peaks are:

$$\begin{aligned} P_{3ds} &= P_3 - p_{m3} \% \text{ of } P_3, & P_{4ds} &= P_4 - p_{m4} \% \text{ of } P_4, & P_{5ds} &= P_5 - p_{m5} \% \text{ of } P_5, \\ P_{6ds} &= P_6 - p_{m6} \% \text{ of } P_6, & & & P_{7ds} &= P_7 - p_{m7} \% \text{ of } P_7, \\ P_{8ds} &= P_8 - p_{m8} \% \text{ of } P_8. & & & & \end{aligned}$$

The peaks of the CCF after deduction for 100 nodes with 100 iterations are shown in Figure 3.66. To demonstrate the effectiveness of the process, the  $R_s$  of the CCF after deduction are plotted for different numbers of nodes with one iteration in Figure 3.67. It is obvious from this figure that the process is adequate for estimating the number of nodes.

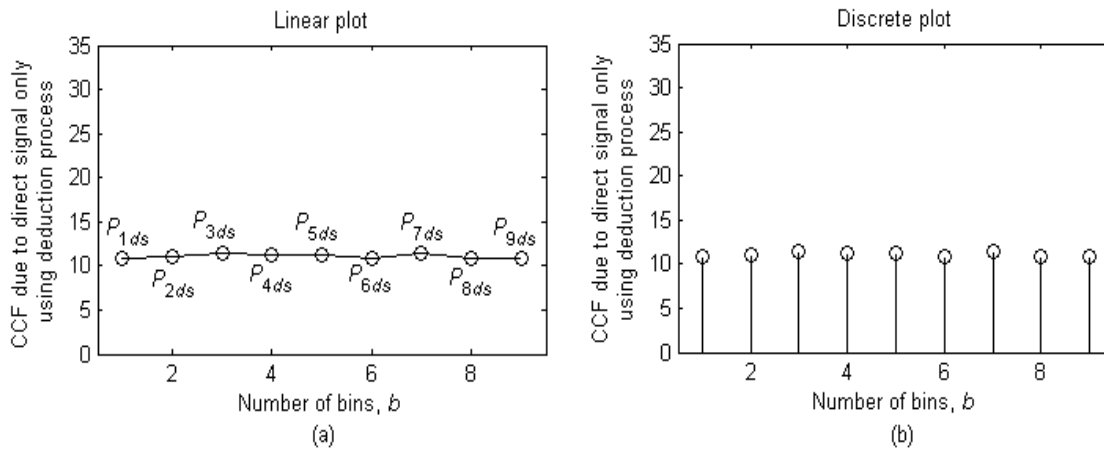


**Figure 3.66 CCFs after deduction**

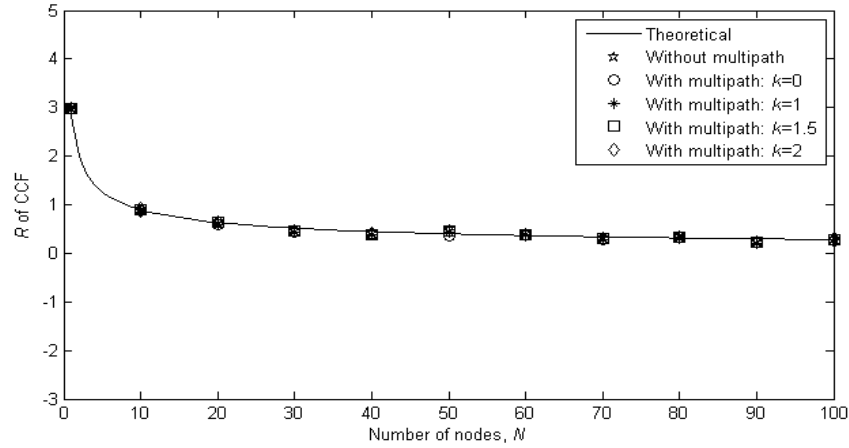


**Figure 3.67 Rs of CCF: comparison of theoretical, simulation without multipath (using earlier proposed technique) and simulation with multipath (using proposed multipath compensation technique) for different  $k$  (0, 1, 1.5 and 2)**

### 3.12.4.2 Considering a direct and two reflected path

The previous analysis was for the multipath effect due to only the bottom (seabed) reflection. A similar process is applied to obtain an estimation in the case of a multipath due to both surface and bottom reflections. Now, to properly demonstrate the robust estimation process with multipath effects due to both surface and bottom reflections, let us consider a similar experimental setup to that for the multipath effect due to only bottom reflections. The only difference between the two is that, in the latter, the sea surface is considered as another reflector, i.e., the cause of the multipath. The results for the CCF from such a setup for 100 nodes with 9 bins, 100 iterations and different  $k$  values, are presented in Figures 3.68 to 3.71. These four figures have different dispersion coefficient,  $k$ , values of 0, 1, 1.5 and 2, respectively, and each has three separate plots: the top for CCFs with multipath, i.e., direct and indirect path signals are responsible for forming the CCF, the middle for CCFs due to reflected (both surface and bottom) signals only; and the bottom for CCFs due to only direct signals, i.e., without multipath, as in the earlier case of the ERP without a multipath. It has already been demonstrated that a delta without a multipath, i.e., with only a direct path, follows a random distribution to form the CCF; this will also be true for deltas with indirect paths. Thus, the CCF with a multipath will be the summation of three random variables.

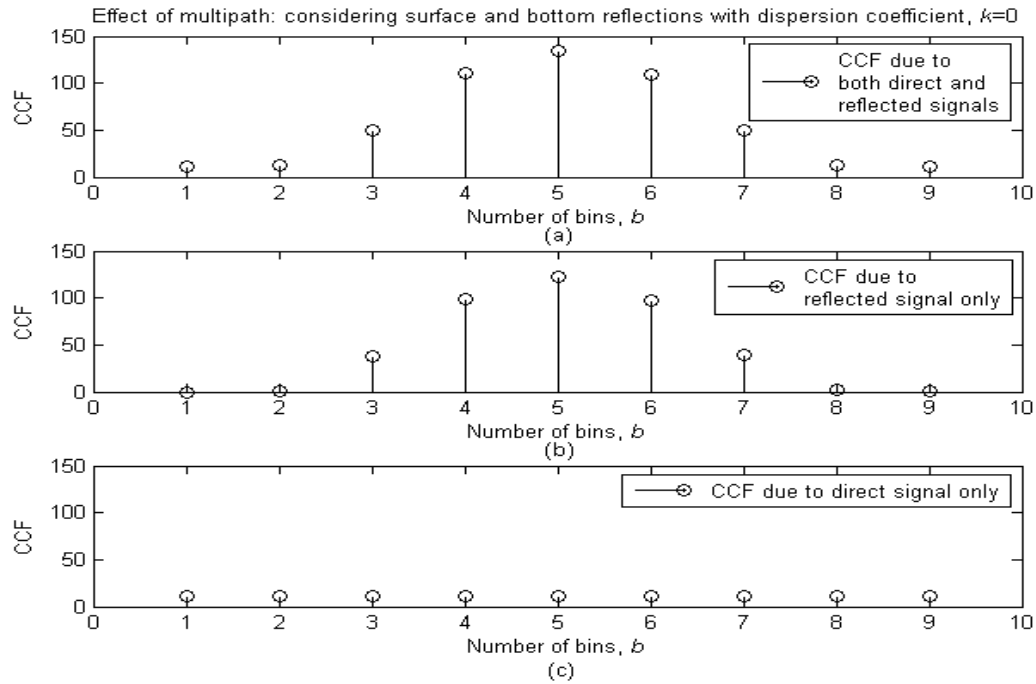


**Figure 3.68 CCF with  $k = 0$  from: both direct and reflected signals (surface and bottom); only reflected signal; and only direct signal**

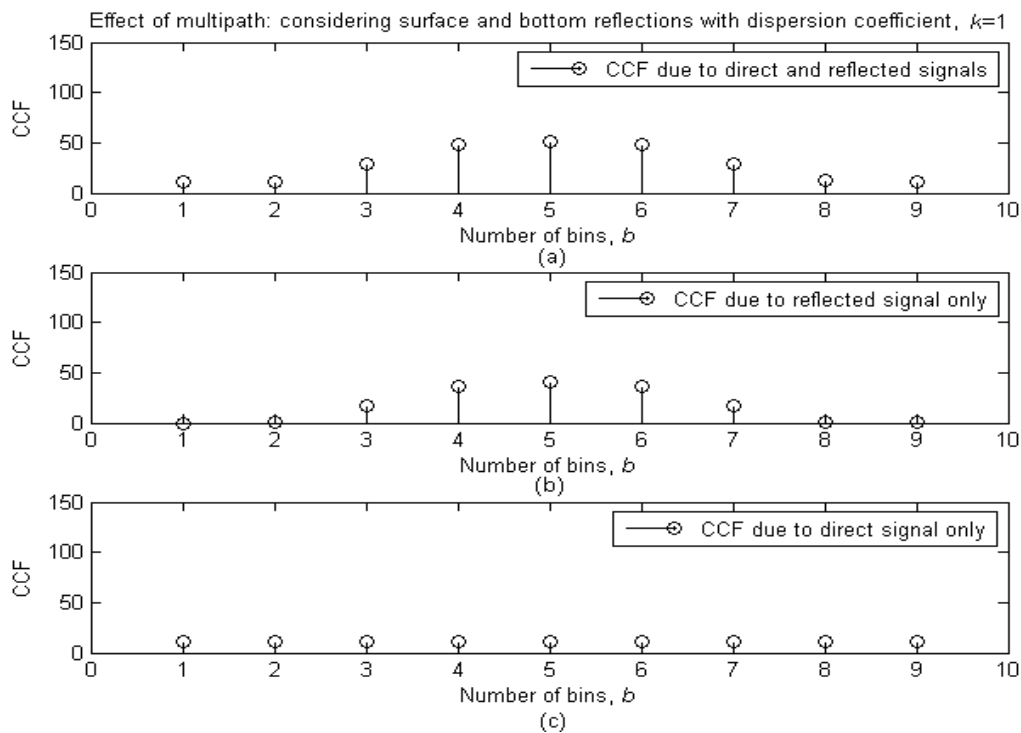


**Figure 3.69 CCF with  $k = 1$  from: both direct and reflected signals (surface and bottom); only reflected signal; and only direct signal**

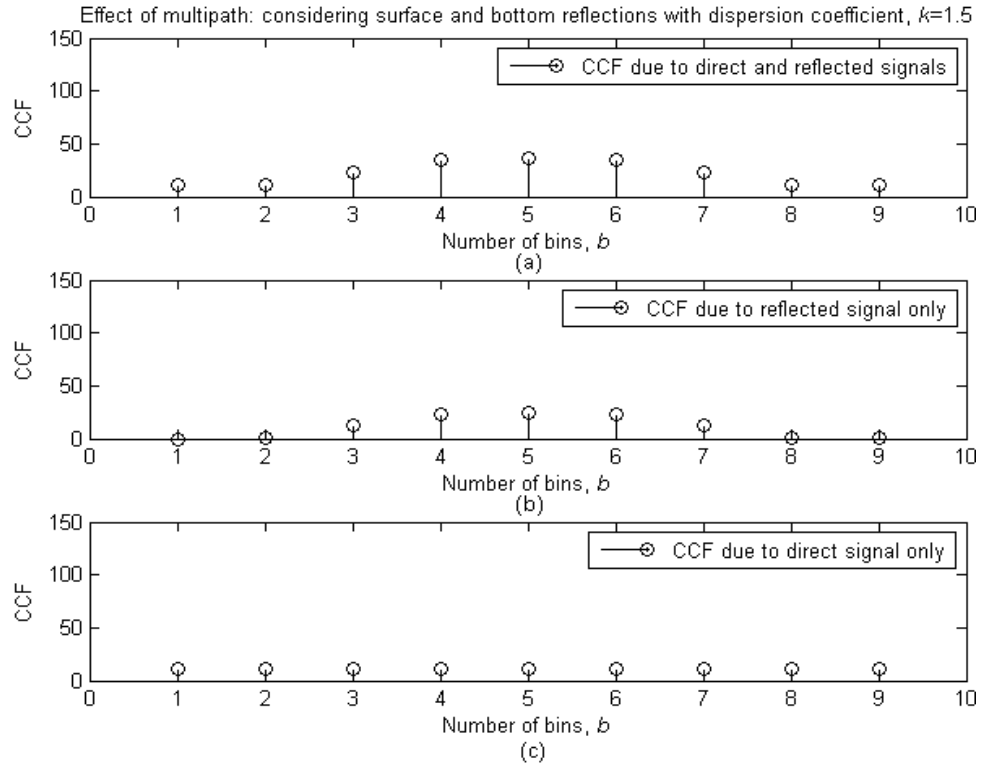


**Figure 3.70 CCF with  $k = 1.5$  from: both direct and reflected signals (surface and bottom); only reflected signal; and only direct signal**

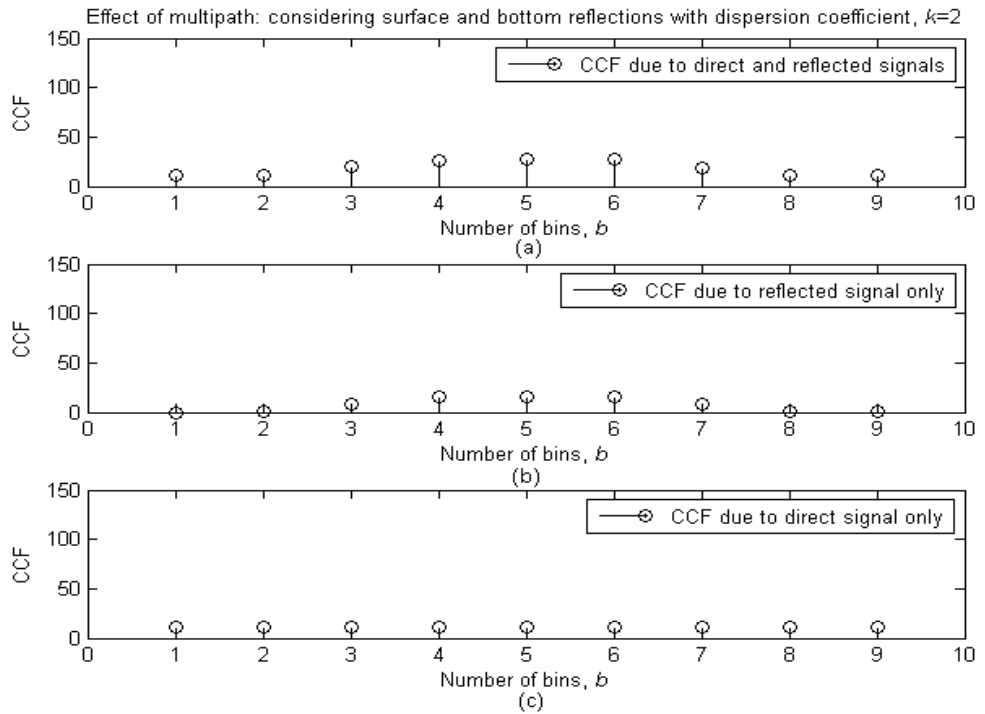


**Figure 3.71 CCF with  $k = 2$  from: both direct and reflected signals (surface and bottom); only reflected signal; and only direct signal**

To clarify the above discussion, Figures 3.72 to Figure 3.74 are plotted.

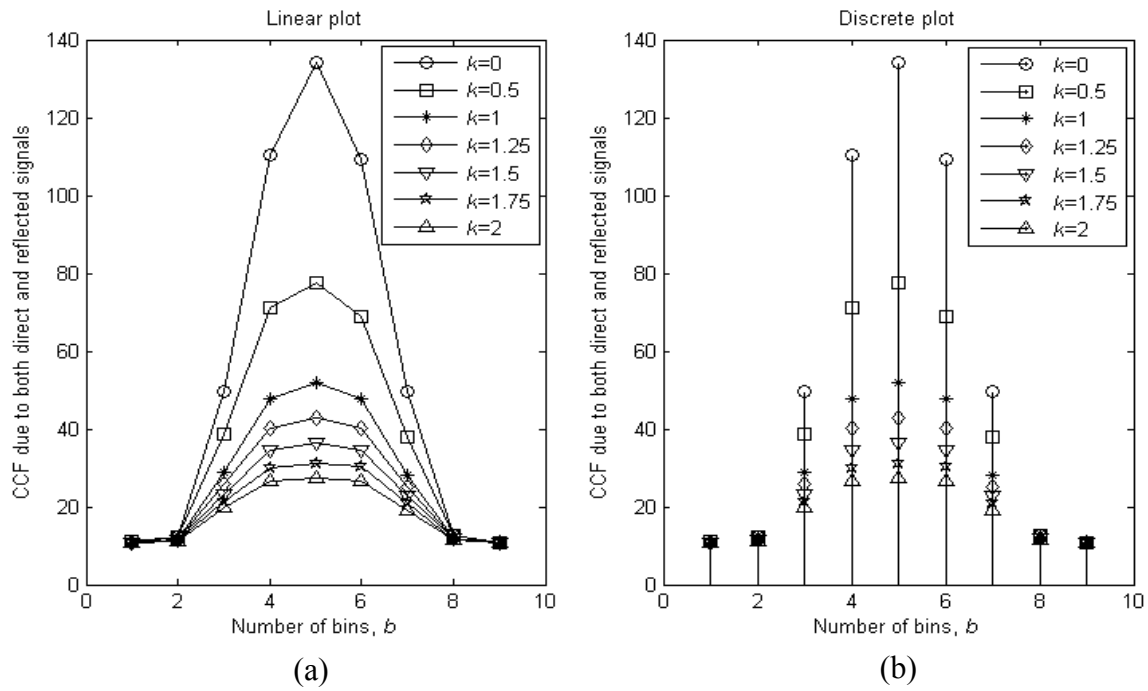


**Figure 3.72 CCF with different  $k$  (0, 0.5, 1, 1.25, 1.5, 1.75 and 2) from both direct and reflected signals (surface and bottom): (a) linear plot; and (b) discrete plot**

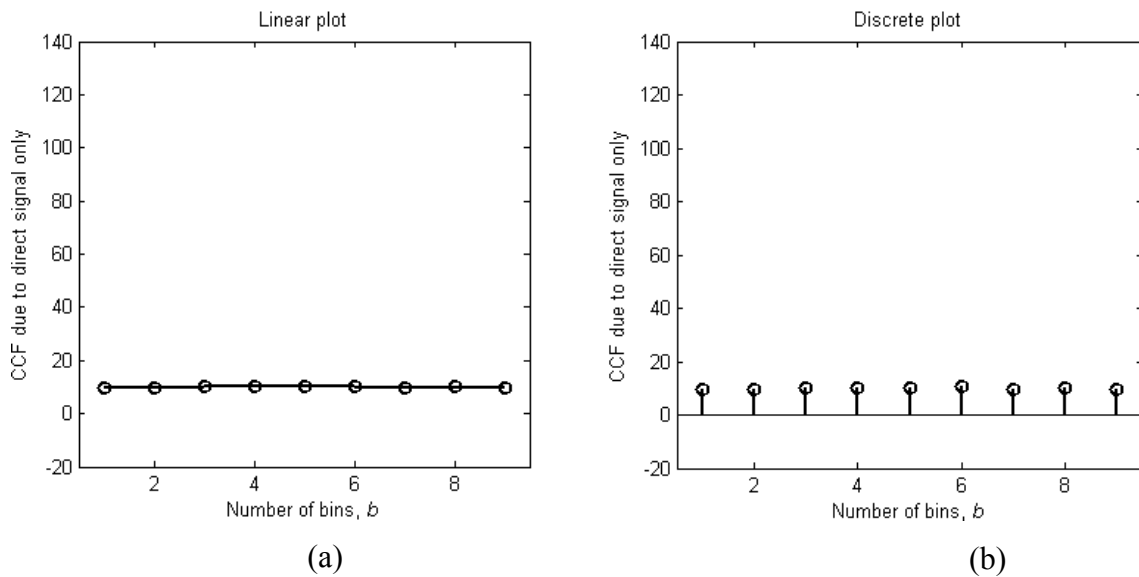


**Figure 3.73 CCF from only direct signal: (a) linear plot; and (b) discrete plot**

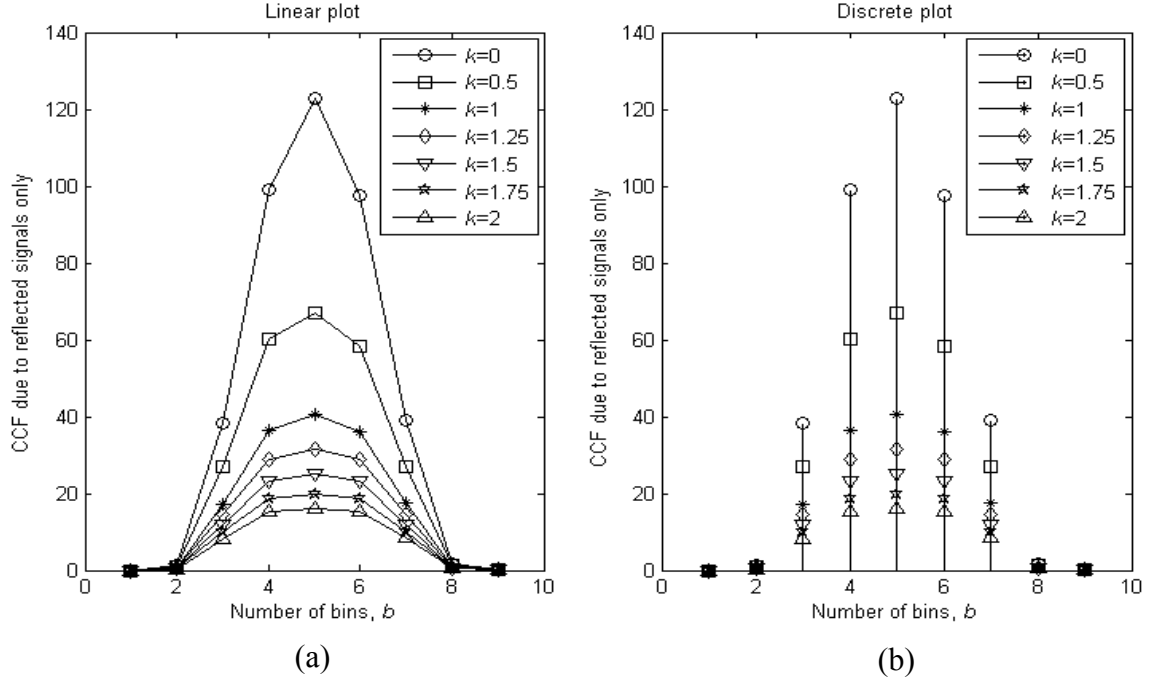


**Figure 3.74 CCF with different  $k$  (0, 0.5, 1, 1.25, 1.5, 1.75 and 2) from only reflected signals (both surface and bottom): (a) linear plot; and (b) discrete plot**

These results demonstrate that the multipath has a similar effect to the bottom reflection case as it decreases with increasing  $k$  and can be neglected because of the higher values of  $k$  in a practical underwater acoustic environment. The process of neglecting a multipath due to both surface and bottom reflections has also been provided in earlier work on the effects of the multipath on estimation.

Now, we obtain a generalised estimation of the number of nodes using the ratio of the standard deviation to the mean of the CCF considering a multipath due to both surface and bottom reflections with any possible values of  $k$ .

Let us consider a CCF with a multipath (one direct and two indirect paths from both surface and bottom reflections) for a 9-bin setup in which the delta peaks in the bins are  $P_{21}$ ,  $P_{22}$ ,  $P_{23}$ ,  $P_{24}$ ,  $P_{25}$ ,  $P_{26}$ ,  $P_{27}$ ,  $P_{28}$  and  $P_{29}$ , as shown in Figure 3.75, and the corresponding peaks for the direct and reflected paths are  $P_{21d}$ ,  $P_{22d}$ ,  $P_{23d}$ ,  $P_{24d}$ ,  $P_{25d}$ ,  $P_{26d}$ ,  $P_{27d}$ ,  $P_{28d}$  and  $P_{29d}$ , and  $P_{21r}$ ,  $P_{22r}$ ,  $P_{23r}$ ,  $P_{24r}$ ,  $P_{25r}$ ,  $P_{26r}$ ,  $P_{27r}$ ,  $P_{28r}$  and  $P_{29r}$ , respectively, as shown in Figure 3.76, where  $P_{21} = P_{21d} + P_{21r}$ ,  $P_{22} = P_{22d} + P_{22r}$ ,



$$P_{23} = P_{23d} + P_{23r}, P_{24} = P_{24d} + P_{24r}, P_{25} = P_{25d} + P_{25r}, P_{26} = P_{26d} + P_{26r}, P_{27} = P_{27d} + P_{27r},$$

$$P_{28} = P_{28d} + P_{28r}, \text{ and } P_{29} = P_{29d} + P_{29r}.$$

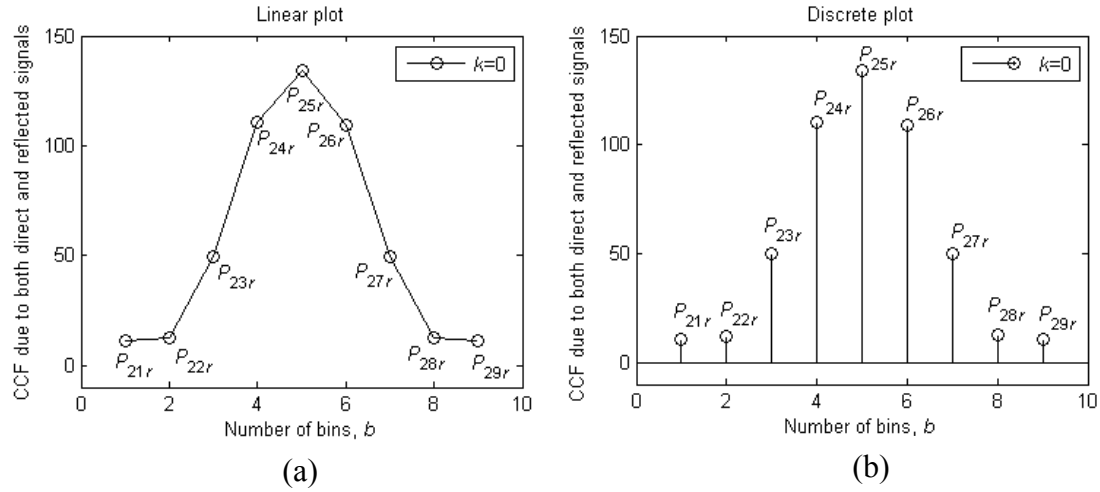


**Figure 3.75 Peaks of deltas in bins of CCF due to both direct and reflected signals with  $k = 0$  (a) linear; and (b) discrete plot**

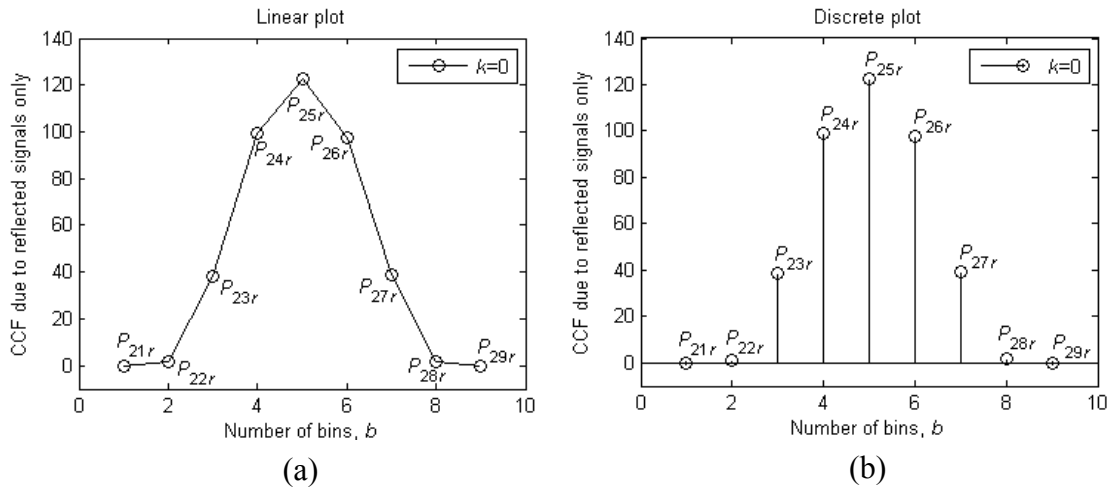


**Figure 3.76 Peaks of deltas in bins of CCF due to only reflected signal with  $k = 0$  (a) linear; and (b) discrete plot**

In the case of two reflections, it is again shown in the above figures that not all bins are affected by the reflected signals and there is a mirror effect with respect to the middle bin. As previously in the case of 9 bins, the affected bins are 2 to 8 and, due to the mirror effect, the peaks of the 2<sup>nd</sup> & 8<sup>th</sup>, 3<sup>rd</sup> & 7<sup>th</sup>, 4<sup>th</sup> & 6<sup>th</sup> bins are similar. As only the CCF with a multipath is available from this experiment, it will have to suffice for the estimation. However, using a similar process to that for finding the

ratio of the standard deviation to the mean of the CCF to estimate the number of nodes without a multipath is not appropriate here because of the extended peaks due to the signals of the reflected paths. But, if we can deduct the extended peaks from the CCF with a multipath, the process will be exactly the same as that for the CCF without a multipath and will be appropriate for estimation.

To do this, we represent the peaks due to both direct and reflected signals (Figure 3.75) as percentages of the peaks due to only reflected signals (Figure 3.76) which will be different from the case with only a bottom reflection.

The process of obtaining percentages is:

$$\text{Percentage at } 2^{\text{nd}} \text{ bin, } p_{m22} = \frac{\text{Peak at } 2^{\text{nd}} \text{ bin due to reflected signal only}}{\text{Peak at } 2^{\text{nd}} \text{ bin due to both direct and reflected signals}} \times 100\%$$

$$\text{i.e., } p_{m22} = \frac{P_{22r}}{P_{22}} \times 100\%$$

Similarly for other affected bins, the percentages are obtained using the following expressions:

$$p_{m23} = \frac{P_{23r}}{P_{23}} \times 100\%, \quad p_{m24} = \frac{P_{24r}}{P_{24}} \times 100\%, \quad p_{m25} = \frac{P_{25r}}{P_{25}} \times 100\%, \quad p_{m26} = \frac{P_{26r}}{P_{26}} \times 100\%,$$

$$p_{m27} = \frac{P_{27r}}{P_{27}} \times 100\%, \quad p_{m28} = \frac{P_{28r}}{P_{28}} \times 100\%$$

Detailed results are provided in Figures 3.77 to 3.79. These percentages are again independent of the number of nodes but dependent on the dispersion coefficient,  $k$ , and the number of bins,  $b$ . We investigate the percentages for different values of  $k$  with 9 bins, as shown in Figures 3.77 and 3.78. Figure 3.77 shows the percentages of deltas due to both direct and reflected signals in each affected bin of the CCF. The percentage contributions of the different affected bins for different  $k$  are presented in Figure 3.78.

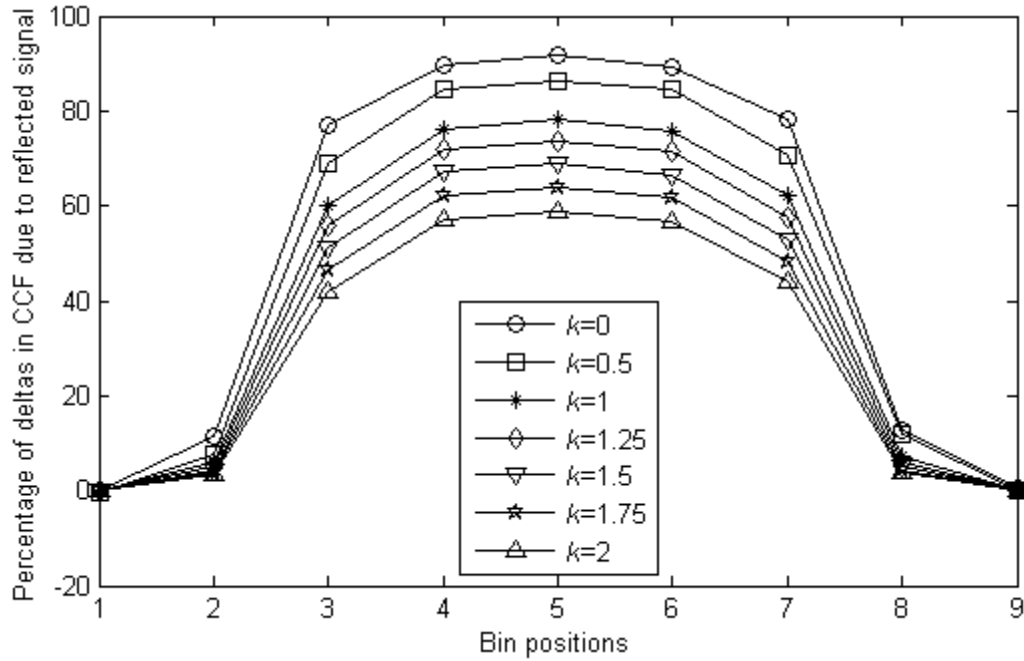


**Figure 3.77 Percentages of deltas in affected bins of CCF due to reflected signals (both surface and bottom) with different  $k$  (0, 0.5, 1, 1.25, 1.5, 1.75 and 2)**

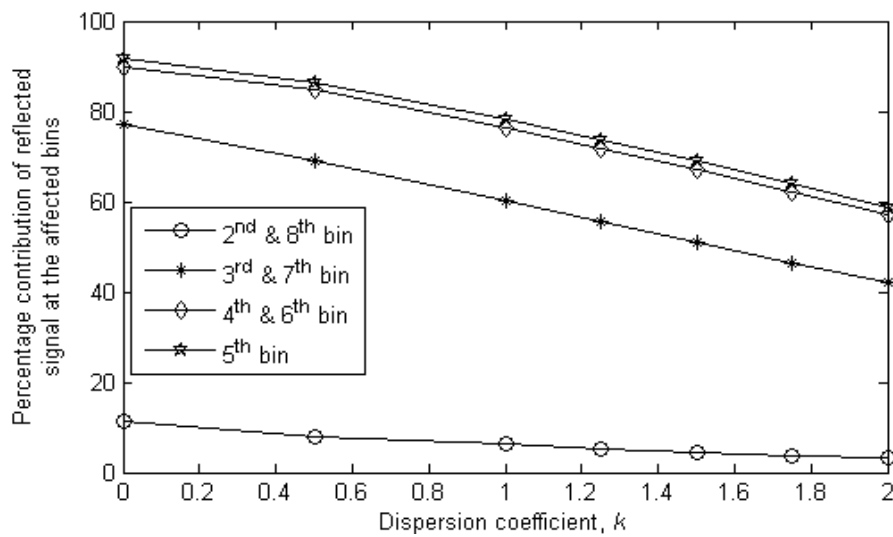


**Figure 3.78 Percentage contributions of reflected signals (both surface and bottom) in affected bins for different  $k$  (0, 0.5, 1, 1.25, 1.5, 1.75 and 2)**

To obtain information on the percentages for any  $k$ , the percentages of all bins are expressed by the 4<sup>th</sup>-degree approximation, as shown in Figure 3.79.

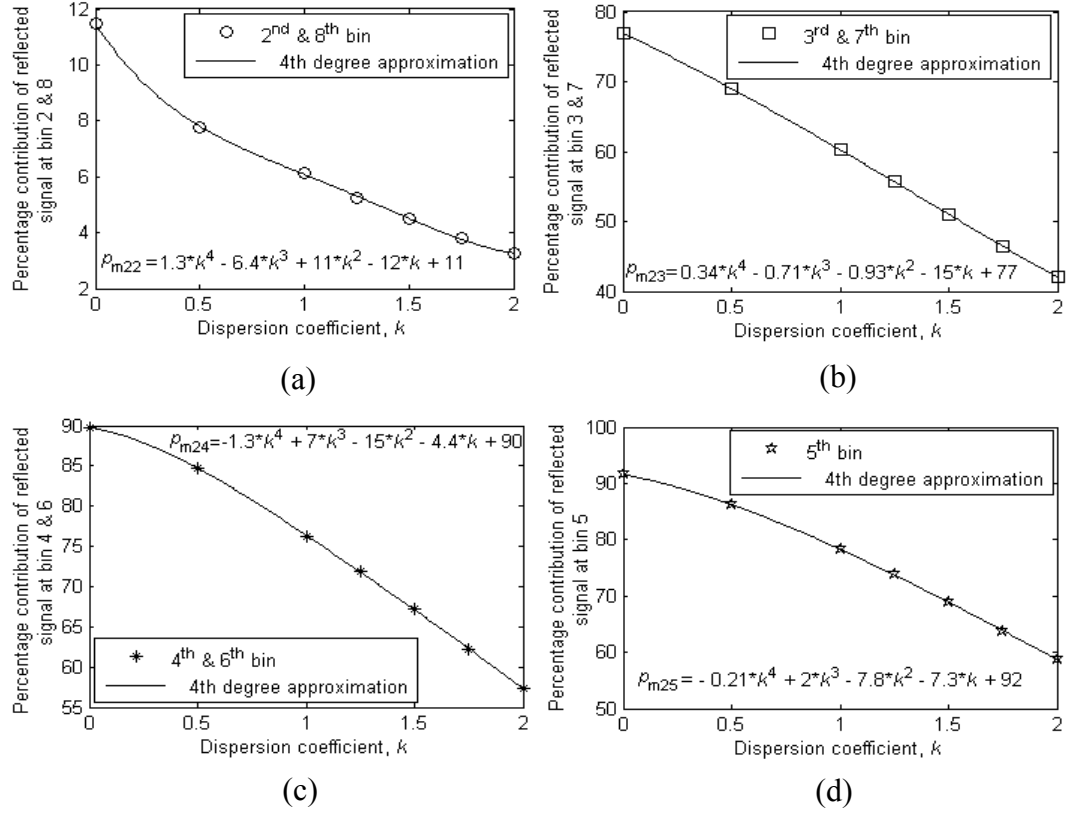


**Figure 3.79 Percentage contributions of reflected signals (both surface and bottom) for different  $k$  (0, 0.5, 1, 1.25, 1.5, 1.75 and 2) in: (a) bin 2 and 8 , (b) bin 3 and 7, (c) bin 4 and 6, and (d) bin 5**

The approximated expressions are:

$$p_{m22} \approx p_{m28} = 1.3k^4 - 6.4k^3 + 11k^2 - 12k + 11 \quad (3.64)$$

$$p_{m23} \approx p_{m27} = 0.34k^4 - 0.71k^3 - 0.93k^2 - 15k + 77 \quad (3.65)$$

$$p_{m24} \approx p_{m26} = -1.3k^4 + 7k^3 - 15k^2 - 4.4k + 90 \quad (3.66)$$

$$p_{m25} = -0.21k^4 + 2k^3 - 7.8k^2 - 7.3k + 92 \quad (3.67)$$

Comparisons of the percentage contributions with one and two reflector in the bins are presented in Figure 3.80.

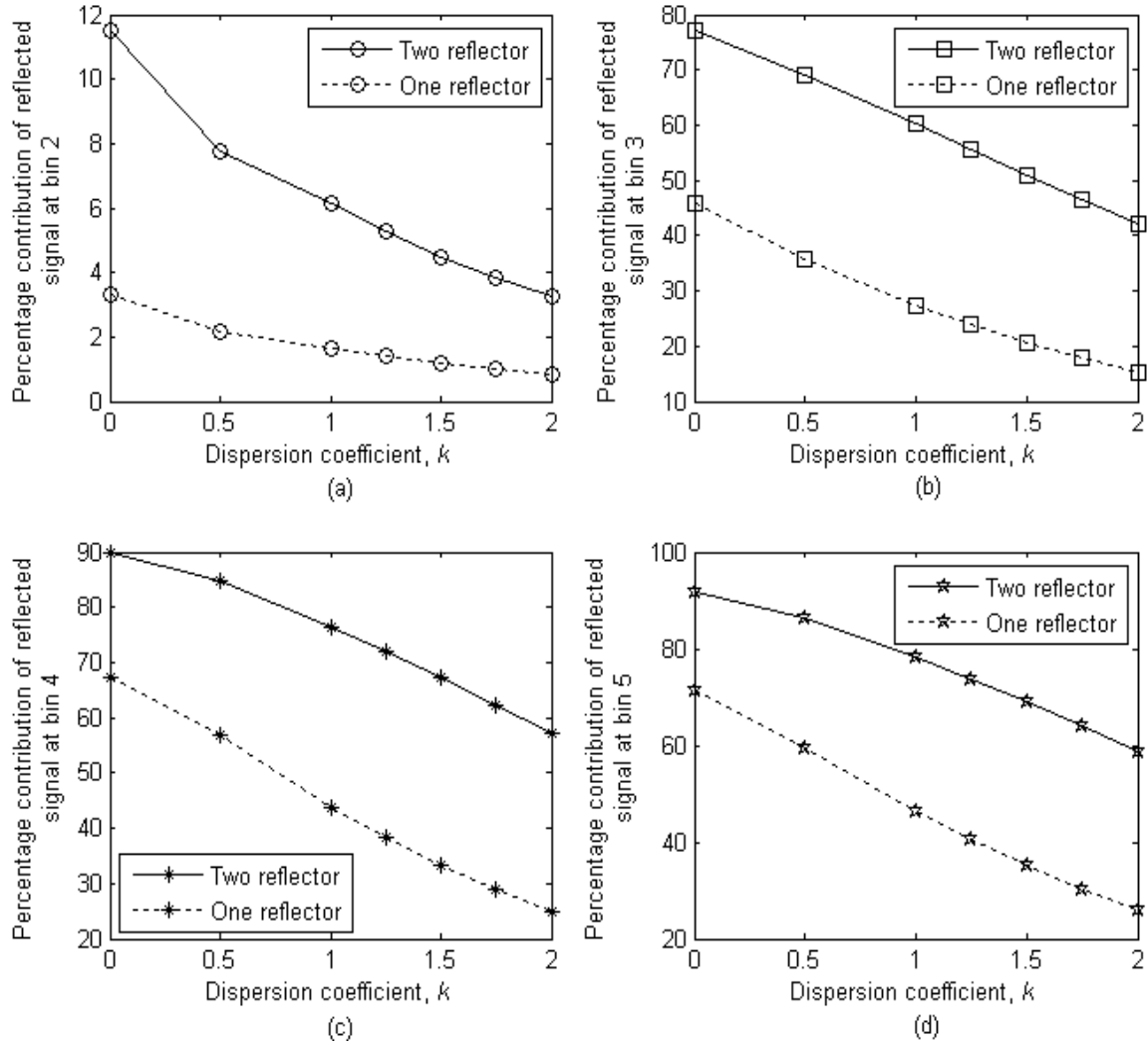


**Figure 3.80 Comparisons of percentage contributions of reflected signals in different affected bins for different  $k$  (0, 0.5, 1, 1.25, 1.5, 1.75 and 2)**

Now, to obtain the estimation parameter, i.e., the ratio of the standard deviation to the mean of the CCF, deductions of the extended peaks of the corresponding bins are obtained as follows.

In bin 2, the deducted peak is:

$$P_{22ds} = P_{22} - p_{m22} \% \text{ of } P_{22}$$

Similarly, for the other affected bins, 3 to 8, the deducted peaks are:

$$P_{23ds} = P_{23} - p_{m23} \% \text{ of } P_{23}, P_{24ds} = P_{24} - p_{m24} \% \text{ of } P_{24}, P_{25ds} = P_{25} - p_{m25} \% \text{ of } P_{25},$$

$$P_{26ds} = P_{26} - p_{m26} \% \text{ of } P_{26}, P_{27ds} = P_{27} - p_{m27} \% \text{ of } P_{27}, P_{28ds} = P_{28} - p_{m28} \% \text{ of } P_{28}$$

The peaks of the CCF after deduction for 100 nodes with 100 iterations are shown in Figure 3.81. To demonstrate the effectiveness of the process, the  $R_s$  of the CCF after deduction for different numbers of nodes with one iteration are plotted in Figure 3.82. It can be seen from the results that the technique is good enough to estimate in multipath environment.

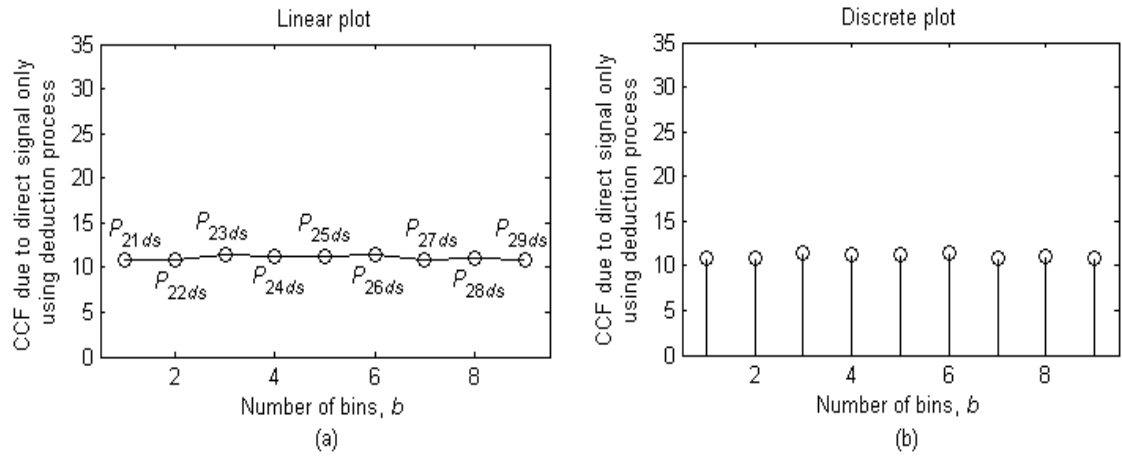


**Figure 3.81 CCFs after deduction**

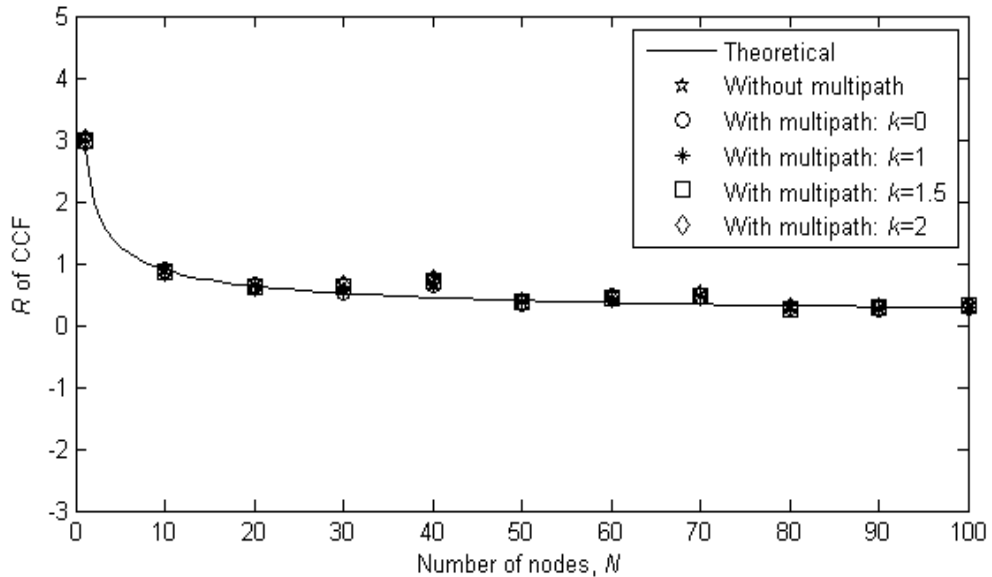


**Figure 3.82  $R_s$  of CCF: comparison of results from theoretical, simulation without multipath (using earlier proposed technique) and simulation with multipath (using proposed multipath compensation technique with both surface and bottom reflections) for different  $k$  (0, 1, 1.5 and 2)**

### 3.12.5 Conclusion

In a practical wireless network, multipath signal propagation is common. This section investigates the effect with two different cases-the multipath with one indirect path and multipath with two indirect paths. Although the effect might be similar, only the ERP case is investigated. In some cases where the received direct path signal is stronger than the indirect path signal, the multipath effect can be neglected and the estimation can be obtained as without multipath. Again if the indirect path signal is not negligible, a technique is investigated to estimate the number of nodes.

### 3.12.6 Multipath effects in protocols

Two main performance criteria for estimation protocols are the estimation range and their speed i.e. the time required to estimate. Range is the maximum distance from which the receiver can sense the signal from the transmitter – that is, the range at which it receives at least  $Q_n$  (the threshold power of the receiver). But in a multipath environment the received power is sometimes lower than  $Q_n$  due to the subtraction of indirect signal power from the direct signal, as multipath reception of some unwanted signal, of which some are additive whereas others are subtractive. Thus some signals can not reach the sensors and the system performance for estimation degrades. Besides, the multipath causes ISI in the received signal, but using the symbol interval sufficiently longer than the delay spread, ISI can be neglected. Thus it takes more time to provide an estimate neglecting the effect of multipath fading.

In the proposed technique of cross-correlation, any multipath effect can be neglected with a process where the power of a signal or time required is not affected. This will be very useful in the energy-limited UWSN in compared to the protocol technique.

## 3.13 Conclusion

Knowing the number of nodes in a network is very useful for practical network operations. Previous techniques proposed for estimating have been based on some

aspect of the protocol(s) in use and most do not take into account the capture effect. In this chapter, we have shown that the cross-correlation of random signals can be used to estimate the number of nodes or transmitters in a network. Mathematically derived expressions were investigated by simulations and the results agreed with those from theory. Two cases - with and without consideration of the fractional parts of the delays - were investigated in the simulation process and the results showed similar performance. The effect of the signal length was investigated and a selection criterion for the finite signal length for both the ERP and ETP cases was proposed. Moreover, the effects on estimation of noise and multipath signal propagation were also investigated. It was found that the impact of multipath propagation is often negligible. In cases where multipath propagation must be taken into account, techniques were presented for the cases of two paths (direct and bottom reflection) and three paths (direct, bottom reflection and surface reflection). However, demonstration of the effectiveness of the proposed estimation technique requires comparisons with conventional technique(s). Later in this thesis, two conventional techniques using protocols are considered and detailed comparisons, including analyses of the error and time required for estimation, are provided.





# Chapter 4

## Estimation of the Dimensionality and numbers of nodes in different dimensions in a communication network

---

### 4.1 Introduction

In the cross-correlation node estimation, placement of a delta in a bin depends on the node position i.e. the formation of the CCF has a significant dependency on the placement of the nodes in the network. Thus it can be said that the estimation of the number of nodes is dependent on the dimensionality of the network. In Chapter 3, estimation of  $N$  is investigated only for a 3D network. As estimation of the number of nodes using cross-correlation depends on the dimensionalities of the networks, it is better to first estimate the latter, that is, whether the nodes are oriented in 1D, 2D or 3D in space. This also helps in obtaining additional information about the network, e.g., localization of the nodes, AOA estimations. As most research conducted on dimensionality has been for a network's architecture before deployment of its nodes, the dimensionality of a deployed unknown network is a relatively new research area. The deployment strategies for 2D and 3D underwater acoustic network is proposed by Pompili (2009) to determine the minimum number of sensors to be deployed to achieve optimal sensing and communication coverage, which are dictated by application requirements; provide guidelines on how to choose the optimal deployment surface area, given a target body of water; study the robustness of the sensor network to node failures, and provide an estimate of the number of redundant sensor nodes to be deployed to compensate for potential failures. The only protocol-based technique for dimensionality estimation in a deployed communication network is proposed in (Howlader 2008; Howlader 2009).

In earlier chapter(s), the fact that the use of protocols is inefficient in harsh environments, such as underwater, underground, has been mentioned. In this chapter, a similar cross-correlation technique to that presented in Chapter 3 for estimating the number of nodes is used to estimate the dimensionality of a communication network after deployment. This process can be concurrent with that of the estimation of the number of nodes. Thus, the proposed cross-correlation techniques for estimating the number of nodes and their dimensionalities are of interest for wireless communication networks such as WSNs and RFIDs.

Two dimensionality and two node count estimation techniques for all dimensions are provided. Firstly, the shape of the CCF (which varies with dimensionality of the network) is used to estimate the dimensionality. Then, the ratio of standard deviation and mean of CCF (obtained from the individual bin of theoretical and simulated CCF) is used to estimate the dimensionality. Like the shape, this ratio also varies with dimensionality. Also, to obtain the node count for any dimensional network, this ratio is used. Though it is useful, it requires prior knowledge of the signal power. To overcome the limitation, the approach similar to that used in Chapter 3 with some manipulations is applied for all dimensions.

## **4.2 Estimation using CCF of dimensionality**

To start the process of cross-correlation for estimating dimensionality, firstly, the shapes of the cross-correlation functions (CCFs) for different dimensions are discussed fully using both analytical and simulated interpretations. The shapes of the CCF varies with dimensionalities. Knowing the proper theoretical shapes, it is easy to estimate the dimensionality by comparing the shape of experimental CCF with that of the theoretical. This section provides theoretical with corresponding simulated shapes of the CCF for 1D (linear), 2D (circle), and 3D (sphere) network. Then an estimation technique is provided using a cost function which is the summation of mean square deviations of the peaks of individual bins of theoretical and simulated CCF. Again, the effect of fractional-samples delays has been investigated.

### 4.2.1 Shapes of CCFs

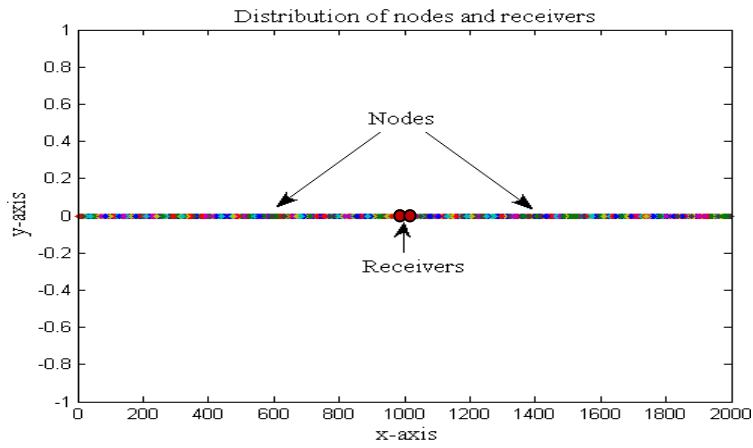
The procedure for obtaining both the analytical and simulated shapes of the CCFs for different dimensions is given step by step.

Step1: We choose 3 types (1D, 2D and 3D) of networks with 10,000 transmitting nodes (to obtain proper fundamental shapes of the networks) and two probing nodes or two receivers in a probing node, as indicated in Figure 4.1. It is clear in the figure that the probing node(s) is/are placed at the centre of the network. It can be seen in the figure that the uniform nodes distribution in 1D network is on a straight line, 2D network is on a circle, and 3D inside a sphere. Though these are very restrictive assumptions, this cross-correlation technique to estimate the dimensionality will help for further work with other type of configurations as for example, 3D but not spherical.

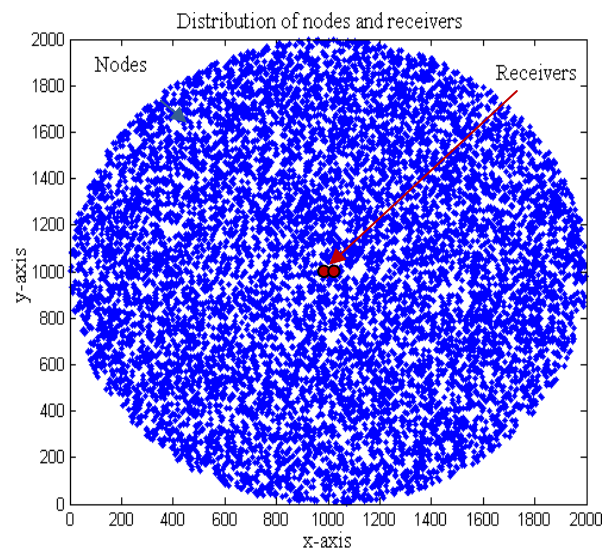
Step2: The probing node(s) send probe requests to the transmitting nodes which send back Gaussian signals as their responses such that the receivers at the probing node(s) receive signals of the same power (ERP case) from the transmitting nodes.

Step3: We sum the signals from all transmitting nodes to two locations of the probing nodes and cross-correlate these two combined signals to produce the CCF. If the network is 3D, the CCF is a series of Dirac deltas of uniform strengths over the width  $2d_{DBS}$  and centred at 0, as shown in Figure 4.2 (c). However, this is not true for the 1D and 2D networks, as shown in Figures 4.2 (a) and 4.2 (b). In the Figure 4.2, the width  $2d_{DBS}$  is replaced by the  $b$  bins, and for 11 bins, the 6<sup>th</sup> is considered as the centre bin.

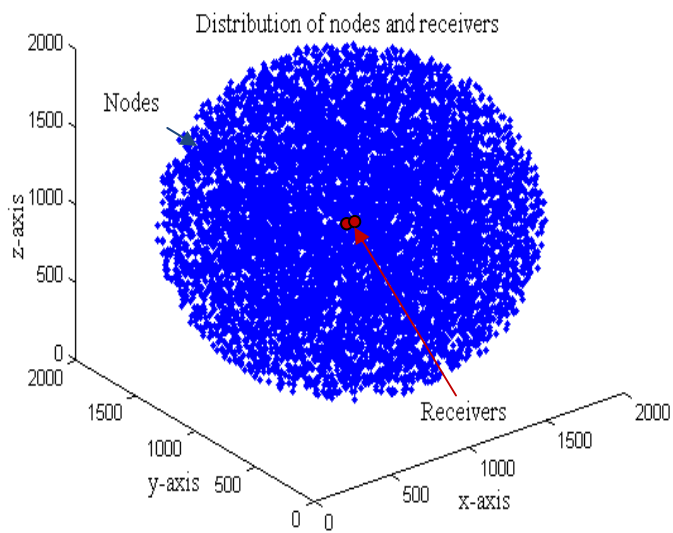
Step4: Now, we discuss the theory regarding this phenomenon using Figure 4.3. If we cross-correlate two signals that are the summation of several Gaussian signals inside a boundary, for each signal we obtain a Dirac delta which occupies a location inside a space of width  $2d_{DBS}$  (which is divided equally into several bins).



(a)

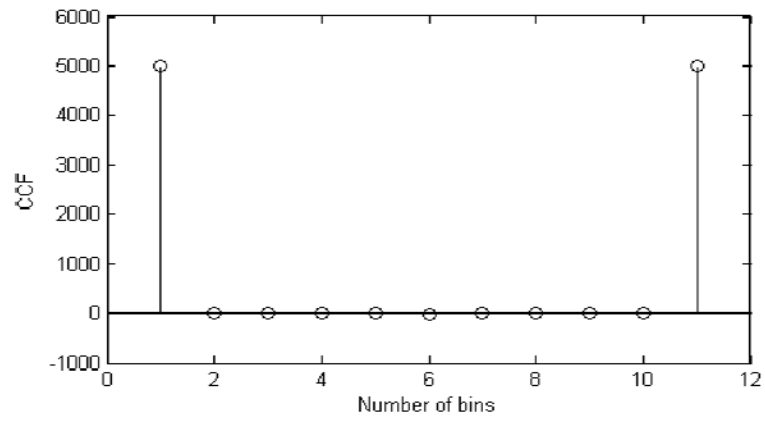


(b)

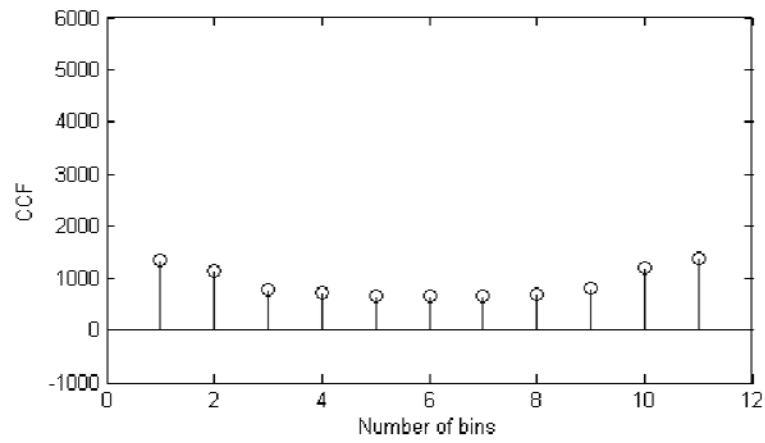


(c)

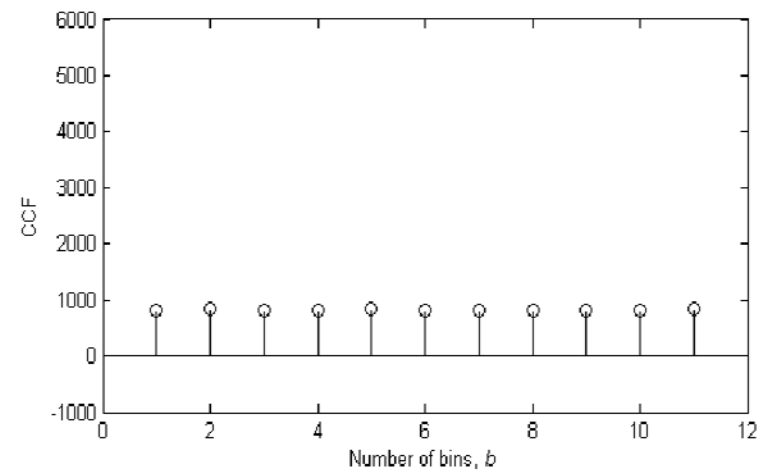
**Figure 4.1 Distributions of (10,000) nodes in (a) 1D; (b) 2D; and (c) 3D**



(a)

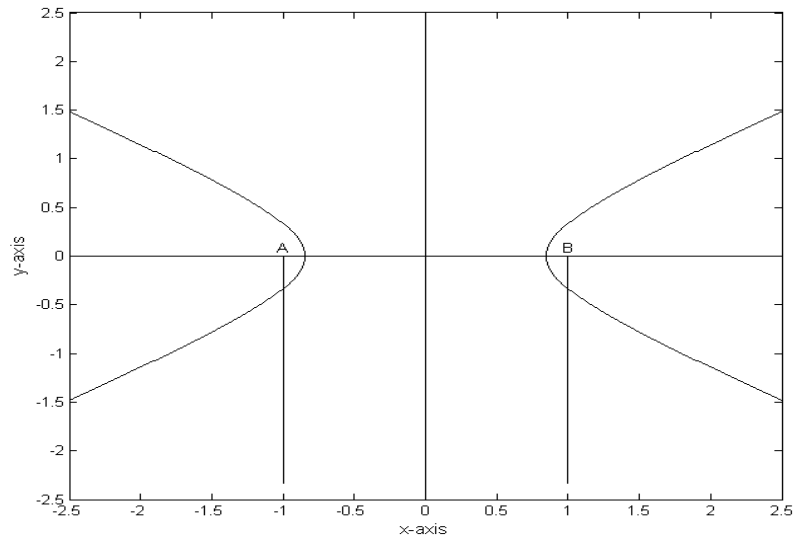


(b)

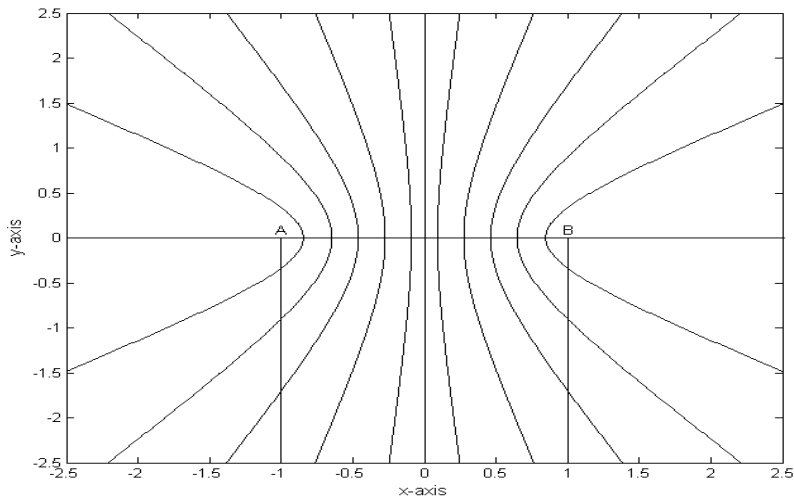


(c)

**Figure 4.2 CCFs versus  $b$ : (a) 1D; (b) 2D; and (c) 3D**



(a)



(b)

**Figure 4.3 Representation of hyperbolas of deltas contributing to the same bin:  
(a) 1D; and (b) 2D**

This location is determined by the delay difference between the signals arriving at the receivers at the probing node(s). The deltas of delay differences equal to a bin distance from the centre bin are placed in that particular bin. It is shown in (Roux 2005) that the deployment of nodes (which determines the placements of deltas) of equal delay difference follows a hyperbola, as shown in Figure 4.3.

Thus, the number of deltas in a certain bin is the number of transmitting nodes inside two hyperbolas placed at the edges of that bin as shown in Figure 4.3 (b). Physically the area inside those two hyperbolas is occupied by a number of hyperbolas to cover all of the nodes in that area. Although there will be some variations in the delay differences, they are considered same for a bin area. As the transmitting nodes are distributed randomly, the number of nodes is proportional to the area inside those hyperbolas.

Step5: Let us consider 11 bins of equal length, as shown in Figure 4.3 (b). To estimate the number of deltas in a particular bin, Figure 4.4 is plotted for the bin at the locations of receivers *A* and *B* at the probing node(s).

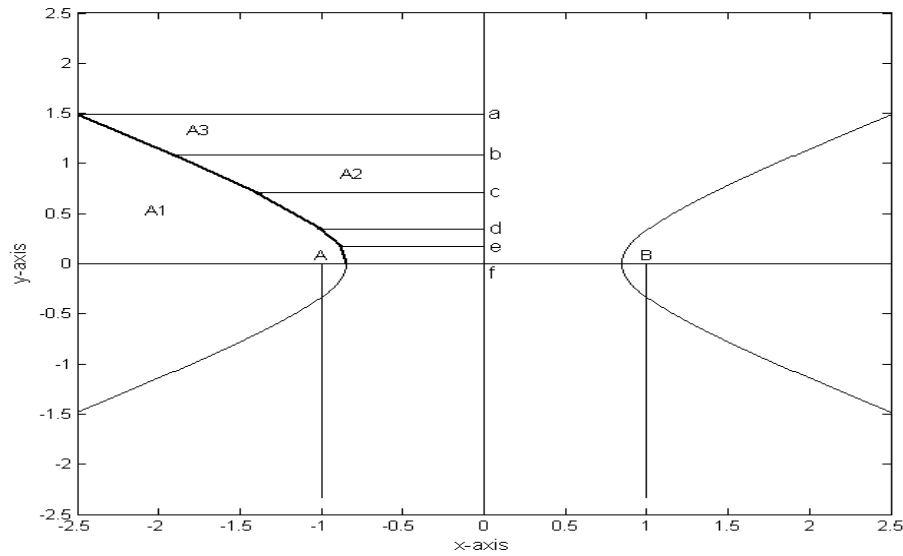


**Figure 4.4 Representation of hyperbolas for theoretically calculating the number of deltas in bin**

Step 6: To obtain the area inside the two hyperbolas shown in Figure 4.4, the trapezoidal rule of numerical integration is used.

From Figure 4.4, the area is calculated as:

$$\text{Area, } A_1 = \text{Area, } A_3 - \text{Area, } A_2 = 1.7 \text{ m}^2$$

So, the percentage of the number of deltas at the bin at location *A* is:



$$\frac{2 \times \text{Area } A_1}{\text{TotalArea}} \times 100\% \approx 13.6\%$$

Distributions of the deltas in the bins can also be formulated as in (Papoulis 2002; Maisel 1983). It is known that it is possible to represent discrete random variables as well as random variables, with a generalized probability density function using Dirac delta function; for example, if a discrete random variable takes only two values  $-1$  or  $1$ , with probability half each, the probability density associated with this variable is (Papoulis 2002; Maisel 1983):

$$f(t) = \frac{1}{2} \{ \delta(t + 1) + \delta(t - 1) \} \quad (4.1)$$

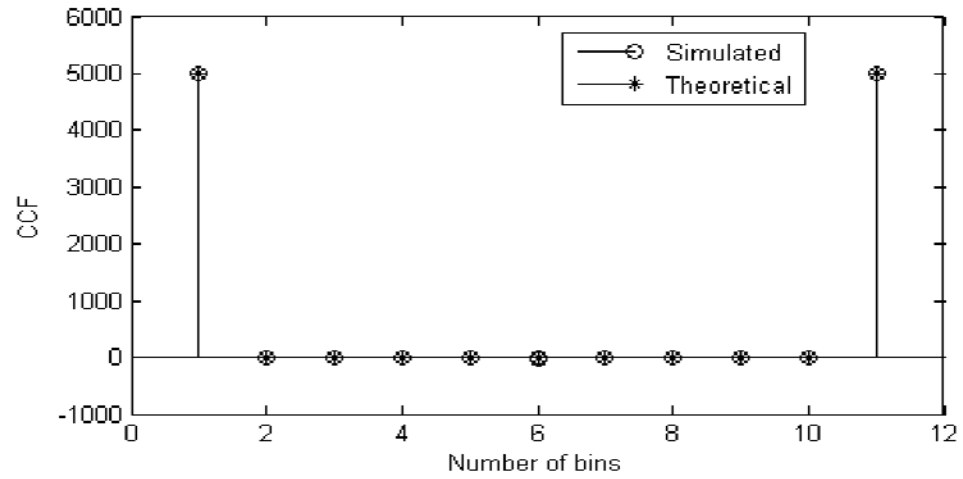
More generally, if a discrete variable can take  $n$  different values among real numbers, the associated probability density function is (Papoulis 2002; Maisel 1983):

$$f(t) = \sum_{i=1}^n P_i \delta(t - x_i) \quad (4.2)$$

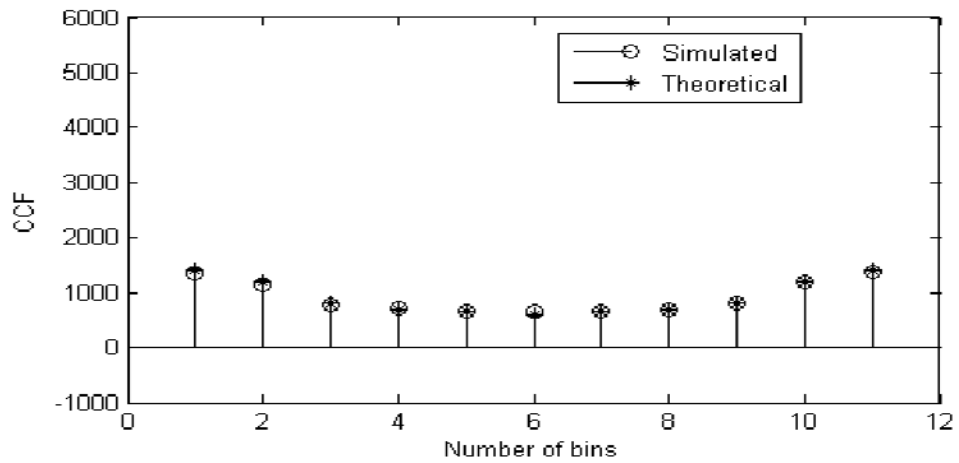
where  $x_1, \dots, x_n$  are the discrete values accessible to the variable and  $P_1, \dots, P_n$  the probabilities, which indicate the amplitudes of the deltas associated with these values.

If we assume that the deltas and number of nodes are of equal strengths, and the percentage of deltas in a bin is the probability, the theoretical distributions can be estimated by equation (4.2) and are plotted in Figure 4.5 with a comparison to the simulation obtained earlier.

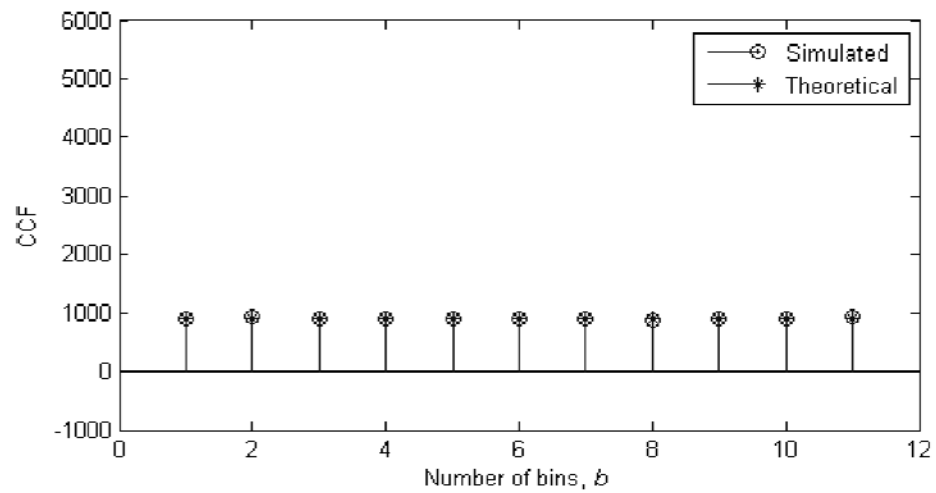
It can be seen from the results that the theoretical CCF matches the simulated CCF in all networks' dimensions.



(a)



(b)



(c)

**Figure 4.5 Simulated and theoretical distributions of CCFs:**

**(a) 1D; (b) 2D; and (c) 3D**

### 4.2.2 Estimation of dimensionality of communication network

The analytical and simulated results in Figure 4.5 show that they are similar for corresponding dimensionalities. However, the shapes of the CCFs vary according to the different dimensionalities of the networks, i.e., the CCF is dependent on a network's dimensionality. By utilising this dependency, the simple process of networks' dimensionality estimation is as follows.

Recalling the cross-correlation process with 10,000 nodes and 11 bins discussed in Section 4.2.1, we have three theoretical shapes of the nodes to the bins for 1D, 2D and 3D, as shown in Figure 4.5.

Now, suppose we have a CCF from a simulation or experiment which is similar in shape of any of the theoretical CCFs according to the dimensionality. By looking at its shape, we can decide whether the network is 1D, 2D or 3D. However, to make this process computationally feasible, these simulated or experimental CCFs are compared with the analytical CCFs using a computational method. The results are helpful in deciding the network's dimension. To do this, recall simulated results with similar parameters as used in Section 4.2.1 for 2D network and the shape of the simulated CCF is shown in the Figure 4.6.

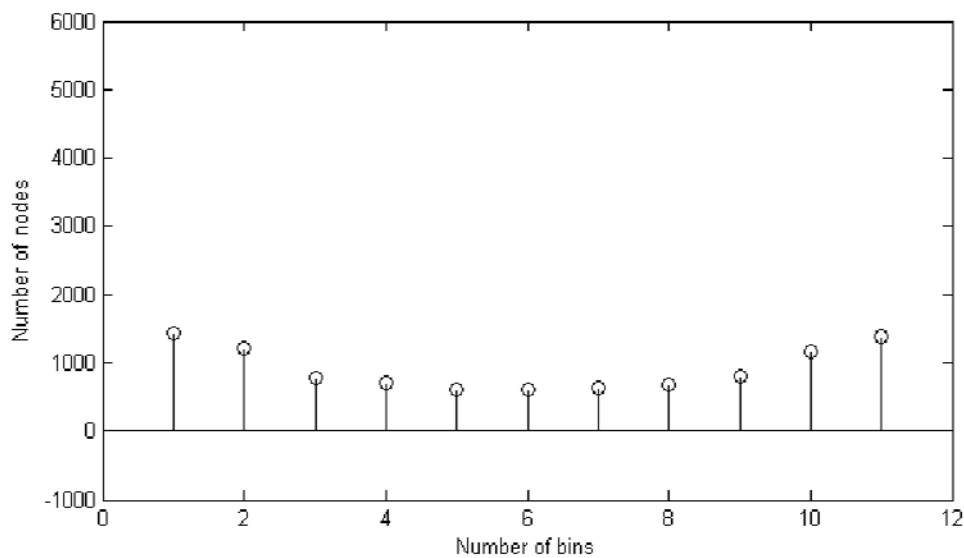


**Figure 4.6 Distributions of nodes in bins from observed (simulated) cross-correlation process**

To estimate the dimensionality of the network, we use the cost function (sum of square errors) (Sirovich 2011) as:

$$\arg \min_{D \in \{1,2,3\}} \sum_{i=1}^b e_{Di}^2 = \arg \min_{D \in \{1,2,3\}} \sum_{i=1}^b (P_{T_{Di}} - P_{O_i})^2$$

where  $P_{T_{Di}}$  is the peak of the theoretical CCF at the  $i^{\text{th}}$  bin for  $D$  dimensional WCN,  $P_{O_i}$  the peak of the observed CCF at the  $i^{\text{th}}$  bin for an observed WCN, and  $e_{Di}$  the error, misfit or deviation between the theoretical and observed peaks in the  $i$ th bin.

In MATLAB, we use the function to obtain the networks' dimensionality:

$$[e_{\min} D] = \min \left( \sum_{i=1}^b e_{Di}^2 \right)$$

where  $D$  gives the position at which the cost function is minimised and  $e_{\min}$  is the minimum value of  $\sum_{i=1}^b e_{Di}^2$ . This position i.e. the value of  $D$  is considered here as the dimensionality of the network.

Using the theoretical CCFs in Figure 4.2, the simulated CCF in Figure 4.6 gives the values of the cost functions for 1D, 2D and 3D as, respectively,

$$\sum_{i=1}^{11} e_{1i}^2 = 3 \times 10^7, \sum_{i=1}^{11} e_{2i}^2 = 3 \times 10^3, \text{ and } \sum_{i=1}^{11} e_{3i}^2 = 1 \times 10^6$$

Now, from the MATLAB expression,

$$[e_{\min} D] = \min(3 \times 10^7 \ 3 \times 10^3 \ 1 \times 10^6),$$

As in the above expression  $e_{\min}$  is  $3 \times 10^3$  at position 2,  $D$  gives the value of 2, i.e., the network is 2D. Thus it is easy to estimate the networks' dimensionality from the CCF.

### 4.2.3 Effect of fractional-samples delays on dimensionality estimation

To show the effect of fractional-sample delays on the estimation of network dimensionality, some simulation results for the CCF are provided in Figures 4.7 to 4.9 for 1D, 2D and 3D networks, respectively. It can be seen that these CCFs are not greatly affected by fractional-sample delays as, although there are slight variations in their shapes with and without them, they are still able to estimate the network's dimensionality using the following expression which was used earlier for integer-sample delays:

$$\arg \min_{D \in \{1,2,3\}} \sum_{i=1}^b e_{Di}^2 = \arg \min_{D \in \{1,2,3\}} \sum_{i=1}^b (P_{T_{Di}} - P_{O_i})^2$$

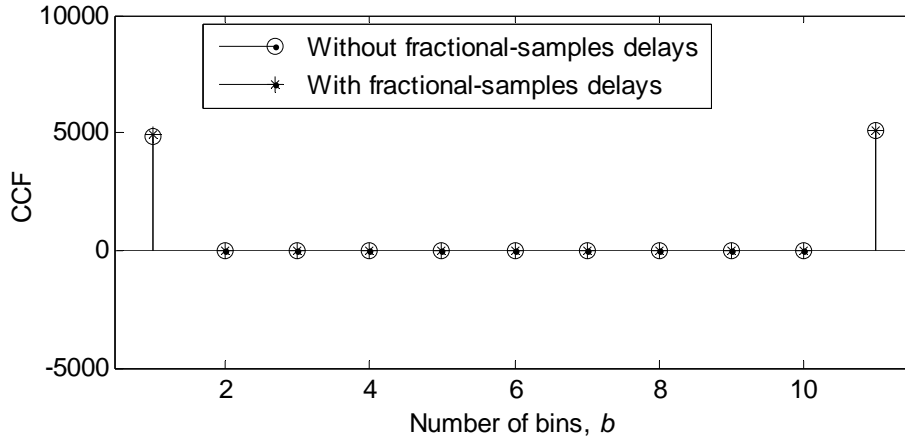


**Figure 4.7 Simulated CCFs with and without fractional-samples delays in 1D network**

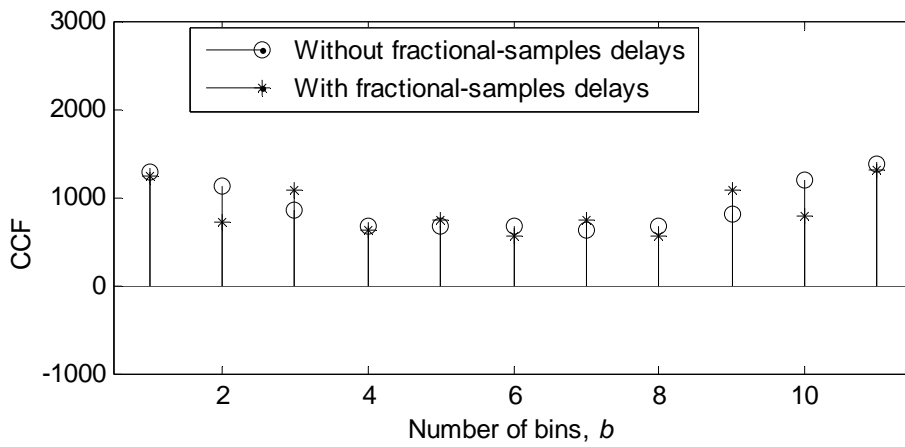


**Figure 4.8 Simulated CCFs with and without fractional-samples delays in 2D network**

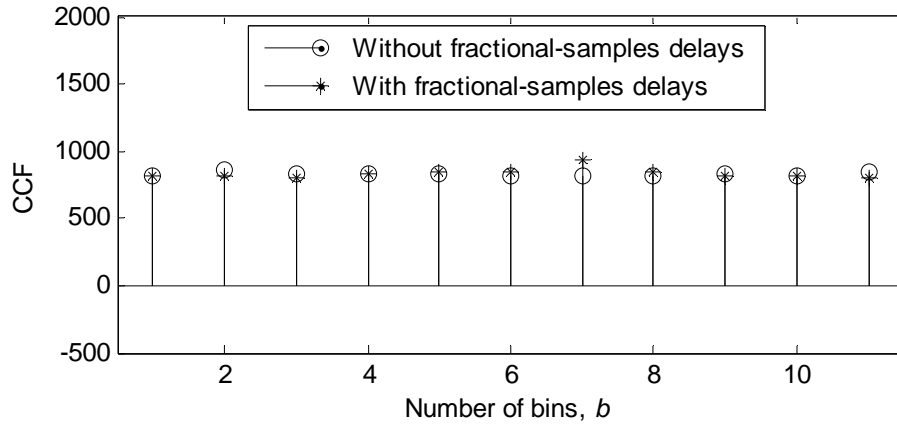


**Figure 4.9 Simulated CCFs with and without fractional-samples delays in 3D network**

#### 4.2.4 Conclusion

Thus, one can estimate the dimensionality of a communication network using the shapes of CCF. Although this system needs equal signal powers from the nodes, it is irrelevant what these powers are. However, as it is an exact method, which gives only three distinct estimations of dimensionality - 1D, 2D and 3D, it will only be accurate if the proper system requirements are maintained. In case of wrong estimation, the estimation will be dramatically different and the error will be higher. For example, in the case of 3D network, if we get the simulated result 1D or 2D, then the estimation will be completely different but if we get 3D then it will be 100% accurate. To mitigate the limitation, another approach is provided in the following section.

### 4.3 Estimation using $R$ of CCF of dimensionality

Estimation of dimensionality using the shape of CCF, discussed in the previous section, is useful but has the limitation of incurring a severe error in the case of a wrong estimation. To overcome this limitation, another estimation technique using the ratio,  $R$ , of the CCF is investigated and discussed in this section. In this process, the  $R$ s are first obtained for all dimensions and then the dimensionality is decided from the variation of these  $R$ s. This approach is very similar to the earlier number of nodes' estimation technique with the exception that the binomial distribution with

unequal probabilities for all bins is considered in order to obtain the standard deviation and mean of the CCF. This is explained further with the following results and discussion.

### 4.3.1 Theoretical estimation

It is known that the placement of nodes in a bin is binomially distributed with the parameters  $n_i$  and  $p_i$  (Vogt 2002a; Vogt 2002b), where the parameters indicate the number of nodes in the  $i^{\text{th}}$  bin and the probability of success of that bin, respectively. This is true for all bins in a cross-correlation process.

Again, the expected values and variances in the total number of successes in  $n$  independent Bernoulli trials with  $p_j$  probability of success at  $j^{\text{th}}$  trial is expressed in (Wang 1993) as:

$$E(X) = \sum_{j=1}^n p_j$$

And the variance is

$$Var(X) = \sum_{j=1}^n p_j(1 - p_j)$$

If the trials are identical, i.e., the probabilities of success are

$$p_1 = p_2 = p_3 = \dots = p_n = p,$$

the expected values and variances are, respectively

$$E(X) = \sum_{j=1}^n p_j = np$$

and

$$Var(X) = \sum_{j=1}^n p_j(1 - p_j) = np(1 - p).$$

In the proposed case, as the trials' probabilities of achieving successes in a bin is equal, the number of groups with identical probabilities is equal to the number of bins,  $b$ .

Thus, the expected value (the mean) of the CCF in this case is

$$\begin{aligned}
 E(X) &= \mu = \sum_{j=1}^n p_j \\
 &= \sum_{i=1}^b n_i p_i, \text{ where } n_i \text{ is the number of trials of equal probabilities of successes} \\
 &= \sum_{i=1}^b (np_i) p_i; \text{ as } n_i = np_i \\
 &= \sum_{i=1}^b np_i^2 \\
 &= n \sum_{i=1}^b p_i^2
 \end{aligned}$$

Similarly, the variance is

$$\begin{aligned}
 Var(X) &= \sigma^2 = \sum_{j=1}^n p_j(1 - p_j) \\
 &= \sum_{i=1}^b n_i p_i(1 - p_i) \\
 &= \sum_{i=1}^b (np_i) p_i(1 - p_i); \text{ as } n_i = np_i \\
 &= \sum_{i=1}^b np_i^2(1 - p_i) \\
 &= n \sum_{i=1}^b (p_i^2 - p_i^3)
 \end{aligned}$$

So, the standard deviation is

$$\sigma = \sqrt{n \sum_{i=1}^b (p_i^2 - p_i^3)}$$

Thus, the ratio of the standard deviation to the mean,  $R$ , is



$$R = \frac{\sigma}{\mu} = \frac{\sqrt{n \sum_{i=1}^b (p_i^2 - p_i^3)}}{n \sum_{i=1}^b p_i^2} = \frac{1}{\sqrt{n}} \left( \frac{\sum_{i=1}^b (p_i^2 - p_i^3)}{\left( \sum_{i=1}^b p_i^2 \right)^2} \right)$$

Using the above relationship, we can obtain the ratio of the standard deviation to the mean of the CCF for different network dimensions to estimate the dimensionality of the network by knowing only the  $p_i$ . The probabilities of successes for the bins are defined in this proposed technique as:

$$p_i = \frac{n_i}{n}; \text{ for } i = 1 \text{ to } b$$

The theoretical probabilities of successes for the bins in a 1D network are:

$$\begin{aligned} p_i &= \frac{n_i}{n} = \frac{1}{2}; \text{ for } i = 1 \text{ and } b \\ &= 0; \text{ otherwise} \end{aligned}$$

The ratio of the standard deviation to the mean,  $R_{1D}$ , is:

$$R_{1D} = \frac{1}{\sqrt{n}} \left( \frac{\sqrt{2 \times \left\{ \left( \frac{1}{2} \right)^2 - \left( \frac{1}{2} \right)^3 \right\}}}{\left\{ 2 \times \left( \frac{1}{2} \right)^2 \right\}^2} \right) = \frac{1}{\sqrt{n}}$$

Similarly, for a 2D network, the theoretical probabilities of successes for the bins are:

$$\begin{aligned} p_1 &= p_{11} = \frac{n_1}{n} = 0.1360; \quad p_2 = p_{10} = \frac{n_2}{n} = 0.1150 \\ p_3 &= p_9 = \frac{n_3}{n} = 0.0780; \quad p_4 = p_8 = \frac{n_4}{n} = 0.0710 \\ p_5 &= p_7 = \frac{n_5}{n} = 0.0626; \quad p_6 = \frac{n_6}{n} = 0.0623 \end{aligned}$$

These values are obtained following the step 6 of Section 4.2.1 where obtaining  $p_1$  is shown for example.

Thus, its ratio of the standard deviation to the mean,  $R_{2D}$ , is:

$$R_{2D} = \frac{1}{\sqrt{n}} \left( \sqrt{\frac{2 \times \{(0.1360)^2 - (0.1360)^3\} + 2 \times \{(0.1150)^2 - (0.1150)^3\} + 2 \times \{(0.0780)^2 - (0.0780)^3\} + 2 \times \{(0.0710)^2 - (0.0710)^3\} + 2 \times \{(0.0626)^2 - (0.0626)^3\} + 1 \times \{(0.0623)^2 - (0.0623)^3\}}{2 \times (0.1360)^2 + 2 \times (0.1150)^2 + 2 \times (0.0780)^2 + 2 \times (0.0710)^2 + 2 \times (0.0626)^2 + 1 \times (0.0623)^2}} \right)$$

$$\approx \frac{3}{\sqrt{n}}$$

Similarly, for a 3D network, the theoretical probabilities of successes for the bins are:

$$p_i = \frac{n_i}{n} = \frac{1}{11} \approx 0.0909 ; \text{ for } i = 1 \text{ to } b$$

Thus, its ratio of the standard deviation to the mean,  $R_{3D}$ , is:

$$R_{3D} = \frac{1}{\sqrt{n}} \left( \sqrt{\frac{11 \times \{(0.0909)^2 - (0.0909)^3\}}{11 \times (0.0909)^2}} \right)$$

$$= \frac{3.1623}{\sqrt{n}}$$

These analytical ratios of the standard deviations to the means of the CCF for different dimensions can be represented as:

$$R_{1D} = \frac{1}{\sqrt{n}} = \frac{c_1}{\sqrt{n}}, \quad R_{2D} = \frac{3}{\sqrt{n}} = \frac{c_2}{\sqrt{n}}, \quad \text{and} \quad R_{3D} = \frac{3.1623}{\sqrt{n}} = \frac{c_3}{\sqrt{n}}$$

where  $c_1$ ,  $c_2$ , and  $c_3$  are the proportionality constants and is obtained from the theoretical data as shown in the above corresponding expressions.

The dimensions are 1, 2, or 3, but if the shape of the 2D, and 3D networks might vary from the basic assumption of circle and sphere, the dimensionality parameter might vary. To show this effect,  $R_{2.5D}$  is obtained from the CCF from the process below:

It is known that the CDF of the distribution of the uniformly distributed nodes are

$$g(d) = d^D$$

In this expression, considering  $D=2.5$ , it is easy to get the distances of the nodes from the centre of the nodes distribution (i.e. from the receivers). Getting the distances, the CCF is obtained using them from the moving average technique of CCF (discussed in Chapter 3) for other dimensions except the basic three discussed here. From that CCF, the dimensionality parameter has been obtained for  $D=2.5$  as shown in Figure 4.10.

In Figure 4.10, denoting the theoretical constants by  $W_T$  and named dimensionality parameter,  $W_T$  versus the dimensions,  $D$  are plotted. The results are approximated by a cubic expression as shown in Figure 4.10.

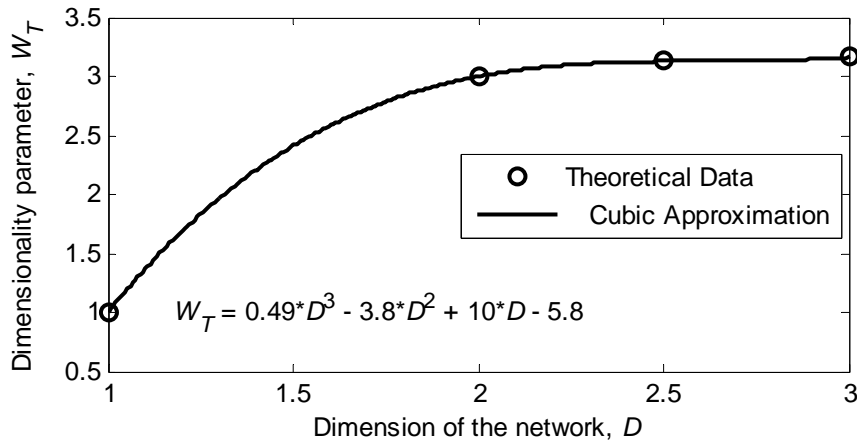


**Figure 4.10 Dimensionality parameter  $W_T$  versus Dimensions  $D$ : theoretical**

Precisely, the approximate expression from theory is:

$$W_T = 0.48657D^3 - 3.8383D^2 + 10.109D - 5.7571 \quad (4.3)$$

### 4.3.2 Estimation from simulation

Similarly with the simulated CCF for all dimensions, using the same procedures as for the theoretical results, we obtain the simulated ratio of the standard deviation to the mean of the CCF which is a parameter for estimating dimensionality.

In the simulation,

$$p_i = \frac{n_i}{\sum_{j=1}^b n_j}; \text{ for } i = 1 \text{ to } b$$

Then we can obtain the simulated ratio of the standard deviation to the mean,  $R_{iD}$ , where  $i = 1, 2, 3$ .

Thus, the ratio,  $R$ , is

$$R_{1D} = \frac{c_{11}}{\sqrt{n}}, \quad R_{2D} = \frac{c_{21}}{\sqrt{n}}, \quad \text{and} \quad R_{3D} = \frac{c_{31}}{\sqrt{n}},$$

where  $c_{11}$ ,  $c_{21}$ , and  $c_{31}$  are the proportionality constants and are obtained from the observed (simulated) data.

Again, as for the theoretical case, in Figure 4.11, denoting the simulated constants by  $W_S$  and named dimensionality parameter,  $W_S$  versus the dimensions,  $D$  are plotted. The results are again approximated by a cubic expression as shown in Figure 4.11. The  $R_{2.5D}$  in simulation is obtained from the same manner as in the theory discussed earlier.

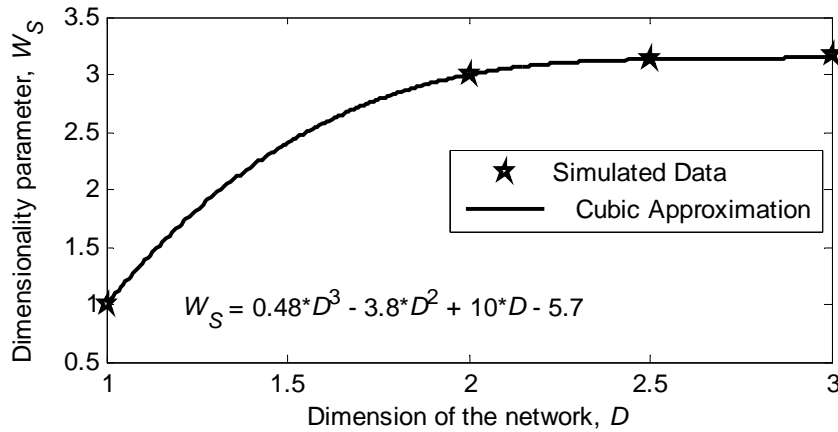


**Figure 4.11 Dimensionality parameter  $W_S$  versus Dimensions  $D$ : simulated**

Precisely, the approximate expression from simulation is:

$$W_S = 0.47753D^3 - 3.7849D^2 + 10.016D - 5.7142 \quad (4.4)$$

To compare the theoretical and simulated results, we plot the constants against the dimensions and number of nodes from the approximated expressions, as shown in Figures 4.12 to 4.14. Figure 4.12 is the comparison of theory and simulation with some fractional dimensions, where the extra points are obtained using the expressions of  $W_T$  and  $W_S$  from (4.3) and (4.4).

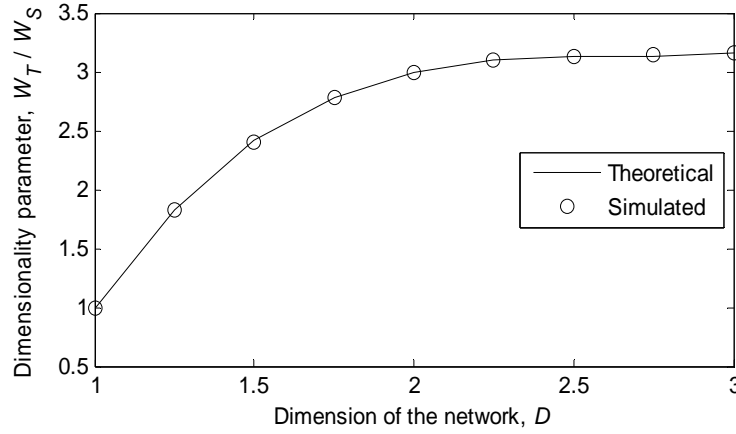


**Figure 4.12 Dimensionality parameter  $W_T$  or  $W_S$  versus Dimensions  $D$ : theoretical and simulated**

To show the effect of  $N$  on the dimensionality parameter, in Figure 4.13 the dimensionality parameters are plotted against  $N$ .

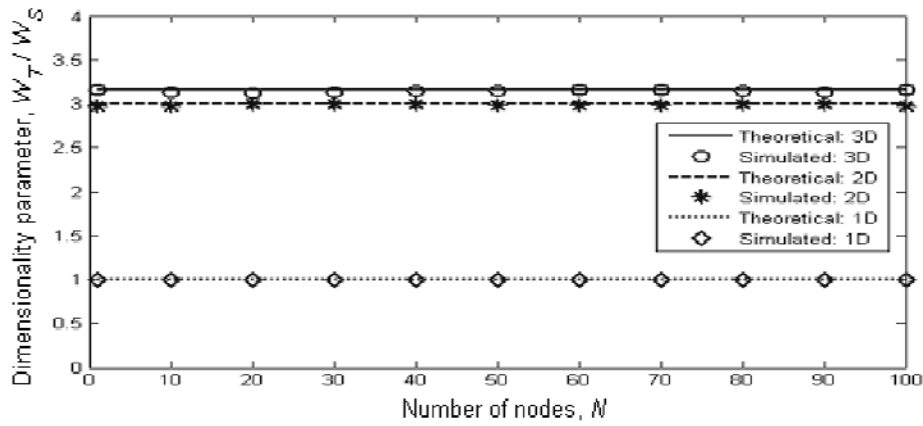


**Figure 4.13 Dimensionality parameter  $W_T$  and  $W_S$  versus Number of nodes  $N$ : theoretical and simulated**

It implies that the dimensionality parameter is independent of  $N$ , which is helpful for any size of network. 1D is a unique case and it is far different from 2D and 3D results. Although the 2D and 3D results are close, the difference is clear enough to

separate them both in theoretical and simulated results. Sometimes, the network might exactly not follow the assumption of 2D a circle and 3D a sphere. But the results of dimensionality parameter will be between 1 and 3 for any 2D network and between 3 and 3.1623 for any 3D network. Thus we can extend this technique to estimate the dimensionality for any network.

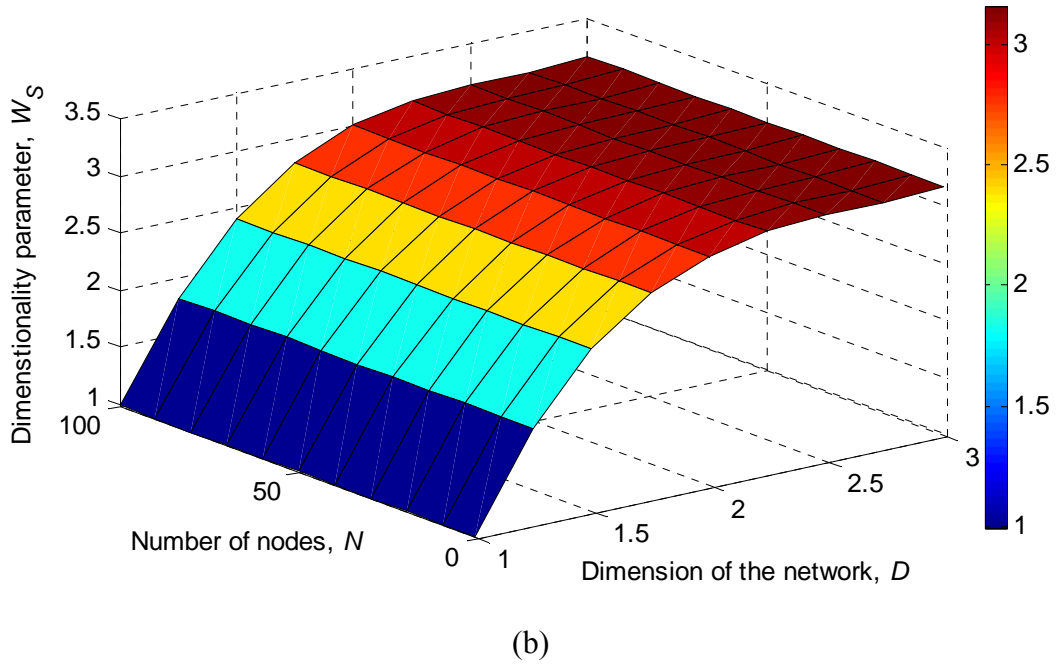
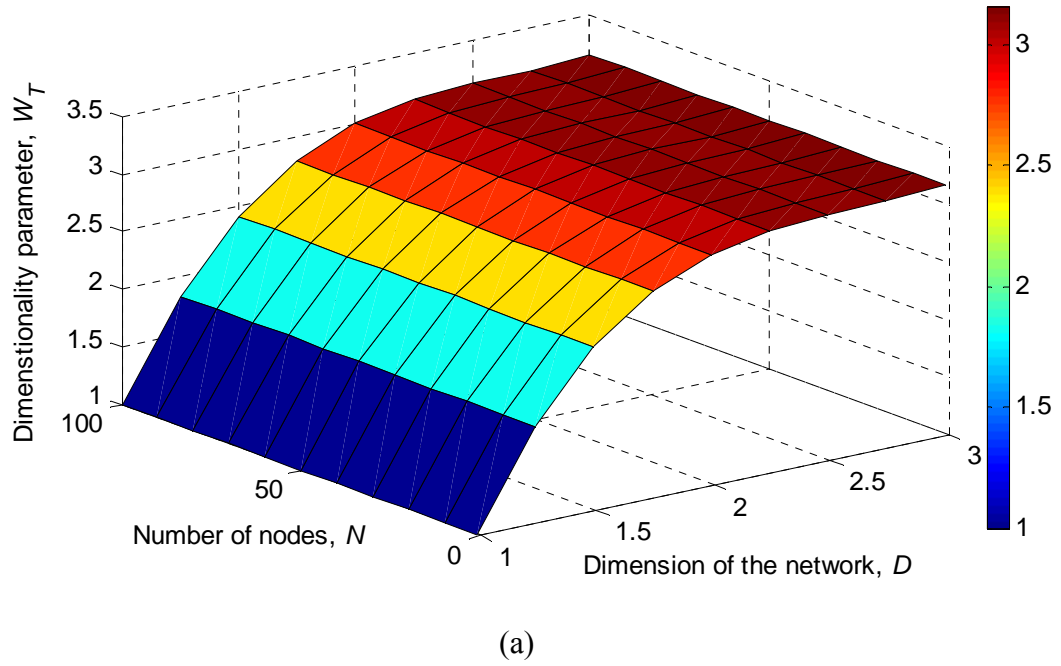


**Figure 4.14** Surface plots Dimensionality parameter  $W$ , Dimensions  $D$ , and Numbers of nodes  $N$ : (a) analytical; and (b) simulated

To show both effects (effect of  $D$  and  $N$ ) on the dimensionality parameter at a time, two surface plots are provided in Figure 4.14. Figure 4.14 (a) shows the theoretical whereas Figure 4.14 (b) the simulated results. It can be seen that the theoretical and simulated results sufficiently match each other to obtain the networks' dimensionality.

### 4.3.3 Effect of fractional-samples delays on dimensionality

The expression of  $R$  using binomial distribution in each bin of the CCF obtained in Section 4.3.1 is:

$$R = \frac{\sigma}{\mu} = \frac{\sqrt{n \sum_{i=1}^b (p_i^2 - p_i^3)}}{n \sum_{i=1}^b p_i^2} = \frac{1}{\sqrt{n}} \left( \frac{\sum_{i=1}^b (p_i^2 - p_i^3)}{\left( \sum_{i=1}^b p_i^2 \right)^2} \right)$$

In Section 4.3.2, the dimensionality parameter varied with different dimensionalities in the expressions of the  $R$  of the CCF and a cubic approximation was used to obtain the dimensionality estimation where the sample delays taken were only of integer values. It is shown in Figure 4.15 that a similar quadratic approximation is also valid for the expression with fractional-samples delays.

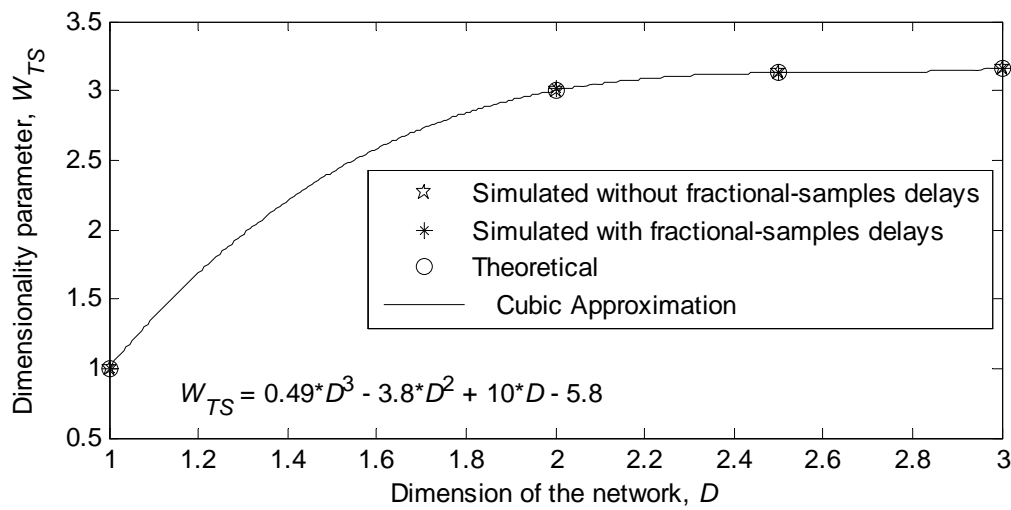


**Figure 4.15 Dimensionality parameter  $W_{TS}$  versus Dimensions  $D$**

#### 4.3.4 Conclusion

This dimensionality estimation proposes another technique for estimating the dimensionality of a communication network. However, it is not an exact method, giving fractional dimensionality of any values between 1 and 3 instead of 1, 2, and 3 only as in exact method, and thus in the case of a wrong estimation, the error will be less because of fractional results. Actually the wrong estimation indicates that the shape of the network is not exactly the same as sphere in 3D, or circle in 2D, so the dimensionality parameter will be different from the value obtained with 3D sphere or 2D circle. Thus the obtained dimensionality  $D$  might change. Suppose we can get the  $D=2.9$  instead of 3 for 3D network, the error is 3.33%, which is very low with compared to the 33.33% with exact method (if I get 2 instead of 3 in 3D network from the exact method). Again, the effect of fractional-samples delays has been investigated for this technique and it is shown that the process is applicable with and without fractional-samples delays.

Although the proposed methods of dimensionality estimation are only discussed for three basic dimensionalities, they can work in other cases, for example where most nodes were on a disc but just a few were off the plane of the disc in a two dimensional network. Both methods will declare the network as 2D. The cost function method is suitable because it compares the CCF shapes. As the shape of the CCF of the test network matches better with 2D theoretical CCF, it will give the estimation as 2D without any error. Although the second method can provide the estimation, there might be some error in estimation for the mismatches in the simulated and theoretical estimation parameters.

The term fractional dimensionality physically indicates the deviated dimensionality from the basic dimensionalities. The basic dimensionalities in this thesis are a straight line in 1D, a circle in 2D, and a sphere in 3D. Consider a network whose shape is exactly neither linear nor circular is a network with fractional dimensionality. Its dimensionality might be of any values between 1 and 2 depending on the closeness of the shape towards 1D or 2D. Although there will be some error in dimensionality estimation, detail error analysis is left for the future work.



## 4.4 Estimation of the numbers of nodes in different dimensions

In this section, the same process of dimensionality estimation discussed in Section 4.3.2 is used to estimate the number of nodes. Actually, the ratio,  $R$ , is used for estimation. To simplify the procedure, suppose we have three analytical and three simulated CCFs from which the corresponding ratios of the standard deviation to the mean are obtained using the expressions discussed in Section 4.3.2.

The parameters for obtaining the analytical and simulated CCFs are:

Number of nodes = 1 to 100

Number of bins = 11

Both the simulated and analytical results for the three dimensions with integer samples delays are shown in Figures 4.16 to 4.18. Simulated results are obtained from the average of 100 iterations. Figure 4.16 for 1D, Figure 4.17 for 2D, and Figure 4.18 for 3D network. The solid lines indicate the theoretical whereas the circles indicate the simulated results. It can be seen from the results that in all dimensions, the theoretical and simulated results match sufficiently to obtain the estimation of  $N$ , which ensures the capability of the process.

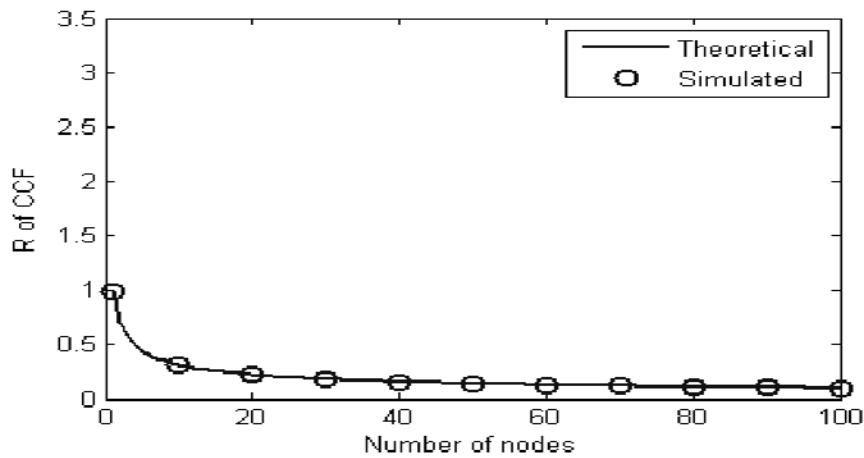


**Figure 4.16 Comparison of ratios,  $R$ , of CCF versus  $N$ : 1D network**

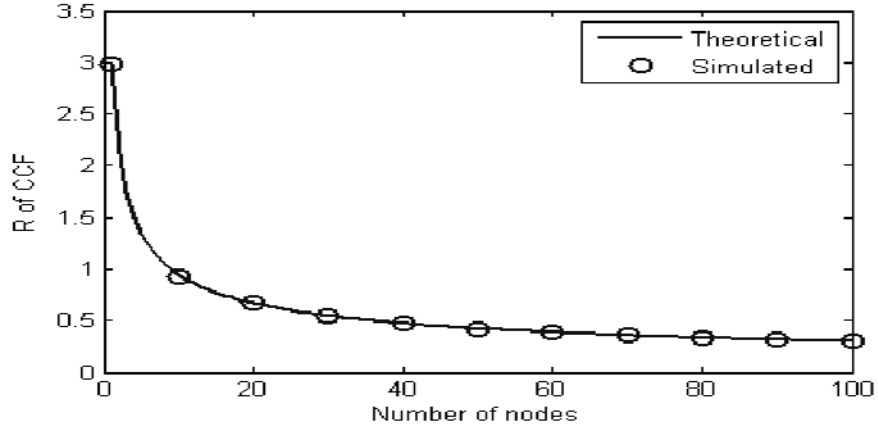


**Figure 4.17 Comparison of ratios,  $R$ , of CCF versus  $N$ : 2D network**

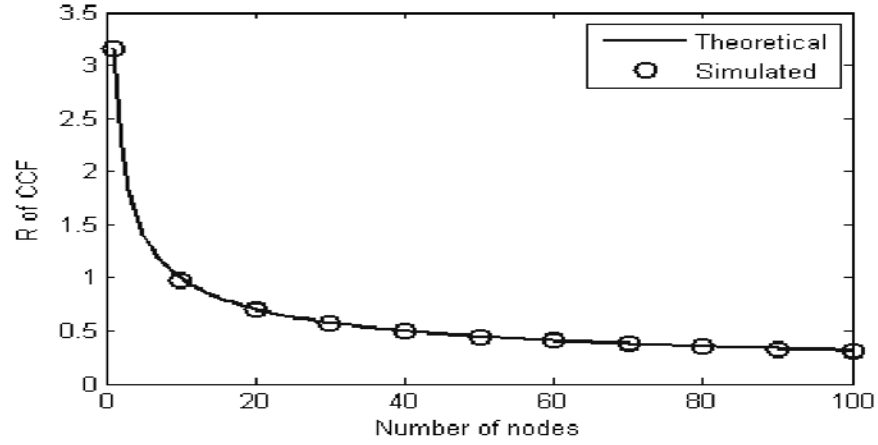


**Figure 4.18 Comparison of ratios,  $R$ , of CCF versus  $N$ : 3D network**

#### **4.4.1 Effect of fractional-samples delays**

In this section, the same process of dimensionality estimation discussed in Section 4.4 is used to estimate the number of nodes considering fractional-sample delays.

Both the simulated and analytical results, with and without fractional-sample delays, are shown in Figures 4.19 to 4.21 in which it can be seen that the process is equally applicable with the fractional-samples delays.

However, this method is only suitable if the signal strengths from the nodes are equal and unity. This is discussed here with the Figures 4.22 to 4.25 in which the signal strengths are doubled from the previous case.

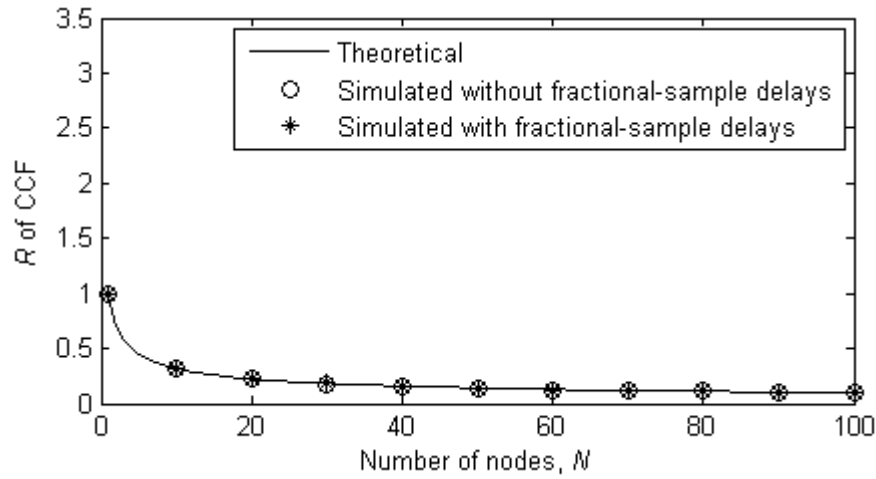


**Figure 4.19  $R$  of CCF versus  $N$ : 1D network**

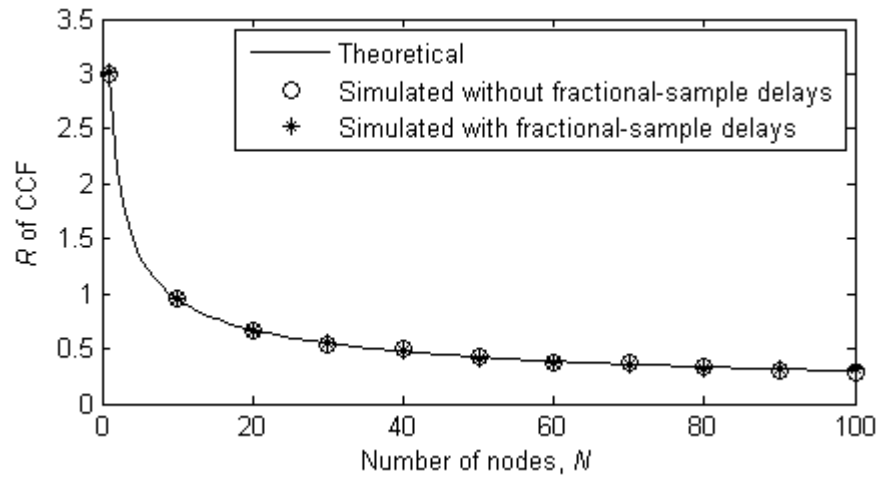


**Figure 4.20  $R$  of CCF versus  $N$ : 2D network**

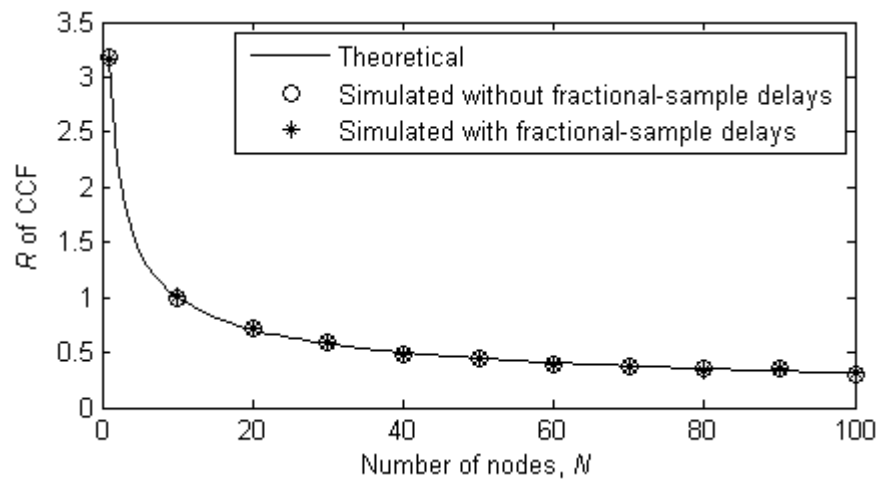


**Figure 4.21  $R$  of CCF versus  $N$ : 3D network**

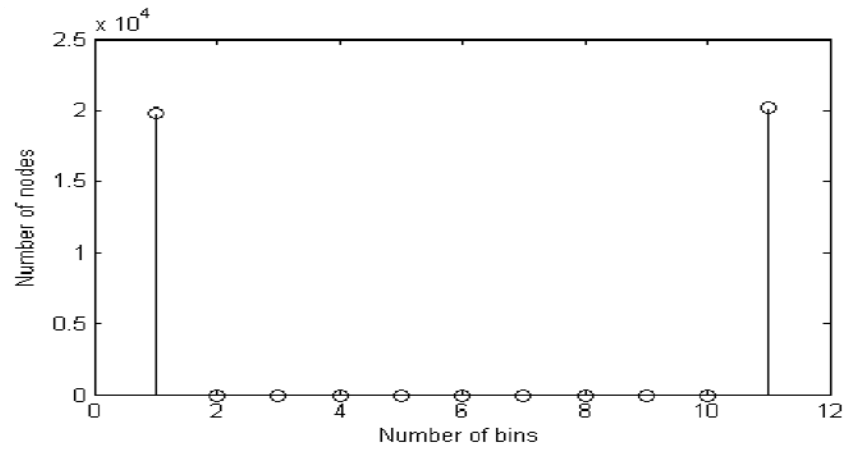


**Figure 4.22 Simulated CCF: 1D**

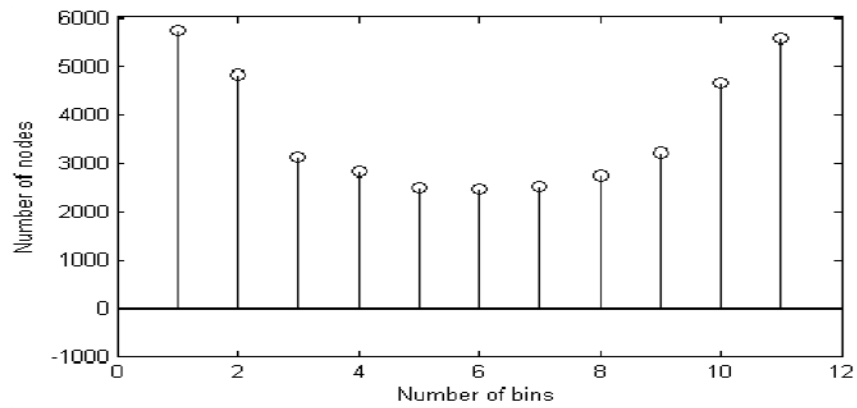


**Figure 4.23 Simulated CCF: 2D**

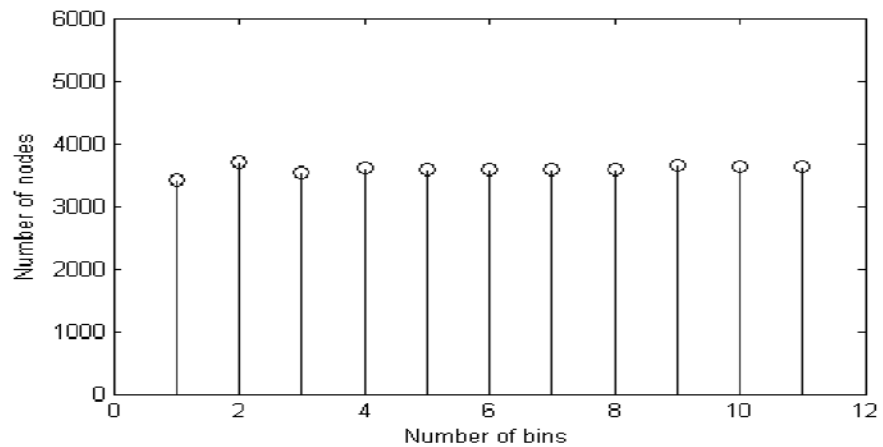


**Figure 4.24 Simulated CCF: 3D**

The resulting ratios of the standard deviations to the means of the CCFs are shown in Figure 4.25. It shows that the simulated line does not follow the theoretical line. But

it follows the theoretical results when they are divided by two. This variation is due to the different signal power in the cross-correlation process.

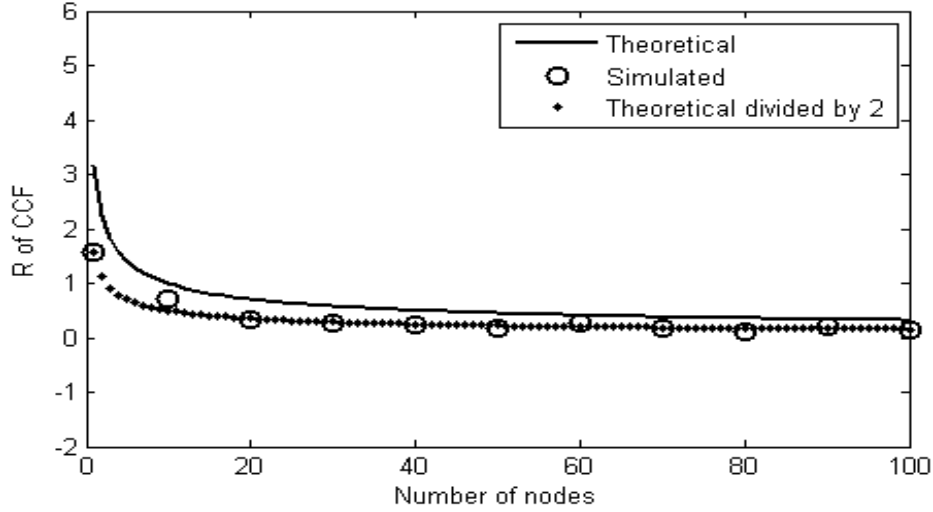


**Figure 4.25 Comparison of ratios,  $R$ , of CCF versus  $N$ : 3D network**

It can be seen that the method for estimating the number of nodes proposed in this work is only suitable when all received signals strength from the nodes are equal and unity. Although obtaining equal signal strengths from the nodes is possible using the probing technique, achieving unity values is not possible without knowing the prior knowledge of the signal strengths. Therefore, another approach is proposed in the following section.

## **4.5 Estimation of the numbers of nodes for different dimensions: another approach**

It is shown in the previous section that the proposed process is adequate for estimation although it has a limitation in terms of signal strength. To overcome this, we propose another approach for estimating the number of nodes which is similar to the basic approach discussed in Chapter 3 for the 3D ERP case. As has already been discussed the shapes of the CCFs are different for different dimensions, so for those other than 3D, we have to scale the results to obtain proper estimations. The following analysis details this estimation process.

In our earlier work of Chapter 3, the theoretical ratio of the standard deviation to the mean of CCF in 3D network,  $R_{3DT}$  is obtained as:

$$R_{3DT} = \frac{\sqrt{npq}}{np} = \sqrt{\frac{q}{np}} \quad (4.5)$$

where

$n$  = number of trials i.e. nodes in CC process,

$p$  = probability of success, and

$q = 1-p$

In addition, from the simulated CCF, the ratio of the standard deviation to the mean of CCF in 3D network,  $R_{3DS}$  is obtained in MATLAB as:

$$R_{3DS} = \frac{\sigma(\text{CCF})}{\mu(\text{CCF})} = \frac{\text{std}(\text{CCF})}{\text{mean}(\text{CCF})} \quad (4.6)$$

In this section, for a 3D spherical network, the estimation is performed by the same manner with the above two expressions.

It is already mentioned that the placement of deltas due to the network nodes in a bin is binomially distributed, from which the theoretical CCF for a 1D network with  $N=10,000$  and  $b=11$  as shown Figure 4.26.

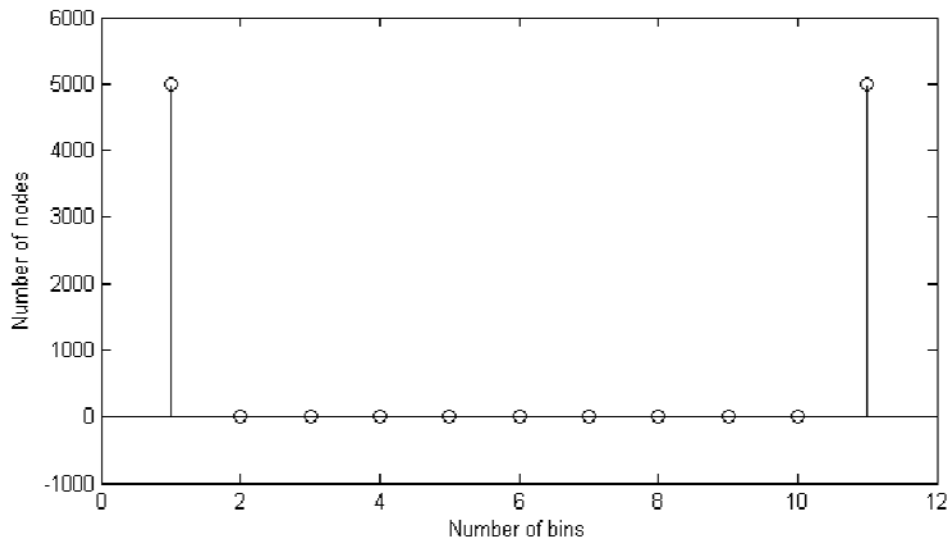


**Figure 4.26 Analytical CCF: 1D**

It can be seen from the figure that the CCF can be considered as two deltas in 11 bins. Thus the theoretical ratio of the standard deviation to the mean of CCF in 1D network,  $R_{1DT}$  is obtained as:

$$R_{1DT} = \sqrt{\frac{q}{np}} = \sqrt{\frac{q}{2p}} \quad (4.7)$$

And from the simulated CCF shown in Figure 4.27, the ratio of the standard deviation to the mean of CCF in 1D network,  $R_{1DS}$  is obtained in MATLAB as:

$$R_{1DS} = \frac{std(CCF_{1D})}{mean(CCF_{1D})} = \frac{\sigma(CCF_{1D})}{\mu(CCF_{1D})} \quad (4.8)$$

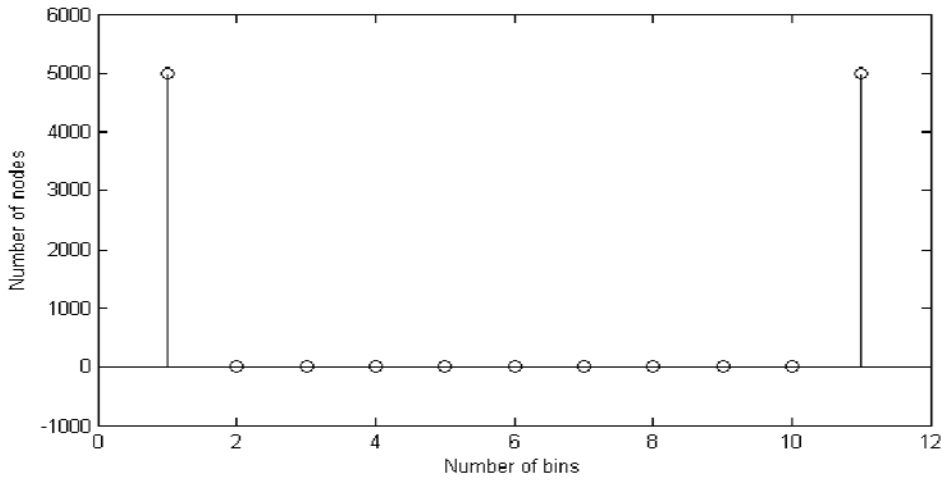


**Figure 4.27 Simulated CCF: 1D**

As it can be seen in the expression (4.7), the  $R_{1DT}$  is constant for all  $N$  and thus the estimation is not possible from that expression. So, another ratio,  $R_{13T}$  (derived from  $R_{1DT}$  and  $R_{3DT}$ ) is used for the estimation in 1D network.

The ratio  $R_{13T}$  is obtained as:

$$R_{13T} = \frac{R_{1DT}}{R_{3DT}} = \sqrt{\frac{\frac{q}{2p}}{\frac{q}{np}}} = \sqrt{\frac{n}{2}} \quad (4.9)$$

Similarly, the corresponding simulated ratio used in 1D network,  $R_{13S}$  is:

$$R_{13S} = \frac{R_{1DS}}{R_{3DS}} = \frac{R_{1DS}}{R_{3DT}} = \frac{\frac{std(CCF_{1D})}{mean(CCF_{1D})}}{\sqrt{\frac{q}{n\left(\sum_{i=1}^b n_i\right)p}}} = \frac{\frac{\sigma(CCF_{1D})}{\mu(CCF_{1D})}}{\sqrt{\frac{q}{n\left(\sum_{i=1}^b n_i\right)p}}} \quad (4.10)$$

Again the analytical CCF for a 3D spherical and a 2D circular networks are shown in Figure 4.28 and 4.29.

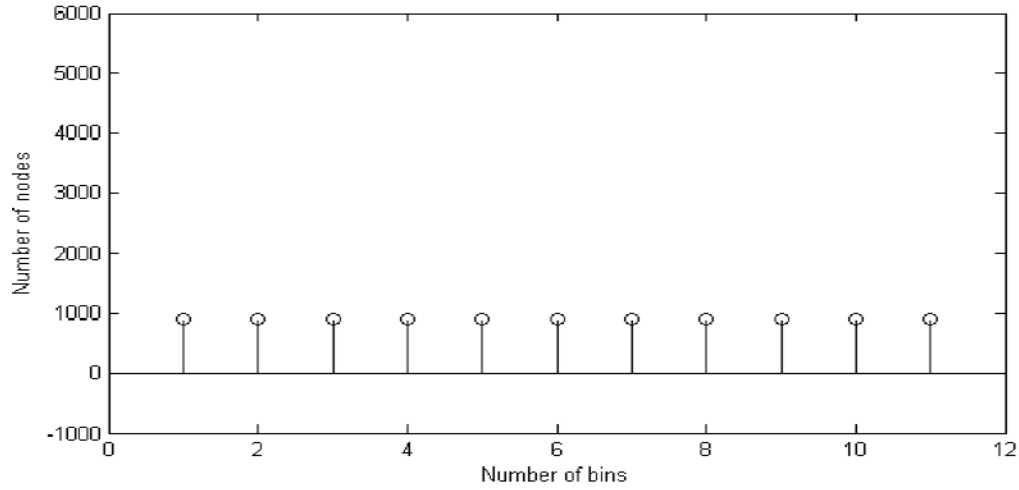


**Figure 4.28 Analytical CCF: 3D**

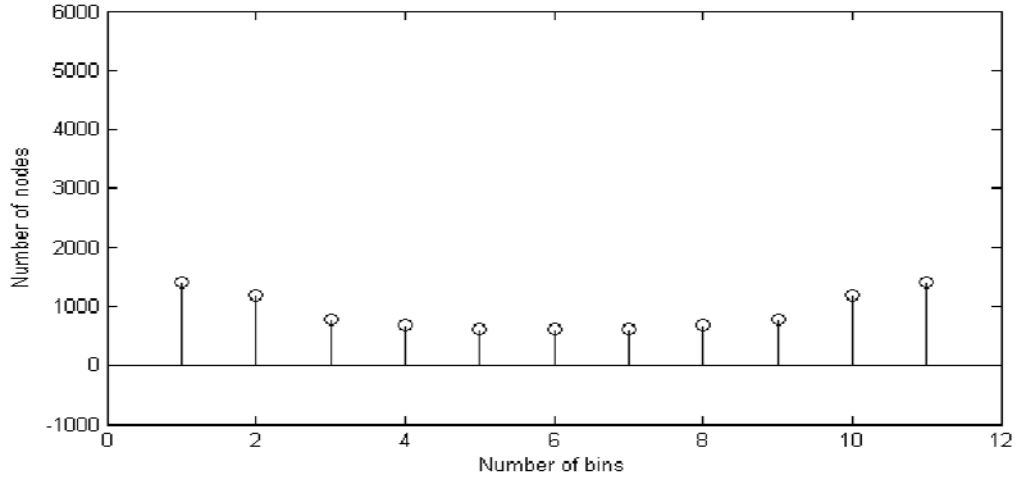


**Figure 4.29 Analytical CCF: 3D**

From these figures it is easy to obtain the percentages of deltas in the bins. Upon getting the percentages, another ratio of those percentages in the corresponding bins is obtained which is used later to convert the 2D CCF to 3D CCF. The following details the process.



The percentage of the deltas (number of nodes) at  $i^{\text{th}}$  bin with respect to summation of deltas (number of nodes) at all bins of the CCF for a  $D$  dimensional network is expressed as

$$V_{iD} = \frac{n_{iD}}{n} \times 100\%$$

Thus, the percentages of deltas in the bins for 2D,

$$V_{\text{deltas2D}} = [V_{12} \ V_{22} \ V_{32} \ V_{42} \ V_{52} \ V_{62} \ V_{72} \ V_{82} \ V_{92} \ V_{102} \ V_{112}]$$

and the percentages of deltas in the bins for 3D,

$$V_{\text{deltas3D}} = [V_{13} \ V_{23} \ V_{33} \ V_{43} \ V_{53} \ V_{63} \ V_{73} \ V_{83} \ V_{93} \ V_{103} \ V_{113}]$$

So, the ratio of  $V_{\text{deltas2D}}$  and  $V_{\text{deltas3D}}$  i.e. the nodes for the corresponding bins are :

$$\begin{aligned} V_{r23} &= \left[ \frac{V_{12}}{V_{13}} \ \frac{V_{22}}{V_{23}} \ \frac{V_{32}}{V_{33}} \ \frac{V_{42}}{V_{43}} \ \frac{V_{52}}{V_{53}} \ \frac{V_{62}}{V_{63}} \ \frac{V_{72}}{V_{73}} \ \frac{V_{82}}{V_{83}} \ \frac{V_{92}}{V_{93}} \ \frac{V_{102}}{V_{103}} \ \frac{V_{112}}{V_{113}} \right] \\ &= [V_{r123} \ V_{r223} \ V_{r323} \ V_{r423} \ V_{r523} \ V_{r623} \ V_{r723} \ V_{r823} \ V_{r923} \ V_{r1023} \ V_{r1123}] \end{aligned}$$

Thus, we can convert 2D percentages of deltas to 3D percentages of deltas by dividing them by the above ratios as:

$$V_{\text{deltas3D from 2D}} = \left[ \frac{V_{12}}{V_{r123}} \ \frac{V_{22}}{V_{r223}} \ \frac{V_{32}}{V_{r323}} \ \frac{V_{42}}{V_{r423}} \ \frac{V_{52}}{V_{r523}} \ \frac{V_{62}}{V_{r623}} \ \frac{V_{72}}{V_{r723}} \ \frac{V_{82}}{V_{r823}} \ \frac{V_{92}}{V_{r923}} \ \frac{V_{102}}{V_{r1023}} \ \frac{V_{112}}{V_{r1123}} \right]$$

Thus, the number of deltas in the bins in 3D derived from 2D are:

$$K_{\text{deltas3D from 2D}} = \left( \frac{V_{\text{deltas3D from 2D}}}{100} \right) \times \sum_{i=1}^b n_i$$

Then, it is easy to estimate the number of nodes using a 3D expression for a 2D network using the estimation expression (4.6) of 3D network as:

$$R_{3D \text{ from 2D}} = \frac{\text{std}(\text{CCF}_{3D \text{ from 2D}})}{\text{mean}(\text{CCF}_{3D \text{ from 2D}})}$$

Some simulated results with corresponding theory are provided in Figures 4.30 to 4.32. The simulation parameters are same as earlier with 11 bins and 1 to 100 nodes. Figure 4.30 shows the theoretical, simulated from 2D (using the expression of

converted 3D CCF from simulated 2D CCF), and simulated from 3D, estimation parameter,  $R$  against  $N$ . Figure 4.31 shows the theoretical and simulated  $R$  in case of 1D network. This theoretical and simulated  $R$  is constants with respect to  $N$ , and thus is not informative to obtain the estimation of the number of nodes. Finally the Figure 4.32 shows the derived estimation parameters,  $R_{13T}$  and  $R_{13S}$  to estimate  $N$  in 1D network. It can be seen that the theoretical and simulated results in Figures 4.30 and 4.32 match properly to estimate the number of nodes in all three dimensions.

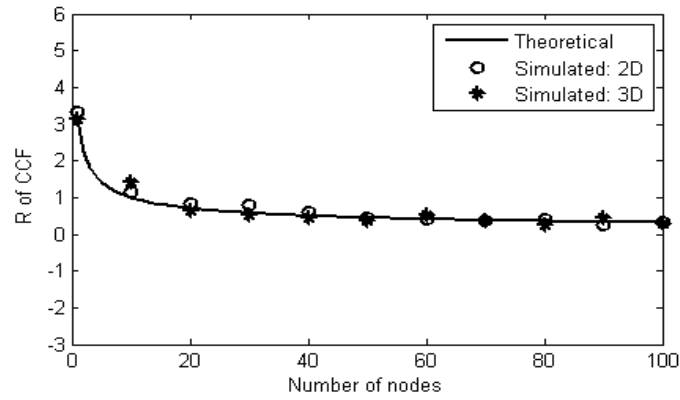


**Figure 4.30  $R$  of CCF for estimations in 2D and 3D**

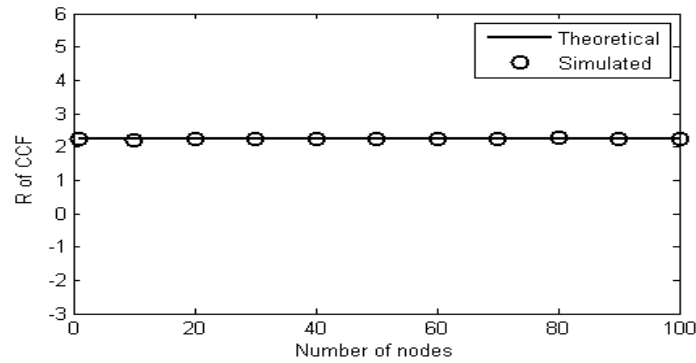


**Figure 4.31  $R$  of CCF in 1D**

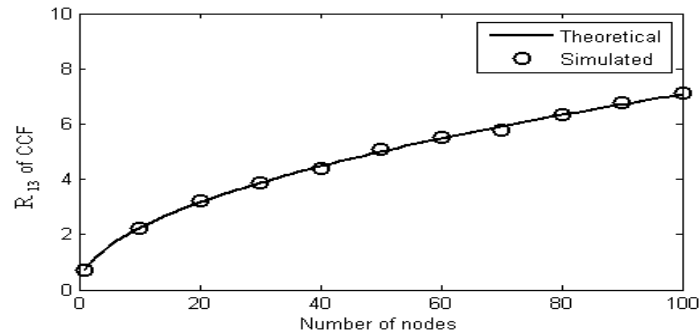


**Figure 4.32 Ratios of  $R$  in 1D and 3D of CCF for estimations in 1D**

This technique for estimating the number of nodes overcomes the limitation of unity powers from the nodes required by the previous method, i.e., although it needs equal signal powers from the nodes, it does not matter what these powers are.

#### 4.5.1 Effect of fractional-samples delays

In this section, we use the ratio of the standard deviation to the mean of the whole CCF with fractional-samples delays in 3D network discussed earlier,  $R_{3D}$ , to estimate the number of nodes. In the 2D network, the CCF is converted to a 3D CCF, and then the  $R_{3D}$  is obtained from that CCF for the estimation in 2D. In the 1D case, firstly, the  $R_{1D}$  (which is independent of the number of nodes) and then another ratio,  $R_{1D}/R_{3D}$ , are used to obtain the estimation. Figures 4.33 to 4.35 show that the fractional-samples delays have no significant effect on estimation.

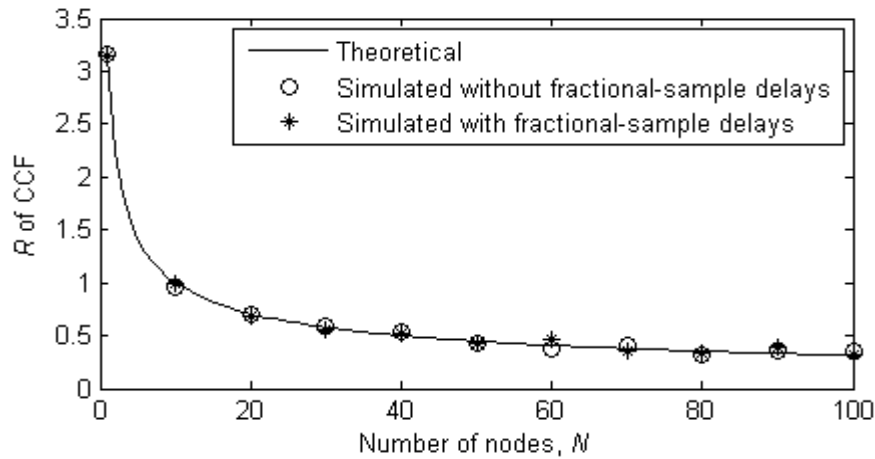


Figure 4.33  $R_{3D}$  from  $2D$  of CCF for estimations in 2D

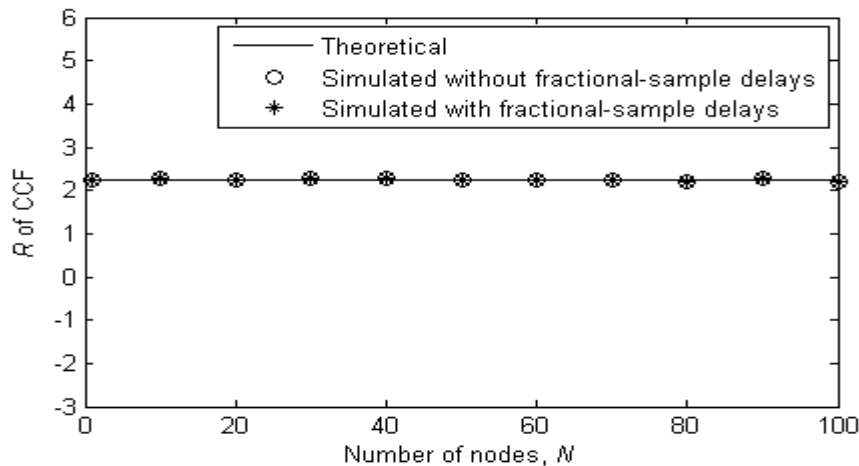
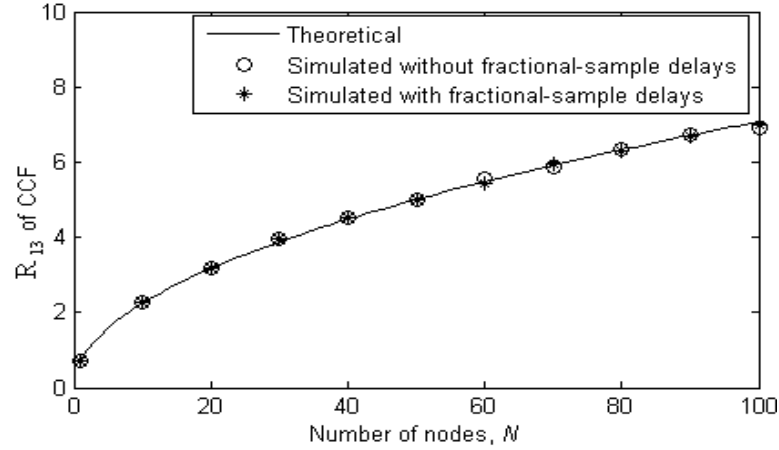


Figure 4.34  $R_{1D}$  of CCF for estimations in 1D



**Figure 4.35 Ratios of  $R_{1D}$  and  $R_{3D}$  of CCF for estimations in 1D**

## 4.6 Conclusion

Estimation of network dimensionality with the number of nodes is also helpful in network applications and maintenance. The method of cross-correlation of the number of nodes estimation also depends on dimensionality. In this chapter, the estimation of dimensionality has been investigated in two different ways using cross-correlation. Besides few more estimation techniques of the number of nodes in different dimensional networks have also been proposed and investigated. All investigations have been obtained in the ERP case based on the basic CCF formation theory. It is obvious from the results that the CCF method is suitable for the dimensionality estimation associated with the estimation of the number of nodes. To validate the accuracy of the estimation process, error in estimation has also been provided in the next chapter with the analysis in the estimation of the number of nodes only.



# Chapter 5

## Analysis of error in estimation

---

### 5.1 Introduction

Every estimation method involves an error which arises from the simple fact that an actual quantity generally differs from its estimation. Numerically, an error in estimation might be represented in different ways: as a true error which is the exact deviation of the estimated value from the true value, or a statistical error which is obtained from several estimated values using the least squares technique. A true error is preferable when the parameter used in the experiment is not random, i.e., it gives a fixed estimation every time for a particular setup. Whereas, in an experiment with random numbers, as the estimated values vary from time to time for a particular setup, thereby indicating a certain statistical property, it is wiser to represent the error statistically. As the proposed cross-correlation is a statistical technique, the statistical error, the coefficient of variation (CV), is used as its error in estimation in order to fully assess the accuracy of the proposed estimation techniques. The CV is defined as the ratio of the standard deviation to the mean taken from several estimations. This chapter analyses the error in estimation of the number of nodes in detail and compares it with the estimation error in the conventional protocol techniques. Section 5.2 provides the theoretical formulation of the CV with detailed verification of it by simulations for both the ERP and ETP cases in which all simulated CVs are obtained using the simulated CCF. The process of obtaining this CV from the theoretical CCF is discussed. In some cases, as it is difficult to obtain an exact mathematical expression of the CV, to ensure the correctness of the simulations, using a CV obtained from the theoretical CCF is helpful. Moreover, the effect of fractional-sample delays on the CV is investigated. In Section 5.3, variations in the CV in terms of  $k$  are investigated and a generalised expression of the CV is obtained. Like estimation, CV is also affected by the  $N_s$  and there is a  $b$  for a particular  $N_s$ , where the CV is minimum, called the optimum CV (OCV), is obtained for some  $N_s$ , a generalised expression for it is obtained in Section 5.4. Selections of the sampling

rate and the distance between sensors for estimation are obtained using the CV in Section 5.5. This sampling rate is useful for obtaining the estimation time and energy. As the CV depends on  $b$  and  $b$  depends on  $S_R$  and  $d_{DBS}$ , if the  $d_{DBS}$  is fixed, the CV depends on only  $S_R$  and vice versa. Section 5.6 provides the effects of noise on the CV and it is shown that, as for estimation, the CV is not affected by the noise if the signal strength is sufficiently dominant. The energy (in terms of the product of SNR and  $N_s$ ) and time required for estimation are obtained in the ERP and ETP cases and compared in Sections 5.7 and 5.8, respectively. The results show that the ERP case performs better than the ETP case. To demonstrate the effectiveness of this novel approach, Section 5.9 provides comparisons of the proposed technique (ERP case) and two conventional protocol techniques using three major performance factors, the CV, the estimation time and the required transmit energy. It is shown that the proposed method performs better overall than the conventional techniques.

In this chapter, simulation results of CV using example networks are presented. Some are based on underwater acoustic networks because this is an interesting possible application area of the techniques presented in this thesis.

## 5.2 Error in estimation

To have confidence in the estimation of  $N$ , an error tool, the ratio of the standard deviation to the mean, also known as the CV (Smith 1999) of estimation, is used. Although the standard deviation is not very significant, the CV is an important tool for identifying the error in estimation - the lower the CV, the better the accuracy of the estimation.

This section provides the theory of the CV, obtains the CV from both theoretical and simulated CCFs, and verifies the theory through simulations of both the ERP and ETP cases. Though there are small differences between the theoretical and simulated results for the ETP case, proper scaling of the former causes them to match with the latter. Moreover, the effect of fractional-sample delays on the CV is investigated. In the ETP case, as the dispersion coefficient,  $k$ , might possess different values, a generalised expression of the CV is obtained.

### 5.2.1 Theory regarding error in estimation in ERP case

In this estimation process, two possible parameters that may affect the CV are  $N$  and  $b$  because they are the only factors that affect the estimation parameter,  $R$ . To express this effect, assuming that the signal characteristics do not change markedly throughout the sampling process. Thus  $N$  will be similar for all samples and the mean number of nodes will be similar to  $N$  at any sampling time.

Consequently, if  $N$  increases by a factor,  $r$ , the standard deviation and mean must also increase by the same factor, indicating that the CV is independent of  $N$ .

To obtain the CV, several  $R$  and thus  $N$  from several CCF have been obtained. Considering a CCF as a sample, the ratio of the standard deviation,  $\sigma_s$ , to the mean,  $\mu_s$ , of that sample CCF is expressed in Chapter 3 as

$$R = \frac{\sigma_s}{\mu_s} = \sqrt{\frac{b-1}{N}} \quad (5.1)$$

Then, the expression for the number of nodes is

$$\begin{aligned} N &= \frac{b-1}{R^2} \\ &= \frac{b-1}{\left(\frac{\sigma_s^2}{\mu_s^2}\right)} \\ &= (b-1) \times \left(\frac{\mu_s^2}{\sigma_s^2}\right) \end{aligned} \quad (5.2)$$

Thus,  $N \propto \left(\frac{\mu_s^2}{\sigma_s^2}\right)$  as  $b$  is constant.

Again, from Chapter 3,

$$\mu_s = N \times \frac{1}{b} \quad (5.3)$$

and



$$\sigma_s^2 = N \times \frac{1}{b} \times \left(1 - \frac{1}{b}\right) \quad (5.4)$$

Then, from (5.3) and (5.4), we have

$$\frac{\mu_s^2}{\sigma_s^2} = \left(\frac{b}{b-1}\right) \mu_s \quad (5.5)$$

Suppose we have  $1000b$  normal variates (population with  $\sigma_p$  and  $\mu_p$ ) from which we draw  $b$  samples at a time and obtain the sample mean,  $\mu_s$ . Then we have 1000 sample means the distribution of which will again follow a normal distribution. We obtain the CV of these means from the ratio of the standard deviation and mean of those sample means which is proportional to the inverse of the square root of sample size,  $b$ .

So,  $CV(N) = CV\left(\frac{\mu_s^2}{\sigma_s^2}\right) = CV(\mu_s)$  and  $CV(\mu_s) \propto \frac{1}{\sqrt{b}}$ ; assuming that the estimation

of  $\mu_s$  is normally distributed. Thus,  $CV(N) \propto \frac{1}{\sqrt{b}}$  as  $N$  is proportional to the ratio

$\frac{\mu_s^2}{\sigma_s^2}$ . To obtain the exact expression of the CV, again from (5.3) and (5.4), we have

$$\frac{\mu_s^2}{\sigma_s^2} = \left(\frac{b}{b-1}\right)^2 \sigma_s^2 \quad (5.6)$$

So, the CV of  $N$  can also be obtained as

$$CV(N) = CV\left(\frac{b^2}{b-1} \sigma_s^2\right) = CV(\sigma_s^2)$$

i.e.,

$$CV(N) = \frac{\sigma(\sigma_s^2)}{\mu(\sigma_s^2)} = \frac{E(std(\sigma_s^2))}{E(\sigma_s^2)} \quad (5.7)$$

The CV of estimation is therefore the CV of the sample variance of the CCF distribution. It is known that the expected value of a sample variance (assuming a normal population, which is possible from a cross-correlation (Hanson 2008b)) is

$$E(\sigma_s^2) = \frac{b-1}{b} \sigma_p^2 \quad (5.8)$$

and that the expected variance of that sample variance is

$$E(\text{var}(\sigma_s^2)) = \frac{2(b-1)}{b^2} \sigma_p^4 \quad (5.9)$$

Therefore, the expected standard deviation of the sample variance is

$$E(\text{std}(\sigma_s^2)) = \sqrt{\frac{2(b-1)}{b^2} \sigma_p^4} = \frac{\sqrt{2(b-1)}}{b} \sigma_p^2 \quad (5.10)$$

Thus, the CV of the estimation is

$$\text{CV}(N) = \frac{E(\text{std}(\sigma_s^2))}{E(\sigma_s^2)} = \sqrt{\frac{2}{b-1}} \approx \sqrt{\frac{2}{b}}; [\text{as } b \gg 1] \quad (5.11)$$

## 5.2.2 Obtaining CV from theoretical CCF

The theory developed in the previous section is suitable for all  $b$  for an infinitely long signal but, for a finite length signal, it is suitable only up to a certain  $b$ . This is because, for an infinitely long signal, in a CCF, we will obtain only the desired peaks which are the delta functions of certain strengths for the nodes. But, for a finite length signal, there will be some undesired peaks associated with the desired peaks which are treated as noise in the CCF. The desired peak for a node can be obtained if the position of the node is known. But, as it is difficult to represent the undesired peaks by a closed form expression, it will be very difficult to obtain one for the theoretical CCF and, thus, the CV, especially in cases of finite length signals. Therefore, we try using the moving average technique of cross-correlation to obtain the peaks (desired and undesired).

In all cases, the CCF for the desired bins can be represented as

$$C(\tau) = \sum_{i=1}^b P_i \delta_i \quad (5.12)$$

where  $i$  indicates the bin number,  $\delta_i$  the Dirac deltas and  $P_i$  their strengths or peaks which might be obtained from this technique.

The CCF, using the moving average technique of cross-correlation, can be represented by (Hanson 2008a; Hanson 2008b)

$$C(\tau) = \frac{1}{N_s - \tau} \sum_{i=1}^{N_s - \tau} x_i y_{i+\tau} - \left( \frac{1}{N_s} \sum_{i=1}^{N_s} x_i \right) \left( \frac{1}{N_s} \sum_{i=1}^{N_s} y_i \right)$$

where  $N_s$  is the signal length in the number of samples,  $\tau$  the time delay of cross-correlation, and  $x_i$  and  $y_i$  are  $i^{\text{th}}$  samples of the two sensors' signals, respectively.

As we use the zero mean Gaussian signal, the product of their means is zero. So, the CCF is reduced to

$$C(\tau) = \frac{1}{N_s - \tau} \sum_{i=1}^{N_s - \tau} x_i y_{i+\tau}$$

This gives the peaks for the desired bins as

$$\frac{1}{N_s + \tau} \sum_{i=1}^{N_s + \tau} x_i y_{i-\tau}, \dots, \frac{1}{N_s + 1} \sum_{i=1}^{N_s + 1} x_i y_{i-1}, \frac{1}{N_s - 0} \sum_{i=1}^{N_s - 0} x_i y_{i+0}, \frac{1}{N_s - 1} \sum_{i=1}^{N_s - 1} x_i y_{i+1}, \dots, \frac{1}{N_s - \tau} \sum_{i=1}^{N_s - \tau} x_i y_{i+\tau}$$

where the peaks are the strengths of the deltas of (5.12) which are

$$\begin{aligned} P_1 &= \frac{1}{N_s + \tau} \sum_{i=1}^{N_s + \tau} x_i y_{i-\tau}, \\ P_2 &= \frac{1}{N_s + (\tau - 1)} \sum_{i=1}^{N_s + (\tau - 1)} x_i y_{i-(\tau - 1)}, \\ &\vdots \\ P_b &= \frac{1}{N_s - \tau} \sum_{i=1}^{N_s - \tau} x_i y_{i+\tau} \end{aligned}$$

Putting these values in (5.12), we obtain the desired CCF and call it in this thesis the theoretical CCF. For a particular simulation setup, we obtain similar theoretical and simulated CCF values. Using this theoretical CCF, the CV, called the 'CV from the theoretical CCF', can be obtained as is the simulated CCF discussed in the following section. Later in this chapter, the CVs from theoretical and simulated CCFs are compared to ensure the correctness of the simulation results.

### 5.2.3 Obtaining CV from simulated CCF in ERP case

It is already known that, after cross-correlating the signals received at two sensors from a number of random Gaussian signal sources, the CCF, which is a rectangular pulse over the space between the sensors, can be obtained. Then, we can easily estimate the mean and standard deviation of this CCF and, therefore, its ratio,  $R$ , as we know the sampling rate,  $S_R$  and distance between the sensors,  $d_{DBS}$ . Reframing the cross-correlation problem as a probability problem, we obtain a relationship of  $N = (b-1) / R^2$ , as discussed earlier. Thus, from the simulation, we can readily estimate the number of nodes by knowing only  $R$ .

To obtain a simulated CV of estimation, a simulation process is run 1000 times for a particular  $N$  and  $b$ . From these 1000 values of estimated  $N$ , the standard deviation and mean of estimation and, thus, the CV, are obtained. To obtain better results, 100 iterations are taken for the simulations unless otherwise mentioned. This process is similar for both the ERP and ETP cases. Some results are provided in the following section to verify the theory expressed in (5.11) for the ERP case.

#### 5.2.3.1 Verification of relationship between CV and $b$

In this section, the proposed theory regarding the CV is verified by the simulation results obtained using the following parameters:

dimension of cube 2000 m; considering the estimation area as a 3D cube  
number of nodes,  $N = 32$ , spherically distributed inside the cube;  
signal length,  $N_s = 1,000,000$  samples;  
sampling rate,  $S_R = 30$  kSa/s;  
speed of propagation,  $S_p = 1500$  m/s;  
distance between sensors,  $d_{DBS} = 0.25$  m; and  
iteration used,  $u = 100$  (to obtain better results).

Firstly, the  $R$  of the CCF from 100 iterations, and then the estimated  $\hat{N}$  using the expression of  $N$  related to this  $R$ , are obtained. Secondly, to obtain the CV, the same

process is continued 1000 times without any change in parameters and the values of all estimated  $\hat{N}$  are recorded. Finally, the CV for one iteration is obtained from the ratios of the standard deviation to the mean of those values as

$$CV = \frac{\sigma(\hat{N})}{\mu(\hat{N})} \quad (5.13)$$

Now, if we use iteration  $u$ , the standard deviation and, thus, the CV, are reduced to  $\frac{1}{\sqrt{u}}$  (Barry 1978; Howlader 2009) so that the CV after the  $u^{\text{th}}$  iteration is

$$CV_u = \frac{1}{\sqrt{u}} \left( \frac{\sigma(\hat{N})}{\mu(\hat{N})} \right). \quad (5.14)$$

To verify the theoretical relationship of the CV and  $b$ , the above process is continued for several distinct values of  $b$  by varying the sampling rate or the  $d_{DBS}$  and the results are presented in Figure 5.1. Figure 5.1 (a) shows the results using a linear plot and, to verify the theoretical relationship between the CV and  $b$  from the simulation, they are re-plotted in Figure 5.1 (b) using the logarithmic axes. Assuming a straight line approximation, the slope,  $s_{co}$  in Figure 5.1 (b) is

$$s_{co} = \frac{\log_{10}(C) - \log_{10}(D)}{\log_{10}(A) - \log_{10}(B)} \approx -\frac{1}{2} \quad (5.15)$$

Therefore,

$$\begin{aligned} \log_{10}(CV_{100}) &= (s_{co}) \log_{10}(b) + c \\ &= (s_{co}) \log_{10}(b) + \log_{10}(c_0) \\ &= \log_{10}(c_0 \times b^{(s_{co})}) \end{aligned}$$

So,

$$CV_{100} = c_0 \times b^{s_{co}} = c_0 \times b^{\left(-\frac{1}{2}\right)} \quad (5.16)$$

where  $c$ , and  $c_0$  are constant and are related as  $c = \log_{10}(c_0)$ . Using a particular point from Figure 5.1 (a) in (5.16), the value of the constant,  $c_0$  is  $c_0 \approx \frac{\sqrt{2}}{10}$ . Putting this  $c_0$

in (5.16), it can be expressed as  $CV_{100} = \frac{\sqrt{2}}{10\sqrt{b}}$ . The results in (5.16) were obtained from 100 iterations, thus, for one iteration; the CV is  $CV_1 = \sqrt{\frac{2}{b}}$  which verifies the theory in (5.11).

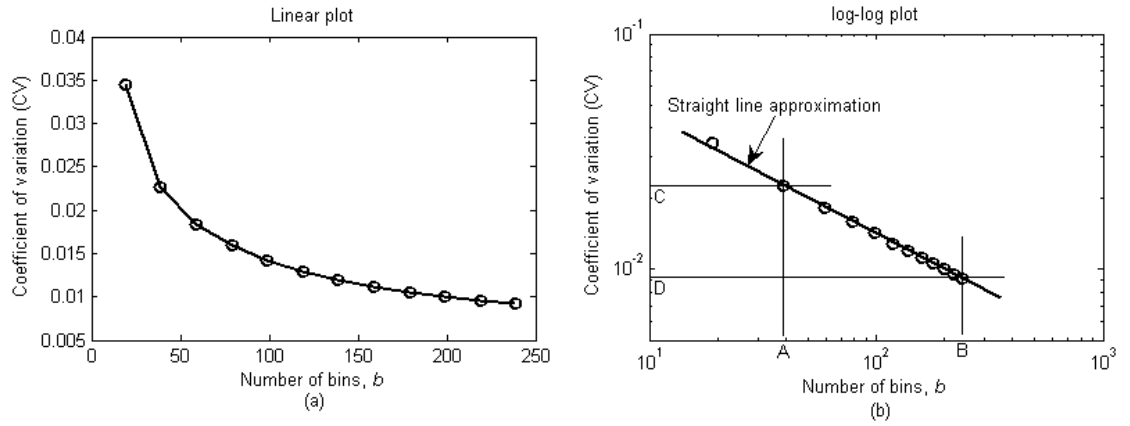


**Figure 5.1 Simulated CV (with  $N=32$ ) in ERP case: (a) linear and (b) log-log scale**

A comparison of the theoretical CV, the CV from the theoretical CCF and the CV from the simulated CCF is provided in Figure 5.2. It can be seen from the figure that the theoretical and simulation results match.

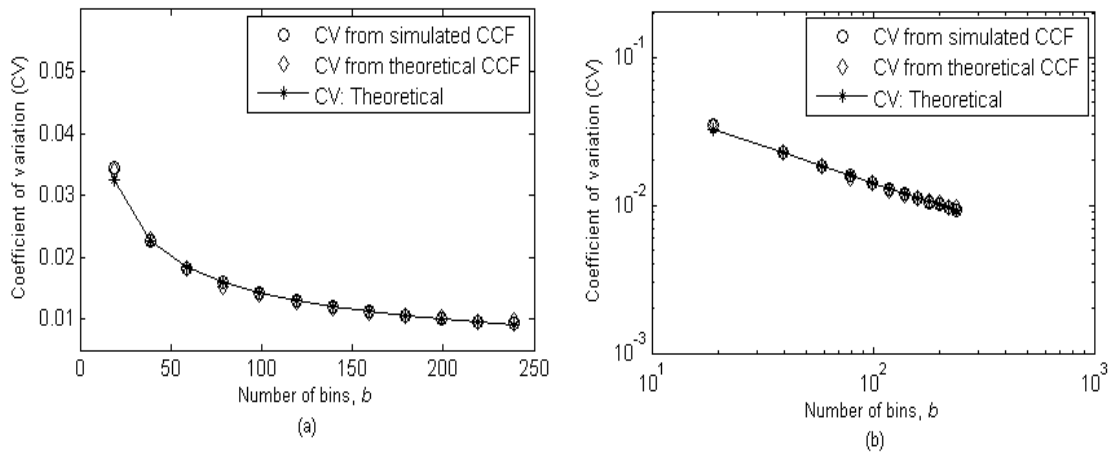


**Figure 5.2 Comparison of theoretical and simulated CVs for 32 nodes in ERP case: (a) linear and (b) log-log scale**

### 5.2.4 Theory regarding error in estimation in ETP case

In the ETP case, the estimation parameters' expression, as obtained in Chapter 3 is

$$\begin{aligned}
 R_k &= (b-1)^{1/2} N^{-|s_k|} \\
 \Rightarrow N^{|s_k|} &= (b-1)^{1/2} R_k^{-1} \\
 \Rightarrow N &= \left\{ (b-1)^{1/2} R_k^{-1} \right\}^{|s_k|} \\
 \Rightarrow N &\propto \left( R_k^{-2} \right)^{|s_k|/2} \\
 \Rightarrow N &\propto \left( \frac{\mu_{ks}^2}{\sigma_{ks}^2} \right)^{|s_k|/2}
 \end{aligned} \tag{5.17}$$

Using (5.6), we have

$$N \propto \left( \sigma_{ks}^2 \right)^{|s_k|/2}$$

So, the CV will be

$$CV(N) = CV \left\{ \left( \sigma_{ks}^2 \right)^{|s_k|/2} \right\} \tag{5.18}$$

Now, the CV of this case can be derived as follows. Suppose  $Y = g(x)$ , where the mean of  $x$  is  $\mu_x$ , and using the Taylor series expansion about the mean, we have

$$Y = g(\mu_x) + (X - \mu_x) \frac{dg}{dx} + \frac{1}{2} (X - \mu_x)^2 \frac{d^2g}{dX^2} + \dots$$

where  $X$  is a random variable and its values are the obtained value of  $x$ .

Then, the expected mean of  $Y$  is

$$E(Y) \approx g(\mu_x)$$

Taking up to the 1<sup>st</sup> derivative term in the Taylor series, we have the variance of  $Y$  as

$$\text{Var}(Y) \approx \text{Var}(X - \mu_x) \left( \frac{dg}{dX} \right)^2$$

Now, if

$$Y = x^K$$

then, the mean of  $Y$  is

$$(5.19)$$

$$E(Y) \approx (E(X))^K$$

and the variance of  $Y$  is

$$(5.20)$$

$$\text{Var}(Y) \approx \{K(E(X))^{K-1}\}^2 \text{Var}(X)$$

So, the  $\text{SD}(Y)$  is

$$\text{SD}(Y) \approx \{K(E(X))^{K-1}\} \text{SD}(X)$$

and, thus, the CV is

$$\text{CV}(Y) = \frac{\text{SD}(Y)}{E(Y)} = \frac{\{K(E(X))^{K-1}\} \text{SD}(X)}{(E(X))^K} = K \frac{\text{SD}(X)}{E(X)} = K \times \text{CV}(X) \quad (5.21)$$

In (5.18), considering that  $K = \frac{1}{2|s_k|}$  and  $x = \sigma_{ks}^2$  (assuming a normal population as in

ERP case), we have the CV as

$$\text{CV}(N) = \frac{1}{2|s_k|} \text{CV}(\sigma_{ks}^2) = \frac{1}{2|s_k|} \sqrt{\frac{2}{b}} \quad (5.22)$$

i.e., the CV is again proportional to the one on the square root of  $b$ , i.e.,

$$\text{CV}(N) \propto \frac{1}{\sqrt{b}}$$

Figure 5.3 shows the results for the CVs in the ETP case for  $k=1.5$  in which the straight line approximation of the simulated results obtained is presented in Figures 5.3 (b).



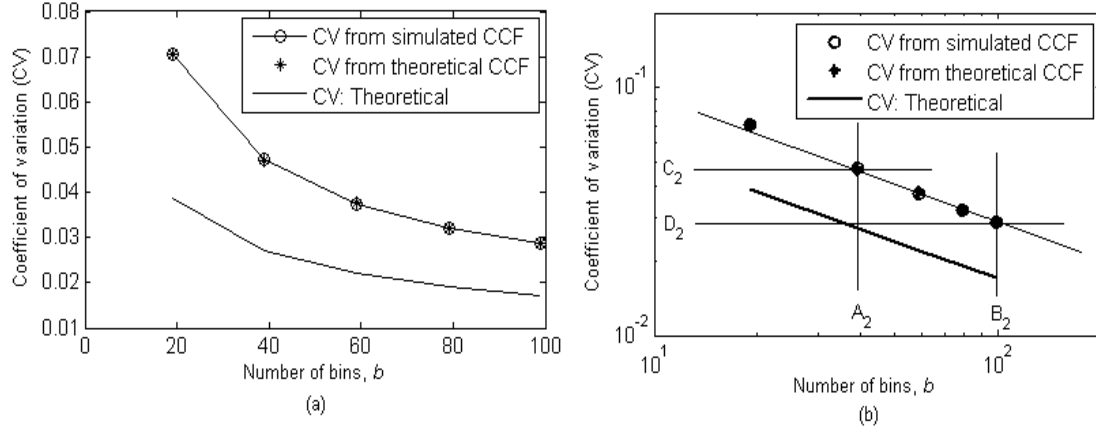


**Figure 5.3 Theoretical and simulated CVs for 32 nodes in ETP case: (a) linear and (b) log-log scale**

Using the straight line approximation, the slope of the simulated results in Figure 5.3 (b) is

$$s_{c1} = \frac{\log_{10}(C_2) - \log_{10}(D_2)}{\log_{10}(A_2) - \log_{10}(B_2)} \approx -\frac{1}{2}$$

So,

$$CV_S = c_S \times b^{(s_{c1})} = c_S \times b^{\left(-\frac{1}{2}\right)}, \quad (5.23)$$

where  $c_S$  is the constant of proportionality.

It is shown in Figure 5.3 that there are differences among the theoretical and simulated results and, also, that the latter are almost a constant multiple of the former (Figure 5.3 (b)). Thus, the theoretical results can be scaled to match the simulated results as follows. Denoting theoretical CV in (5.22) as  $CV_{Th}$ , it is in the ETP case is

$$CV_{Th} = \frac{1}{2|s_k|} \sqrt{\frac{2}{b}} = \frac{c_{Th}}{\sqrt{b}} \quad (5.24)$$

where  $c_{Th}$  is the constant and defined as  $c_{Th} = \frac{\sqrt{2}}{2|s_k|}$ .

Again from (5.23), the simulated  $CV_S$  in the ETP case is

$$CV_S = \frac{c_S}{\sqrt{b}} \quad (5.25)$$

Thus, by combining (5.24) and (5.25), we have the corresponding scaled theoretical  $CV_{STh}$  as

$$CV_{STh} = \frac{c_s}{c_{Th}} CV_{Th} \quad (5.26)$$

where  $CV_{STh}$  is the scaled theoretical CV in the ETP case.

Later in this chapter, the theoretical CV in the ETP case indicates the above scaled theoretical CV. Using a particular point from Figure 5.3 (a) in (5.26), we obtain the constants  $c_s$  as  $c_s \approx 2.16\sqrt{2}$ . Thus, expression (5.25) can be written as

$$CV_{STh} = 4.32|s_k| CV_{Th}$$

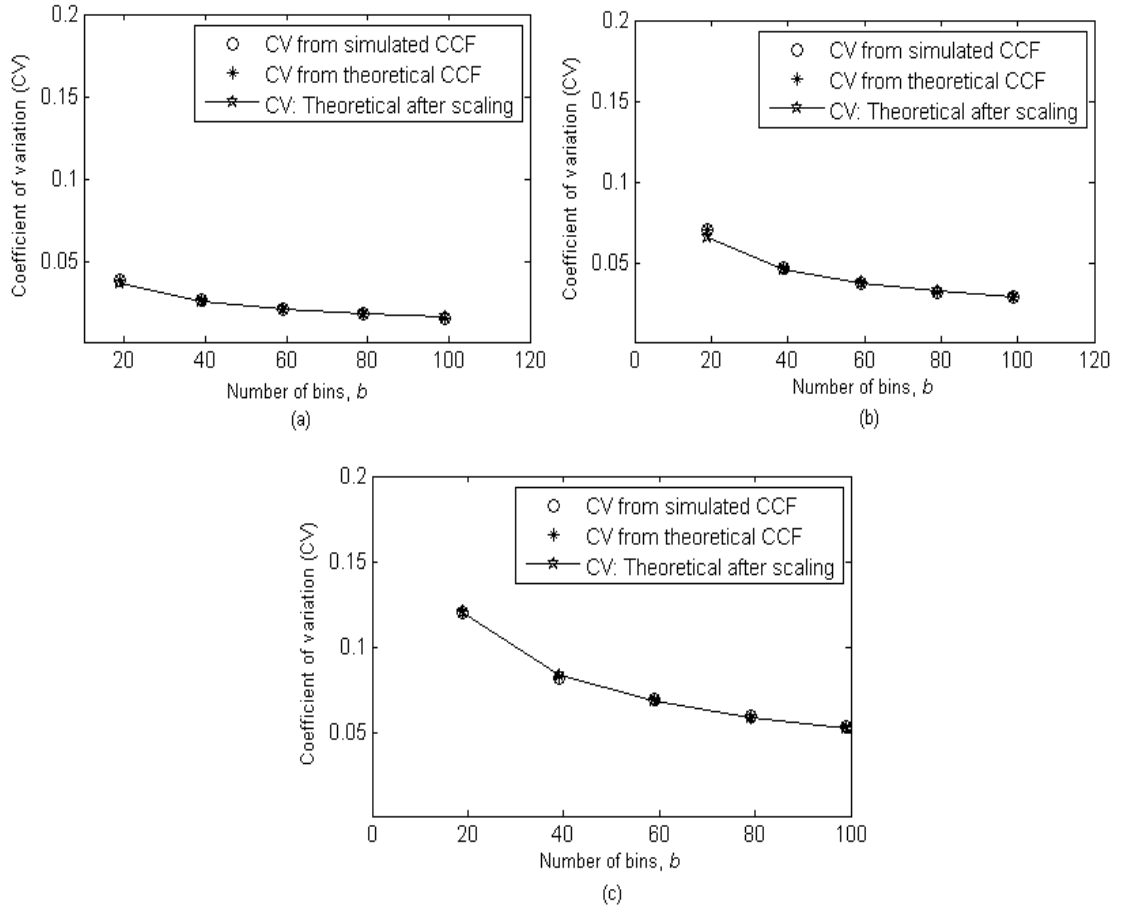


**Figure 5.4 Comparison of theoretical and simulated CVs for 32 nodes: (a)  $k=1$ ; (b)  $k=1.5$ ; and (c)  $k=2$**

Some CV results (obtained from the theoretical and simulated CCFs) along with the scaled theoretical CV for three cases with different  $k$  (1, 1.5 and 2) are shown in Figure 5.4. It can be seen that, after scaling, the theory matches the CVs from both the simulated and theoretical CCFs.

Now, from (5.16) and (5.23), the relationship between the simulated CV and  $b$  when  $N$  remains constant can be generalised as

$$CV \propto \frac{1}{\sqrt{b}} \quad (5.27)$$

Therefore, the CV is proportional to the inverse square root of  $b$  for both the ERP and ETP cases which verify the theory discussed in Section 5.2.1 regarding the relationship between the CV and  $b$ . The only differences in exact values are due to changes in  $k$ .

Comparisons of the CVs for two distinct values of  $k$  (0 and 1.5) are listed in Table 5.1 and four distinct values of  $k$  (0, 1, 1.5 and 2, where  $k = 0$  indicates the ERP case) are presented in Figure 5.5.

**Table 5.1 Comparison of CVs**

Parameter		Coefficient of variation (CV) (all values from 100 iterations)				
		$b = 19$	$b = 39$	$b = 59$	$b = 79$	$b = 99$
$k=0$	Theoretical	0.0324	0.0226	0.0184	0.0159	0.0142
	From simulated CCF	0.0320	0.0227	0.0183	0.0160	0.0138
	From theoretical CCF	0.0321	0.0225	0.0181	0.0161	0.0139
$k=1.5$	Theoretical	0.0710	0.0489	0.0398	0.0344	0.0307
	From simulated CCF	0.0714	0.0490	0.0395	0.0346	0.0298
	From theoretical CCF	0.0712	0.0486	0.0391	0.0348	0.0300

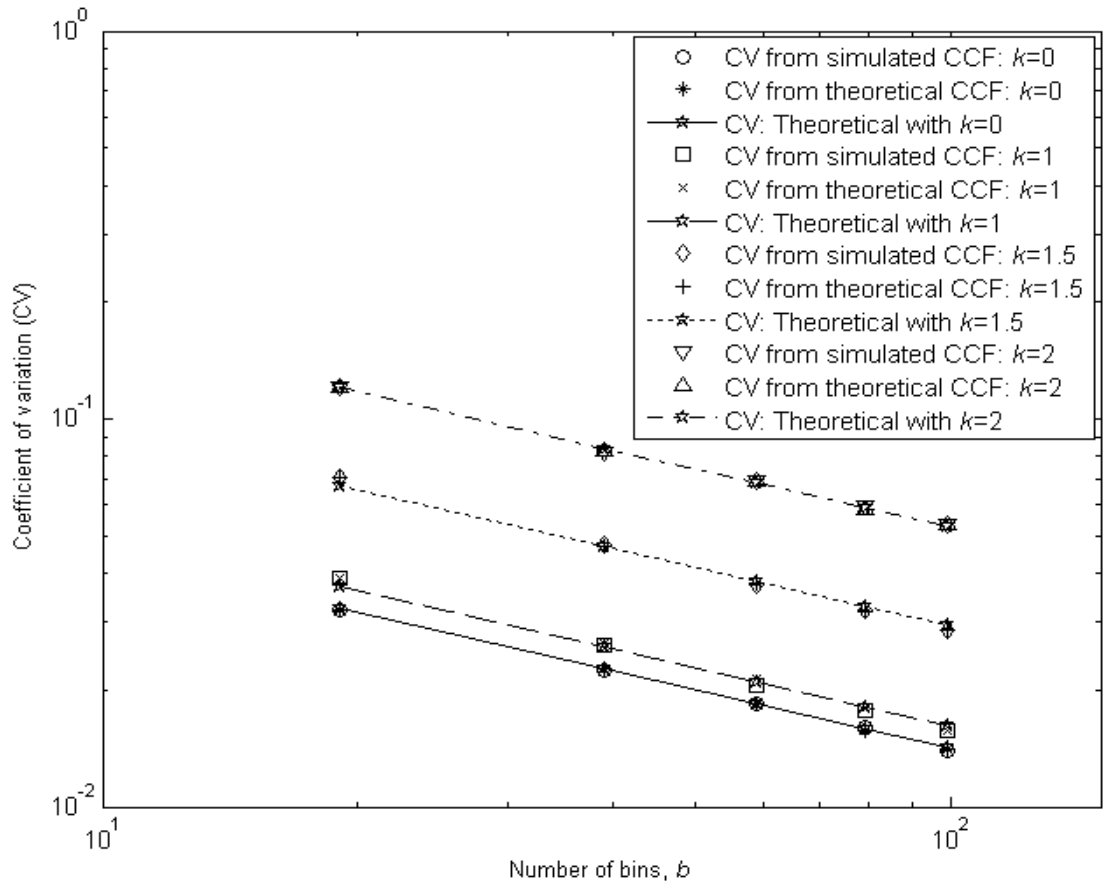


**Figure 5.5 CV vs  $b$ : comparison of CVs due to four distinct values of dispersion coefficient,  $k$  (0, 1, 1.5 and 2)**

#### 5.2.4.1 Verification of relationship between CV and $N$

It has already been explained that, if we increase the number of nodes, the standard deviation and mean of estimation increase by the same amount. Thus, the CV remains the same for all  $N$ , i.e., it is independent of  $N$ . It can also be seen from the expression of the CV, which is depicted in (5.27) for both the ERP and ETP cases as

$$CV \propto \frac{1}{\sqrt{b}}, \text{ that it is only dependent on } b.$$

Now, we change the simulation for different values of  $N$  and perform the estimation 1000 times for each  $N$ , keeping  $b$  fixed at 19 bin in order to obtain the relationship between the CV and  $N$ . The results are plotted in Figures 5.6 (a) for the ERP and 5.6 (b) for the ETP (with  $k=1.5$ ) cases. It can be seen in both figures that, if  $N$  is greater

than 10, the CV is virtually independent of  $N$ , which follows the theory. This is an important finding because, even if the environment is totally unknown, the estimation system can be designed without knowing  $N$ .

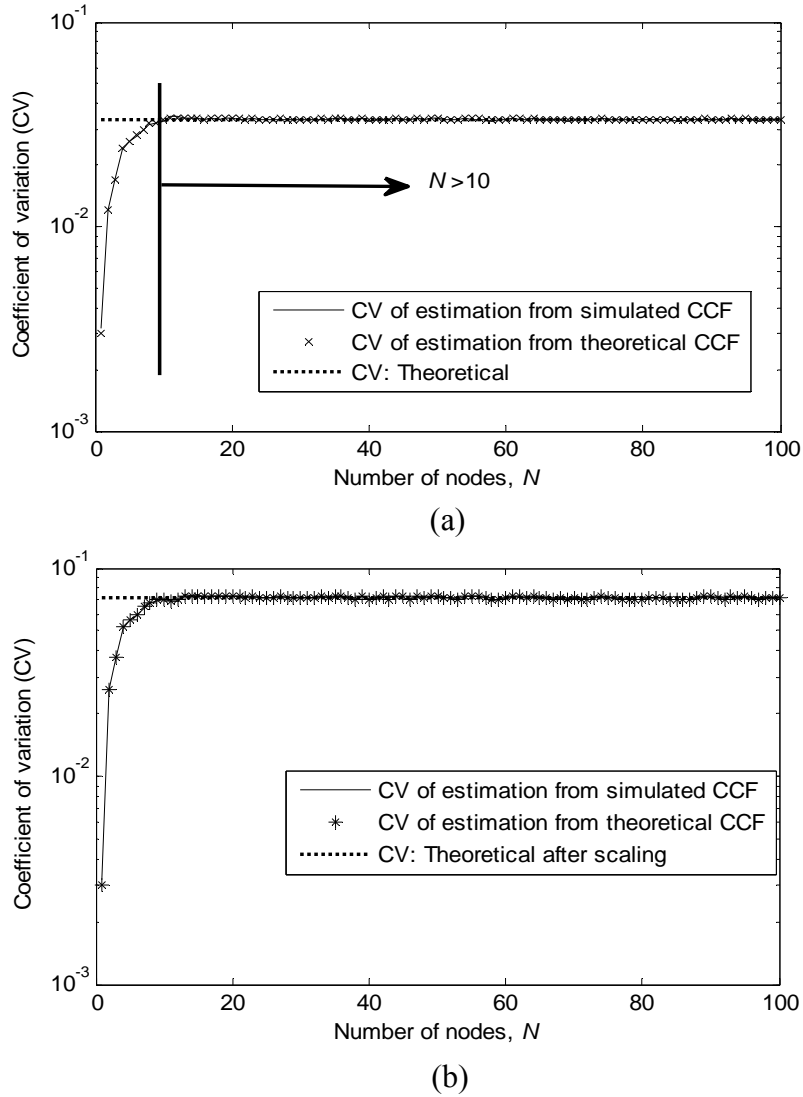


**Figure 5.6 CV versus  $N$ : semi-log plots in (a) ERP case; and (b) ETP case**

Two comparisons of the CVs for the ERP and ETP (with  $k=1.5$ ) cases are provided in Figure 5.7 with (a)  $b=19$  ( $N=10$  to 100) and (b)  $b=99$  ( $N=10$  to 100). It can be seen that the CV in the ERP case is lower than the CV in the ETP case. Besides, although the CVs varies with  $b$ , they are independent of  $N$ .

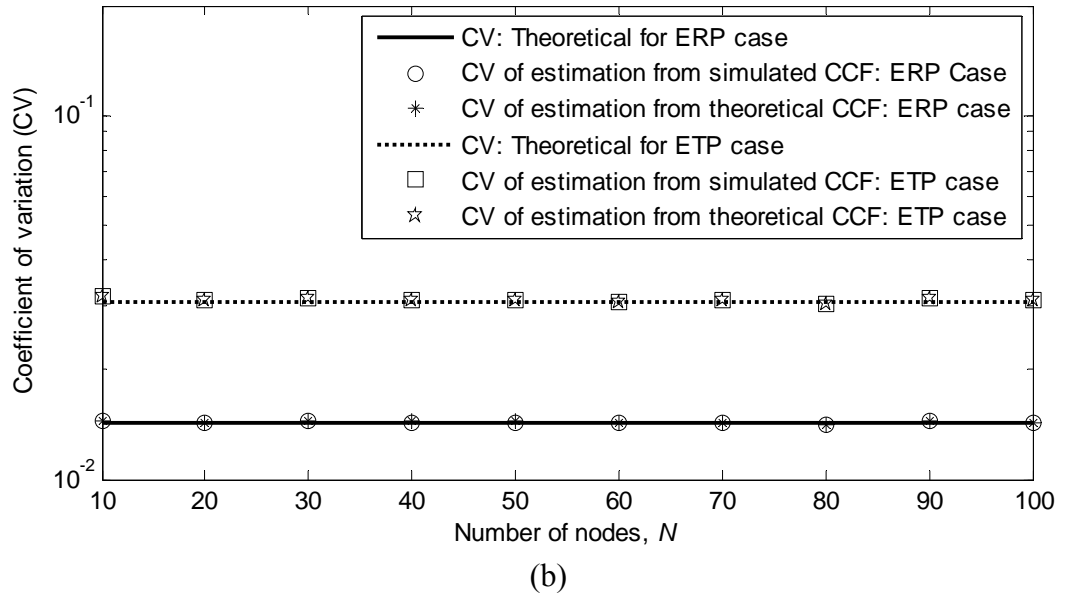
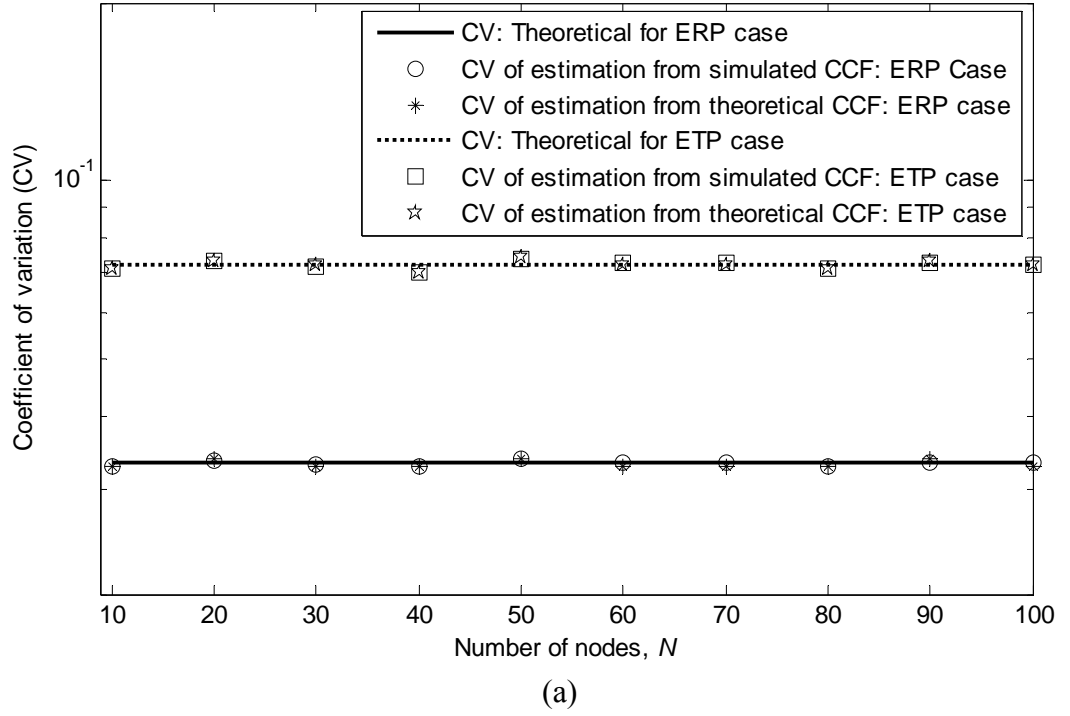


**Figure 5.7 CV versus  $N$ : comparisons of ERP and ETP cases for:**  
**(a)  $b = 19$ ; and (b)  $b = 99$**

To clarify the relationships among the CV,  $N$  and  $b$ , some other results are provided in Figures 5.8 and 5.9 in which the CVs for 10 to 100 nodes with different  $b$  ( $= 19, 59$  and  $99$ ) and for three distinct  $N$  (32, 64, and 100) with respect to  $b$ , respectively, for both the ERP and ETP cases are shown. It can be seen that there are significant variations (which follow (5.27)) in the estimated CVs with respect to  $b$  but, with

respect to  $N$ , they are almost constant for a given  $b$ . These discussions further verify the relationships among the CV,  $N$  and  $b$  discussed in Section 5.2.

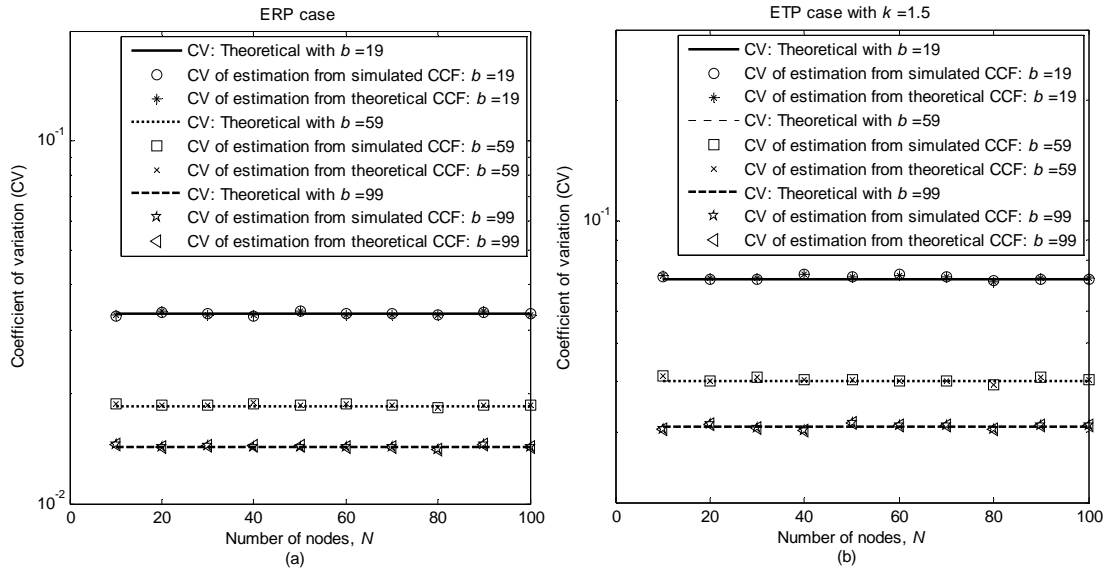


**Figure 5.8 CV versus  $N$  for three distinct  $b$  (19, 59 and 99):**

**(a) ERP case; and (b) ETP case**

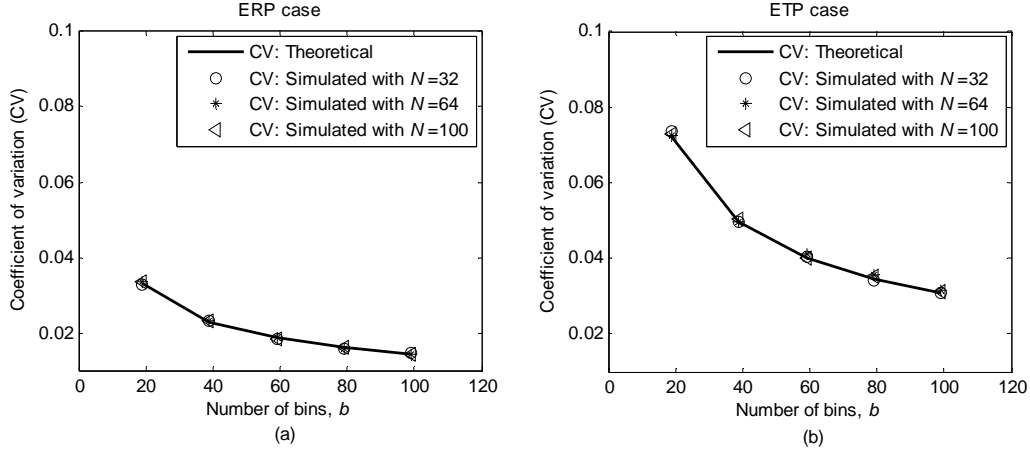


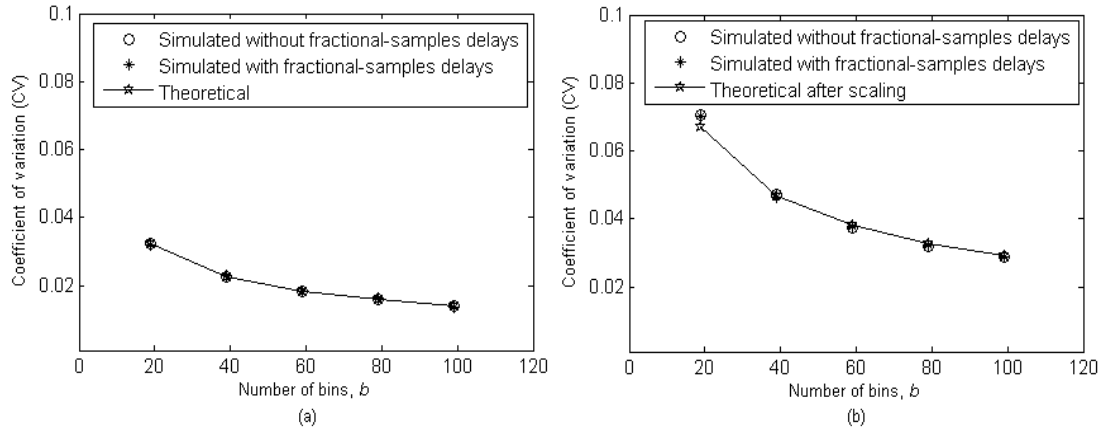
**Figure 5.9 CV versus  $b$  for three distinct  $N$  (32, 64 and 100):**

**(a) ERP case; and (b) ETP case**

### 5.2.5 Effect of fractional-samples delays

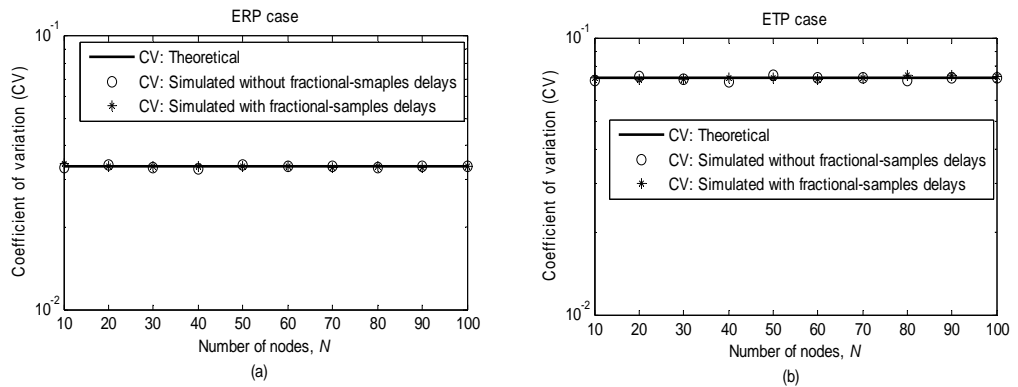
The effects of fractional-samples delays on estimation have already been investigated in Chapter 3. Figures 5.10 and 5.11 show that they have similar effects on the CV.

Figure 5.10 (a) and (b) show the CV versus  $b$  plots for the ERP and ETP cases, respectively, with and without considering the fractional-samples delays. In both figures, the stars and circles indicate the CVs with and without considering the fractional-samples delays, respectively, whereas the lines with pentagon markings indicate the theoretical results.



**Figure 5.10 CV versus  $b$  with and without fractional-sample delays: (a) ERP case and (b) ETP case**

Figure 5.11 (a) and (b) shows the CV versus  $N$  plots with and without considering the fractional-sample delays with a certain  $b$  of 19 for the ERP and ETP cases, respectively. In both figures, the stars and circles indicate the CVs with and without considering the fractional-sample delays, respectively, whereas the lines with pentagon markings indicate the theoretical results. All these results indicate that the fractional parts of the sample delays have no significant effect on CV (the same as for estimation).



**Figure 5.11 Semi-log plot of CV versus  $N$  with and without fractional-samples delays: (a) ERP case; and (b) ETP case**



### 5.2.6 Deriving generalised expression for CV

It can be seen from the above sections that the actual value of the CV is also dependent on  $k$ , i.e., the powers of the received signals. This relationship is discussed in this section. It has already been shown in Figure 5.5 that CV is proportional to the inverse square root of  $b$  for 4 distinct  $k$  ( $= 0, 1, 1.5$  and  $2$ ). Assuming this relationship holds for all  $k$ , i.e., the CV follows the proportional expression (5.27), we can express it using a generalised expression.

To obtain the expression, CVs for five distinct  $k$  with  $b=19$  are listed in Table 5.2.

**Table 5.2 CVs for different  $k$  with 19 bins**

Parameters		Values (100 iterations)				
		$k = 0$	$k = 0.5$	$k = 1$	$k = 1.5$	$k = 2$
CV	Theoretical	0.0324	0.0349	0.0396	0.0710	0.1223
	From simulated CCF	0.0320	0.0347	0.0406	0.0714	0.1217
	From theoretical CCF	0.0321	0.0346	0.0404	0.0712	0.1219

From the Table 5.2, for  $b=19$ , we can express the CV for  $k = 0, 0.5, \dots, 2$  as

$$CV_{19}(k = 0) = (0.1414)(19^{-\frac{1}{2}})$$

$$CV_{19}(k = 0.5) = (0.1521)(19^{-\frac{1}{2}})$$

$$\vdots$$

$$CV_{19}(k = 2) = (0.5331)(19^{-\frac{1}{2}})$$

Similarly, for  $b=39$  bins, the expressions are obtained as

$$CV_{39}(k = 0) = (0.1414)(39^{-\frac{1}{2}})$$

$$CV_{39}(k = 0.5) = (0.1521)(39^{-\frac{1}{2}})$$

$$\vdots$$

$$CV_{39}(k = 2) = (0.5331)(39^{-\frac{1}{2}})$$

From these two series of expressions, we can obtain the generalised expression as

$$CV_b(k) = c_{CV}(b)^{-\frac{1}{2}} \quad (5.28)$$

where the  $c_{CV}$  is a constant whose values are those shown in Table 5.3 for 5 distinct  $k$ .

**Table 5.3 Constant  $c_{CV}$  related to  $k$  in CV expression (5.28)**

Parameter		Values (100 iterations)				
		$k = 0$	$k = 0.5$	$k = 1$	$k = 1.5$	$k = 2$
$c_{CV}$	Theoretical	0.1414	0.1521	0.1726	0.3095	0.5331
	From simulated CCF	0.1395	0.1511	0.1768	0.3110	0.5303
	From theoretical CCF	0.1417	0.1522	0.1723	0.3098	0.5327

It can be seen from the above expressions and the results that there are two parts in the CV, one of which is dependent on only  $k$  and the other on only  $b$ . The dependency of the CV on  $b$  has already been discussed. Now, its relationship to  $k$ , i.e., the constant part in the expression of the CV related to  $k$ ,  $c_{CV}$ , is expressed by a cubic approximation in Figure 5.12.

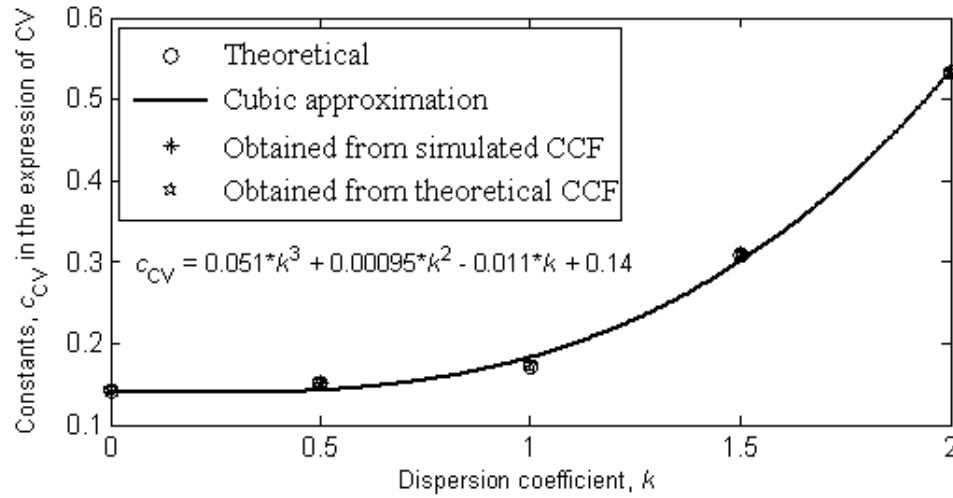


**Figure 5.12 Constant,  $c_{CV}$ , in expression of CV versus dispersion coefficient,  $k$**

Therefore, the expression of the constant,  $c_{CV}$  in the generalized expression of the CV is

$$c_{CV}(k) = 0.051k^3 + 0.00095k^2 - 0.011k + 0.14$$

Thus once the  $b$ , and  $k$  are known, obtaining  $c_{CV}$ , the error in estimation (CV) is easy obtainable from the expression (5.28).

### 5.2.7 Conclusion

Theories of error (CV) and their verification by the simulated results are provided in this section. It can be concluded that in both the ERP and ETP cases, the CV is independent of  $N$  and only proportional to the inverse square root of  $b$ , and that  $b$  is proportional to the  $S_R$  and  $d_{DBS}$ . Thus, we can obtain an error in estimation as low as desired by increasing  $b$  (without exceeding the limit of the  $S_R$  and  $d_{DBS}$ ). Besides, CV is affected by the  $k$ , and a generalised expression of CV for all  $k$  is obtained, which is very helpful to obtain CV in ETP case. All the above results are taken for a very long fixed signal length,  $N_S$ , of 1,000,000 samples. As has already been shown in Chapter 3,  $N_S$  affects the estimation performance and, therefore, might be another factor which could affect the CV. The effects of  $N_S$ , the  $S_R$  and  $d_{DBS}$  (on the CV) are discussed with the CVs obtained from both theoretical and simulated CCFs in the following sections which might help to select their proper values.

## 5.3 Selection of signal length from Optimum CV (OCV)

As the  $N_S$  plays a vital role in estimation performance, its selection is important and a selection process using the minimum CV, called the OCV (in the sense that it is the minimum for that  $N_S$ ) for different  $N_S$  is proposed. The OCVs from ERP case are plotted against  $N_S$  in Figure 5.13 in both linear and log-log scales for values from 100 iterations and the relationship between the OCV and  $N_S$  is obtained.

Figure 5.13 (b) shows that the values of the OCV with respect to  $N_S$  can be approximated by a straight line, the slope of which is approximately  $-0.283$ . As this is a log-log plot, the OCV can be expressed as

$$\begin{aligned}\log_{10}(\text{OCV}) &= -0.283 \times \log_{10}(N_S) + c \\ \Rightarrow \log_{10}(\text{OCV}) &= \log_{10}(N_S)^{-0.283} + \log_{10}(c_3) \\ \Rightarrow \text{OCV} &= c_3 \times N_S^{-0.283}\end{aligned}\tag{5.29}$$

where  $c$ , and  $c_3$  are constant and are related as  $c = \log_{10}(c_3)$ .

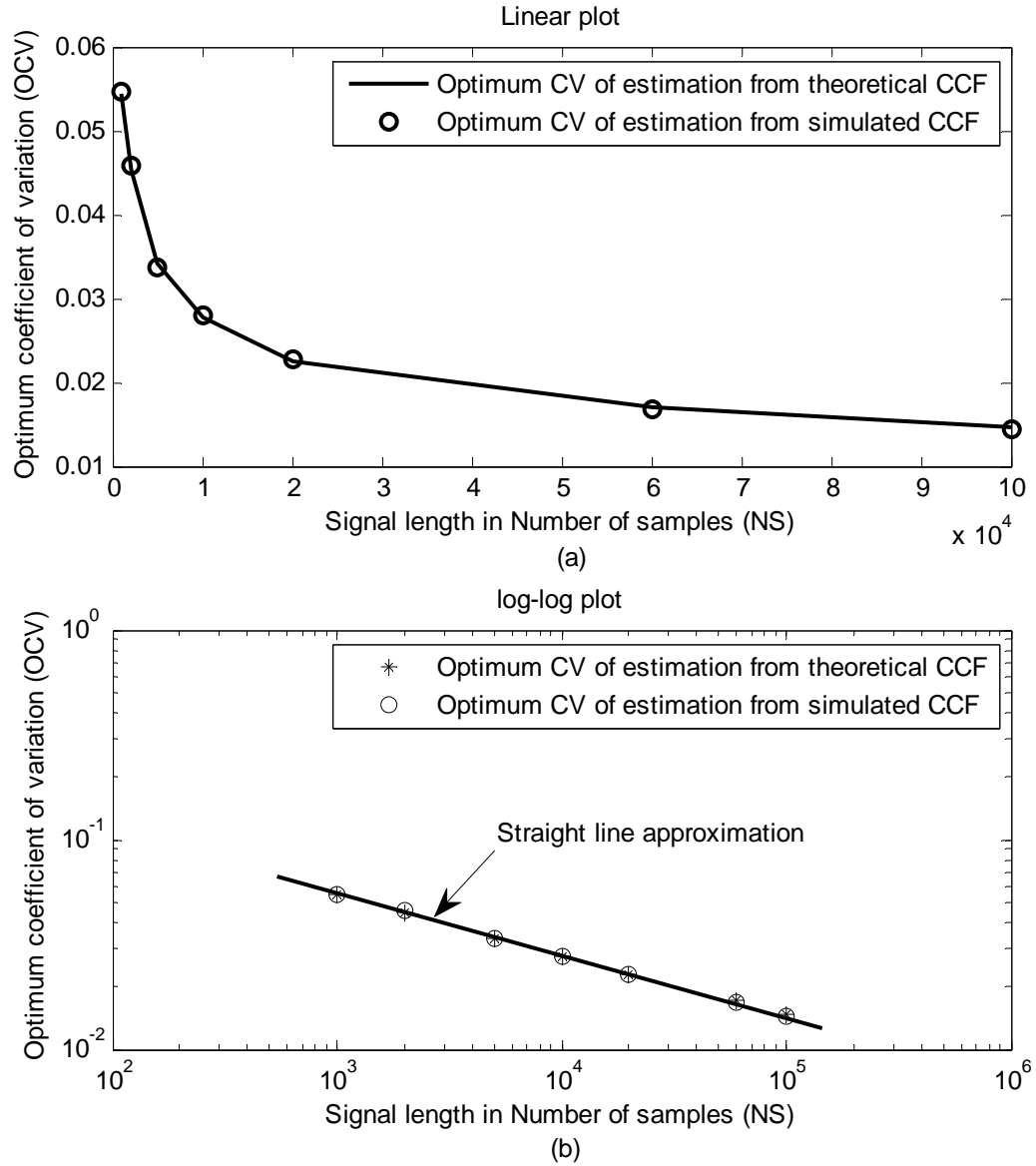


**Figure 5.13 OCV vs  $N_s$  for selection of signal length in ERP case with  $N=32$  (a) linear and (b) log-log scale.**

The value of constant  $c_3$  is obtained using a particular point from Figure 5.13 (a) in (5.29) as approximately 0.385. Finally, the relationship between the OCV (with 100 iterations) and  $N_s$  in the ERP case is expressed as

$$\text{OCV} = 0.385 \times N_s^{-0.283} \quad (5.30)$$

Therefore, OCV for 1 iteration can be expressed as

$$\text{OCV} = 3.85 \times N_s^{-0.283} \quad (5.31)$$

Similarly, Figure 5.14 shows the results for the OCV in the ETP case. Although the slope in Figure 5.14 (b) is almost the same as that in Figure 5.13 (b), i.e., approximately  $-0.283$ , the constant value is different, being  $0.8314$  instead of  $0.385$ .

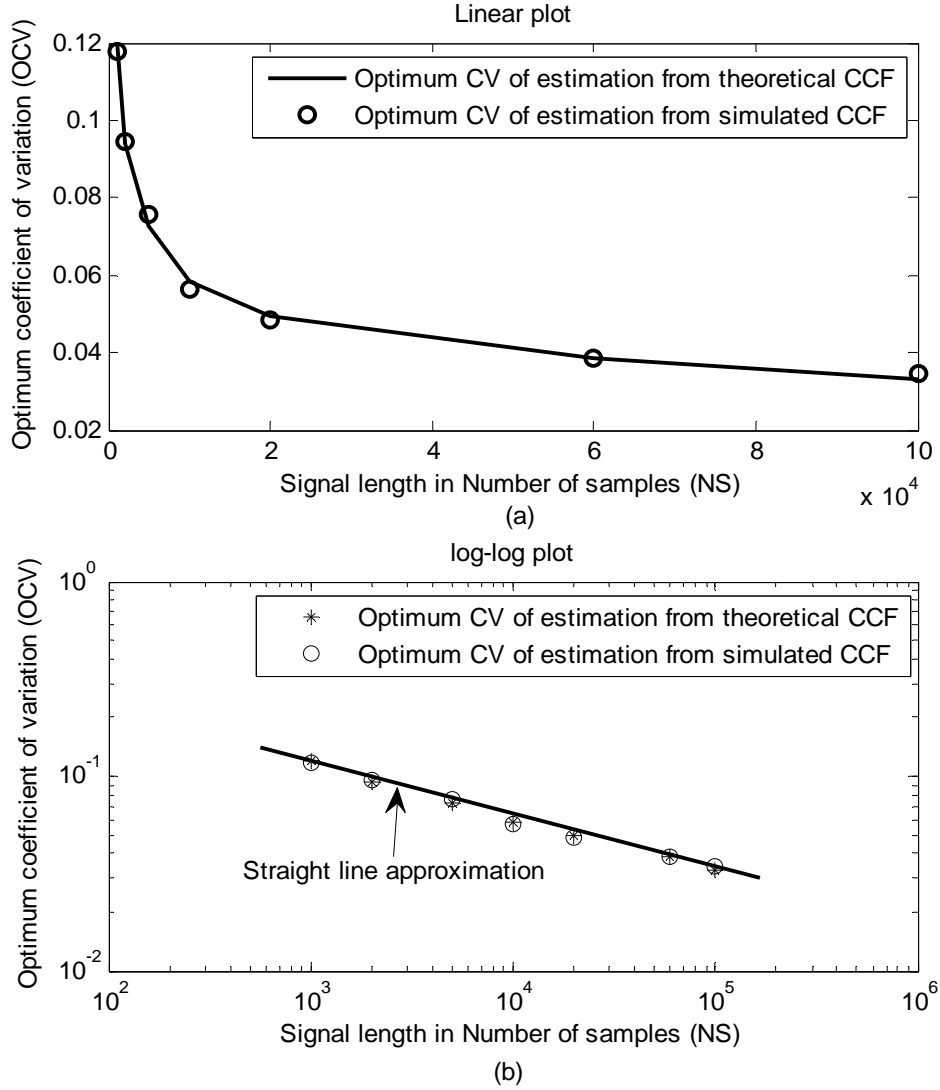


**Figure 5.14 OCV vs  $N_s$  for selection of signal length in ETP case with  $N=32$  (a) linear and (b) log-log scale.**

Therefore, the OCV in the ETP case is

$$\text{OCV} = 0.8314 \times N_s^{-0.283} \quad (5.32)$$

Thus, we can select  $N_s$  using the above expressions for the desired CV (considering the desired CV is OCV) in estimation. This gives the lowest possible  $N_s$  which leads to obtaining the energy efficient estimation technique.

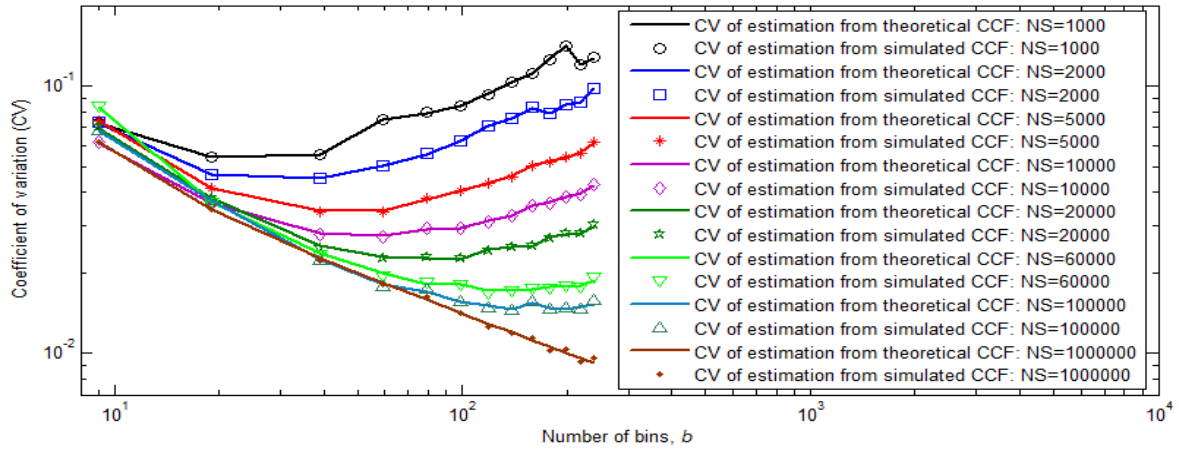
## 5.4 Selection of sampling rate, $S_R$ , distance between sensors, $d_{DBS}$ , and number of bins, $b$

To obtain proper estimations, it is necessary to know  $S_R$  and  $d_{DBS}$  as well as  $N_S$ . The selection process of  $N_S$  is discussed in the previous section. In this section, selections of  $S_R$ ,  $d_{DBS}$ , and  $b$  are investigated from the CVs of the estimated number of nodes.

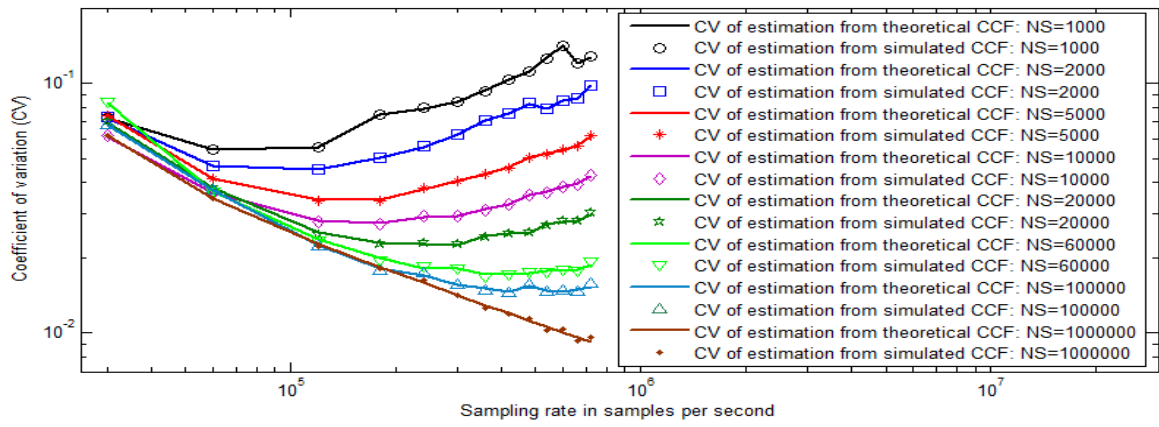
Figures 5.15 (ERP case) and 5.16 (ETP case) show the CVs for different  $N_S$  with respect to (a) the number of bins,  $b$ , (b) the sampling rate,  $S_R$ , and (c) the distance between the sensors,  $d_{DBS}$ . The CVs obtained from the theoretical and simulated CCFs are provided and can be seen to be similar. The results are obtained from 100 iterations for the 32 operating nodes for different  $b$  ( $= 9, 19, 39, \dots, 239$ ) and  $N_S$  ( $= 1000, 2000, 5000, 10,000, 20,000, 60,000, 100,000$  and  $1,000,000$ ). It can be seen in Figures 5.15 (a) and 5.16 (a) that there is an OCV for every  $N_S$  at which the CV is the minimum with a certain  $b$ . If the  $N_S$  used in the estimation process is 10,000 samples, it can be seen in Figures 5.15 (a) and 5.16 (a) that the OCV occurs with the 59 bin. Thus,  $b$  can be selected to obtain optimum performance in estimation.

It is also known that  $b$  is dependent on only  $d_{DBS}$  and  $S_R$ , the values of which are irrelevant for the CV (which varies only with variations in  $b$ ). Thus, if  $d_{DBS}$  is fixed to a certain value,  $b$  and, therefore, the CV for a particular  $N_S$ , only change with changes in the  $S_R$ . So, the CV can be plotted against  $S_R$  for different  $N_S$  taking a constant  $d_{DBS}$  at 0.25 m (to obtain the receivers in the same node), as shown in Figures 5.15 (b) and 5.16 (b). If the  $N_S$  used in the estimation process is 10,000 samples, it can be seen in Figures 5.15 (b) and 5.16 (b) that the OCV occurs at the sampling rate of 180,000 Sa/s. Thus, one can select the  $S_R$  for the estimation process keeping  $d_{DBS}$  fixed.

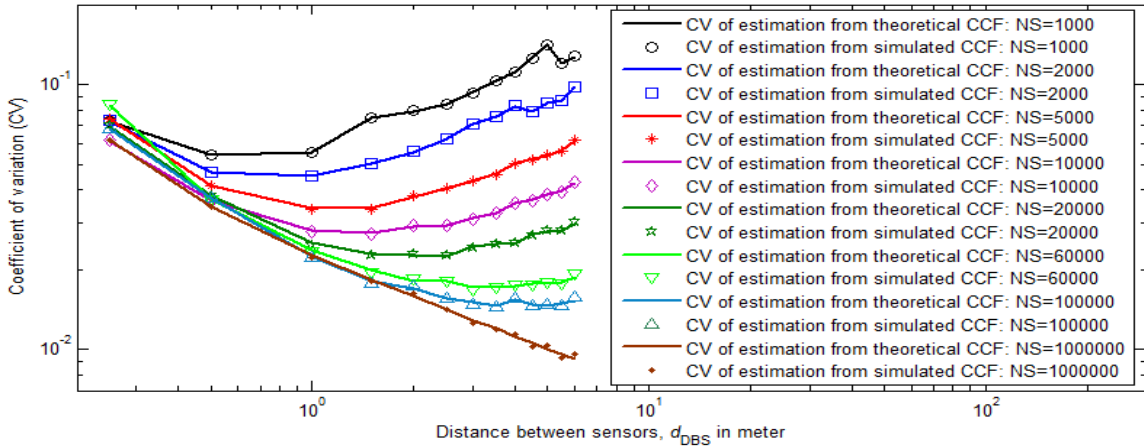
Similarly, the selection of  $d_{DBS}$  can be obtained from Figures 5.15 (c) and 5.16 (c) with  $S_R$  fixed. However, as for a particular  $b$ ,  $S_R$  and  $d_{DBS}$  might be combined in any way without violating the sampling theorem for obtaining corresponding CV, they can be selected at a time with compromising each other.



(a)



(b)



(c)

**Figure 5.15: CVs in ERP case for different  $N_s$  with respect to: (a) number of bins,  $b$ ; (b) sampling rate,  $S_R$ ; and (c) distance between sensors,  $d_{DBS}$**

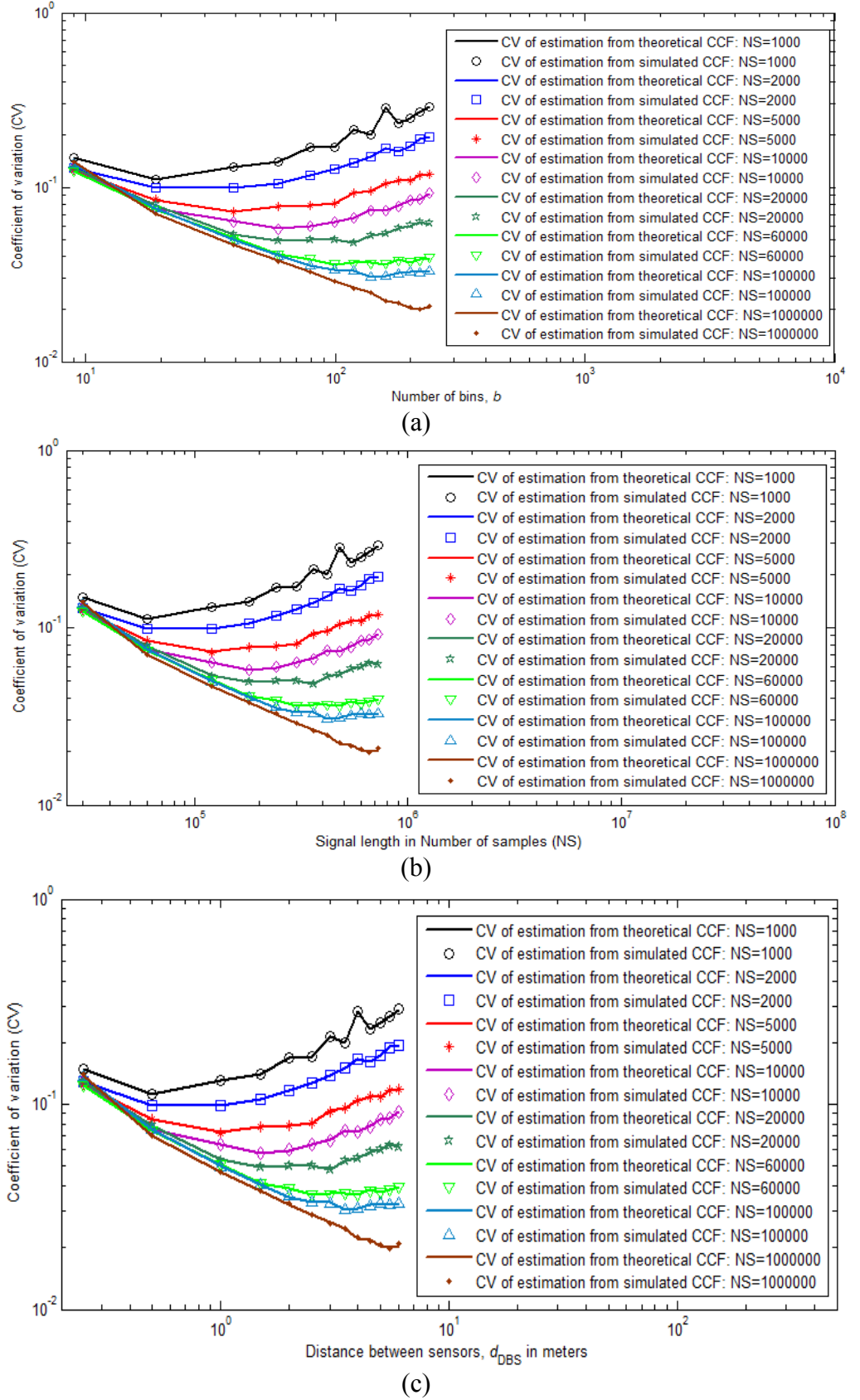


**Figure 5.16 CVs in ETP case for different  $N_S$  with respect to: (a) number of bins,  $b$ ; (b) sampling rate,  $S_R$ ; and (c) distance between sensors,  $d_{DBS}$**



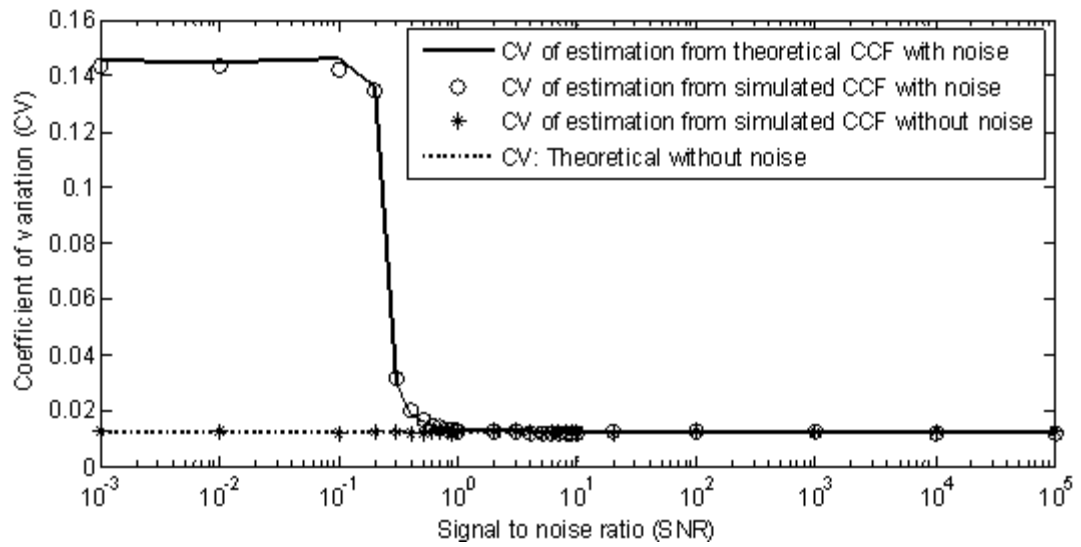
## 5.5 Effect of noise on CV

Noise (background and/or internal receiver noise) affects estimations of the number of nodes using the cross-correlation process, as discussed in Chapter 3. There might be similar effects on the estimation error, i.e., the CV, as discussed in this section. It is known that, if the integration time is finite, the cross-correlation process depends on both it and the signal to noise ratio, SNR. As the CV comes from the CCF of this cross-correlation process, it is dependent on the same parameters, i.e., integration time and SNR.

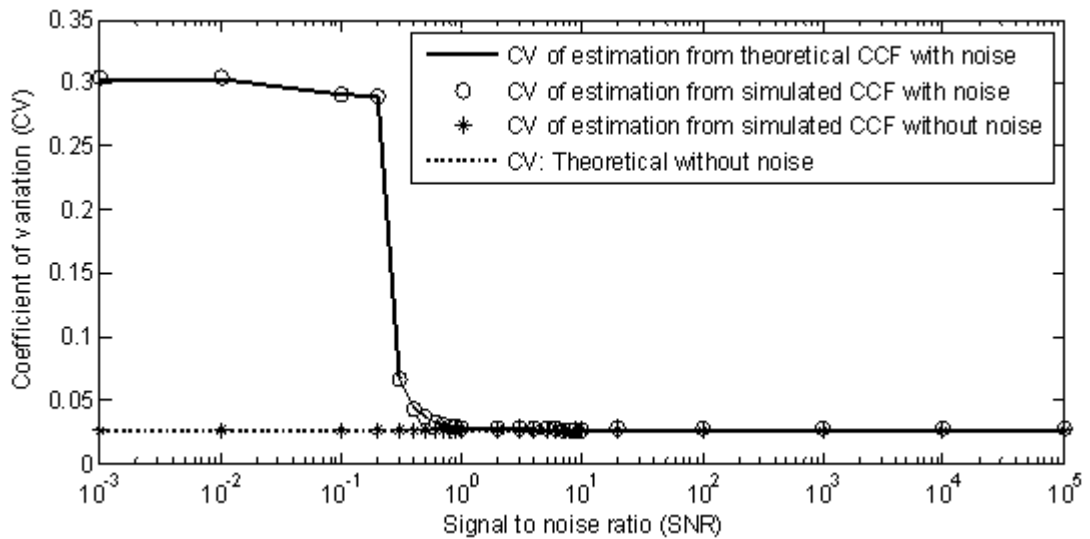
To show the effect of noise, internal receiver noise is added into the received signals in the estimation process. Table 5.4 shows the CVs with different SNRs for a signal length of 800,000 samples which are illustrated in Figure 5.17. The solid lines indicate the CVs with noise from the theoretical CCFs obtained using the moving average technique of cross-correlation, as discussed in section 5.2.2. The circles indicate the simulated results with noise, the stars the simulated results without noise and the dotted lines the theoretical without noise. It can be seen from these results that the CVs from the theoretical CCFs coincide with those from the simulated CCFs. Thus, hereafter, we present only the simulated results. Simulations for the CV, with varying  $N_S$  and SNRs of the receivers for a certain number (32) of operating nodes, are conducted and the results for both the ERP and ETP cases provided in Figures 5.18 to 5.21. Figure 5.18 shows the surface plots for the CV, SNR and  $N_S$  in which it can be seen that, for particular  $N_S$  up to a certain SNR ( $\text{SNR} \leq 0.05$ ), the CV is constant at the worst possible value but, with increases in the SNR (up to  $\text{SNR} = 1$ ), improves and, finally, becomes constant again at the best possible value for the case without noise. It can also be seen in Figure 5.18 that the worst possible value continues longer and the best possible value starts later if the  $N_S$  is lower. In other words, there is a transition zone in which the CV varies with the SNR, the start and end points of which vary with changing  $N_S$ , being earlier with a higher  $N_S$  and later with a lower  $N_S$ , respectively.

**Table 5.4 Noise effects in ERP and ETP cases**

SNR	CV: ERP	CV: ETP
0.001	0.1453	0.3161
0.01	0.1359	0.2932
0.1	0.0296	0.0639
0.5	0.0140	0.0300
1	0.0129	0.0277
2	0.0125	0.0275
10	0.0123	0.0271
100	0.0120	0.0272
1000	0.0121	0.0265

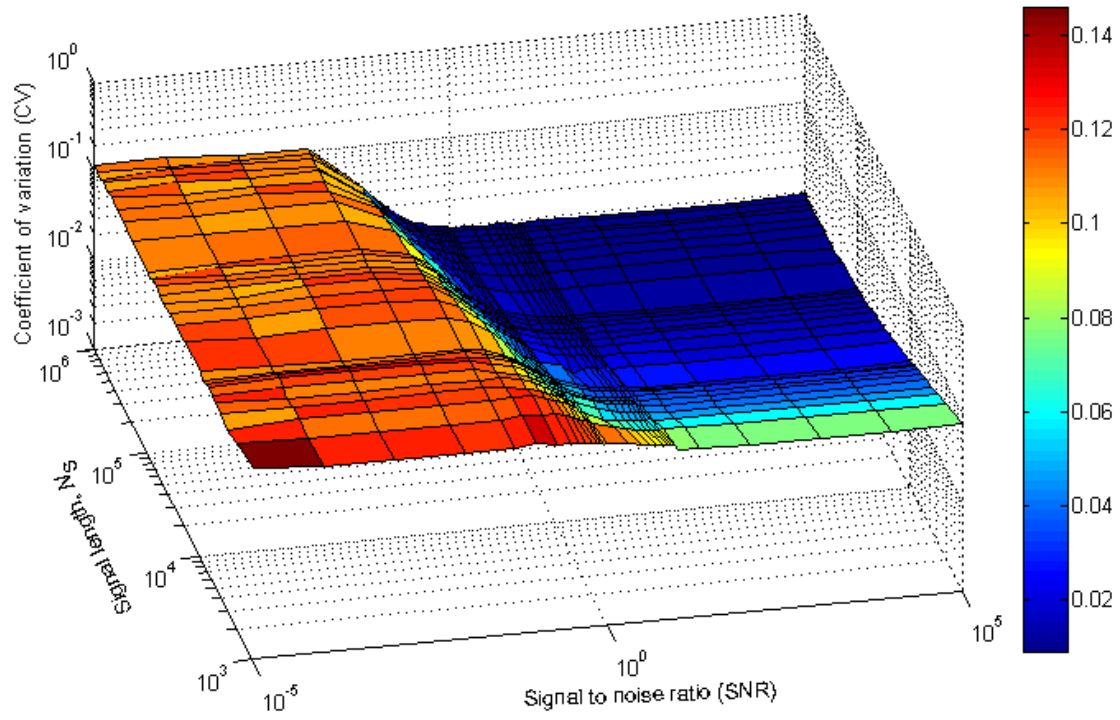


**(a)**

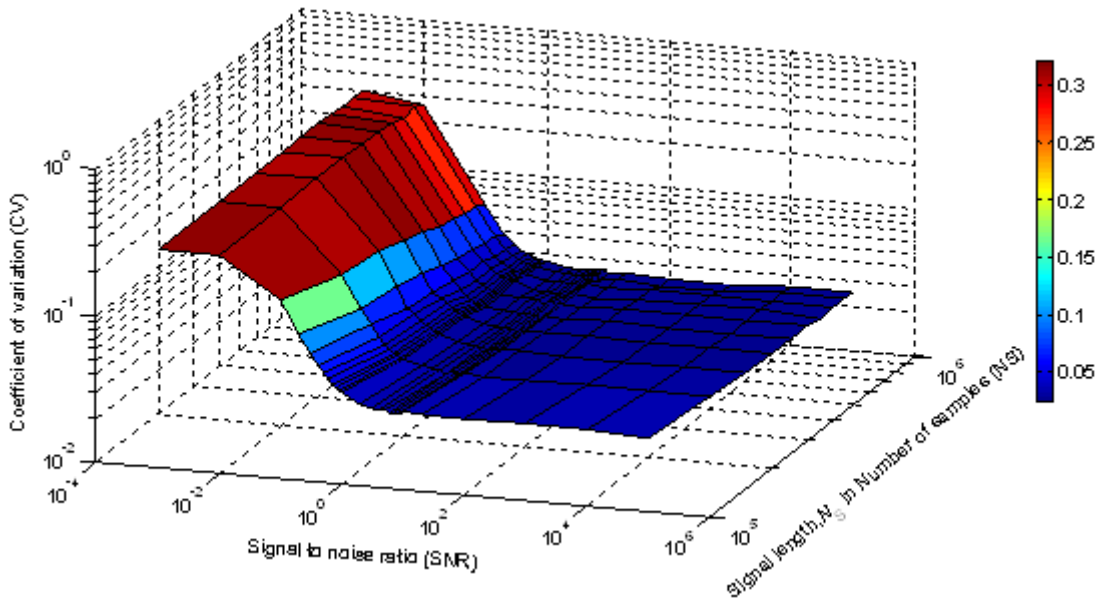


**(b)**

**Figure 5.17 CV versus SNR: (a) ERP; and (b) ETP case ( $N_S = 800,000$  samples)**



(a)

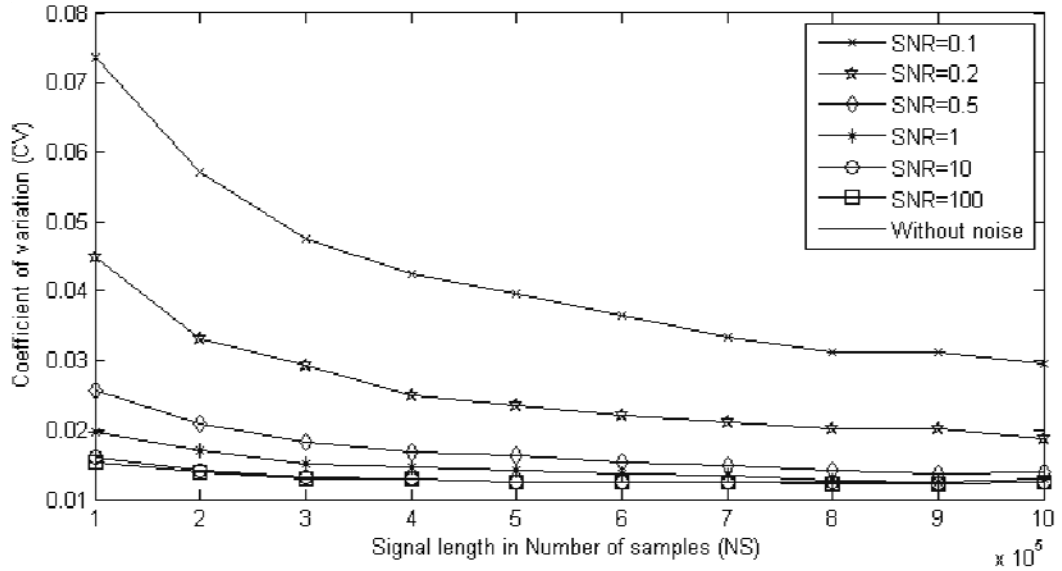


(b)

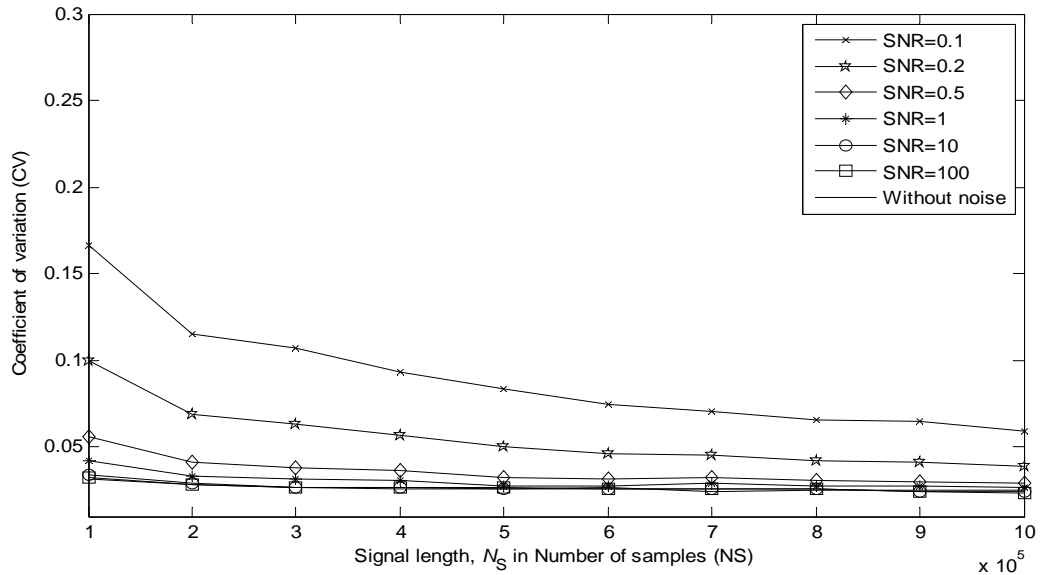
**Figure 5.18 Log-log-log plots of SNR,  $N_s$  and CV with  $N_s = 1000$  to 1,000,000:**

**(a)ERP case; and (b) ETP case**

In Figure 5.19, the CVs are plotted with respect to  $N_s$  (values from  $10^5$  to  $10^6$  samples) for different SNRs (0.1, 0.2, 0.5, 1, 10, 100 and without noise). It can be seen again that, for a particular SNR, the CV improves with higher  $N_s$ .



(a)

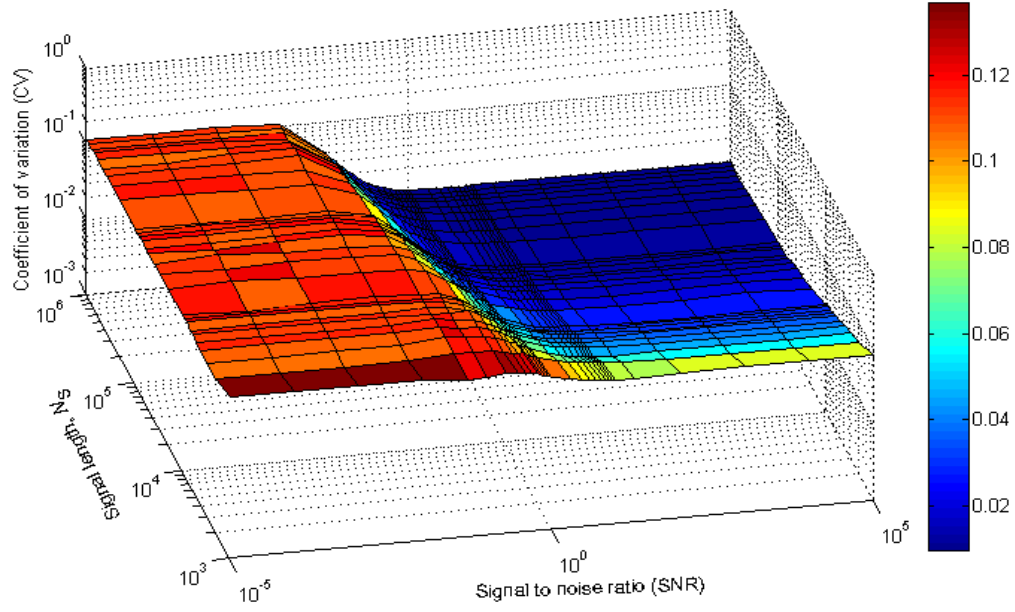


(b)

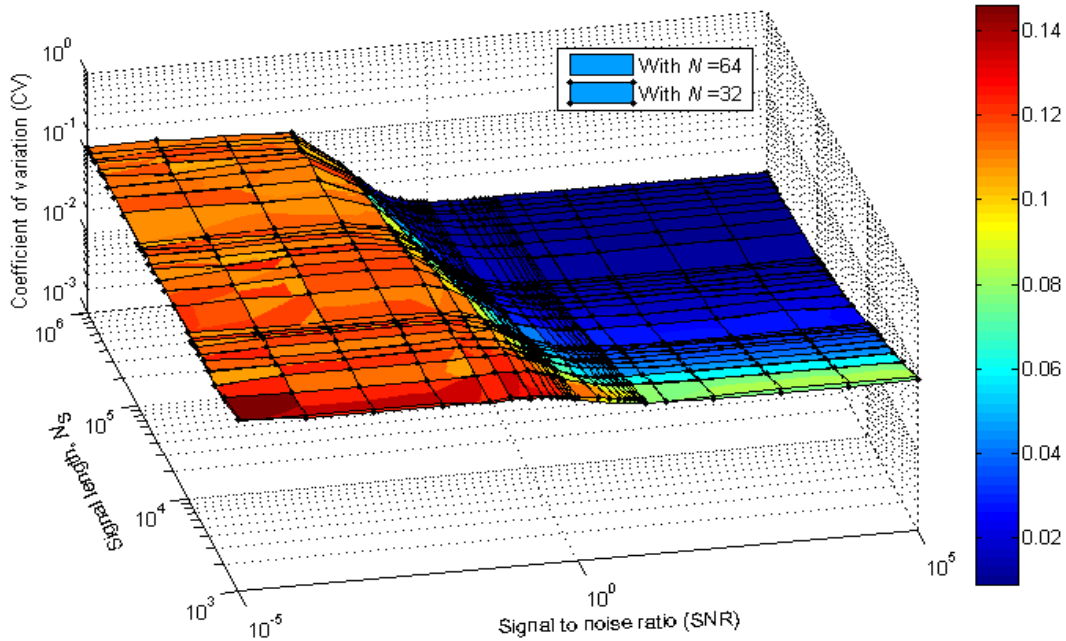
**Figure 5.19 CV versus signal length for different SNR:**

**(a) ERP case; and (b) ETP case**

It has already been mentioned that all the above results for the effect of noise on the CV are from investigations using 32 operating nodes. It has been shown that the CV is independent of the number of nodes in the case without noise. To determine whether the same relationship exists for the case with noise, the results for 64 operating nodes are provided in Figure 5.20 (a) and compared with those for 32 operating nodes in Figure 5.20 (b) and 5.21.



(a)



(b)

**Figure 5.20 Log-log-log plots of SNR,  $N_s$  and CV with  $N_s = 1000$  to  $1,000,000$ :**

**(a) original  $N = 64$ ; and (b) comparison of  $N = 32$  and  $64$**

Figure 5.20 shows the surface plots and Figure 5.21 the corresponding contour plots of the SNR,  $N_s$  and CV for both the 32- and 64-node cases. The comparisons in Figure 5.20 (b) and 5.21 show that  $N$  still has no significant effect on the CV when noise is considered.

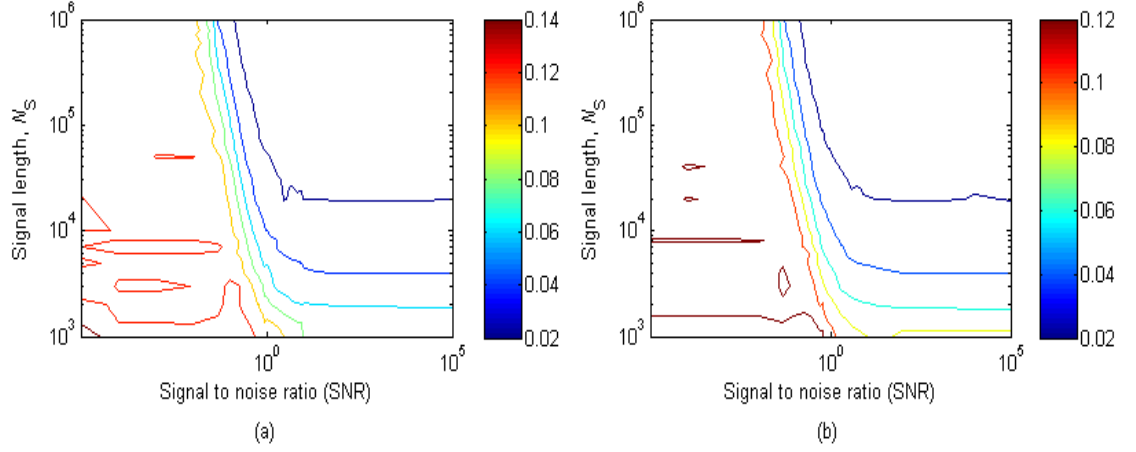


**Figure 5.21 Contour plots of SNR,  $N_s$ , and CV with  $N_s = 1000$  to  $1,000,000$ :  
(a) original  $N = 32$ ; and (b) original  $N = 64$**

It can be seen from the results that for an SNR greater than a certain value (1 in voltage ratio), the CV of the estimation are almost the same as those in the without noise case (with a little variation due to the randomness of the experiments). For a lower SNR (less than 1 in voltage ratio), the CV of the estimation increases and finally reaches the fixed worst possible value. The meaning of these phenomena can be described as follows: when the SNR is less than 1, the noise dominates the signal but, as some signals are strong enough to count, we obtain a reduced number of nodes rather than the appropriate number. As with the lower SNRs, the original number of nodes is far beyond those of the estimation; this wide variation leads to the CV being worse.

## 5.6 Required estimation time in the proposed method

As the energy is directly related to time, it is important to know the estimation time, especially for the UWCN where the limited energy is a challenge. Estimation time is related with the performance of the cross-correlation which in turn related with the signal length, sampling rate, and the number of probes required to achieve that performance. The process of obtaining estimation time is discussed here. In the proposed CC technique, using the  $N_s$ ,  $S_R$ , and  $u$ , the estimation time,  $T_{CC}$  is expressed as

$$\begin{aligned}
T_{CC} &= \text{Number of iteration} \times (\text{Number of samples per iteration}) \\
&\quad \div (\text{Sampling rate}) \\
&= \text{Number of iteration} \times (\text{Number of samples per iteration}) \\
&\quad \div (\text{Number of samples per unit time}) \\
&= \text{Number of iteration} \times \text{Number of samples per iteration} \\
&\quad \times (\text{Time per sample}) \\
&= \text{Number of iteration} \times \text{Time per sample} \\
&\quad \times \text{Number of samples per iteration} \\
&= \text{Number of iteration} \times \left( \frac{1}{\text{Sampling rate}} \text{ second/sample} \right) \\
&\quad \times (N_s \text{ sample per iteration}) \\
&= \frac{N_s}{S_R} \times u \text{ second}
\end{aligned} \tag{5.33}$$

This expression shows that obtaining the required estimation time in the proposed estimation process requires knowing the value of  $N_s$ ,  $S_R$ , and  $u$ . Actually, to obtain a certain CV, required  $N_s$ ,  $S_R$ , and  $u$  are used to obtain the estimation time.

To obtain the estimation time using (5.33), a method is proposed as follows. Firstly, CVs are obtained from simulations for the different possible combinations of  $N_s$  (1000, 2000, ..., 10,000, 20,000, ..., 100,000, 200,000, ..., 1,000,000) and  $b$  (19, 39, ..., 239), keeping the other parameters same as in Section 5.2.3.1. Upon obtaining the CVs, they,  $b$  and  $N_s$  are visualised using contour plots, as shown in Figure 5.22, from which a point with certain  $N_s$  and  $b$  is selected to obtain the estimation time. Figure 5.22 shows the contour plots of  $b$ ,  $N_s$  and CV with 100 iterations for ERP and ETP cases. The x-axis indicates  $b$ , the y-axis  $N_s$  and 'Level' is the  $\log_{10}(\text{CV})$ . So,

$$\text{CV} = 10^{\text{Level}} \tag{5.34}$$

Considering a particular point in the contour plot of Figure 5.22 (a), e.g., in the ERP case in which Level =  $-1.9136$  at  $b = 219$  and  $N_s = 200,000$  then, from (5.34),  $\text{CV} = 0.0122$ .

To obtain the above accuracy, i.e., to obtain the value of  $\text{CV} = 0.0122$ , the required time,  $T_{\text{ERP}}$  in the ERP case can be obtained with a sampling rate of 30,000 Sa/s (this

is chosen arbitrarily with the  $d_{\text{DBS}}$  for  $b=219$  without violating the sampling theorem) from (5.33) as

$$\begin{aligned} T_{\text{ERP}} &= 100 \times \left( \frac{1}{30000} \text{ second/sample} \right) \times (200000 \text{ sample}) \\ &= 100 \times 6.67 \left( \frac{\text{second} \times \text{sample}}{\text{sample}} \right) \\ &= 667 \text{ second} \end{aligned}$$

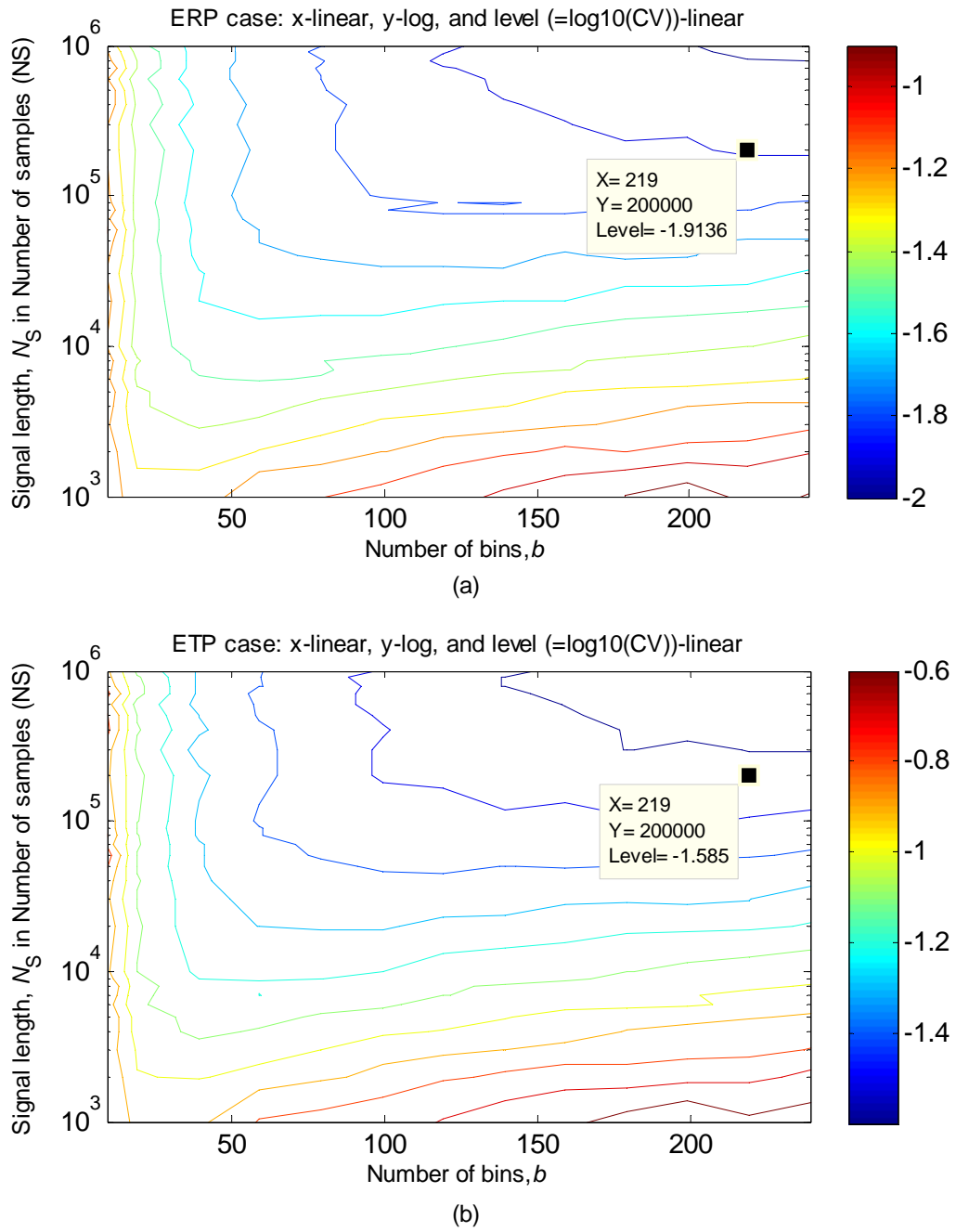


**Figure 5.22** Contour plots of  $b$ ,  $N_s$  and CV: (a) ERP case; and (b) ETP case



Similarly, for a particular point in the contour plot of Figure 5.22 (b), e.g., in the ETP case in which Level =  $-1.585$  at  $b = 219$  and  $N_s = 200,000$  then, from (5.34),  $CV = 0.026$ .

To obtain the above accuracy, i.e., the value of  $CV = 0.026$ , the required time,  $T_{ETP}$  in ETP case can be obtained from (5.33) with a sampling rate of 30 kSa/s (as is chosen in ERP case) as

$$\begin{aligned} T_{ETP} &= 100 \times \left( \frac{1}{30000} \text{ second/sample} \right) \times (200000 \text{ sample}) \\ &= 100 \times 6.67 \left( \frac{\text{second} \times \text{sample}}{\text{sample}} \right) = 667 \text{ second} \end{aligned}$$

Again, we recall the results for the OCV in Figure 5.23 which shows linear plots of the OCV against the signal length,  $N_s$ , for the ERP (a) and ETP (b) cases. From these results, an optimal value of  $N_s$  can be picked for a certain CV, i.e., accuracy. The required time can be obtained using (5.33) from this optimal  $N_s$  and the selected  $S_R$  (obtained from the process in Section 5.4).

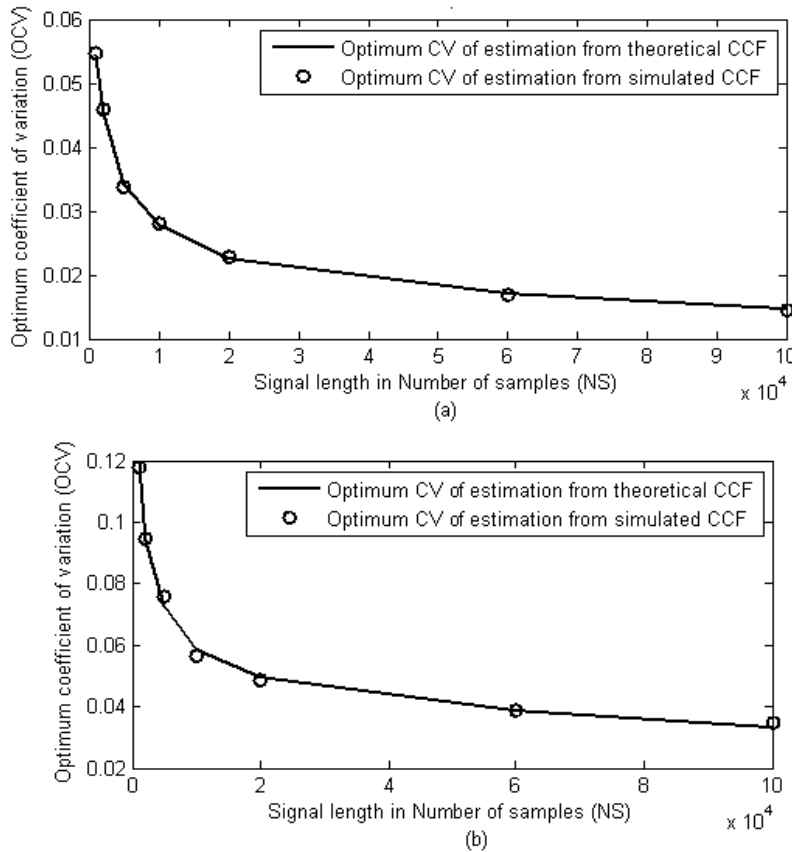


**Figure 5.23 OCV versus  $N_s$ :  $N=32$  for (a) ERP and (b) ETP cases**

It can be seen from the Figure 5.23 that at OCV of 0.0233 with 100 iterations in the ERP case and 0.0504 in the ETP case, the optimal  $N_S=20,000$  samples. If the selected  $S_R = 360$  kSa/s, the required estimation time using (5.33) is

$$\begin{aligned} T_{\text{ERP}} = T_{\text{ETP}} &= 100 \times \left( \frac{1}{360000} \text{ second/sample} \right) \times (20000 \text{ sample}) \\ &= 100 \times 0.0556 \left( \frac{\text{second} \times \text{sample}}{\text{sample}} \right) = 5.56 \text{ second} \end{aligned}$$

As the ratio of OCVs of ETP and ERP cases is  $\frac{0.8314}{0.385} \approx 2.2$ , the iteration required for same CV is about 5 times more in ETP case than that in ERP case. Therefore, it requires about 5 times more time to obtain same CV in ETP case than that in ERP case.

A comparison of the required estimation times for the same CV (0.026) in both ERP and ETP cases is provided in Figure 5.24. It is shown that both estimation times ( $T_{\text{ERP}}=143$  second and  $T_{\text{ETP}}=667$  second) are independent of  $N$  but that the ETP case takes about 5 times the time required by the ERP case to achieve similar performances. However, the ETP technique has some advantages which were discussed earlier.

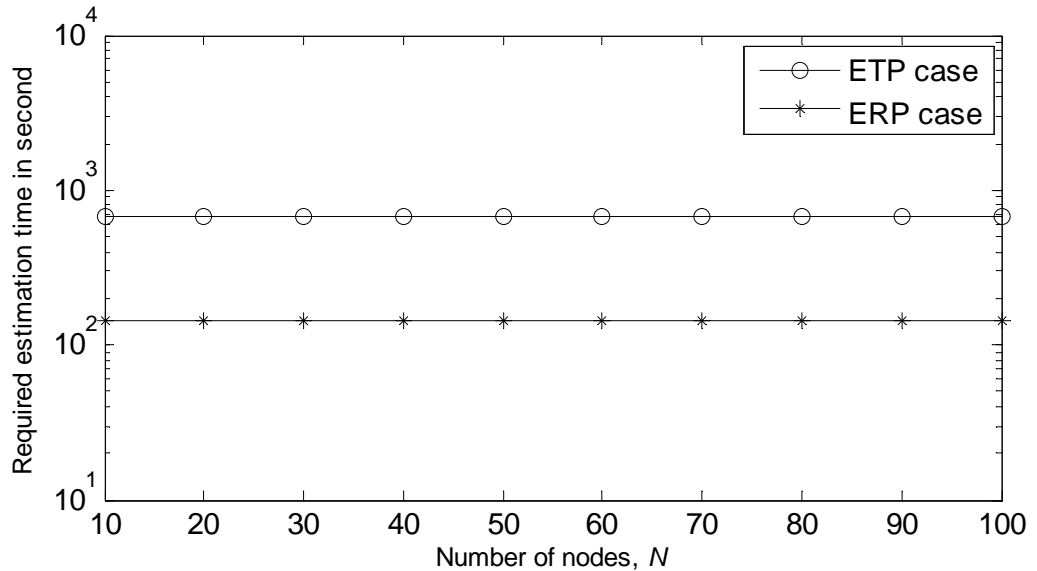


**Figure 5.24 Performance comparison in terms of required estimation times for proposed technique in ERP and ETP cases**

## 5.7 Required energy in terms of the product of SNR and $N_S$

As the WCNs especially UWCNs are energy limited, knowing the required energy is also important for the proposed estimation techniques. To obtain it, the results (of  $N$  and CV) shown in previous sections (Section 3.6 in Chapter 3 and Section 5.6 in Chapter 5) for some  $N_S$  with noise are plotted in Figures 5.25 to 5.28. Figure 5.25 shows the CV from 10 iterations in ERP case against  $A$ , where  $A$  is the product of the SNR and  $N_S$  values, and evidence that, for equal  $A$ , the CVs are similar despite the SNR and  $N_S$  values (without exceeding the lower limit of  $N_S$  for which one can obtain a similar CV without noise). Again, Figure 5.26 shows the estimation ( $\hat{N}$ ) with respect to  $A$ .

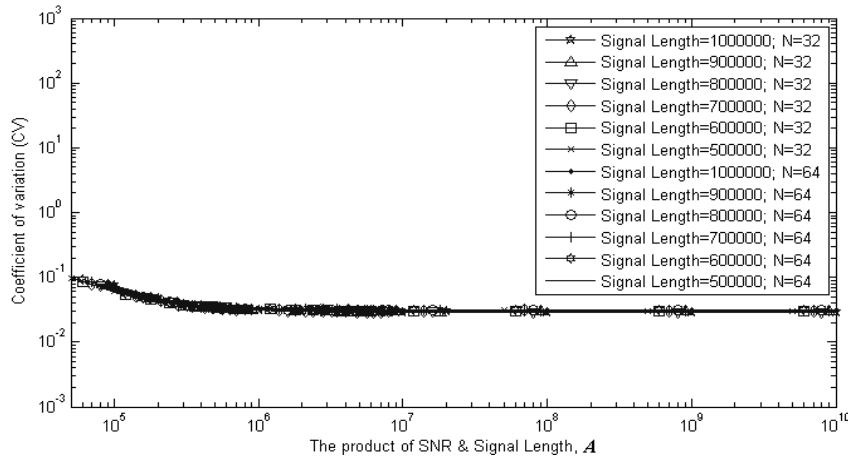


Figure 5.25 CV (from 10 iterations) versus  $A$

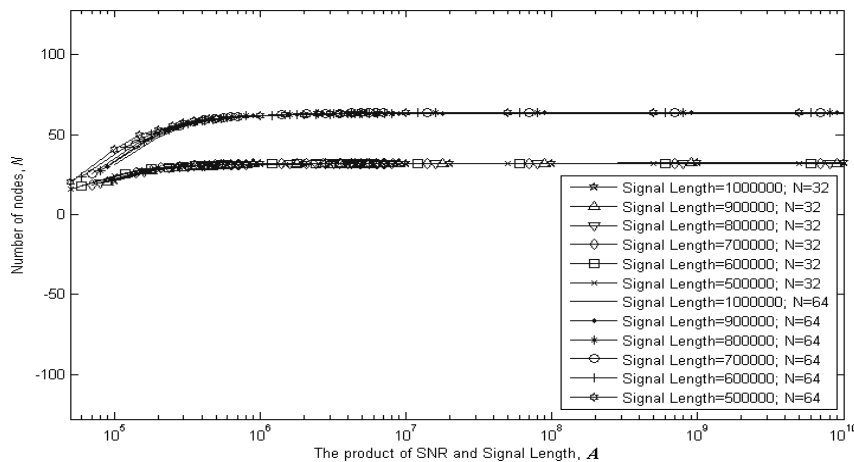
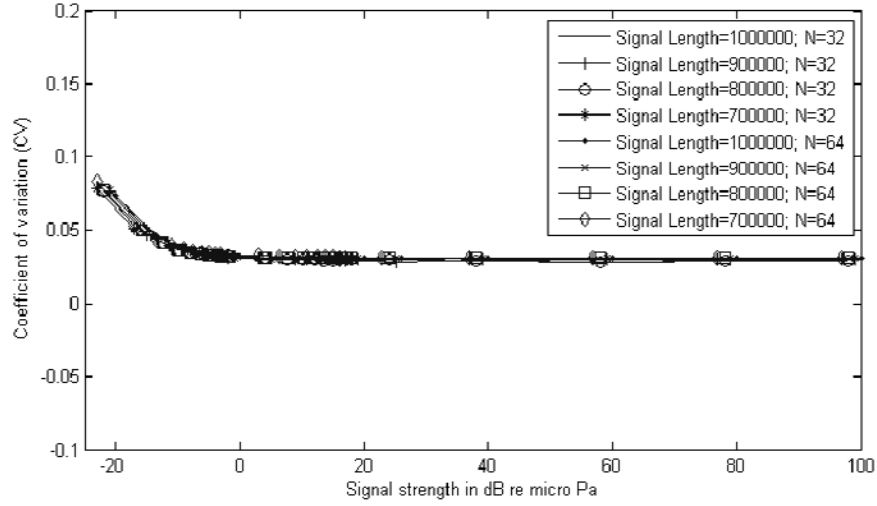
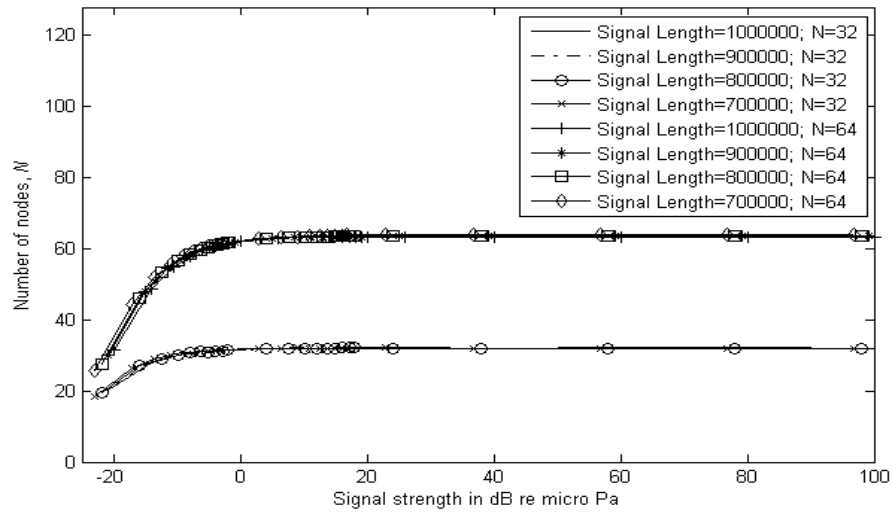


Figure 5.26  $N$  versus  $A$

Both results show the effective values of  $A$  which, when greater than 500,000, give similar performances. Thus, one can estimate the number of nodes using the process of cross-correlation by compromising among the CV, SNR and  $N_S$ , i.e., CV and  $A$ . This is useful because now it is necessary to be careful about one parameter,  $A$  instead of two (SNR and  $N_S$ ) for the estimation.



**Figure 5.27 CV (from 10 iterations) versus signal strength in dB re micro-Pa**



**Figure 5.28  $N$  versus signal strength in dB re micro-Pa**

The product,  $A$ , is proportional to the signal strength above the noise. If one considers it the acoustic pressure in Pascal (Pa) above the noise, it can be converted to the signal pressure level above the noise in dB re 1 micro-Pa using the well-established expression

$$A_{\text{dB re } \mu \text{ Pa}} = 20 \log_{10} \left( \frac{A \text{ in Pa}}{1 \mu \text{ Pa}} \right) \quad (5.35)$$

In Figure 5.27, the CV is plotted with respect to  $A_{\text{dB re } \mu\text{Pa}}$  whereas the estimated number of nodes is plotted against  $A_{\text{dB re } \mu\text{Pa}}$  in Figure 5.28. These figures show that, if the signal level is 0 dB or greater than the noise level, it is possible to estimate the number of nodes with a certain error, the CV, of 0.0389 with 10 iterations. The above energy estimation is for only the ERP case. Now, for the ETP case, the energy required to estimate the number of nodes,  $N$ , is obtained and compared with that for the ERP case in three different forms. Figure 5.29 shows the performance comparison in terms of the CV with the same energy per node per iteration for 100 iterations in order to achieve better performances. It can be seen again that a signal energy of 0 dB greater than the noise level is sufficient for estimations with certain accuracies of  $\text{CV} = 0.0123$  and  $\text{CV} = 0.0266$  for the ERP and ETP cases, respectively. Thus, an almost 2.2 times better performance in terms of CV is possible in the ERP case than in the ETP case when the same energy is provided. Figure 5.30 shows the performance comparison of both cases in terms of the energy used to obtain the same CV in both the ERP and ETP cases. It can be seen that, to obtain a CV of 0.02465, the signal energy has to be about 0 dB and -13.37 dB greater than the noise level in the ETP and ERP cases, respectively. This implies that about 5 (exact value is 4.66) times more signal strength is needed in the former than the latter to achieve the same performance.

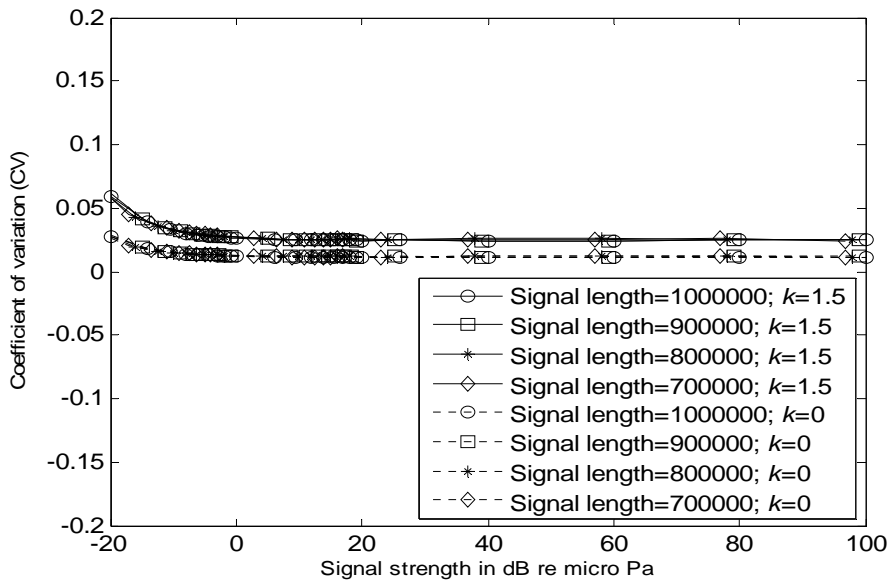


**Figure 5.29 CVs versus signal strengths in dB re 1 micro-Pa: performance comparison in terms of CVs of ERP and ETP cases using same energy**

Finally, Figure 5.31 shows the performance comparison of both cases in terms of the energy used to obtain several distinct CVs. It is again shown that the required energy is always around 13.37 dB greater in the ETP case than in the ERP case, i.e., about 5 times more signal strength is needed in the former than the latter to achieve the same performance.

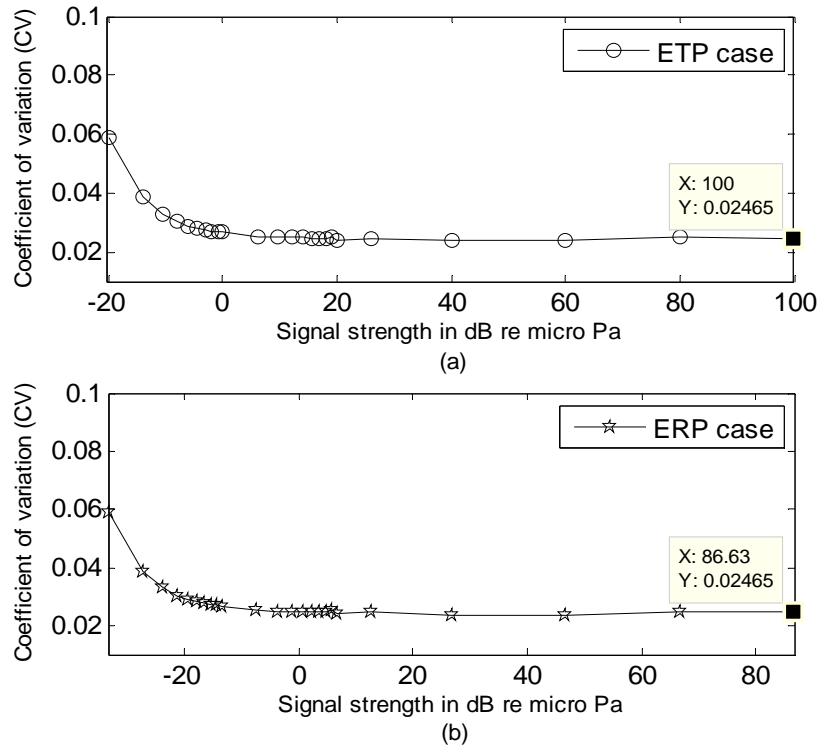


**Figure 5.30 Performance comparison in terms of energy required to obtain same CV in: (a) ERP case for CV = 0.02465; and (b) ETP case for CV = 0.02465**

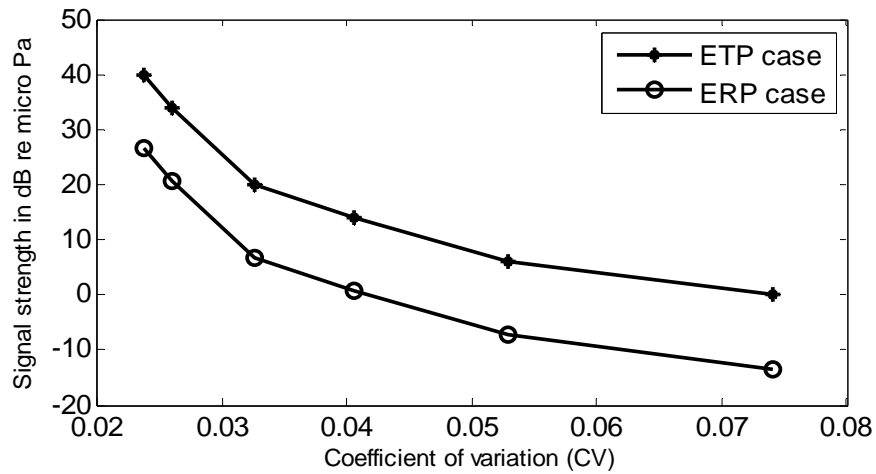


**Figure 5.31 Performance comparison in terms of energy required in ERP and ETP cases**

## 5.8 Comparison with conventional protocol-based techniques

To date, the conventional techniques used for the estimation of the number of nodes in a WCN have been based only on the network protocol in use. This thesis proposes a new estimation technique based on random signal cross-correlation which is very different from the conventional ones in terms of the estimation process; for example, in the proposed technique, the transmitter is required to transmit a Gaussian signal whereas, in a protocol technique, it is required to transmit some data (in the form of bits) to the receiver. Transmission of a Gaussian signal directly through a channel is possible but transmission of bits through the channel requires modification by converting them to a physical signal. Again, after reception of the signal in the CC technique, it is possible to directly use the signal for the cross-correlation process to obtain the CCF from which estimation is obtained. But, in the protocol, after reception of the modified signal, further modification is required to make the received signal a packet of bits and then the estimation is obtained from the proper reception of these bits. Thus, it is difficult to compare the techniques on the same platform without having sufficient field results. Despite wide application of the number of nodes estimation, only one conventional method in UWCN is investigated using analysis and simulation and, although an energy-related performance parameter is investigated, the energy required in joules is not clear. Moreover, both the protocol and CC techniques require more investigation to address the practical issues of obtaining field results. Despite the difficulties, some performance parameters are compared on the same platform in the following way.

To show the effectiveness of the proposed technique, its performances in terms of times and energy required for, and errors (CVs) in, estimation are compared with those of the two conventional protocol-based techniques: the probabilistic framed slotted ALOHA (PFSA) (Howlader 2009) and the Good-Turing (GT) (Budianu 2006) estimator protocol. The CVs are compared keeping the estimation time fixed, actual estimation times are compared keeping the CVs fixed and transmit energies are compared keeping the CVs fixed. Moreover, virtual estimation times are obtained and compared keeping the CVs and transmit energies fixed for all techniques.

As the CV is obtained from the standard deviation and mean of the estimation, it basically depends on the estimation which might be affected by many factors which, in turn, might affect the CV in all methods. In the CC technique, a physical (Gaussian) signal is generated and transmitted directly through the channel to the receiver. It requires some amplifier circuitry, as shown in Figure 5.32 (a), to raise the signal level to overcome attenuation. On the other hand, in the protocol techniques, a packet of bits is generated which (after some signal processing) transmits its physical equivalent signal through the channel to the receiver. It requires some complicated signal processing circuitry, as shown in Figure 5.32 (b), to convert the bits to a physical signal along with the amplifier circuitry. It is clear from the figure that, as both the CC and protocol techniques require signal transmission through the channel, there will be some common factors which might affect the estimations and, thus, the CVs in all techniques.

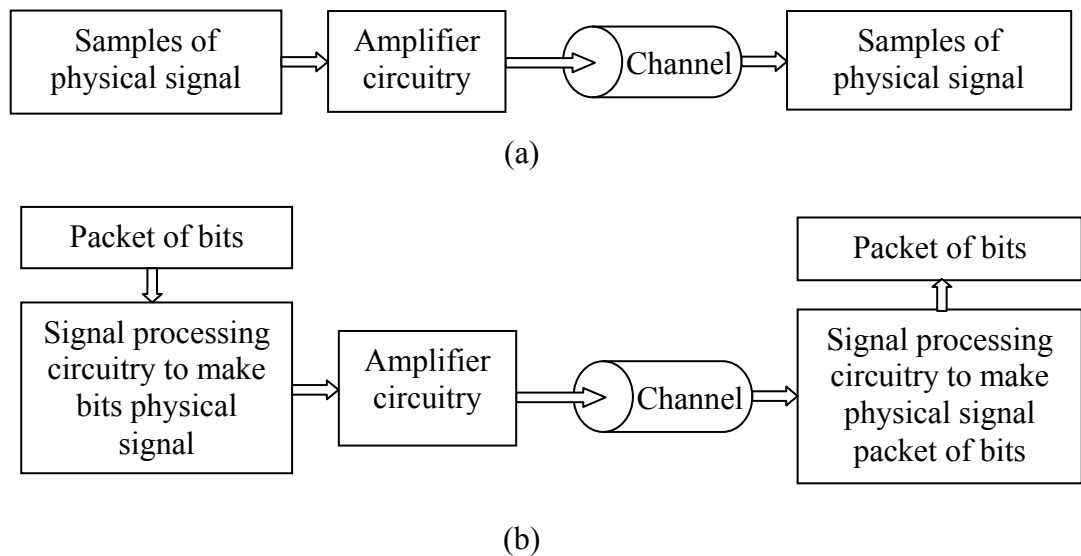


**Figure 5.32 Simple block diagram of signals and their transmission: (a) CC technique; and (b) protocol technique**

Common factors that might contribute to the CV are:

1. the effect of the multipath propagation of signals;
2. the effect of the Doppler spread;
3. attenuation or path loss;
4. the effect of noise and consideration of the SNR;



5. the power of the transmitted and received signals;
6. channel BW;
7. the speed of signal propagation;
8. placements of the sensor(s); and/or
9. distribution of the nodes.

Besides, the CV might be affected in protocols by the following factors:

10. the capture effect;
11. the number of slots; and/or
12. the bit rate.

and in the CC techniques by the following factors:

13. the number of samples; and/or
14. the sampling rate.

The effects and assumptions of these factors are briefly described below.

### ***1. Effect of multipath propagation of signals***

Transmitted signals in both the CC and protocol techniques are affected by multipath propagation in the channel. As the multipath propagation of signals is sometimes additive and sometimes subtractive in nature, signals reach the receiver with either more or less power (Lazaro 2009; Islam 2010). So, to achieve a successful reception, i.e., to obtain at least the sensitive power of the receiver, requires more transmit power for a signal or the system performance for estimation degrades. Besides, the multipath causes ISI in the received signal but, by using a symbol interval which is sufficiently longer than the delay spread, ISI can be neglected (Lazaro 2009). Thus, it takes more estimation time to neglect the effect of multipath fading.

In the proposed technique of cross-correlation, any multipath effect can be neglected using the multipath suppression process (discussed in Section 3.12 of Chapter 3) where the power of a signal and the time required are not affected. This is very useful for an energy-limited UWCN.

As in conventional protocols the multipath effect is not considered in the estimation of the number of nodes, in order to be able to compare the techniques on the same platform, this effect is neglected for all methods.

## **2. *Effect of Doppler spread***

The Doppler effect is one of the important practical issues in underwater acoustic networks. It sometimes compresses and sometimes spreads the frequency of the received signal according to the movements of the source and receiver towards or away from each other.

When a signal is spread, the transmitter and receiver are turned on for a longer time than when it is not spread and, when it is compressed, the transmitter and receiver are turned on for a shorter time than when it is not compressed. Therefore, sending and receiving a Doppler spread signal requires more energy than sending and receiving a non-spread signal. Thus, extra energy is required to compensate for the Doppler effect. However, although both the protocol and CC techniques might be affected by this, it has not yet been considered in the estimation process, and the Doppler effect is neglected in the comparison of techniques.

## **3. *Attenuation or path loss***

Considering attenuation or path loss is important in terms of transmitted signals reaching a receiver. If any attenuation is not compensated for by the appropriate signal strength, the transmitted signal will not reach the receiver. In an underwater channel, attenuation means absorption and dispersion losses. Below about 70 kHz (Heidemann 2006) the dispersion loss is sufficiently higher than the absorption loss and only the dispersion loss can be considered as the total loss. As the higher frequencies cause severe absorption loss, it is not practical to use it in long-distance transmission. Therefore, absorption loss is neglected in all techniques. To compare dispersion losses, appropriate distances and the practical dispersion coefficient,  $k$  ( $=1.5$ ), are considered in all techniques.

#### 4. *Effect of noise and consideration of SNR*

Both the protocol and CC techniques require a receiver to properly collect a signal the strength of which has to be such that its power will be greater than or equal to the threshold power of the receiver which is determined from its noise floor (internal noise power). In the CC technique, the receiver is simply a hydrophone but, in the protocol techniques, it is a hydrophone with some signal processing circuitry (as shown in Figure 5.33) to make the physical signal a packet of bits. Thus, in all techniques, the receiver is the major component of the noise floor contributions to which from other parts are negligible in comparison. So, the noise floor of the hydrophone can be considered the noise floor of the whole receiver. Thus, it is assumed that the threshold power of the receiver is the same for all cases and is the internal noise (AWGN) power of the hydrophone. In the proposed CC technique, it is shown that a 20 dB SNR (10 in voltage ratio) is sufficient to estimate the number of nodes with the same error as in the without noise case. Although the effect of noise is not considered in the protocol techniques for estimating the number of nodes, it is mentioned in the literature (Heinzelman 2000) that a 30 dB SNR is sufficient to properly collect a signal. Besides, for BPSK modulation with AWGN, typically an SNR of 10 dB gives a BER of  $10^{-05}$  which is too low and can be neglected. Based on these discussions, a 20 dB SNR is considered in the energy calculations for all techniques when compared on the same platform. Again, from the testing conducted at Jervis Bay, Australia (details in Appendix A), the channel's background noise is about 25 dB greater than the internal noise of the receiver. Although the strength of the background noise might vary with the frequency, it will be shown in Figure A.3 (See in Appendix A) that, at frequencies beyond 5 kHz, the power spectrum is almost flat and that values greater than 25 dB will be sufficient compared with the internal noise of the receiver. As internal noise of the receiver, assuming the background noise (which is almost flat after 5 kHz) of the channel is Gaussian in nature, like internal noise another 20 dB SNR will have to be added for it in the estimation process. Details of this calculation are provided in the energy comparison in this section.

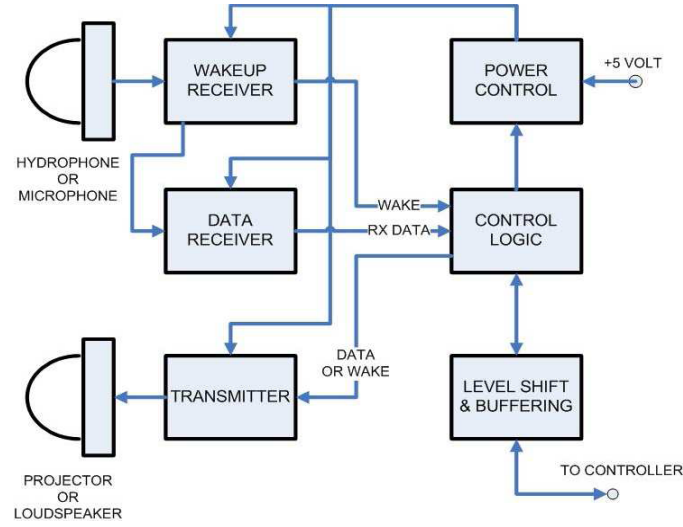


**Figure 5.33 Block diagram of modem hardware (Wills 2006)**

### 5. *Power of transmitted and received signals*

As power is limited in underwater nodes, it has to be carefully considered. It has already been discussed that, according to the powers of the transmitted and received signals, three possible cases might arise in practical situations, the ERP, ETP and RTRP. The signal strengths at a receiver affect the estimation performance, as discussed for the ETP case using the proposed technique. But, as only the ERP case is studied using both the protocol and CC techniques, it is considered for comparison.

In the ERP case, the received powers from all nodes have to be equal which is possible using a probing technique. It has been mentioned previously that, as transmitted signals have to overcome the receiver threshold power,  $Q_n$ , with a 20 dB SNR (i.e., 100 times more power than the  $Q_n$ ) and an attenuation of  $d^{-k}$ , the transmitted power has to be  $100 \times Q_n \times d^k$ . This gives a received power of  $100 \times Q_n$  for all nodes if the background noise is neglected. If the background noise (which is tested at Jervis Bay, Australia, at about 25 dB greater than the  $Q_n$ ) is considered with a 20 dB SNR as previously, for the proper signal to be received at the receiver, the transmitted power has to be

$$100 \times 10^{2.5} \times Q_n \times d^k + 100 \times Q_n \times d^k = (10^2 + 10^{4.5}) \times Q_n \times d^k$$

which will give received powers of  $(10^2 + 10^{4.5}) \times Q_n$  for all nodes.

It is important to note that the power considered here is for the SNR, attenuation and threshold power of the receiver. But, as in the protocol techniques the signals are sent to the modem as a bit stream, the modem has transmit electronics (as shown in Figure 5.34) for digital coding, modulation and filtering which require a fixed amount of power (typically in a wattage range (Benson 2010) for an underwater modem). Similarly, receiver electronics also require a fixed but lesser (than transmitter) amount of power for the reverse process of the transmitter (i.e., filtering, decoding and demodulation). In the figure,  $B_n$  is the packet size,  $Q_{te}$  is power dissipated in the transmit electronics,  $Q_{re}$  is power dissipated in the receive electronics,  $E_T$  the total required energy in the transmitter, and  $E_R$  the total required energy in the receiver. Thus, the protocol technique requires a huge amount of extra power over the above considered amount to estimate the number of nodes. In contrast, in the proposed CC technique, as the transmitter and receiver do not require any coding, decoding, modulation, demodulation or filtering power is only required for the SNR, attenuation and threshold power of the receiver.

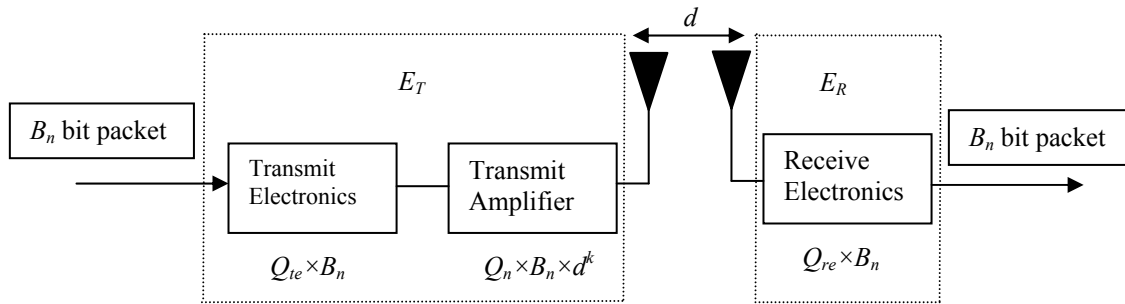


**Figure 5.34 Energy dissipation model in protocol (Heinzelman 2002)**

## 6. Channel bandwidth (BW)

A channel's BW has an effect on a signal's BW. As previously discussed, because the estimation techniques (protocol and CC) require some sort of signal transmission in the physical channel, they might be affected by the channel BW. But this issue is not investigated in the protocol techniques. Although it will be suggested in Chapter 6 (with some simulated results) that the effect of BW ( $>10\text{kHz}$ ) in the proposed technique is negligible, more investigations are required to confirm this decision. However, obtaining the estimation time and energy requires knowledge of the bit rates in the protocol methods and the sampling rate in the proposed method, both of which depend on the channel BW. As this estimation is investigated in underwater

networks, the possible underwater BW of 15 kHz is chosen for the time and energy calculation and comparison. However, as the effect is not considered in the estimation process, other possible BW could be used to obtain the estimation time and energy.

#### **7. *Speed of propagation***

All techniques require acoustic signal propagation in the channel (water). Although there are significant variations (1450 m/s to 1540 m/s) in the propagation speed of an acoustic signal underwater, the techniques do not consider this as all their results are obtained using the typical value of 1500 m/s. Thus, in the comparisons, 1500 m/s is taken as the propagation speed.

#### **8. *Placement of sensor(s)***

All techniques require equal amounts of data from all directions to use the binomial distribution of the placement of balls in the bins (in CC, the balls are the deltas and, in protocol techniques, the number of slots) and, using the same network, their receiver(s) have to be placed in the centre of it. In the protocol techniques, a receiver is a node in receiving mode and, in the CC approach, two hydrophones attached in a node. Although estimations might be different with different receiver placements, this is not investigated. Thus, comparisons are conducted using the receiver(s) at the centre of the network.

#### **9. *Distribution of nodes***

As, in order to achieve the proper placement of balls in the bins, the distribution of the nodes is equally important to the placement of the receiver(s), a uniformly random distribution of nodes is required. Moreover, all estimation techniques use this distribution inside a 3D sphere which is a reasonable distribution for an underwater network. Although the GT protocol is investigated in a 2D terrestrial network, as it is shown in (Howlader 2009) that its performance is similar for 2D and 3D, it is reasonable to extend the 2D GT protocol to the 3D GT protocol. In this case, the MAP will be the same as the receiving node of the PFSA protocol and the

transmitting nodes will surround the MAP with a uniformly random distribution inside a sphere.

#### **10. Capture effect**

In the conventional GT method, which is obtained for a terrestrial sensor network, the capture effect is negligible and no adjustment is provided for the underwater network. However, the severe capture effect underwater may make its direct use difficult or even impossible. Besides, long propagation delays affect the protocol's performance and complicate its design. But, for comparison, it is assumed that similar performances of the GT protocol in a terrestrial network are possible in an underwater network (it can be assumed, as the proposed and conventional PFSA methods are equally suitable for all environments).

The conventional PFSA protocol method uses an estimation parameter which is not affected by the capture effect and the capture effect is not a concern in the proposed CC technique.

#### **11. Number of slots in protocol**

In the protocol technique (Howlader 2009), estimation performance is expressed in terms of the number of slots,  $\eta$ , for different accuracy parameters,  $\beta$ , keeping  $Z$  (percentile of unit normal distribution) fixed at 2.576,  $\phi$  at 0.01, the number of successful slots in a frame,  $\rho_\xi$ , at 1.59 and the number of probes,  $u$ , at 10. Using these values with some manipulation, the CV can be obtained. With the help of the bit rate (discussed next) and the number of minimum bits in a slot, the time can be obtained in a slot and extended for  $\eta$  slots. Thus, the estimation time and CV are obtained in the protocol technique. Detail processes are shown later in this section.

#### **12. Bit rate in protocol**

The bit rate,  $B_R$  is obtained from the used modulation technique and BW. It is known that if the modulation technique used is BPSK, the bit rate in bps is equal to the BW in Hz. Therefore, as the BW used is 15 kHz, the bit rate is 15 kbps.

### **13. *Number of samples in CC technique***

The  $N_s$  is an energy-related term in the CC technique required to obtain the estimation time and CV. Proper selection of this parameter for a particular CV is provided in Section 5.3 and its value is used to obtain the time, CV and energy in the CC technique.

### **14. *Sampling rate in CC technique***

As with the bit rates in the protocol techniques, the sampling rate in the CC technique is required to obtain the estimation time, CV and energy, and also depends on the BW. According to the sampling theorem, the sampling rate will have to be twice as much or more than the BW. Proper selection of this parameter following the sampling theorem is discussed in Section 5.4.

## **5.8.1 Performance comparisons in terms of CV**

In this section, for a particular estimation time, the CV of the proposed technique, which is a performance measure of estimation, is compared with those of the conventional methods (in which estimations are performed using a PFSA protocol and the Good-Turing estimation technique). The constraints of the comparison are: i) the estimation times have to be the same for all cases; ii) the available BW is taken as 15 kHz; iii) there is no impact of noise and the multipath is considered; and iv) other parameters, such as the dimensions of the experimental area and the placements of the nodes and receiver(s), are the same. There are two different parameters: the numbers of slots in the protocol techniques; and the signal lengths in the proposed CC techniques. Based on these, the estimation times are obtained with the help of the bit rates in the protocol techniques and the sampling rate in the proposed technique. As the BW is chosen as 15 kHz and, if the assumed modulation technique used is BPSK, the bit rate in the protocol technique will be equal to the BW, i.e., 15 kbps, and the sampling rate in the proposed technique will have to be either more than or equal to twice it according to the sampling theorem, i.e., greater than or equal to 30 kSa/s. Actually, using the proposed CC technique, an OCV for a particular  $N_s$ , which is assumed to be independent of  $N$ , is chosen for the comparison parameter. Again, it



has already been shown that, in a particular  $N_s$ , the OCV depends on  $b$ , where  $b$  is dependent on the  $S_R$ , and the  $d_{DBS}$ . Thus, by keeping the  $d_{DBS}$  at a fixed value for the chosen OCV, the required estimation time can be obtained with  $N_s$ ,  $S_R$ , and  $u$ . Based on this estimation time, the CVs in the conventional protocols are obtained and compared with that of the proposed technique.

### 5.8.1.1 CV in the proposed technique

As previously discussed, let the OCV (with 100 iteration) is chosen as 0.01, i.e., a 1% statistical error. Thus, its signal length can be obtained using (5.30) which is around 400,000 samples at  $b = 319$ , as shown in Figures 5.35 and 5.36 which illustrate the logarithmic plot of CV versus  $b$  ( $= 99$  to  $439$ ) and the corresponding normal plot which clarifies the optimal points, respectively. In this experiment, as  $d_{DBS}$  is set to 0.25 m (to obtain receivers in the same node), the required  $S_R$  can be obtained from the expression of  $b$  in Section 3.6.2.3, as 960 kSa/s. So, the time required in CC technique (the ERP case) to obtain this CV (0.01) is

$$\begin{aligned}
 T_{CC} &= \left( \frac{1}{\text{Sampling rate}} \text{ second/sample} \right) \times (N_s \text{ sample/iteration}) \\
 &\quad \times \text{Number of iteration} \\
 &= \frac{1}{960000} \times 400000 \times 100 \\
 &= 41.67 \text{ second}
 \end{aligned}$$

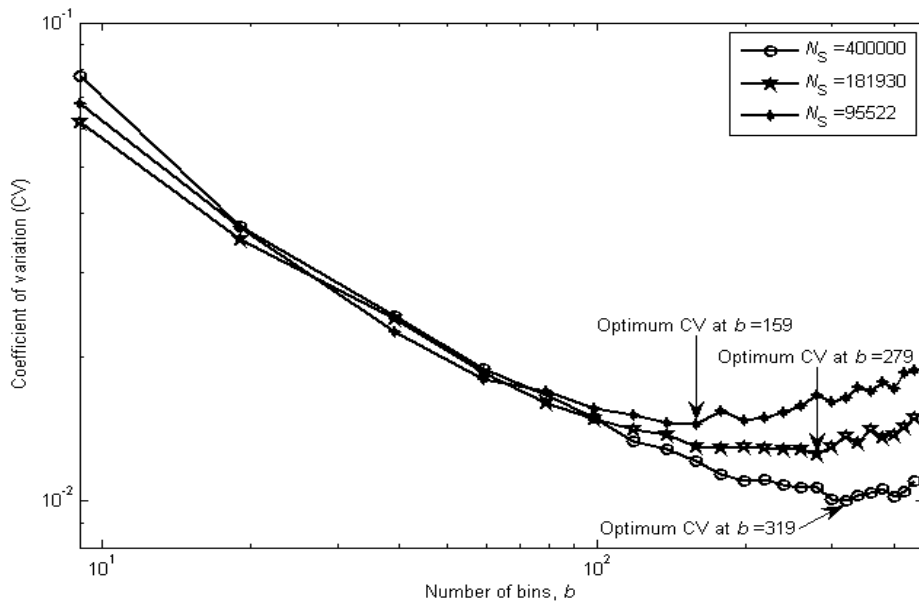
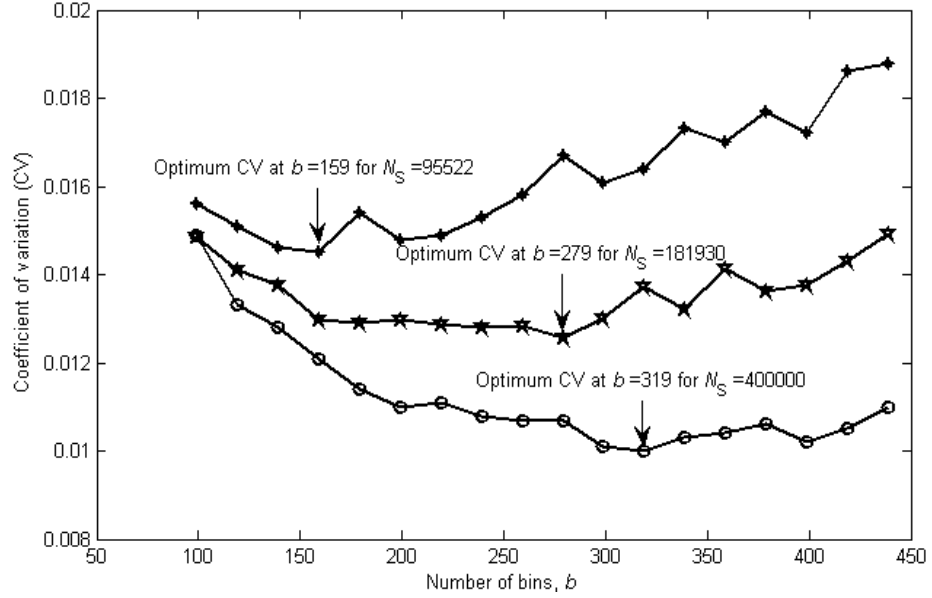


Figure 5.35 CV versus  $b$ : logarithmic plot

This time is then used to obtain the CVs in the conventional protocols, as discussed in the following sections.



**Figure 5.36 CV versus  $b$ : normal plot**

### 5.8.1.2 CV in the conventional PFSA protocol

In the protocol(s) for estimating the number of nodes, estimation performance is investigated using the number of slots needed for certain accuracy. Now, the required time,  $T_{\text{pro}}$  for estimation is calculated for the conventional protocol methods as

$$\begin{aligned}
 T_{\text{pro}} &= (\text{Time per slot}) \times (\text{Number of slots}) \\
 &= (\text{Time per packet}) \times (\text{Number of packets per slot}) \times (\text{Number of slot}) \\
 &= (\text{Time per bit}) \times (\text{Number of bits per packet}) \times \\
 &\quad (\text{Number of packets per slot}) \times (\text{Number of slot}) \\
 &= \left( \frac{1}{\text{Bit rate, } B_R} \text{ second/bit} \right) \times (B_n \text{ bit/packet}) \times (\rho_\xi \text{ packet/slot}) \times (\eta \text{ slot}) \\
 &= \frac{B_n \times \rho_\xi \times \eta}{B_R}
 \end{aligned} \tag{5.36}$$

where  $\rho_\xi$  is the number of packets per slot and its value is taken as 1.59 from (Howlader 2009).

For a wireless communication network, the packet size is the bits or bytes in a MAC (Medium Access Control) frame and depends on the frame format. Tables 5.5 and 5.6 indicate the general and IEEE 802.11 MAC frame formats (IEEE-Standard-Association 2007), respectively, for a wireless communication network.

**Table 5.5 General MAC frame format**

Frame Control	Duration ID	Address1	Address2	Address3	Sequence Control	Address4	QoS Control	Frame Body	FCS
2	2	6	6	6	2	6		0-2312	4

**Table 5.6 IEEE 802.11 MAC packet (frame) format**

Frame Control	Duration ID	Address 1	Address 2	Address 3	Sequence Control	Address 4	Data	Checksum
2	2	6	6	6	2	6	0-2312	4

Each format comprises a set of fields that occur in a fixed order in all frames. The first three (frame control, duration/ID and address1) and the last (frame check sequence (FCS)) constitute the minimal frame format and are present in all frames (IEEE-Standard-Association 2007). So, to create wireless communication in a WCN, we have to transmit at least  $B_n = 14$  bytes = 112 bits per packet (2 bytes for frame control, 2 for duration/ID, 6 for address and 4 for the FCS).

Thus, to obtain an estimation of the CV within 41.67 seconds (to compare the CV with the same estimation time as in the proposed CC technique) from the conventional PFSA technique with  $B_R = 15$  kbps,  $B_n = 112$  bit/packet,  $\rho_\xi = 1.59$  packets/slot, the required number of slots,  $\eta$ , from (5.36) is

$$\eta = \frac{T_{\text{PFSA}} \times B_R}{B_n \times \rho_\xi} \quad (5.37)$$

Inputting the values of the parameters in (5.37) gives

$$\eta \approx 3510$$

In conventional protocol techniques,  $\phi$  and  $\beta$  are considered the performance or accuracy parameters where  $\beta$  is related to  $\eta$ , as (Howlader 2009)

$$\eta = \frac{1.54 \times Z^2}{\beta^2} \quad (5.38)$$

where  $Z$  is the  $Z$ -value of the estimation from the normal distribution (considering the estimated  $N$  follows the normal distribution)  $Z$ -table for the accuracy parameter,  $\phi$ .

Thus, from (5.38),

$$\beta = 0.054$$

as the value of  $Z$  is 2.576 for  $\phi = 0.01$ , i.e., the probability of obtaining the actual number of nodes is greater than or equal to 99%.

For the purpose of comparison, in this proposed work, the accuracy parameter,  $\beta$ , is required to be converted to the CV.

For a particular  $\phi$ , factor  $\beta$  is related to the standard deviation and mean of the estimation as (Howlader 2009)

$$u = \frac{\sigma^2 Z^2}{N^2 \beta^2}, \quad (5.39)$$

where  $u$  is the number of probes required to obtain a certain accuracy in estimation using this  $\beta$ ,  $\sigma$  the standard deviation in this case and  $N$  the number of nodes. To make the performance factor similar to that in the proposed technique,  $\beta$  is converted to the CV as follows.

After some manipulation with denoting  $\sigma$  as  $\sigma_u$  for  $u^{\text{th}}$  iteration, expression (5.39) can be written as

$$\frac{\frac{\sigma_u}{\sqrt{u}}}{N} = \frac{\beta}{Z} \quad (5.40)$$

The left-hand side of the expression is equivalent to the ratio of the standard deviation to the mean of estimation,  $\frac{\sigma(\hat{N})}{\mu(\hat{N})}$ , with  $u^{\text{th}}$  probes. Thus, (5.40) can be rewritten as

$$\frac{\sigma(\hat{N})}{\mu(\hat{N})} = \frac{\frac{\sigma_u}{\sqrt{u}}}{N} = \frac{\beta}{Z} \quad (5.41)$$

This is defined as the CV with  $u$  probes in the proposed technique as

$$\frac{\sigma(\hat{N})}{\mu(\hat{N})} = \text{CV} = \frac{\beta}{Z} \quad (5.42)$$

where  $\hat{N}$  indicates the estimated value of  $N$  considering that  $\mu(\hat{N}) \approx N$ .

Thus, the CV in the PFSA protocol with an equal estimation time to that of the proposed technique can be obtained from (5.42) as

$$\begin{aligned} \text{CV} &= \frac{\beta}{Z} \\ &= 0.0209 \end{aligned}$$

### 5.8.1.3 CV in conventional Good Turing (GT) protocol

In the GT protocol, all the parameters are kept the same as in the PFSA protocol except for the slot size,  $\rho_\xi$ . In this case, the value of  $\rho_\xi$ , is about 4 (Budianu 2006) instead of 1.59 in PFSA.

Thus, to obtain an estimation of the CV within 41.67 seconds (to compare the CV with the same estimation time as in the proposed CC technique) from the

conventional GT technique with  $B_R = 15$  kbps,  $B_n = 112$  bit/packet,  $\rho_\xi = 4$  packets/slot, the required number of slots,  $\eta$ , from (5.36) is

$$\eta_{GT} = \frac{T_{GT} \times B_R}{B_n \times \rho_\xi} \approx 1395$$

Again, in the GT method, the required number of slots is expressed as (Howlader 2009)

$$\eta_{GT} = \sqrt{N} \left( \sqrt{\frac{-2(1+\beta)\ln\left(\frac{\phi}{2}\right)}{\beta - \ln(1+\beta)}} \right) \quad (5.43)$$

where  $\phi$  and  $\beta$  are the performance parameters and  $N$  the number of nodes to be estimated, as discussed for the conventional PFSA protocol.

It is already known that, for a particular  $\phi$ , factor  $\beta$  is related to the standard deviation and mean of estimation from which an expression of the CV has already been obtained as

$$CV = \frac{\beta}{Z} \quad (5.44)$$

where  $Z$  is the Z-value of the estimation from the normal distribution Z-table for a certain accuracy parameter,  $\phi$ .

Now, to solve (5.43) for  $\beta$ ,

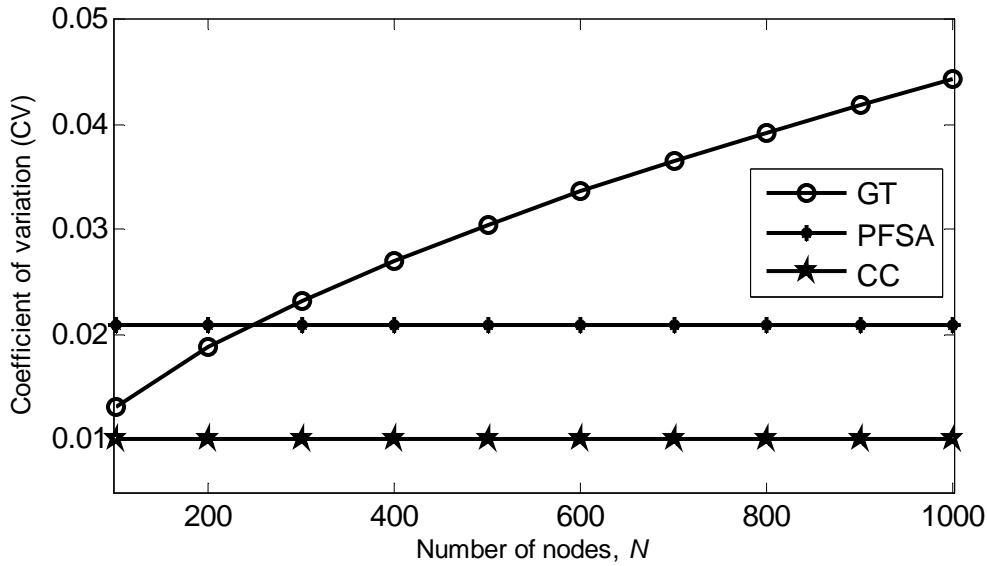
$$\begin{aligned} \left( \frac{\eta_{GT}}{\sqrt{N}} \right)^2 &= \frac{-2(1+\beta)\ln\left(\frac{\phi}{2}\right)}{\beta - \ln(1+\beta)} \\ \Rightarrow \{\beta - \ln(1+\beta)\} \left( \frac{\eta_{GT}}{\sqrt{N}} \right)^2 &= -2(1+\beta)\ln\left(\frac{\phi}{2}\right) \end{aligned} \quad (5.45)$$

Thus, for a particular number of nodes, we can solve (5.45) numerically for  $\beta$ . Table 5.7 shows the values of  $\beta$  for different numbers of nodes for an estimation time of 41.67 seconds.

**Table 5.7 Performance parameter,  $\beta$  in GT method**

$N$	100	200	500	800	1000
$\beta$	0.0339	0.0486	0.0786	0.1012	0.1142

As  $Z$  is known, we can easily obtain the CV from (5.44) for the conventional GT case from these values of  $\beta$ . For a particular estimation time of 41.67 seconds, the CVs of the different estimation techniques are compared in Figure 5.37. It can be seen that, with respect to the number of nodes, they are constant in our proposed and the PFSA technique but increase in the GT technique.

**Figure 5.37 Performance comparison in terms of CV: estimation time = 41.67 s**

Similarly, in the proposed method, if the OCV is chosen as 0.0125, i.e., a 1.25% statistical error, its corresponding  $N_s$  can be obtained using (5.30) which is 181,930 samples at around  $b = 279$ . In this experiment, as  $d_{DBS}$  is set to 0.25 m, the required  $S_R$  is 840 kSa/s. So, the required time to obtain this CV (0.0125) is

$$\begin{aligned}
 T_{CC} &= \left( \frac{1}{\text{Sampling rate}} \text{ second/sample} \right) \times (N_s \text{ sample/iteration}) \\
 &\quad \times \text{Number of iteration} \\
 &= \frac{1}{840000} \times 181930 \times 100 \\
 &= 21.67 \text{ second}
 \end{aligned}$$

Using this required estimation time, the CVs are obtained from the PFSA technique as 0.029 and the GT technique as in Table 5.8.

**Table 5.8 Performance parameters, CV in GT method:  $T=21.67$  second**

$N$	100	200	500	800	1000
CV	0.026	0.038	0.0624	0.0818	0.0933

Similarly, as in the CC techniques for another operating point with  $OCV = 0.015$ , a signal length of 95,522 samples and a sampling rate of 600 kSa/s (as the required  $b = 199$ ), the required estimation time is 15.92 seconds with which the CVs in the PFSA and GT techniques are obtained. The CV in the PFSA protocol is constant at around 0.0339 and those for different numbers of nodes in the GT technique (as its CV depends on  $N$ ) are provided in Table 5.9.

**Table 5.9 Performance parameters, CV in GT method:  $T=15.92$  second**

$N$	100	200	500	800	1000
CV	0.0361	0.0528	0.0892	0.1187	0.1367

Comparisons of these CVs for the two abovementioned operating points are provided in Figures 5.38 and 5.39.

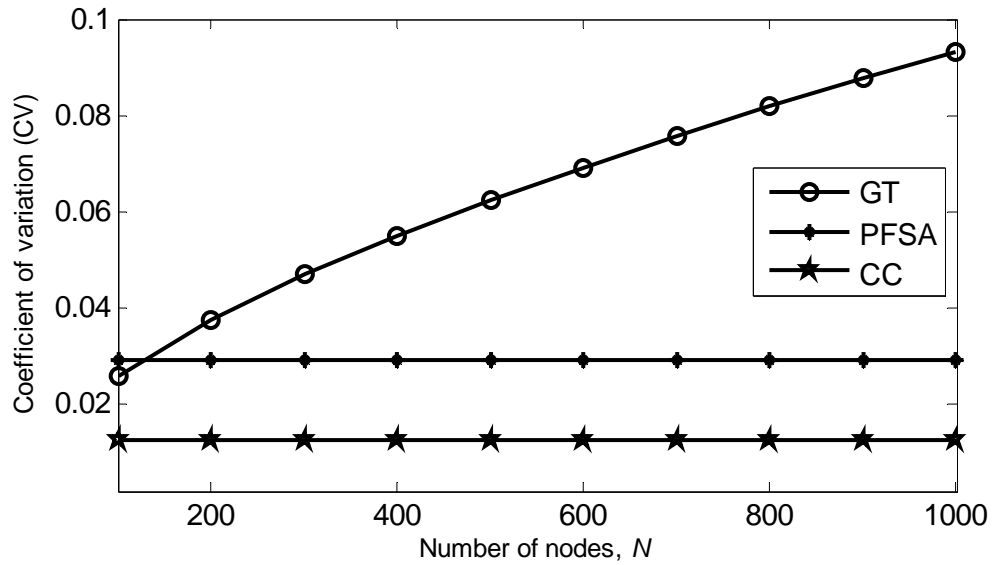


**Figure 5.38 Performance comparison in terms of CV: estimation time = 21.67 s**



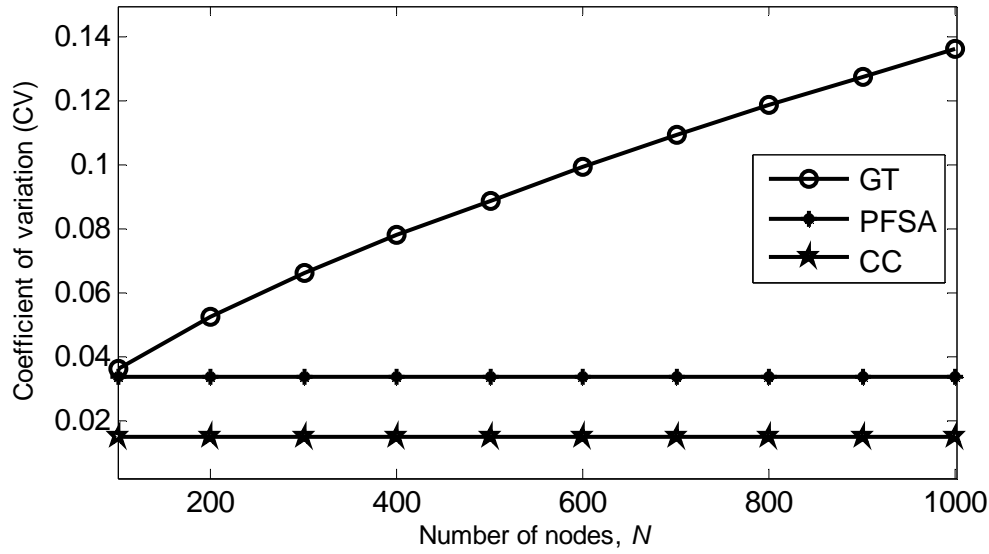


**Figure 5.39 Performance comparison in terms of CV: estimation time = 15.92 s**

It can be seen in Figures 5.37, 5.38 and 5.39 that the CVs with the same required time for estimations of the number of nodes are constant in the proposed CC and conventional PFSA technique but vary with the number of nodes in the GT technique. The proposed technique always performs better than the conventional techniques.

### 5.8.2 Performance comparisons in terms of required estimation time

In this section, the required estimation times of the proposed and conventional methods are compared. The constraints of this comparison are: i) errors in estimation, i.e., the CVs have to be the same for all methods; ii) the available BW is taken as 15 kHz; iii) there is no impact of noise and the multipath is considered; and iv) other parameters, such as the dimensions of the experimental area and placements of the transmitting and receiving node(s), etc., are the same. There are two different parameters: the  $\eta$  in the protocol techniques; and the  $N_s$  in the number of samples in the proposed CC technique. Based on these two parameters, the estimation times are obtained with the help of the  $B_R$  in the protocol techniques and the  $S_R$  in the proposed technique. Actually, using the proposed CC technique, an OCV for a particular  $N_s$ , which is independent of  $N$ , is chosen as the comparison parameter. It has already been shown that, for a particular  $N_s$ , the OCV depends on  $b$ , where  $b$  is dependent on the  $S_R$ , and the  $d_{DBS}$ . Thus, keeping  $d_{DBS}$  at a fixed value for an OCV, the required

estimation time can be obtained. For the same CV as in the proposed technique, the estimation times in the conventional protocols are obtained and compared with that of the proposed technique.

### 5.8.2.1 Estimation time in CC technique

To obtain the estimation time in the proposed technique after one iteration, as the OCV is taken as 0.1, i.e., a 10% statistical error, its corresponding  $N_s$  can be obtained using (5.31) which is about 400,000 samples at around  $b = 319$  (similar as for CV=0.01 with 100 iteration; as we are using only 1 iteration instead of 100, thus keeping the other parameters same, the CV increases to 0.1). In this experiment, as the  $d_{DBS}$  is set to 0.25 m (to have the sensors in the same node), the required  $S_R$  can be obtained from the expression of  $b$  in Section 3.6.2.3 which is 960 kSa/s. So, the required estimation time to obtain this CV (0.1) is

Thus, the estimation time in the CC method,

$$\begin{aligned} T_{CC} &= \left( \frac{1}{\text{Sampling rate}} \text{ second/sample} \right) \times (N_s \text{ sample/iteration}) \\ &\quad \times \text{Number of iteration} \\ &= \frac{1}{960000} \times 400000 \times 1 \\ &\approx 0.4167 \text{ second} \end{aligned}$$

Since the CV is independent of  $N$ , the estimation time obtained above will hold for all  $N$ .

### 5.8.2.2 Estimation time in PFSA protocol

To compare the conventional PFSA protocol technique with the proposed approach, the estimation time is obtained for the same CV (0.1) for different  $N$ .

Now, from expressions (5.38) and (5.42),

$$\eta_{PFSA} = \frac{1.54}{CV^2} = 154$$

Thus, by keeping the parameters the same as previously, i.e.,  $B_R = 15\text{kbps}$ ,  $B_n = 112$  bits/packet and  $\rho_\xi = 1.59$  packets/slot, the required estimation time,  $T_{\text{PFSA}}$ , can be obtained from the following expression (which is derived from (5.37)).

$$T_{\text{PFSA}} = \frac{\eta_{\text{PFSA}} \times B_n \times \rho_\xi}{B_R},$$

$$\approx 1.8283\text{second}$$

Since the CV is again independent of  $N$  in PFSA technique, the estimation time obtained above will hold for all  $N$ .

### 5.8.2.3 Estimation time in GT protocol

To compare the estimation times of the GT protocol technique and proposed approach, they are obtained for the same CV (0.1) for different  $N$ .

Now, from expression (5.42),

$$\beta = Z \times \text{CV} = 0.2756$$

As the performance parameter ( $\phi = 0.01$ ) is known and using the above  $\beta$  for different  $N$ ,  $\eta_{\text{GT}}$  can be obtained from (5.43). The obtained  $\eta_{\text{GT}}$  for different  $N$  are presented in Table 5.10.

**Table 5.10  $\eta_{\text{GT}}$  in GT method: CV = 0.1**

$N$	100	200	500	800	1000
$\eta_{\text{GT}}$	217	307	486	614	687

Keeping the other parameters the same as previously, i.e.,  $B_R = 15\text{kbps}$ ,  $B_n = 112$  bits/packet and  $\rho_\xi = 4$  packets/slot, the required estimation time,  $T_{\text{GT}}$ , can be easily obtained from the following expression.

$$T_{\text{GT}} = \frac{\eta_{\text{GT}} \times B_n \times \rho_\xi}{B_R}$$

Figure 5.40 shows the comparison of estimation times required to obtain similar performances.

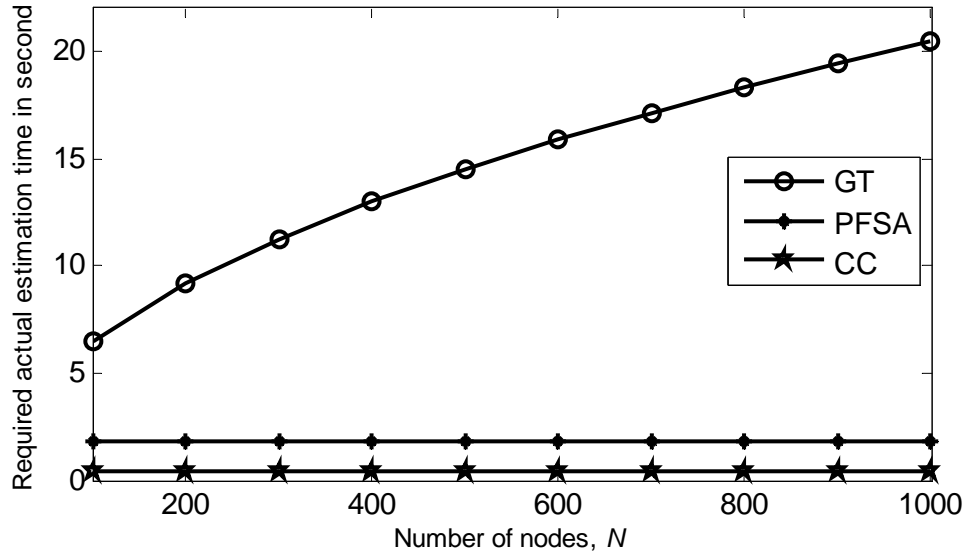


**Figure 5.40 Performance comparison in terms of estimation time required to obtain CV = 0.1**

Similarly, if the OCV is taken as 0.125, i.e., a 12.5% statistical error, its corresponding signal length is about 181,930 samples at around  $b = 279$ . In this experiment, as the  $d_{\text{DBS}}$  is set to 0.25 m, the required sampling rate is 840 kSa/s. So, the required time to obtain this CV (0.125) is

$$\begin{aligned}
 T_{\text{CC}} &= \left( \frac{1}{\text{Sampling rate}} \text{ second/sample} \right) \times (N_s \text{ sample/iteration}) \\
 &\quad \times \text{Number of iteration} \\
 &= \frac{1}{840000} \times 181930 \times 1 \\
 &= 0.2167 \text{ second}
 \end{aligned}$$

The obtained estimation times for the same CV are 1.17 seconds in the PFSA technique and as shown in Table 5.11 in the GT technique.

**Table 5.11  $T_{\text{GT}}$  in GT method: CV = 0.125**

$N$	100	200	500	800	1000
$T_{\text{GT}}(\text{s})$	5.4	7.6368	12.0748	15.2735	17.0763

Similarly, for another operating point with  $OCV = 0.15$  in the proposed method, the signal length is about 95,522 samples and the sampling rate 600 kSa/s (as the required  $b = 199$ ). So, the required estimation time is 0.1592 s. With the same CV, the required estimation times in the PFSA and GT techniques are obtained.

The estimation times in the PFSA protocol are constant at around 0.8126 second for different  $N$  but variable in the GT protocol (in which the CV depends on  $N$ ), as shown in Table 5.12.

**Table 5.12  $T_{GT}$  in GT method: CV = 0.15**

$N$	100	200	500	800	1000
$T_{GT}(s)$	4.6856	6.6264	10.4773	13.2529	14.8172

Comparisons of these estimation times for the two abovementioned operating points are also provided in Figures 5.41 and 5.42.

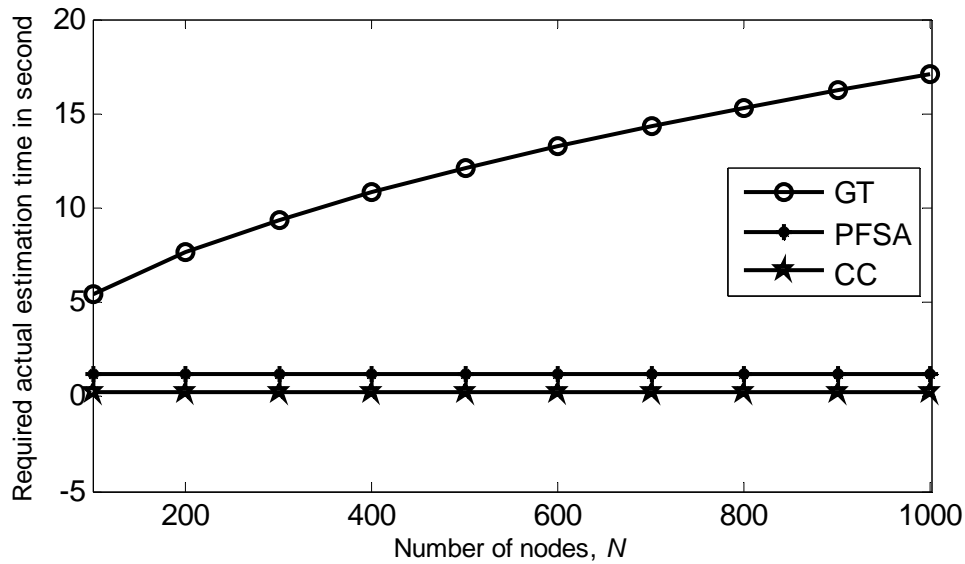


**Figure 5.41 Performance comparison in terms of estimation time required to obtain CV = 0.125**

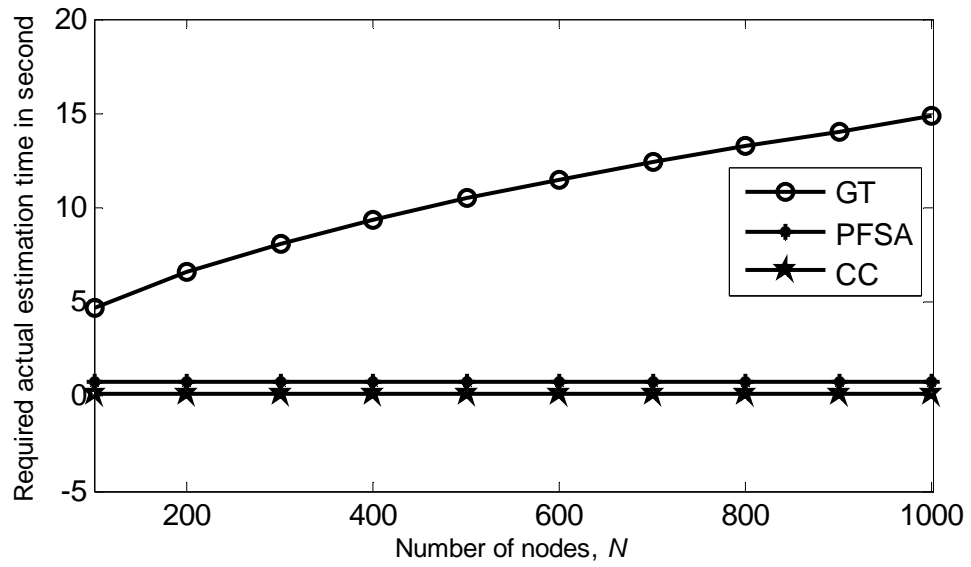


**Figure 5.42 Performance comparison in terms of estimation time required to obtain  $CV = 0.15$**

It can be seen in Figures 5.40, 5.41 and 5.42 that, like the CV comparisons, the required time for estimations of the number of nodes is constant in the proposed and PFSA techniques whereas it varies with the number of nodes in the GT technique. In terms of the required estimation time for a particular CV, the proposed cross-correlation technique always performs better than the PFSA and GT techniques.

### 5.8.3 Performance comparisons in terms of required transmit energy

All the above comparisons do not take into account the transmit energy required for estimation. In this section, the transmit energies required for a certain CV are compared, as are the virtual times (not the actual times) needed when assuming the same power, for all methods.

The constraints of the comparison are: i) the same CV in estimation,  $CV (=0.1)$ , has to be obtained in all cases to compare the energy and assuming the same power for all methods to compare virtual times; ii) the available BW is taken as 15 kHz; iii) the same impact of noise is assumed in all cases, iv) no multipath is considered; and v) other parameters, such as the dimensions of the experimental area and the placements of the transmitting and receiving node(s), are the same.

### 5.8.3.1 Transmit energy required in proposed CC technique

In our simulations, from the  $n^{\text{th}}$  node, a sensor receives an array of samples of a continuous time signal (Gaussian). The numeric values (which follow the zero mean unity standard deviation Gaussian distribution) of the samples are normalised (in terms of original received signal) with units of volts and referenced to a normalised (in terms of receiver equivalent) resistance of 1 ohm. The sampling frequency,  $S_{R_n}$ , is 960,000 Sa/s (although other frequencies might also be used, we use this one for a certain  $d_{\text{DBS}}$  to obtain the optimal  $b$ , in order to obtain a certain CV of estimation).

Suppose the sampled transmitted signal is  $x(s)$ , where  $s$  is the index of the sample number. The instantaneous power of a sample in watts will be the value of that sample squared and the average power of the signal will be the average of the instantaneous power of every sample in the signal. If we use the signal of  $N_{S_n}$  samples, the average power will be

$$Q_{\text{avg}} = \frac{1}{N_{S_n}} \sum_{s=1}^{N_{S_n}} x^2(s) = E(x^2(s))$$

Again, the variance in the sampled signal can be defined as

$$\sigma^2(x(s)) = E(x^2(s)) - (E(x(s)))^2$$

As we use zero mean unity variance samples, the variance will be

$$\sigma^2(x(s)) = E(x^2(s)) = 1$$

Thus, the normalised average received power will be

$$Q_{\text{avg}} = \frac{1}{N_{S_n}} \sum_{s=1}^{N_{S_n}} x^2(s) = E(x^2(s)) = \sigma^2(x(s)) = 1 \text{ watt}$$

Now, the energy of a signal is the time integral of its average power and the integration is converted to a summation for the sampled signal.

If the time per sample is denoted by  $T_{S_n} \left( = \frac{1}{S_{R_n}} \right)$ , the total normalised received energy for the  $n^{\text{th}}$  node in joules will be

$$\begin{aligned}
 E_{rn} &= \sum_{n=1}^{N_s} (Q_{avg} \times T_{S_n}) \\
 &= Q_{avg} \sum_{n=1}^{N_s} T_{S_n} \\
 &= Q_{avg} \times \frac{1}{S_{R_n}} \times N_{S_n} \\
 &= \frac{N_{S_n}}{S_{R_n}} \text{ joule}
 \end{aligned}$$

If the original received power is the  $Q_{R_n}$  watt, the total received energy required for the  $n^{\text{th}}$  node is

$$E_{trn} = Q_{R_n} \times \frac{N_{S_n}}{S_{R_n}} \text{ joule}$$

Multiplying this by the appropriate path loss factor,  $d_n^k$  (where  $d_n$  is the distance between the receiver and the  $n^{\text{th}}$  node and  $k$  the spreading factor), the required transmitted energies for the nodes are

$$\begin{aligned}
 E_{t1} &= d_1^k \times Q_{R_1} \times \frac{N_{S_1}}{S_{R_1}} \\
 E_{t2} &= d_2^k \times Q_{R_2} \times \frac{N_{S_2}}{S_{R_2}} \\
 &\vdots \\
 E_{tN} &= d_N^k \times Q_{R_N} \times \frac{N_{S_N}}{S_{R_N}}
 \end{aligned}$$

Thus, the total transmitted energy for  $N$  nodes is

$$E_t = E_{t1} + E_{t2} + \dots + E_{tN} = d_1^k \times Q_{R_1} \times \frac{N_{S_1}}{S_{R_1}} + d_2^k \times Q_{R_2} \times \frac{N_{S_2}}{S_{R_2}} + \dots + d_N^k \times Q_{R_N} \times \frac{N_{S_N}}{S_{R_N}}$$



As the received powers, number of samples and sampling frequencies for all nodes are considered equal in the estimation process and, thus, assuming

$$Q_{R_1} = Q_{R_2} = \dots = Q_{R_N} = Q_R, N_{S_1} = N_{S_2} = \dots = N_{S_N} = N_S, \text{ and } S_{R_1} = S_{R_2} = \dots = S_{R_N} = S_R,$$

we have the total transmitted energy as

$$E_t = \left( \sum_{n=1}^N d_n^k \right) \times Q_R \times \frac{N_S}{S_R} \text{ Joule} \quad (5.46)$$

Using this expression, we then obtain the energy in two cases, as discussed below.

**(a) Channel without noise but receiver with internal noise**

It has been shown in the estimation process that, if we consider the internal noise of the receiver to obtain similar performances to those of estimation without noise, the SNR has to be at around 1 (in voltage ratio), as also depicted in Figure 5.43 and 5.44 for a signal length of 100,000 samples. Again, it is estimated in our lab (Underwater Lab, UNSW@ADFA, Australia. See Appendix A for the details) that the voltage level of the internal noise of a receiver (hydrophone) is about  $3.16 \text{ nV}/\sqrt{\text{BW in Hz}}$  and the equivalent resistance of a typical hydrophone is  $z=1\text{kohm}$ .

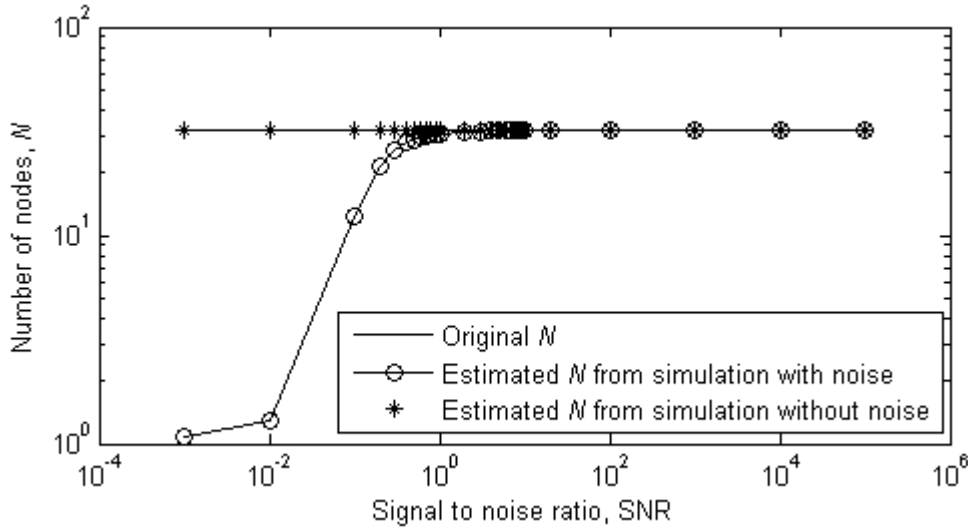


**Figure 5.43 Number of nodes,  $N$ , versus SNR**

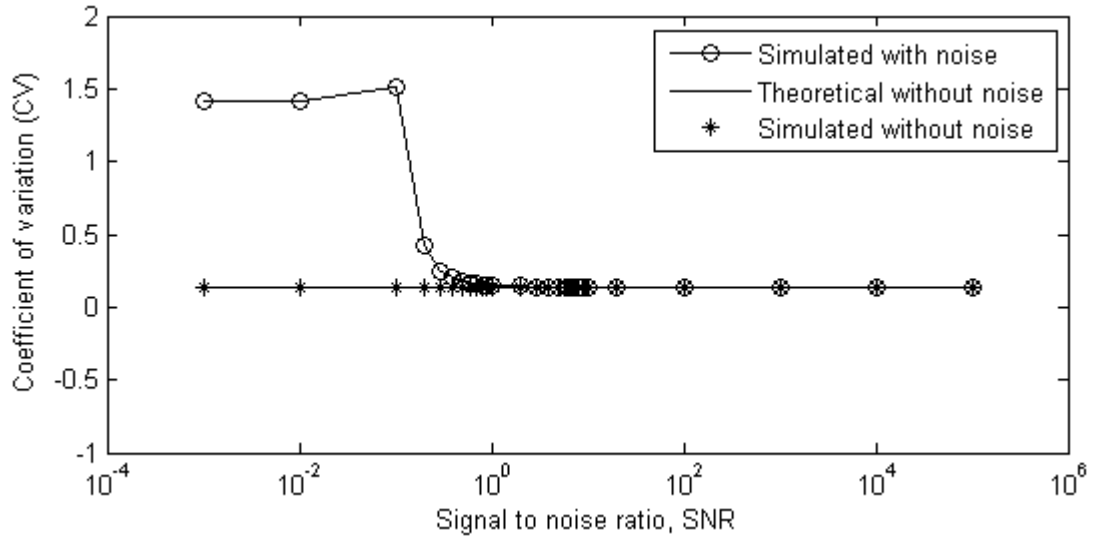


**Figure 5.44 Coefficient of variation, CV, versus SNR**

Therefore, the hydrophone can receive a signal voltage of at least  $3.16 \times 10^{-9} \times \sqrt{15000} = 3.87 \times 10^{-7}$  volts (as the chosen BW is 15 kHz). Thus the internal noise power of the receiver (which is the receiver threshold power) is

$$Q_n = \frac{(3.16 \times 10^{-9})^2}{1000} \approx 1.5 \times 10^{-16} \text{ W.}$$

So, to confirm the reception and perfect matching of the without noise case with 10 times more received voltage, the average received power per node will have to be

$$Q_{R_n} = 10^2 \times Q_n = 1.5 \times 10^{-14} \text{ W}$$

This can also be calculated as follows. The internal noise power in a receiver is

$$Q_n = c_B \theta B = 1.38 \times 10^{-23} \times 725 \times 15000 = 1.5 \times 10^{-16} \text{ W}$$

where,

$$c_B = \text{Boltzman constant} = 1.38 \times 10^{-23} \text{ Watt/K - kHz}$$

$\theta$  = Noise temperature in Kelvin = 725 K (It is obtained for the receiver used here as shown in Appendix A)

B = Bandwidth = 15 kHz

So, to confirm the reception and perfect matching of the without noise case with 100 times more received power, the average received power per node will have to be  $Q_{R_n} = 100 \times Q_n \approx 1.5 \times 10^{-14}$  W.

For a particular case in which the CV is 0.1, as the OCV expression for 1 iteration  $\left(OCV = 3.85 \times N_s^{-0.283}\right)$  gives the signal length of  $N_s \approx 400000$  samples, the total transmitted energy required for a  $N$  nodes estimation is

$$E_t = \left( \sum_{n=1}^N d_n^k \right) \times 1.5 \times \frac{400000}{960000} \times 10^{-14} \text{ joule} \quad (5.47)$$

#### (b) Channel with background and receiver with internal noise

If we consider both the receiver and channel with noise, the procedure is similar to (a) above but the transmitted signal needs extra energy to overcome the background noise of the channel in a similar manner to that of only the receiver with internal noise.

Again, as it is shown in testing at Jervis Bay, Australia (See Appendix A for the details), that the background noise level underwater is around 25 dB greater than the internal noise of the receiver used above, another noise to be overcome is  $10^{2.5} \times 1.5 \times 10^{-16} = 1.5 \times 10^{-13.5}$  W; this is properly achieved by again using 100 times more power. Thus, the average received power per node in presence of background noise is

$$Q_{R_n} = 1.5 \times 10^{-14} + 1.5 \times 10^{-11.5} = 1.5 \times (10^{-14} + 10^{-11.5}) \text{ W}$$

For the earlier case in which the CV is 0.1 with  $N_s \approx 400000$  samples, the total energy required for  $N$  nodes estimation is

$$E_t = \left( \sum_{n=1}^N d_n^k \right) \times 1.5 \times (10^{-14} + 10^{-11.5}) \times \frac{400000}{960000} \text{ joule} \quad (5.48)$$

### 5.8.3.2 Distance estimation in CC technique

Estimations of distances are similar in all CC techniques and the number of distances is equal to the number of nodes, where the nodes are uniformly placed inside a 3D sphere. Thus, if we want to estimate  $N$  nodes, the number of distances will be  $N$  which is obtained using the formula for the distance between two points ,

$$d_n = \sqrt{(x_n - x_o)^2 + (y_n - y_o)^2 + (z_n - z_o)^2}$$

where  $d_n$  is the distance between the sensor and the  $n^{\text{th}}$  node which are in positions  $(x_o, y_o, z_o)$  and  $(x_n, y_n, z_n)$ , respectively.

### 5.8.3.3 Transmit energy required in PFSA protocol approach

It is known from (Howlader 2009) that, in the PFSA protocol technique, to obtain a certain accuracy in an estimation requires a certain number of packets. It is also known that each node transmits one packet in a probe (Howlader 2009). In this technique, the required energy for a node to transmit the  $w^{\text{th}}$  packet to a distance,  $d_w$ , is defined from (Howlader 2011; Bhardwaj 2002) as

$$E_{tpw} = E_{pp} \times d_w^k \quad (5.49)$$

The parameter  $E_{pp}$  is the energy/packet which depends on the required receiver sensitivity, i.e., the receiver's internal noise floor energy for which the transmit power needs to be adjusted so that the power at the receiver is equal to, or above, the sensitive threshold power of the receiver. As previously discussed the receiver threshold power can be considered same in both in the protocol and CC techniques and, thus, considering same threshold power,  $Q_n$  in PFSA protocol, the average received power per node will be same as CC technique, which is

$$Q_{R_n} = 1.5 \times 10^{-14} \text{ W}$$

Now, choosing unity gain omnidirectional receiver and the bit rate,  $B_r = 15000$  bps (as previously discussed the use of BPSK modulation with 15000 Hz BW allow the

bit rate of 15000 bps), the received energy per bit,  $E_{pb}$  is obtained as (Heinzelman 2000)

$$E_{pb} = \frac{Q_{R_n}}{B_R} = \frac{1.5 \times 10^{-14}}{15000} \approx 10^{-18} \text{ Joule/bit}$$

As it has already been shown that the minimum packet size in protocol is 112 bits and, thus, assuming this packet size in protocol technique of estimation of the number of nodes, the received energy per packet is

$$E_{pp} \approx 112 \times 10^{-18} \text{ J/packet} = 1.12 \times 10^{-16} \text{ J/packet}$$

Now, the transmitted energies required for the 1<sup>st</sup>, 2<sup>nd</sup>, ...,  $N_p$ <sup>th</sup> packet to transmit to distances  $d_1, d_2, \dots, d_{N_p}$  respectively are

$$\begin{aligned} E_{tp1} &= E_{pp} \times d_1^k \\ E_{tp2} &= E_{pp} \times d_2^k \\ &\vdots \\ E_{tpN_p} &= E_{pp} \times d_{N_p}^k \end{aligned}$$

So, the total transmitted energy in PFSA technique will be

$$E_{tPFSA} = E_{tp1} + E_{tp2} + \dots + E_{tpN_p} = E_{pp} \times d_1^k + E_{pp} \times d_2^k + \dots + E_{pp} \times d_{N_p}^k$$

Finally, we have the total transmitted energy as

$$E_{tPFSA} = \left( \sum_{w=1}^{N_p} d_w^k \right) \times E_{pp} = \left( \sum_{w=1}^{N_p} d_w^k \right) \times 1.12 \times 10^{-16} \text{ Joule} \quad (5.50)$$

where  $N_p$  is calculated as the number of slots multiplied by the number of successful packets per slot.

The number of slots in the PFSA protocol is (Howlader 2009)

$$\eta_{\text{PFSA}} = \frac{\left\{ e^{\rho_\xi} - \left( 1 + \frac{F\rho_\xi^2}{N} \right) \right\} Z^2}{\beta^2 \rho_\xi^2}; \text{ where, } \frac{F\rho_\xi}{N} = \text{Probability, } M,$$

the value of which will be between 0 and 1

and the number of successful packets per slot is  $\rho_\xi \approx 1.59$  (Howlader 2009).

Thus, the final expression of the total number of packets is

$$N_p = \rho_\xi \eta_{\text{PFSA}} = \frac{\left\{ e^{\rho_\xi} - \left( 1 + \frac{F\rho_\xi^2}{N} \right) \right\} Z^2}{\beta^2 \rho_\xi}$$

For the case in which CV=0.1, the performance factor,  $\beta$  (the product of the CV and the normal percentile, Z, which is chosen to be 2.576 with the  $\phi$  constant at 0.01), is 0.2576.

So, the total number of packets (for  $F=100$  (used in (Howlader 2009))) is

$$N_p = 245.5188 - \frac{15900}{N}; \text{ where } N \geq 159 \quad (5.51)$$

Thus, for lower numbers of nodes (less than 159),  $N_p$  will be fixed at the value with  $N=159$ .

### 5.8.3.4 Transmit energy required in GT protocol approach

It is known from (Howlader 2009) that, in the GT protocol technique, to obtain estimations with a certain accuracy requires a certain number of packets. It is also known that each node transmits one packet in a probe (Venkitasubramaniam 2004; Budianu 2006). In this technique, again the energy required for a node to transmit the  $w^{\text{th}}$  packet to a distance,  $d_w$ , is defined from (Howlader 2011; Bhardwaj 2002) as

$$E_{\text{tpw}} = E_{pp} \times d_w^k$$

where  $E_{pp}$  is the energy per packet, the value of which is the same as in the PFSA protocol, i.e.,  $E_{pp} = 1.12 \times 10^{-16}$  J/packet.

Thus, the transmitted energies required for the 1<sup>st</sup>, 2<sup>nd</sup>, ...,  $N_p$ <sup>th</sup> packet to transmit to distances  $d_1, d_2, \dots, d_{N_p}$  respectively are

$$\begin{aligned} E_{tp1} &= E_{pp} \times d_1^k \\ E_{tp2} &= E_{pp} \times d_2^k \\ &\vdots \\ E_{tpN_p} &= E_{pp} \times d_{N_p}^k \end{aligned}$$

So, the total energy will be

$$E_{tGT} = E_{tp1} + E_{tp2} + \dots + E_{tpN_p} = E_{pp} \times d_1^k + E_{pp} \times d_2^k + \dots + E_{pp} \times d_{N_p}^k$$

Finally, we have the total transmitted energy as

$$E_{tGT} = \left( \sum_{w=1}^{N_p} d_w^k \right) \times E_{pp} = \left( \sum_{w=1}^{N_p} d_w^k \right) \times 1.12 \times 10^{-16} \text{ Joule} \quad (5.52)$$

where  $N_p$  is calculated from the number of slots multiplied by the number of successful packets per slot.

The number of slots in the GT protocol is (Howlader 2009)

$$\eta_{GT} = \sqrt{N} \left( \sqrt{\frac{-2(1+\beta) \ln\left(\frac{\phi}{2}\right)}{\beta - \ln(1+\beta)}} \right)$$

and the number of successful packets per slot is about 4 (Venkitasubramaniam 2004).

Thus, the final expression for the total number of packets is

$$N_p = \sqrt{16N} \left( \sqrt{\frac{-2(1+\beta) \ln\left(\frac{\phi}{2}\right)}{\beta - \ln(1+\beta)}} \right)$$

For the case in which CV=0.1 same as CC and PFSA techniques), the performance factor,  $\beta$  (the product of the CV and the normal percentile Z which is chosen to be 2.576 with the  $\phi$  constant at 0.01), is 0.2576.

Therefore, the total number of packets is

$$N_p = \sqrt{16N} \left( \sqrt{\frac{-2(1+0.2576)\ln\left(\frac{0.01}{2}\right)}{0.2576-\ln(1+0.2576)}} \right) = 86.7\sqrt{N} \quad (5.53)$$

### 5.8.3.5 Distance estimation in protocol technique

In the protocol techniques, the number of distances indicates the number of packets. If, for a  $N$  node estimation with  $u$  probes  $N_{pu}$  packets are needed, the number of packets per probe is  $N_{pu}/u$  and, in each probe, a node can transmit only one packet, i.e., the number of transmitting nodes per probe is  $N_{pu}/u$ . Thus, for all probes, the number of transmitting nodes is  $N_{pu}/u$  and their placements are uniformly random. So, we can consider that, whatever the number of nodes to be estimated, we need  $N_{pu}$  nodes uniformly randomly distributed inside the estimation area.

Thus, if we want to estimate  $N$  nodes, the number of distances will be  $N_{pu}$  which are obtained using the formula for the distance between two points,

$$d_w = \sqrt{(x_w - x_o)^2 + (y_w - y_o)^2 + (z_w - z_o)^2}$$

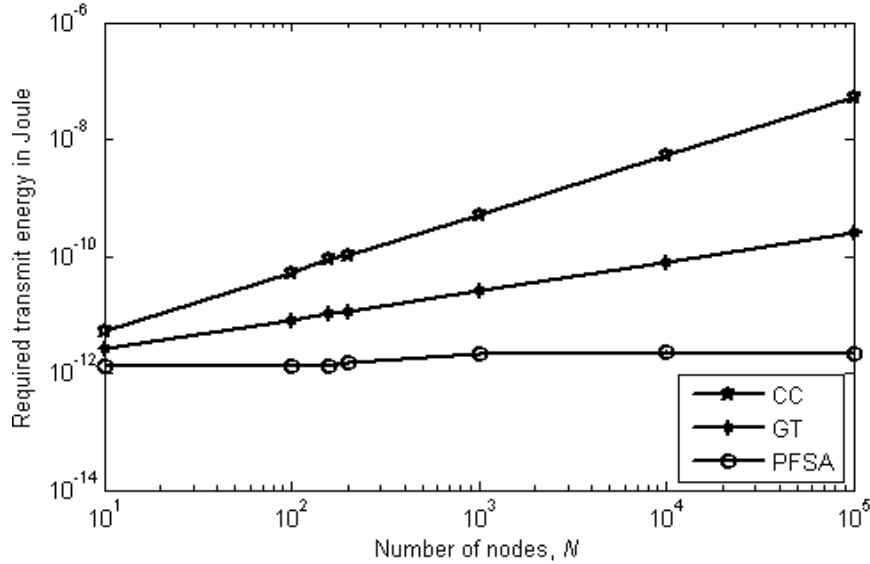
where  $d_w$  is the distance between the receiver and the  $w^{\text{th}}$  node which are in positions  $(x_o, y_o, z_o)$  and  $(x_w, y_w, z_w)$ , respectively.

### 5.8.3.6 Comparison of required transmit energies in estimation techniques

The required transmit energies are obtained from (5.47), (5.50), and (5.52) with the distribution of nodes in a 50 m diameter 3D sphere. Results from comparisons of the proposed CC, conventional PFSA, and conventional GT techniques are shown in Figures 5.45 to 5.48. Figure 5.45 shows the transmit energy required (in joules) considering only the internal noise of the receiver. This transmit energy is the energy required to overcome the receiver's threshold power using an appropriate SNR and



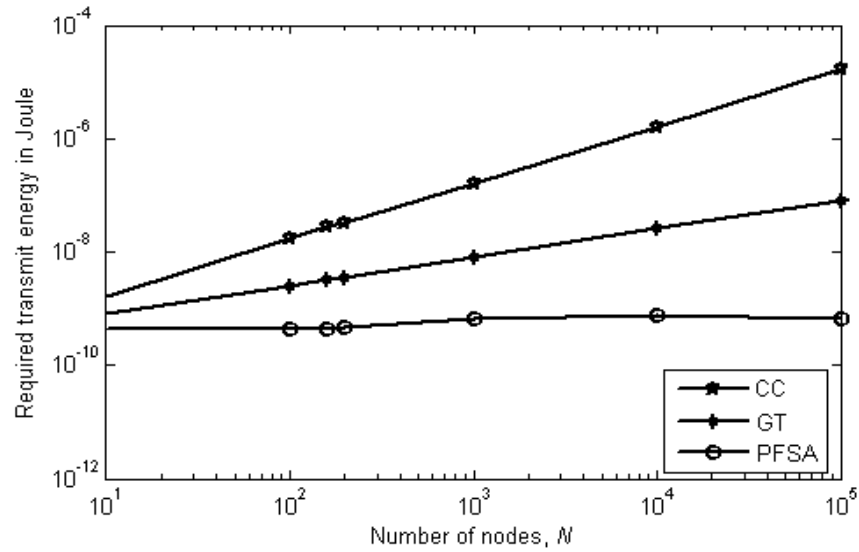
attenuation in the channel. However, as previously discussed, the required large amounts of fixed energy in the protocol techniques for the transmitter and receiver are not considered. The top line indicates the cross-correlation (CC) method, the middle the Good Turing (GT) approach and the bottom the probabilistic framed slotted ALOHA (PFSA) technique.



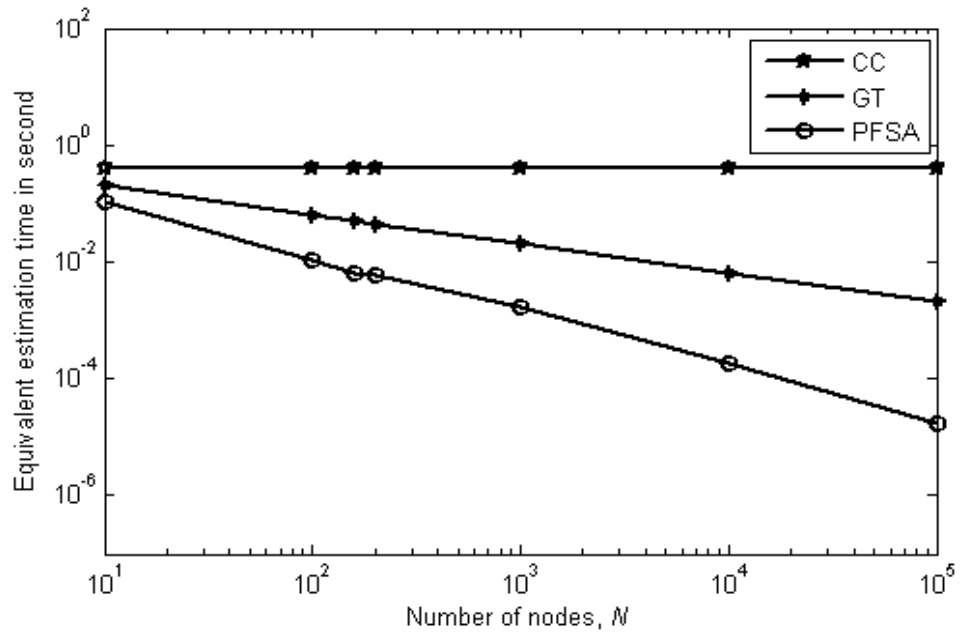
**Figure 5.45 Comparison of required energies with only internal receiver noise**

Figure 5.46 shows the results from the comparison of the required transmit energies in joules considering both the internal noise of the receiver and the background noise of the channel. The top line indicates the CC method, the middle the GT approach and the bottom the PFSA technique. Again, only the energy required to overcome the attenuation, the receiver threshold and the channel background noise using an appropriate SNR, with no fixed power (which is required for the protocol techniques) are considered.

Figure 5.47 shows the results from the comparison of the virtual transmit times for the same power used in the CC method when applied to the conventional methods. The top line indicates the CC method, the middle the GT approach and the bottom the PFSA technique. These are not the actual estimation times but provide suggestions as to what they would be if the same power was applied for estimations in all techniques.



**Figure 5.46 Comparison of required energies with both background and internal receiver noises**



**Figure 5.47 Comparison of equivalent times considering same power used in all techniques**

The actual estimation times were compared in Section 5.8.2. Figure 5.48 shows the results from one such comparison with the power being different for each method. The top line indicates the GT method, the middle the PFSA approach and the bottom line the CC technique.

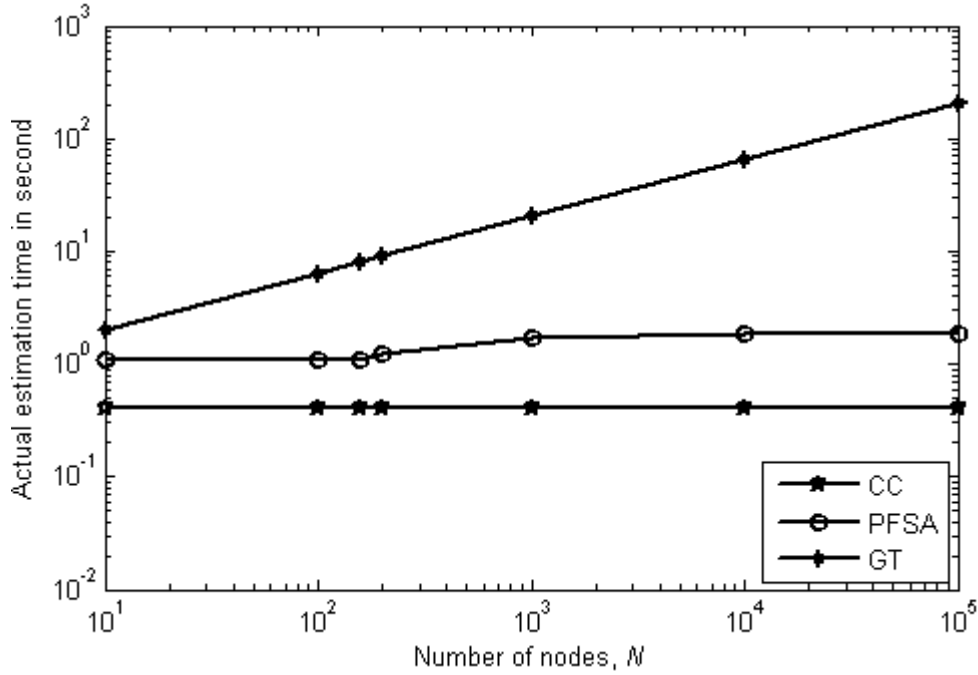


**Figure 5.48 Comparison of actual times required with different actual powers**

### 5.8.3.7 Conclusion

It can be seen from the above comparisons that the actual estimation time required is improved significantly in the proposed technique. This will be very helpful for arriving at quick decisions about the number of nodes needed for proper network operation and maintenance. However, the required transmit energy is higher in the proposed technique because all nodes transmit for the entire estimation time whereas, in the protocol methods, fractions of nodes transmit for fractions of the whole estimation times. It can be noted that the original estimation energy in the protocols will be very high as they require large amounts of extra power in their transmitter and receiver circuitries.

### 5.8.4 Results and discussion

In this chapter, the proposed estimation technique is compared with two conventional protocol techniques in terms of four different performance parameters, a CV with a constant estimation time, an estimation time with a constant CV, the actual transmit energy with a constant CV, and the virtual estimation time assuming constant

transmit power to obtain constant CV. The results from comparisons of the CVs (Figure 5.37 keeping a constant estimation time of 41.67 seconds) of the proposed and conventional protocol-based techniques show that, when estimating 1000 nodes, the CVs are approximately 0.01, 0.0209 and 0.0443 in the proposed, conventional PFSA and conventional GT techniques, respectively, i.e., the proposed method can obtain a CV almost 52.15% and 77.43% lower than those from the PFSA and GT techniques, respectively. Similarly, the results from comparisons of estimation times (Figure 5.40 to obtain a constant CV of 0.1) of the proposed and conventional protocol-based techniques show that, when estimating 1000 nodes, the times are about 0.41s, 1.83s and 20.52s in the proposed, conventional PFSA and conventional GT techniques, respectively, i.e., the proposed method takes almost 77.6% and 98% less time than the PFSA and GT techniques, respectively.

All results indicate the superior performance of the proposed technique without considering the actual transmit energy needed for estimation but, as the transmit energy is a vital factor for an underwater network, it is compared for a particular CV. It is shown in the results that, to estimate 1000 nodes, with a CV of 0.1, the proposed method requires about  $500 \times 10^{-12}$  J, the conventional PFSA method about  $2 \times 10^{-12}$  J and the conventional GT method  $25 \times 10^{-12}$  J. It can be seen that, although the transmit energy is comparatively very high in our proposed technique, it is still within the pJ range.

Also, although the actual transmit energy and, thus, the transmit power only for the estimation, are comparatively very high in our proposed CC technique, they are in the pW range (shown in Figures 5.45 and 5.46) which is insignificant compared with the underwater transmitter power which is typically in the wattage range. Thus, this transmit energy for estimation is not very important in the number of node estimation. Moreover, the proposed method is very time-efficient compared with existing protocol techniques.

It is important to note that the transmit power considered here is for the SNR, attenuation and threshold power of the receiver. But, as the protocol sends a signal into the modem as a bit stream, the modem has transmit electronics for digital

coding, modulation and filtering which require a fixed amount of power (typically in the wattage range (Benson 2010) for an underwater modem) as does the receiver, The protocol techniques require huge amounts of extra power to estimate the number of nodes compared with that considered above. In contrast, in the proposed CC technique, as the transmitter and receiver do not require any coding, decoding, modulation, demodulation or filtering, only the power considered for the SNR, attenuation and threshold power of the receiver is necessary. Therefore, the total estimation energy will be very high in the conventional techniques.

Another performance parameter, virtual time (obtained from the required actual transmitted energy), is compared. Virtual time indicates the imagined time required when assuming the same power (used in the CC technique) for all methods. It is shown that, for a constant total transmit power of  $1219 \times 10^{-12}$  W, the proposed CC technique requires 0.41 second, the conventional PFSA 0.0016 second, and the conventional GT technique 0.0205 second. Although this time is high in the proposed technique, it is not the actual time of estimation.

Again, the proposed method can adjust the multipath effect such that a similar performance to that without a multipath is possible. Although the multipath effect degrades performances in terms of estimation or time (discussed in Section 3.12.6 in Chapter 3), in the protocols, no multipath is considered. Moreover, for the ETP case, estimations from the proposed technique are investigated but not those from the conventional techniques. In the case of an uncontrolled node (e.g., fish), estimation using the protocols is not possible whereas it is easy to estimate employing the proposed method in ETP case.

Besides, in both the CC and PFSA cases, the CV and time are independent of  $N$  which is very efficient for networks with high numbers of nodes. The proposed method also has the advantage that it is useful when all the nodes are in operating condition for their usual purposes.

## 5.9 Conclusion

An estimation error acts as a mirror of the performance of the estimation process. In this chapter, this was discussed by comparing the proposed CC technique with conventional protocol-based approaches. The error is expressed as a CV which is the ratio of the standard deviation to the mean of the estimated number of nodes. As the proposed estimation technique possesses significant statistical properties, this statistical tool is appropriate for performance analyses. The error is analysed in terms of the practical issues of fractional-sample delays, noise, etc. The results follow a similar trend to those for estimation, i.e., where the estimation is good, the error is less and vice versa, which proves the effectiveness of the proposed technique. When some cases are compared with the two conventional techniques proposed in (Budianu 2006; Howlader 2009), their performance improve significantly, thereby indicating the superiority of the proposed technique.



# Chapter 6

## Conclusion & Further Work

---

### 6.1 Introduction

It is important in a communication network to know the number of nodes and networks' dimensionality for a number of practical reasons as network operation, maintenance. Cross-correlation, a statistical signal processing approach is applied for these purposes. Basically, the estimations are obtained using the statistical property of the cross-correlation (of two composite signals) function. Although several estimation strategies have been proposed (Budianu 2003; Budianu 2004; Budianu 2006) using existing protocols in TCN, their use in UCN requires extreme modifications (as the performances of the TCN protocols heavily degrade due to the harsh underwater channel property for wireless communications) and only one such method has been proposed as yet. Moreover, literature on these estimation techniques indicates that the accuracy is dependent on the number of nodes except the only method proposed in UCN where the accuracy is almost independent on the number of nodes. Also the existing methods are time inefficient. In contrast, the cross-correlation of signals contains various important information about signals and their sources, and is used in the literature extensively for various purposes other than the proposed here. Thus the motivation to use of cross-correlation for estimation of the number of nodes (which are the sources of signal in WCN), and network's dimensionality. The proposed cross-correlation technique is suitable for any environment networks with more accurate estimation than with the conventional techniques. It is also time efficient. Initially, a basic approach with some practically reasonable assumptions has been investigated, and then the effects of those assumptions are investigated. Effects of possible practical issues such as long propagation delay, fractional part of samples, multipath, signal length, noise are discussed and analysed. Error in estimation of the number of nodes is investigated



with both theoretical and simulated analysis. The proposed method is compared with the conventional protocol techniques that demonstrate the superior performance of this technique to protocol-based methods. The thesis includes an initial verification of the performance of the proposed techniques and suggests other issues for future verification.

## **6.2 Future directions**

The proposed method is a new technique in this area of research. It therefore requires considerable research as well as field work to implement the proposed method practically to estimate the number of nodes and network dimensionality. Within the limited scope of this thesis, we have provided some estimation techniques to estimate the number of nodes and network dimensionality with detail analysis and recommendation for some major works are left here as the future directions for the researchers in this area of interest. These include the wide area of the method applications, consideration of arbitrary signal strength, further estimation technique, and practical implementation.

### **6.2.1 The proposed CC technique can be used in networks in any environment.**

Although this thesis only analyses the estimation techniques in underwater environments, the technique is equally applicable for any environment, underwater to space and for any network such as wireless sensor networks to any communication network (for example RFID system, sound-making animals or vehicles etc.). The process of estimation will be similar with only the difference in parameters used such as channel bandwidth, signal (electromagnetic, acoustic etc.) used, speed of signal propagation, dispersion factor, absorption coefficient etc. If one uses acoustic communication in terrestrial network, the speed of propagation will be about 330 m/s instead of 1500 m/s underwater. Moreover dispersion factor for electromagnetic signal is varied from 2 to 6 with typical value 4 in TCN, and 6 in UEN. The speed of propagation of electromagnetic waves is  $3 \times 10^8$  m/s in TCN, whereas in UEN it is around  $3.33 \times 10^7$  m/s. Typical values of absorption coefficient (Howlader 2009) is 0

dB/m for TCN, greater than 1 dB/m for UEN and between 0 and 0.5 dB/m in UAN. According to the used bandwidth, the sampling rate requires to change. The proposed technique is equally suitable for all environments using the appropriate parameters.

### 6.2.2 Random transmitted and received power (RTRP) case

In this thesis, the proposed techniques are investigated in two cases: ERP and ETP. In a practical network, another situation might arise where signals are transmitted (and received) with arbitrary strength. Investigating such cases might be helpful to estimate the number of nodes in any network, even a ‘network’ of fish. Although it is considered that a school of fish such as croakers make similar sounds where it is helpful to assume the equal transmitted power (ETP) case, it would be more realistic to obtain estimation with the assumption of random transmitted powers. The estimation will be similar to the ERP and ETP cases, except that the transmitted signal strengths will be random and the received signal strengths will be the result of the distance-dependent attenuation multiplied by those random transmitted strengths. The process has been briefly described here for future work.

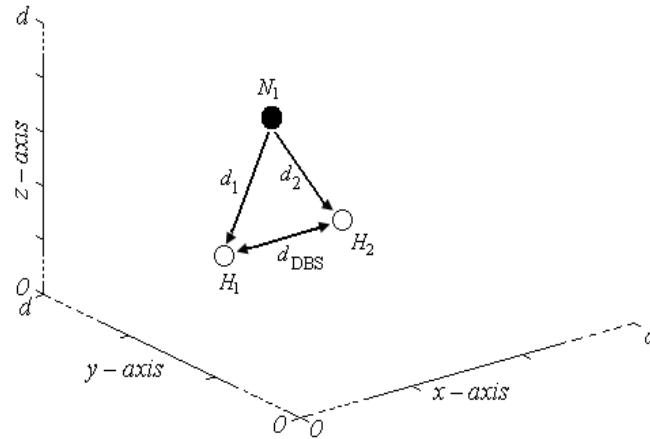


**Figure 6.1 Distributions of underwater network nodes in 3D space**

Recalling the transmitter receiver system of Figure 3.1 (b) at Figure 6.1. Consider that  $N_1$  emits an infinite long signal,  $A_1 S_1(t)$ , where  $A_1$  is its random strength. Then, the signals received by  $H_1$  and  $H_2$  will, respectively, be:

$$S_{r_{11}}(t) = A_1 \alpha_{11} S_1(t - \tau_{11}) \quad (6.1)$$

and

$$S_{r_{12}}(t) = A_1 \alpha_{12} S_1(t - \tau_{12}) \quad (6.2)$$

where the symbols indicating there usual meanings discussed in Chapter 3.

Similarly, the received signals from the second node are:

$$S_{r_{21}}(t) = A_2 \alpha_{21} S_2(t - \tau_{21}) \quad (6.3)$$

and

$$S_{r_{22}}(t) = A_2 \alpha_{22} S_2(t - \tau_{22}) \quad (6.4)$$

Then, for the third node:

$$S_{r_{31}}(t) = A_3 \alpha_{31} S_3(t - \tau_{31}) \quad (6.5)$$

and

$$S_{r_{32}}(t) = A_3 \alpha_{32} S_3(t - \tau_{32}) \quad (6.6)$$

Thus, for the  $N^{th}$  node, they are:

$$S_{r_{N1}}(t) = A_N \alpha_{N1} S_N(t - \tau_{N1}) \quad (6.7)$$

and

$$S_{r_{N2}}(t) = A_N \alpha_{N2} S_N(t - \tau_{N2}) \quad (6.8)$$

Summing (6.1), (6.3), (6.5) and (6.7), the total signal at sensor  $H_1$  is:

$$\begin{aligned} S_{r_{11}}(t) + S_{r_{21}}(t) + S_{r_{31}}(t) + \dots + S_{r_{N1}}(t) \\ = A_1 \alpha_{11} S_1(t - \tau_{11}) + A_2 \alpha_{21} S_2(t - \tau_{21}) + A_3 \alpha_{31} S_3(t - \tau_{31}) + \dots \\ + A_N \alpha_{N1} S_N(t - \tau_{N1}) \\ = \sum_{k=1}^N A_i \alpha_{k1} S_k(t - \tau_{k1}) \end{aligned}$$

Denoting the total signal at sensor  $H_1$  by  $S_{r_{t1}}(t)$  gives:

$$S_{r_{t1}}(t) = \sum_{k=1}^N A_i \alpha_{k1} S_k(t - \tau_{k1}) \quad (6.9)$$

Similarly, denoting the total signal at sensor  $H_2$  by  $S_{r_{t2}}(t)$  gives:

$$S_{r_{i2}}(t) = \sum_{k=1}^N A_k \alpha_{k2} S_k(t - \tau_{k2}) \quad (6.10)$$

Thus, the final CCF between the signals at the sensors is:

$$C(\tau) = \int_{-\infty}^{+\infty} S_{r_{i1}}(t) S_{r_{i2}}(t - \tau) dt \quad (6.11)$$

which takes the form of a series of delta functions as it is a cross-correlation of two signals which are the summations of several white Gaussian signals.

Thus the CCF expression will be similar as (3.16) as shown in the following expression (6.12), but the strength of deltas will be different not only with the distance dependent attenuations but also with the random signal strengths.

$$C(\tau) = \sum_{i=1}^b P_i \delta_i \quad (6.12)$$

Using this CCF, the estimation parameters of the number of nodes can be obtained. Though it might not follow exactly the theory developed in Section 3.7.1 of Chapter 3, proper scaling as in ETP case might give the proper estimation. Thus the works done in ERP and ETP cases are equally possible in RTRP case as well but due to limited time it has been left for future works.

### 6.2.3 Estimation using more than 2 sensors

These estimation techniques might be performed with an array of more than two elements. In that case, the cross-correlation between possible equal distant sensor pairs are performed to get the estimation parameter  $R$  and then average them to get better  $R$  closer to the theoretical, which might give better performance in estimation of the number of nodes and network dimensionality. Actually, this technique is similar as with more than one probe. Thus if we get two set of CCF, it is similar as the CCF in 2 probe with only two sensors, and the performance parameter CV will be one on square root of 2 times less than that with the one CCF. Thus one can improve the performance of this estimation technique with more sensors instead of using more probes. Use of more probes need more time, but more sensors require only the time of one probe. Thus we can obtain a time and error efficient method of estimation, though it costs extra but reasonable charge for the sensor itself. Several

placements of 3 sensors in an estimation system have been provided in Figure 6.2. It can be seen from the figures that for the distribution of sensors in (a) and (b) we will get two  $R$  with same  $b$  and for (c) three  $R$  with same  $b$ . Averaging of these  $R$  from a particular configuration gives an  $R$  closer to the theoretical. This improves the estimation performance.

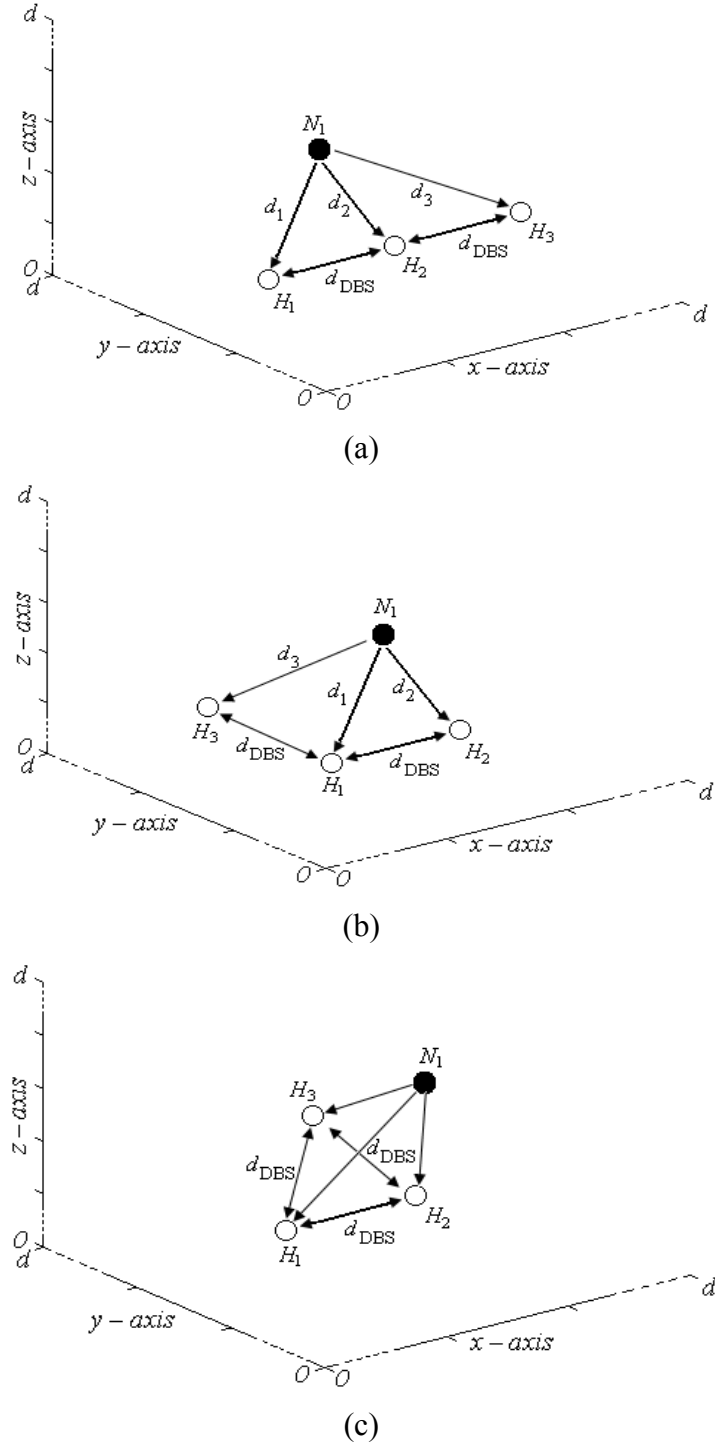


**Figure 6.2** Distribution of nodes and sensors to get (a) two set of CCF (1), (b) two set of CCF (2), and (c) three set of CCF

#### 6.2.4 Practical implementation

The proposed method has been analysed theoretically and by simulation with considering almost all dominant practical issues. Field tests are required to validate the theory and simulation and to obtain the real world implementation. Current underwater nodes are very expensive. Though it is possible to implement practically after some field tests but due to the lack of means and time practical estimation is not performed yet.

#### 6.2.5 Effect of Doppler shift

The Doppler effect is one of the important practical issues in underwater acoustic networks. This effect sometimes compresses and sometimes spreads the frequency of the received signal according to the movement of the source and receiver moving towards or away from each other.

The generalized expression of the received frequency with the Doppler effect is:

$$f = \left( \frac{S_p + S_{p_r}}{S_p + S_{p_t}} \right) f_o \quad (6.13)$$

where,  $S_{p_r}$  and  $S_{p_t}$  are the receiver and transmitter speed. If the movement of the transmitter and receiver are very slow with compared to the speed of signal propagation, the (6.13) can be approximated as:

$$f = \left( 1 - \frac{S_{p_{rt}}}{S_p} \right) f_o$$

where,  $S_{p_{rt}}$  is the difference of  $S_{p_r}$  and  $S_{p_t}$ .

Spreading of a signal requires more time to reach the sensors. So it requires more time and energy for estimation. To investigate the estimation performance with Doppler effect, the frequency of the received signal has to be adjusted with the above expression.

### **6.2.6 Estimation where sensors are not at the centre of the network**

It is assumed in the whole thesis that sensors are placed in the centre of the network. This helps to get proper shape of the CCF, which in turns help to get estimation parameter,  $R$  as theoretical. If the sensors in the centre, this gives a uniform binomial distribution of the deltas in the whole CCF. But in case of sensors not in the centre, though the individual bins are occupied by the binomially distributed deltas (as the signals are Gaussian), it is not uniform for all bins. Thus it is not possible to use  $\frac{\sigma(\text{CCF})}{\mu(\text{CCF})}$  directly in that case to obtain the estimation parameter. Instead we have to obtain the estimation parameter in the way discussed in Sections 4.3 and 4.4 of Chapter 4.

### **6.2.7 Distribution of nodes being sufficiently non-random**

The shape of a CCF depend not only the sensors position at the network but also on the placement of the nodes. Uniform random distribution of nodes with sensors at the centre of the network gives the proper shape of the CCF. If we choose the distribution other than random the individual cross-correlations will give delta function but the shape of CCF will be changed. So the estimation parameter will be changed, and deviated from the theoretical values. Thus again it is not useful to use  $\frac{\sigma(\text{CCF})}{\mu(\text{CCF})}$  directly in this case to obtain the estimation parameter. Instead we have to obtain the estimation parameter in the way discussed in Sections 4.3 and 4.4 of Chapter 4 similarly as for the changed sensors position.

### **6.2.8 Estimation with Non-Gaussian signals**

The Gaussian nature of the signals ensures the delta function in the bins of CCF. Similar delta functions are possible from delta signal as well as from the signal which fulfils the Gaussian property. If the signals are non-Gaussian we will not get only the desired peaks, we will get some undesired peaks as well in the CCF. This may degrade the estimation performance or require additional manipulation to match

with the theoretical results . To show the effect some simulated results are shown as follows with the lognormal signal. It shows that the CCF is giving a desired peak in the desired position but other bins are occupied by almost a constant peak less than the desired peak. Thus if we want to get estimation parameter from this CCF directly, it will give erroneous result.

However, if we manipulate the CCF as we subtract the constant peaks from the CCF, we will get only the desired peak. So we will get the CCF with only the desired peaks. Now obtaining the estimation parameter gives similar result as with Gaussian signal. Thus if the statistical characteristics of the signal is changed, to get the estimation, it requires proper manipulation of the CCF, sometimes it might not possible at all to get the estimation.

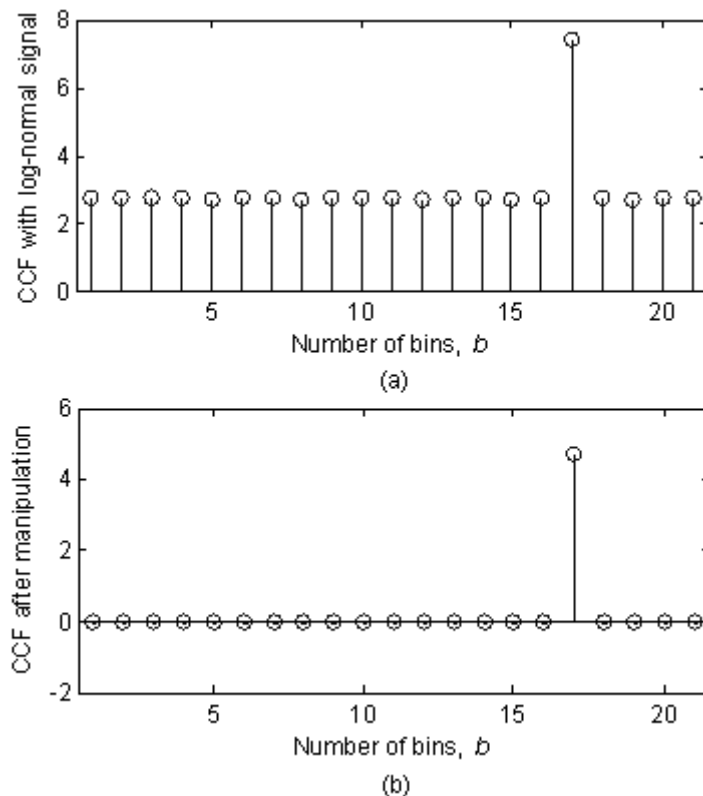


**Figure 6.3 CCF versus  $b$  with a source of lognormal signal (a) before manipulation; and (b) after manipulation**



### 6.2.9 Effect of bandwidth

Channel bandwidth restricts the signal bandwidth which might affect the estimation performance. The reason is that because of limited bandwidth, we will get sinc function (Alam 2009) instead of delta function of infinite band signal. So it will give undesired peaks in the bins. So the CCF is corrupted as well as the estimation. To show the effect of BW, a 10 kHz (lowpass is better in underwater to avoid unwanted high frequency attenuation) Gaussian signal is used in the simulation instead of infinite BW signal. The ratio of standard deviation and mean of CCF for this finite BW case is obtained and denoted by  $R_{\text{finiteBW}}$  and for infinite BW case  $R_{\text{infiniteBW}}$ . Now the ratio of that two  $R$  is obtained and plotted against  $N$  in Figure 6.4. It can be seen in the figure that  $R_{\text{finiteBW}}$  is almost the constant multiple of  $R_{\text{infiniteBW}}$  and the mean of that constants are 0.8093 for this case.

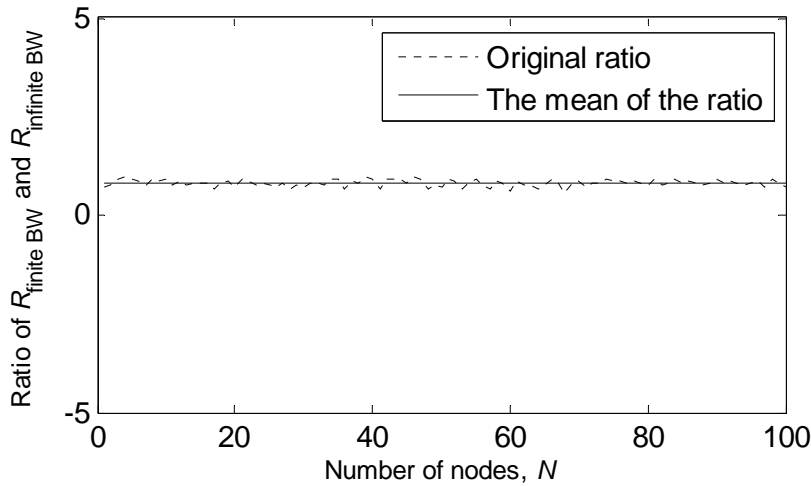


**Figure 6.4** Ratio of  $R_{\text{finiteBW}}$  and  $R_{\text{infiniteBW}}$

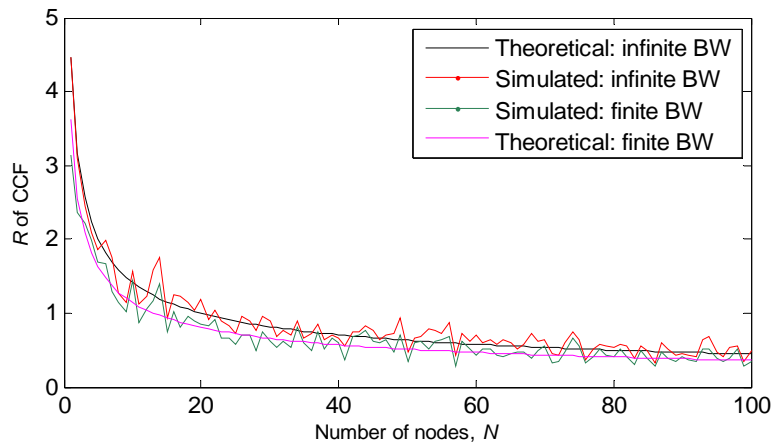


**Figure 6.5**  $R$  of CCF

Now, multiplying theoretical infinite BW  $R$  by this mean gives the theoretical approximation of the finite BW  $R$  which is shown in Figure 6.5 of the previous page. To make the figure more clear, in Figure 6.6 and 6.7, separate plots are provided for infinite and finite BW cases.

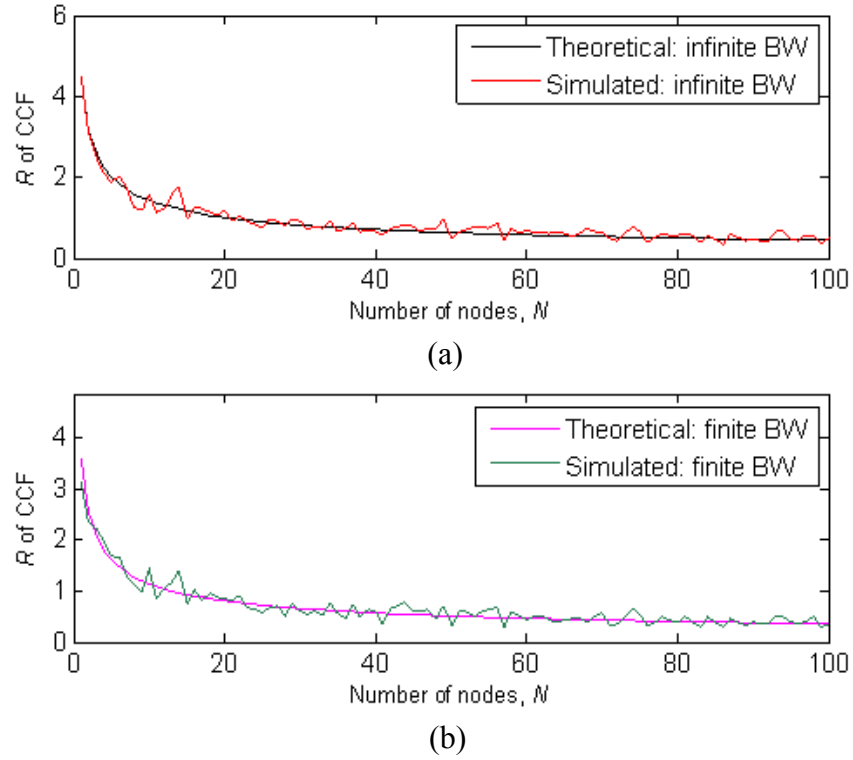


**Figure 6.6  $R$  of CCF in separate plot**

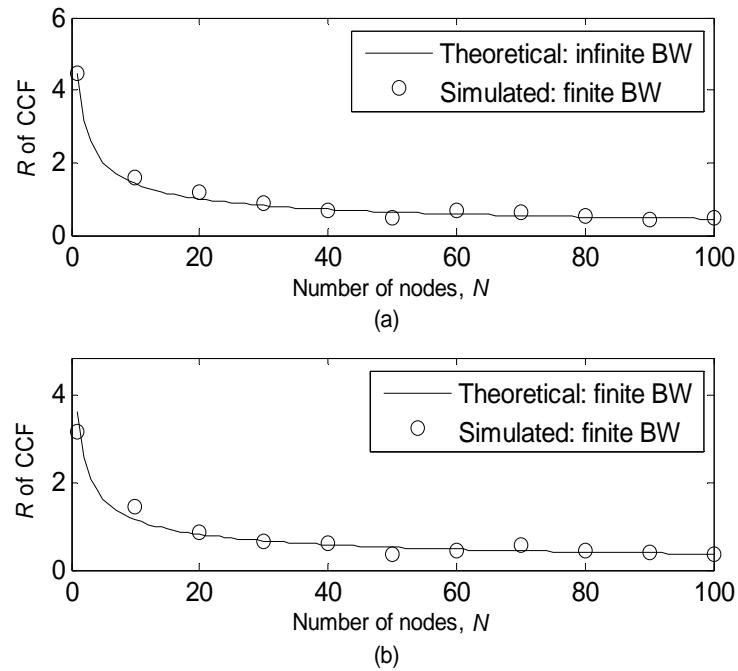


**Figure 6.7  $R$  of CCF in separate plot with less points**

It is shown that the scaling is good enough to get estimation in finite BW case as in infinite BW case. As the  $R_{\text{finiteBW}}$  is a constant multiple of  $R_{\text{infiniteBW}}$ , the power (which affects the CV) of  $R_{\text{finiteBW}}$  in estimation expression is not changed. So the CV is not affected by the BW (10 kHz). Thus from intuition it can say that no problem will occur with the BW greater than 10 kHz but we have to check whether it is affected or not with the BW less than 10 kHz.

### **6.2.10 Effect of shape of the network**

Shape of the network is another factor which might affect the formation of CCF and thus might affect the estimation performance. It is seen in the dimensionality estimation, how the shape of a network affects the estimation process. Based on that analysis, we can describe the estimation process for the other shapes.

### **6.2.11 Effect of non-Gaussian noise**

Performance of estimation is affected by the both receiver internal and channel background noises. It is shown that both noise sources have similar effect and detail is investigated adding internal noise of the receiver. It is assumed that the noises are additive Gaussian in nature. Internal noise of the receiver is the thermal noise and Gaussian assumption is not a problem. Due to the random, large, and undetermined nature of sound sources, Gaussian distribution might be the assumption (Urick 1983), but practically background noises might not follow the exact Gaussian properties (Llor 2009). This non-Gaussianity of the noises might affect the estimation performance. To show the effect it requires to use exact expressions (Coates 1989) of the background noises or the practical underwater noise in the simulation process, which are left for the future work.

### **6.2.12 Effect of more than two reflected path**

It is shown in Section 3.12 of Chapter 3 that one can estimate the number of nodes properly in a multipath environment. This description was described only for one and two reflected paths, but in practical environment there might be such situation of

more than two reflected paths. However, the similar process can be extended for any number of paths, which will be very helpful in estimation in large number of multipath environment.

### 6.2.13 Effect of variable propagation delays

It is assumed in the whole thesis that the propagation speed of sound wave is constant at 1500 m/s. But in a real environment, it varies between 1450 and 1540 m/s (the typical speed is taken as 1500 m/s) according to the properties of water and depth of the sea. This low and variable speed makes long and variable propagation delay, which might effect on estimation process. The underwater sound propagation speed is expressed empirically as (Brekhovskikh 1991):

$$S_p = 1449.2 + 4.6\theta - 0.055\theta^2 + 0.00029\theta^3 + (1.34 - 0.01\theta)(s_f - 35) + 0.016d$$

where,  $\theta$  is the temperature in  $^{\circ}C$  and  $s_f$  is the salinity factor .

Though the long propagation delay is considered in the estimation process, the effect of variable propagation delay is still not considered. But for practical implementation of the technique, it is necessary to investigate the effect by using the proper propagation speed from the above expression in the estimation process.

### 6.2.14 Effect of $N$ on CV of estimation.

It is shown in the results that error in estimation of the number of nodes is independent of  $N$ . It is again shown that CV is dependent on  $b$  as  $CV \propto \frac{1}{\sqrt{b}}$ . Thus, if

$b$  is increasing the CV is decreasing. But it can be seen in Chapter 5 that, CV is not decreasing after a certain  $b$  ( $=239$ ) for a particular  $N$  ( $=32$ ). This can be explained as follows. The CV will be minimum when each delta for the nodes occupy separate bin. As the delta placement is binomially distributed, this will need enough  $b$  (large enough with compared to  $N$ ) to get one delta per bin. So definitely there will be lots of empty bins. But after the required  $b$  for a certain  $N$ , if  $b$  is further increased, it does not help to get better CV. Besides, empty bins are increasing and if the system have

some undesired delta (as in the case of smaller  $N_s$ ) in the empty bins it will degrade the performance of the process. Now if  $N$  increases, the required  $b$  increases to get the minimum CV. Thus CV is affected by the  $N$ . But when the CV reaches again at  $CV \propto \frac{1}{\sqrt{b}}$  for a particular  $N$ , it is again independent of the number of nodes beyond this  $N$ .

### 6.2.15 Further works on dimensionality estimation

Estimation of dimensionality has been investigated only for three fundamental structures of 1D, 2D, and 3D networks. It is assumed that in 1D the nodes are placed on a straight line, in 2D on a circle, and in 3D inside a sphere. But the nodes in the real networks might place in different shape beyond the fundamental three. Although the proposed method can work in those networks, they require more investigations and might require some modifications of the proposed estimation expressions. This thesis considers only the ERP case for dimensionality estimation. As the other (ETP, RTRP) cases in dimensionality estimation requires further work, they are left for the future work. The proposed dimensionality estimations uses 11 bins in the cross-correlation process for the ease of calculation. In Chapter 3 and 5 the effect of the number of bins,  $b$ , on the node estimation is discussed properly. It shows that until a certain number of bins the performance of the estimation improves, after which the performance decays. This cross-correlation process of dimensionality estimation might have the similar performance and the analysis is left for the future work. Besides all other further works in estimation of the number of nodes will equally require for dimensionality estimation because both estimations are using similar cross-correlation approach.

## 6.3 Conclusion

A novel and unique number of networks' node and dimension estimation using cross-correlation is proposed with detail analysis which is equally applicable in networks of all environments. The information from this estimation is useful at any point in time from initial formation of the network to network operation by providing

network maintenance. The process might be used as a stand-alone or a concurrent method with other purposes as DOA, TDOA estimation etc. Due to lack of means, no field experiment is done yet but extensive simulation and analysis are provided. It can be seen from the results that the proposed methods are sufficiently accurate and robust to be used in any type and size of network. Time required and error in estimation is compared with those of the conventional methods, which prove the superiority of the proposed technique. Although required transmit energy is higher in the proposed technique than in the conventional techniques, the energy range is very low with respect to the total energy of the nodes.



# Appendix A

## Obtaining receiver internal noise and channel background noise

---

To obtain the strength of the internal noise of the receiver and channel background noise, two experiments were conducted by our research group (Underwater Lab group, SEIT, UNSW@ADFA, Australia). For internal noise of the receiver, the experiment was conducted in our lab tank, whereas, for the channel background noise, the experiment was done at Jervis Bay, NSW, Australia in April 2010. In the experimental set up of the later, a hydrophone was deployed underwater at the depth of about 6 m from the surface. Since the strength of noise is very low, a 30dB preamplifier was used to amplify the noise before recording. 50 minutes of data was recorded at a sampling rate of 96 kSa/s. Data was recorded at 1 km away from the shore. The experimental setup is shown in Figure A.1.

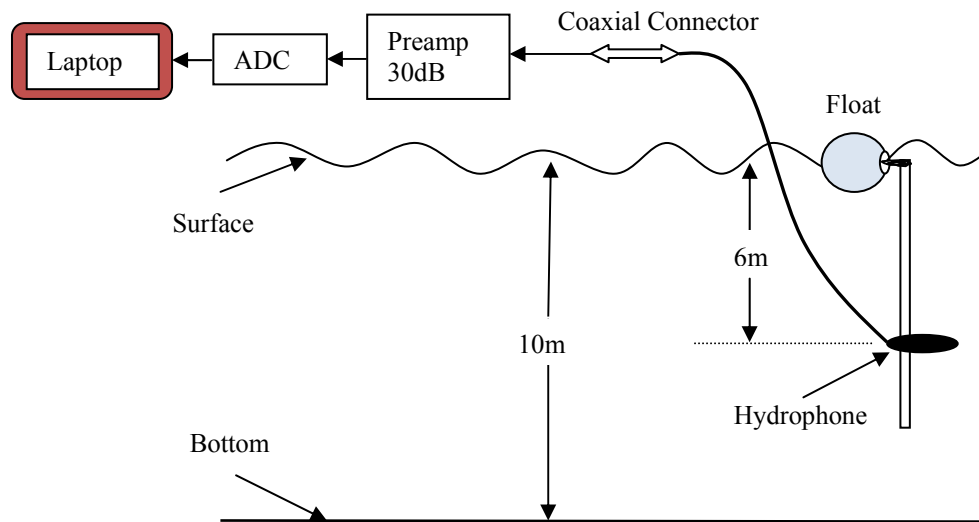


**Figure A.1** Experimental setup to obtain the ocean background noise

To obtain the internal noise of the hydrophone, it was deployed in noiseless water in our laboratory tank as shown in Figure A.2.



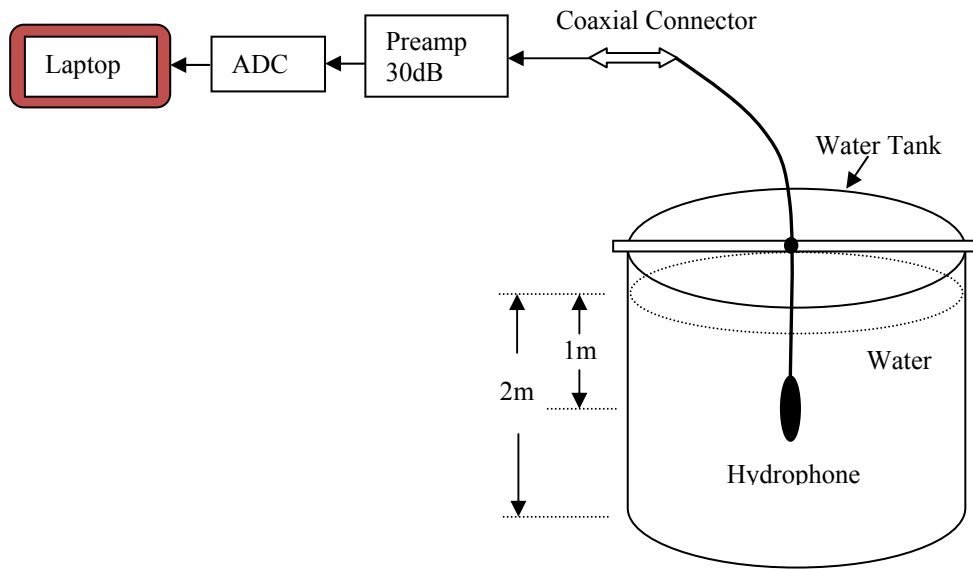


**Figure A.2 Experimental setup to obtain the internal noise of the hydrophone**

Obtained power spectrums of the noise fields recorded at two sensors are shown in Figure A.3. It follows almost a  $1/f$  distribution which is depicted in the figure. The ocean background noise is indicated by the blue colour and internal noise of the receiver by the red colour. It can be seen from the results that the ocean background noise power is about 10 to 25 dB more compared to the internal receiver noise. Voltage level of internal noise is calculated from this power spectrum (assuming flat power spectrum at -170 dB) , which is  $3.16 \text{ nV}/\sqrt{\text{BW in Hz}}$  . Using this value with proper BW and Boltzmann constant, the noise temperature is obtained as 725K.

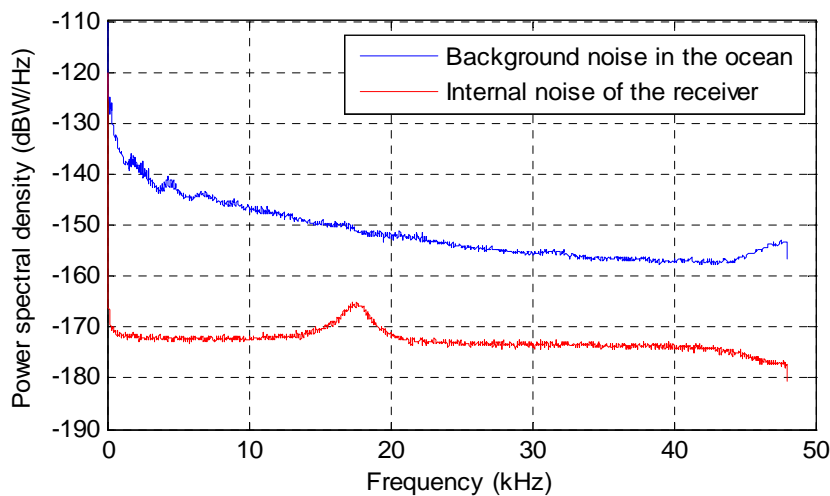


**Figure A.3 Power spectrums of noise from the experiment**

# Appendix B

## List of Symbols

Some symbols may be used to denote more than one entity, but their uses are clearly defined in the context. Common symbols used in this thesis are listed below.

Sym bols	Meaning	Sym bols	Meaning
$\alpha$	Signal attenuation	$\mu_r$	Relative permeability
$\alpha_{ij}$	Attenuation in the direct signal travelling from $i^{th}$ node to $j^{th}$ receiver	$\mu_s$	Sample mean
$\alpha_{mij}$	Attenuation in the reflected signal travelling from $i^{th}$ node to $j^{th}$ receiver	$\rho$	Normalised offered load
$\beta$	Accuracy parameter in protocol	$\rho_\xi$	Effective normalised offered load
$\delta(\cdot)$	Dirac delta function	$\rho_{XY}$	Correlation coefficient between $X$ and $Y$ random variable
$\delta_i$	Dirac delta at $i^{th}$ bin	$\sigma$	Standard deviation of a random variable
$\varepsilon_r$	Relative permittivity	$\sigma_s$	Sample standard deviation
$\phi$	Probability of error in estimation in protocol	$\sigma_p$	Population standard deviation
$\varphi_k$	Power of $(b-1)$ in the expression of simulated $R$ with dispersion factor $k$	$\tau$	Time delay
$\gamma$	Capture constant	$\tau_{ij}$	Time delay for the signal of $i^{th}$ node to the $j^{th}$ receiver
$\eta$	Number of slots	$\tau_{mij}$	Time delay for the reflected signal of $i^{th}$ node to the $j^{th}$ receiver
$\eta_c$	Total collided slots	$\omega$	Angular frequency
$\eta_{GT}$	Number of slots in GT protocol	$\psi$	Throughput
$\eta_{PFSA}$	Number of slots in PFSA protocol	$a$	Absorption coefficient
$\lambda$	Signal wavelength	$b$	Number of bins
$\mu$	Mean of a random variable	$c$	Constant of proportionality
$\mu_0$	Mean of the number of empty slots	$c_{\text{water}}$	Speed of electromagnetic wave underwater
$\mu_p$	Population mean	$d$	Path length

$d_{\text{DBS}}$	Distance between receivers	$p_j$	Probability of success for the $j^{\text{th}}$ node i.e. trial
$d_{ij}$	Path length between $i^{\text{th}}$ node from $j^{\text{th}}$ receiver	$p_{mi}$	Percentage of reflected signal with respect to total signal in $i^{\text{th}}$ bin
$d_j$	Path length between interfering node and receiver in capture	$p_{m2i}$	Percentage of reflected signal with respect to total signal in $i^{\text{th}}$ bin in the multipath case of one direct and two reflected path.
$d_{mc}$	Path length with capture	$q$	Probability of failure to occur
$d_{\text{max}}$	Maximum range	$s$	Slope of a straight line
$d_{mij}$	Path length of indirect signal of $i^{\text{th}}$ node to the $j^{\text{th}}$ receiver	$s_a$	Shipping activity factor
$d_{\text{min}}$	Minimum range	$s_k$	Slope of the straight line approximation of $R$ versus $N$ plot in log-log scale with dispersion factor $k$
$d_t$	Path length between transmitting node and receiver	$t$	Time variable
$d_w$	Path length of $w^{\text{th}}$ node or tag from the receiver in protocol	$x_i$	$i^{\text{th}}$ sample of a signal $x$
$e_{Di}$	Deviation in $i^{\text{th}}$ bin off observed value from the theoretical value of $D$ dimensional network	$y_i$	$i^{\text{th}}$ sample of the signal $y$
$f$	Signal frequency	$w$	Wind speed
$g(d)$	Cumulative distribution function	$B_n$	Packet size in number of bits
$h_0$	Number of slots without having any transmission	$B_R$	Bit rate
$h_1$	Number of slots with having transmission	$C(\cdot)$	Cross-correlation function
$k$	Dispersion factor	$C_i(\cdot)$	CCF for $i^{\text{th}}$ node
$m_0$	Number of empty slots	$C_{\text{rate}}$	Collision rate
$m_1$	Number of singleton slots	$C_{\text{ratio}}$	Collision ratio
$m_{1c}$	Number of singleton slots with capture	$C_R$	Capture ratio
$m_c$	Number of collision slots	$D$	Spatial dimensionality of WCN
$n$	Number of trials	$\hat{D}$	Estimation of $D$
$n_i$	Number of trials placed in the $i^{\text{th}}$ bin	$E(\cdot)$	Expected value of a random variable
$P$	Probability of success	$E_{\text{pb}}$	Energy per bit
$p_i$	Probability of success in the $i^{\text{th}}$ bin	$E_{\text{pp}}$	Energy per packet

$E_t$	Total transmitted energy	$N_{p_1}$	Number of packets appear exactly once in $N_p$
$E_{tGT}$	Total transmitted energy in GT protocol technique	$N_{p_d}$	Number of distinct packets
$E_{tn}$	Transmitted energy from $n^{th}$ node	$N_s$	Signal length
$E_{tpw}$	Transmitted energy in protocol for $w^{th}$ node	$N_{S_n}$	Signal length for $n^{th}$ node
$E_{tPFSA}$	Total transmitted energy in PFSA protocol technique	$P_i$	Peak of dirac delta in the $i^{th}$ bin
$F$	Frame size	$P_j$	Peak of Dirac delta for $j^{th}$ node
$H_0$	Number of missing mass	$P_{id}$	Peak of delta in the $i^{th}$ bin for the direct signal in multipath case
$\hat{H}_0$	Estimation of $H_0$	$P_{ir}$	Peak of dirac delta in the $i^{th}$ bin for the reflected signal in multipath case
$I_{12}(\omega)$	Normalised cross-spectral density	$P_{ids}$	Peak after deduction of reflected peak from the total peak in $i^{th}$ bin
$L_p$	Path loss	$P_{2i}$	Peak of dirac delta in the $i^{th}$ bin for one direct and two reflected signal in multipath case
$M$	Total probability	$P_{2id}$	Peak of dirac delta in the $i^{th}$ bin only for direct signal in multipath case
$M_0$	Random variable of number of empty slots without capture	$P_{2ir}$	Peak of dirac delta in the $i^{th}$ bin only for two reflected signal in multipath case
$M_1$	Random variable of number of singleton slots without capture	$P_{2ids}$	Peak after deduction of reflected peak from the total peak in $i^{th}$ bin in the multipath case of one direct and two reflected path.
$M_c$	Random variable of number of collided slots without capture	$Q_t$	Received power from the transmitting node in a capture
$M_{1c}$	Random variable of number of singleton slots with capture	$Q_j$	Received power from the interfering node in a capture
$N$	Number of nodes or tags to be estimated	$Q_n$	Receiver threshold power
$\hat{N}$	Estimation of $N$	$Q_R$	Received power
$N_{coll}$	Number of tags in a collided slot	$Q_{R_n}$	Received power by the receiver from $n^{th}$ node
$N_p$	Number of packets	$Q_T$	Transmitted power
$N_{p_0}$	Number of packet that do not appear	$R$	Theoretical estimation parameter (ratio of standard deviation to the mean of CCF)

$R_b(k)$	$R$ with number of bins, $b$ and dispersion factor, $k$		
$R_{iD}$	$R$ in $i$ dimensional network		
$R_{iDT}$	Theoretical $R$ in $i$ dimensional network		
$R_{iDS}$	Simulated $R$ in $i$ dimensional network		
$R_k$	Simulated estimation parameter (ratio of standard deviation to the mean of CCF) with dispersion factor $k$		
$S_i(\cdot)$	Signal from $i^{th}$ node or source		
$S_{r_{ij}}(\cdot)$	Received signal in $j^{th}$ receiver from $i^{th}$ node		
$S_{n_i}(\cdot)$	Noise signal received in $i^{th}$ receiver		
$S_p$	Speed of acoustic wave propagation		
$S_R$	Sampling rate		
$S_{R_n}$	Sampling rate for the signal from $n^{th}$ node		
$S_{r_{ij}}(\cdot)$	Total received signal in $j^{th}$ receiver		
$T$	Estimation time		
$T_{ERP}$	Estimation time in ERP case		
$T_{ETP}$	Estimation time in ETP case		
$T_{CC}$	Estimation time in CC technique		
$T_{PFSA}$	Total time in PFSA protocol technique		
$T_{GT}$	Total time GT protocol technique		
$V_{iD}$	Percentages of deltas in $i^{th}$ bin of CCF from $D$ dimensional network		
$V_{i23}$	Ratio of $V_{i2}$ and $V_{i3}$		
$u$	Number of probes or iterations		
$X$	A random variable		
$Y$	A random variable		
$Z$	Percentile of unit normal distribution		

# Appendix C

## Used Abbreviations

---

ADC	Analog to Digital Converter
AOA	Angle of Arrival
AUV	Autonomous Underwater Vehicle
AWGN	Additive White Gaussian Noise
BPSK	Binary Phase Shift Keying
BW	BandWidth
CC	Cross-Correlation
CCF	Cross-Correlation Function
CDF	Cumulative Distribution Function
CV	Coefficient of Variation
DBS	Distance Between Sensors
DOA	Direction of Arrival
EM	ElectroMagnetic
EO	Earth Observation
ERP	Equal Received Power
ETP	Equal Transmitted Power
FCS	Frame Check Sequence
FSA	Framed-Slotted ALOHA
GEO	Geostationary Earth orbit
GF	Green's Function
GT	Good-Turing
ISI	Inter Symbol Interference
LEO	Low Earth Orbit
MAC	Media Access Control
MANET	Mobile Ad-hoc NETwork
MAP	Mobile Access Point
MEO	Medium Earth Orbit
OCV	Optimum CV
PFSA	Probabilistic FSA
PW	Pulsed Wave
QT	Query Tree
RF	Radio Frequency
RFID	Radio Frequency Identification
RSDM	Ratio of Standard Deviation to the Mean
RTRP	Random Transmitted and Received Power
SCN	Space Communication Network
SENMA	Sensor Network with Mobile Access
SNR	Signal to Noise Ratio
SWCN	Space Wireless Communication Network

SWSN	Space Wireless Sensor Network
TCN	Terrestrial Communication Network
TDGF	Time Domain Green's Function
TDOA	Time Delay of Arrival
TWCN	Terrestrial Wireless Communication Network
TWSN	Terrestrial Wireless Sensor Network
UAN	Underwater Acoustic Network
UCN	Underwater Communication Network
UEN	Underwater Electromagnetic Network
UGCN	Underground Communication Network
UGWCN	Underground Wireless Communication Network
UGWSN	Underground Wireless Sensor Network
UUV	Unmanned Underwater Vehicle
UWASN	Underwater Wireless Acoustic Sensor Network
UWCN	Underwater Wireless Communication Network
UWSN	Underwater Wireless Sensor Network
WCN	Wireless Communication Network
WSN	Wireless Sensor Network

# References

---

- Akyildiz**, I. F., Sun, Z., et al. (2009). Signal propagation techniques for wireless underground communication networks. *Physical Communication* **2**(3): 167-183.
- Akyildiz**, I. F., and Stuntebeck, E. P. (2006). Wireless underground sensor networks: Research challenges. *Ad Hoc Networks* **4**(6): 669-686.
- Akyildiz**, I. F., Pompili, D., et al. (2005). Underwater acoustic sensor networks: research challenges. *Ad Hoc Networks* **3**(3): 257-279.
- Akyildiz**, I. F., Su, W., et al. (2002). A Survey on Sensor Networks. *IEEE Communications Magazine* **40**: 102-114.
- Alam**, M. J., Frater, M. R., et al. (2010). Improving resolution and SNR of correlation function with the increase in bandwidth of recorded noise fields during estimation of bottom profile of ocean. *OCEANS 2010 IEEE* - Sydney.
- Alotaibi**, M., Postula, A., et al. (2009). An enhanced method of estimating number of tags using signal strength properties in RFID systems. *The 2nd International Multi-Conference on Engineering and Technological Innovation (IMETI 2009)* Orlando , Florida, USA: 337-341.
- Anguita**, D., Brizzolara, D., et al. (2008a). Smart Plankton: a Nature Inspired Underwater Wireless Sensor Network. *International Conference on Natural Computation*.
- Anguita**, D., Brizzolara, D., et al. (2008b). Smart plankton: a new generation of underwater wireless sensor network. *Artificial Life XI: Proceedings of the Eleventh International Conference on the Simulation and Synthesis of Living Systems, MIT Press*.
- Azaria**, M., and Hertz, D. (1984). Time delay estimation by generalized cross correlation methods. *IEEE Trans. Acoust., Speech, Signal Process.* **ASSP-32**(2): 280-285.
- Bainbridge**, S., and Eggeling, D. (2009). Application of Wireless Sensor Networks to Coastal Observing Systems, An Example from the Great Barrier Reef. *OceanObs'09*, Venice, Italy. From



<https://abstracts.congrex.com/scripts/jmevent/abstracts/FCXNL-09A02-1660403-1-OCeanObs09AbstractforFAIMMSFinal.pdf>.

- Barclay, L. W. (2003).** Propagation of radiowaves. *Institution of Electrical Engineers*, London.
- Barry, B. A. (1978).** Errors in practical measurement in science, engineering, and technology. New York, *John Wiley & Sons*, Inc.
- Benson, B., Li, Y., et al. (2010).** Design of a low-cost underwater acoustic modem. *IEEE Embedded Systems Letters* **2**(3).
- Bhardwaj, M., and Chandrakasan, A. P. (2002).** Bounding the lifetime of sensor networks via optimal role assignments. *INFOCOM 2002*. Twenty-First Annual Joint Conference of the IEEE Computer and Communications Societies. Proceedings. IEEE.
- Blumenthal, J., Handy, M., et al. (2004a).** SeNeTs - test and validation environment for applications in large-scale wireless sensor networks. *2nd IEEE International Conference on Industrial Informatics, 2004 (INDIN '04)*.
- Blumenthal, J., Golatowski, F., et al. (2004b).** Software Development for Large-Scale Wireless Sensor Networks. *The Industrial Information Technology Handbook*, CRC Press. **1**.
- Bogena, H. R., Huisman, J. A., et al. (2009).** Hybrid Wireless Underground Sensor Networks: Quantification of Signal Attenuation in Soil. *Vadose Zone Journal* **8**(3): 755-761.
- Bonnefous, O., and Presque, P. (1986).** Time domain formulation of pulse-Doppler ultrasound and blood velocity estimation by cross-correlation. *Ultrason. Imaging* **8**: 73-85.
- Bonuccelli, M. A., Lonetti, F., et al. (2008).** Perfect tag identification protocol in RFID networks. From [http://arxiv.org/PS\\_cache/arxiv/pdf/0805/0805.1877v1.pdf](http://arxiv.org/PS_cache/arxiv/pdf/0805/0805.1877v1.pdf).
- Bonuccelli, M. A., Lonetti, F., et al. (2006).** Tree Slotted Aloha: a New Protocol for Tag Identification in RFID Networks. *Proceedings of the 2006 International Symposium on on World of Wireless, Mobile and Multimedia Networks*, IEEE Computer Society.
- Brekhovskikh, L. M., and Lysanov, Y. P. (1991).** Fundamentals of Ocean Acoustics. *Springer-verlag*, New York.

- Brekhovskikh, L. M., and Lysanov, Y. P. (1982).** Fundamentals of Ocean Acoustics. Springer-verlag, New York.
- Budianu, C., Ben-David, S., et al. (2006).** Estimation of the number of operating sensors in large-scale sensor network with mobile access. IEEE Trans. Signal Process. **54**(5).
- Budianu, C., and Tong, L. (2004).** Good–Turing estimation of the number of operating sensors: A large deviations analysis. Int. Conf. Acoust., Speech, Signal Process.
- Budianu, C., and Tong, L. (2003).** Estimation of the number of operating sensors in a sensor network. Asilomar Conf. Signals, Syst., Comput., Monterey, CA.
- Buettner, M., Greenstein, B., et al. (2008).** Revisiting Smart Dust with RFID Sensor Networks. 7th ACM Workshop on Hot Topics in Networks (Hotnets-VII), Calgary, Alberta, Canada.
- Burdet, L. A. (2004).** RFID Multiple Access Methods. Seminar on Smart Environments, ETH Zürich.
- Callaghan, T., Czink, N., et al. (2010).** Correlation-based Radio Localization in an Indoor Environment. Draft- EURASIP JWCN.
- Capetanakis, J. (1979).** Tree algorithms for packet broadcast channels. IEEE Transactions on Information Theory, **25**(5): 505-515.
- Cha, J.-R., and Kim, J.-H. (2006).** Dynamic framed slotted ALOHA algorithms using fast tag estimation method for RFID system. IEEE Consumer Communications and Networking Conference, IEEE. **2**: 768-772.
- Cha, J.-R., and Kim, J.-H. (2005).** Novel anti-collision algorithms for fast object identification in RFID system. Int. Conf. Parallel and Distributed Systems Computing.
- Che, X., Wells, I., et al. (2010).** Re-evaluation of RF electromagnetic communication in underwater sensor networks. Comm. Mag. **48**(12): 143-151.
- Chen, Q., Hoilun, N., et al. (2008).** Cardinality Estimation for Large-scale RFID Systems. Sixth Annual IEEE International Conference on Pervasive Computing and Communications (PerCom 2008).
- Chen, W.-C., Horng, S.-J., et al. (2007).** An enhanced anti-collision algorithm in RFID based on counter and stack. Second Int. Conf. Systems Networks Communications (ICSNC 2007).

- Cheng, E., Burnett, I. S., et al. (2007).** Time Delay Estimation of Reverberant Meeting Speech: On the Use of Multichannel Linear Prediction. *International IEEE Conference on Signal-Image Technologies and Internet-Based System*.
- Chiang, K. W., Hua, C., et al. (2006).** Prefix-Randomized Query-Tree Protocol for RFID Systems. *IEEE Int. Conf. on Communications*. **4**: 1653-1657.
- Choi, J. H., Lee, D., et al. (2006).** Bi-slotted tree based anti-collision protocols for fast tag identification in RFID systems. *Communications Letters, IEEE* **10**(12): 861-863.
- Choi, H.-S., Cha, J.-R., et al. (2005).** Improved Bit-by-Bit Binary Tree Algorithm in Ubiquitous ID System. *Advances in Multimedia Information Processing (PCM 2004)*: 696-703.
- Coates, R. (1989).** Underwater Acoustic Systems. *Wiley*, New York.
- Colitti, W., Steenhaut, K., et al. (2008).** Satellite based wireless sensor networks: global scale sensing with nano- and pico-satellites. In *Proceedings of the 6th ACM conference on Embedded network sensor systems (SenSys '08)*. ACM, New York, NY, USA, 445-446.
- Cox, H. (1973).** Spatial correlation in arbitrary noise fields with application to ambient sea noise. *J. Acoust. Soc. Am.* **54**: 1289-1301.
- Dunkels, A., Feeney, L. M., et al. (2004).** An integrated approach to developing sensor network solutions. *Proceedings of the 2nd International Workshop on Sensor and Actor Network Protocols and Applications (SANPA'04)*. Boston, Massachusetts, USA.
- Elson, J., Girod, L., et al. (2002).** Fine-grained network time synchronization using reference broadcasts. *Fifth Symposium on Operating Systems Design and Implementation (OSDI 2002)*, Boston, MA, USA.
- EPC-Global (2005).** EPC Radio-Frequency Identity Protocols Class-1 Generation-2, UHF RFID Protocol for Communications at 860 MHz-960 MHz. *EPC global Inc.* **1.0.9**.
- Feller, W. (1968).** An Introduction to Probability Theory and its Applications, *John Wiley*.
- Feng, Z., Chunhong, C., et al. (2004).** Evaluating and Optimizing Power Consumption of Anti-Collision Protocols for Applications in RFID Systems. *International*

Symposium on Low Power Electronics and Design (ISLPED '04), Newport Beach, California, USA.

- Floerkemeier, C. (2006).** Transmission control scheme for fast RFID object identification. Fourth Annual IEEE International Conference on Pervasive Computing and Communications Workshops (PerCom Workshops 2006).
- Frater, M. R., Ryan, M. J., et al. (2006).** Electromagnetic communications within swarms of autonomous underwater vehicles. 1st ACM international workshop on Underwater networks, Los Angeles, CA, USA.
- Freitag, L., Grund, M., et al. (2005).** A Shallow Water Acoustic Network for Mine Countermeasures Operations with Autonomous Underwater Vehicles. Underwater Defense Technology (UDT).
- Freitas, d., Débora, M., et al. (2009).** Linking science and management in the adoption of sensor network technology in the Great Barrier Reef coast, Australia. Computers, Environment and Urban Systems **33**(2): 111-121.
- Ganeriwal, S., Kumar, R., et al. (2003).** Timing-sync protocol for sensor networks. First International ACM Conference on Embedded Networked Sensor Systems (SenSys'03), Los Angeles, California, USA.
- Gao, S., Xu, G., et al. (1998).** The application of cross-correlation method in blood flow sonography. 20th Annual International Conference of the IEEE Engineering in Medicine and Biology Society.
- Garnier, J., and Papanicolaou, G. (2009).** Passive sensor imaging using cross correlations of noisy signals in a scattering medium. SIAM Journal on Imaging Sciences **2**: 396-437.
- Godin, O. A. (2006).** Recovering the Acoustic Green's Function from Ambient Noise Cross Correlation in an Inhomogeneous Moving Medium. Physical Review Letters **97**(5): 054301.
- Goh, J. H., Shaw, A., et al. (2009).** Underwater wireless communication system. Journal of Physics: Conference Series **178**(1): 012029.
- Good, I. (1953).** The population frequencies of species and the estimation of population parameters. Biometrika **40**: 237-264.
- Hanson, J. A., and Yang, H. (2008a).** A general statistical test for correlations in a finite-length time series. J Chem Phys. 128(21): 214101.

- Hanson, J. A., and Yang, H. (2008b).** Quantitative evaluation of cross-correlation between two finite-length time series with applications to single-molecule FRET. *J Phys Chem B*. 112(44): 13962-13970.
- Heidemann, J., Y. Wei, et al. (2006).** Research challenges and applications for underwater sensor networking. *Wireless Communications and Networking Conference (WCNC 2006)*. IEEE.
- Heinzelman, W., Chandrakasan, A., et el. (2002).** An Application-Specific Protocol Architecture for Wireless Microsensor Networks. *IEEE Transactions on Wireless Communications* 1(4): 660-670.
- Heinzelman, W. (2000).** Application-specific protocol architectures for wireless networks. Ph.D. Dissertation, *Massachusetts Institute of Technology*.
- Howlader, M. S. A., Frater, M. R., et el. (2011).** Multi-step power-efficient distributed target tracking using very-low-accuracy bearing-only sensors. Submitted in *IEEE Trans. on Parallel and Distributed Systems*.
- Howlader, M. S. A. (2009).** Estimation and Identification of Neighbours in Wireless Networks Considering the Capture Effect and Long-delay. *SEIT, University of New South Wales at Australian Defense Force Academy, Canberra. PhD*.
- Howlader, M. S. A., Frater, M. R., et el. (2008).** Estimating the Number and Distribution of the Neighbors in an Underwater Communication Network. *Second International Conference on Sensor Technologies and Applications (SENSORCOMM'08)*.
- Howlader, M. S. A., Frater, M. R., et el. (2007).** Estimation in underwater sensor network taking into account capture. *IEEE OCEANS '07, Aberdeen, Scotland*.
- Hu, W., Bulusu, N., et el. (2009).** Design and evaluation of a hybrid sensor network for cane toad monitoring. *ACM Trans. Sen. Netw.* 5(1): Article 4.
- Ianniello, J. P. (1982).** Time delay estimation via cross-correlation in the presence of large estimation errors. *IEEE Trans. Acoust., Speech, Signal Process.* 30: 998-1003.
- IEEE-Standard-Association (2007).** Part 11: Wireless LAN Medium Access Control (MAC) and Physical Layer (PHY) specifications. *IEEE Std 802.11-2007, IEEE Standard for Information Technology-Telecommunications and information exchange between systems-Local and metropolitan area network-Specific requirements*.

- Islam, M., Hannan, M. A., et al. (2010).** Performance of RFID with AWGN and Rayleigh Fading Channels for SDR Application. *Proceedings of the World Congress on Engineering 2010*, London, UK.
- ISO-Standard (2003).** Information technology automatic identification and data capture techniques--Radio frequency identification for item management Air interface. Part 6. Parameters for Air interface communications at 860-960 MHz. *Final Draft International Standard ISO 18000-6*.
- Jian-fei, L., Jia-yu, L., et al. (2009).** Application of Cross-Correlation Algorithm in Radio Weak Signal Detection. *Seventh Annual Communication Networks and Services Research Conference*, Moncton, NB.
- Jiang, Z. (2008).** Underwater Acoustic Networks – Issues and Solutions. *International Journal of Intelligent Control and Systems* **13**(3): 152-161.
- Kay, S. M. (2003).** Fundamentals of Statistical Signal Processing, Volume I: Estimation Theory. *Beijing China Machine Press*.
- Kininmonth, S., Bainbridge, S., et al. (2004).** Sensor Networking the Great Barrier Reef. *Spatial Sciences Qld.*(Spring): 34-38.
- Klair, D.K., Chin, K., Raad, R (2007).** On the Suitability of Framed Slotted Aloha based RFID Anti-collision Protocols for Use in RFID-Enhanced WSNs. 16th International Conference on Computer Communications and Networks (ICCCN), 13-16 Aug, pp.583-590.
- Knapp, C. H., and Carter, G. C. (1976).** The generalized correlation method for estimation of time delay. *IEEE Trans. Acoust., Speech, Signal Process.* **24**(4): 320-327.
- Kodialam, M., and Nandagopal, T. (2006).** Fast and reliable estimation schemes in RFID systems. *12th annual international conference on Mobile computing and networking (MobiCom'06)*, Los Angeles, CA, USA, ACM.
- Krishnamurthy, A., and Preis, R. (2005).** Satellite formation, a mobile sensor network in space. *Proc. of the 19th IEEE International Parallel and Distributed Processing Symposium, 2005*
- Kumar, A., and Bar-Shalom, Y. (1993).** Time-domain analysis of cross correlation for time delay estimation with an autocorrelated signal. *IEEE Transactions on Signal Processing* **41**(4): 1664-1668.

- Lanbo, L., Shengli, Z., et al. (2008).** Prospects and problems of wireless communication for underwater sensor networks. *Wireless Communications and Mobile Computing* **8**(8): 977-994.
- Larose, E., Derode, A., et al. (2004).** Imaging from one-bit correlations of wideband diffuse wavefields. *J. Appl. Phys.* **95**: 8393- 8399.
- Law, C., Lee, K., et al. (2000).** Efficient memoryless protocol for tag identification (extended abstract). *Proceedings of the 4th international workshop on Discrete algorithms and methods for mobile computing and communications*. Boston, Massachusetts, USA, ACM: 75-84.
- Lazaro, A. Girbau, D., et el. (2009).** Radio Link Budgets for UHF RFID on Multipath Environments. *IEEE Transactions on Antennas and Propagation* **57**(4): 1241-1251.
- Lee, D. (2008).** Wireless and Powerless Sensing Node System Developed for Monitoring Motors. *Sensors* **8**: 5005-5022.
- Lee, S., Joo, S., et al. (2005).** An Enhanced Dynamic Framed Slotted ALOHA Algorithm for RFID Tag Identification. *Second Annual International Conference on Mobile and Ubiquitous Systems: Networking and Services*, IEEE Computer Society.
- Lee, J., Kwon, T., et al. (2004).** Analysis of RFID anti-collision algorithms using smart antennas. *SenSys'2004*.
- Llor, J., Torres, E., et el. (2009).** Analyzing the behavior of acoustic link models in underwater wireless sensor networks. *Proceedings of the 4th ACM workshop on Performance monitoring and measurement of heterogeneous wireless and wired networks (PM2HW2N '09)*, Tenerife, Canary Islands, Spain, ACM, New York, NY, USA.
- Lu, B., Wu, L., et al. (2005).** On the application of wireless sensor networks in condition monitoring and energy usage evaluation for electric machines. *32nd Annual Conference of IEEE Industrial Electronics Society (IECON 2005)* IEEE: 2674-2679.
- Lucani, D. E., M'edard, M., et al. (2007).** Network Coding Schemes for Underwater Networks: The Benefits of Implicit Acknowledgement. *WUWnet '07*, Montreal, Quebec, Canada.
- Maisel, L. (1983).** *Probability, Statistics and Random Processes*, Simon & Schuster.

- Malcolm**, A. E., Scales, J. A., et al. (2004). Retrieving the green function from diffuse equipartitioned waves. *Phys. Rev.* **70**: 015601R.
- Maroti**, M., Kusy, B., et al. (2004). The flooding time synchronization protocol. *Second International ACM Conference on Embedded Networked Sensor Systems (SenSys'04)*, Baltimore, MD, USA, ACM Press.
- Medwin**, H., and Colleagues (2005). Sounds in the Sea: From Ocean Acoustics to Acoustical Oceanography. Cambridge, UK, *Cambridge University Press*.
- Micic**, A., Nayak, A., et al. (2005). A hybrid randomized protocol for RFID tag identification. *First IEEE International Workshop on Next Generation Wireless Networks (IEEE WoNGeN '05)*. Goa, India.
- MIT-Auto-ID-Center** (2003). Draft Protocol Specification for a 900MHz Class 0Radio Frequency Identification Tag. From [www.epcglobalinc.org](http://www.epcglobalinc.org). 23rd Feb.
- Moore**, T., and Sadler, B. (2006). Maximum-Likelihood Estimation and Scoring under Parametric Constraints. *Army Research Lab, Aldelphi, MD, Tech. Rep. ARL-TR-3805*.
- Myung**, J., Wonjun, L., et al. (2007). Tag-Splitting: Adaptive Collision Arbitration Protocols for RFID Tag Identification. *IEEE Transactions on Parallel and Distributed Systems* **18**: 763-775.
- Myung**, J., and Lee, W. (2006a). Adaptive splitting protocols for RFID tag collision arbitration. *7th ACM international symposium on Mobile ad hoc networking and computing (MobiHoc '06)* New York, NY, USA ACM.
- Myung**, J., Lee, W., et al. (2006b). Adaptive binary splitting for efficient RFID tag anti-collision. *IEEE Communications Letters* **10**(3): 144-146.
- Myung**, J., Lee, W., et al. (2006c). An Adaptive Memoryless Protocol for RFID Tag Collision Arbitration. *IEEE Trans. on Multimedia* **8**(5): 1096-1101.
- Ong**, K. G., Yang, X., et al. (2004). A Wireless Sensor Network for Long-term Monitoring of Aquatic Environments: Design and Implementation. *Sensor Letters* **2**(1): 48-57.
- Papoulis**, A. and Pillai, S.U. (2002). Probability, Random Variables and Stochastic Processes. *New York: McGraw-Hill Inc., Fourth Edition*.
- Partan**, J., Kurose, J., et al. (2006). A survey of practical issues in underwater networks. *Proceedings of the 1st ACM international workshop on Underwater networks (WUWNet '06)*, ACM Press.



- Peng, Q., Zhang, M. (2007).** Variant Enhanced Dynamic Frame Slotted ALOHA Algorithm for Fast Object Identification in RFID System. *IEEE Int. Workshop on Anti-counterfeiting*.
- Pompili, D., Melodia, T., et al. (2009).** Three-dimensional and two-dimensional deployment analysis for underwater acoustic sensor networks. *Ad Hoc Networks* 7(4): 778-790.
- Pompili, D., Melodia, T., et al. (2006).** Deployment analysis in underwater acoustic wireless sensor networks. *WUWNet'06*. Los Angeles, California, USA.
- Preisig, J. (2006).** Acoustic Propagation Considerations for Underwater Acoustic Communications Network Development. *WUWNet'06*. Los Angeles, California, USA.
- Proakis, J. G., Rice, J. A., et al. (2003).** Shallow water acoustic networks. *Encyclopedia of telecommunications*. J. G. Proakis, John Wiley and Sons.
- Quazi, A., and Konard, W. (1982).** Underwater Acoustic Communication. *IEEE Communications Magazine* 20(2): 24-30.
- Rickett, J., and Claerbout, J. (1999).** Acoustic daylight imaging via spectral factorization: Helioseismology and reservoir monitoring. *The Leading Edge* 18: 957-960.
- Roux, P., Sabra, K. G., et al. (2005).** Ambient noise cross correlation in free space: Theoretical approach. *The Journal of the Acoustical Society of America* 117(1): 79-84.
- Roux, P., Kuperman, W. A., et al. (2004).** Extracting coherent wave fronts from acoustic ambient noise in the ocean. *The Journal of the Acoustical Society of America* 116(4): 1995-2003.
- Ryu, J., Lee, H., et al. (2007).** A Hybrid Query Tree Protocol for Tag Collision Arbitration in RFID systems. *IEEE Int. Conf. on Communications*, IEEE.
- Sabra, K. G., Gerstoft, P., et al. (2005a).** Extracting time-domain Green's function estimates from ambient seismic noise. *Geophys. Res. Lett.* 32: L 03310-(03311-03315).
- Sabra, K. G., Roux, P., et al. (2005b).** Arrival-time structure of the time-averaged ambient noise cross-correlation function in an oceanic waveguide. *The Journal of the Acoustical Society of America* 117(1): 164-174.

- Sabra, K. G., Roux, P., et al. (2005c).** Emergence rate of the time-domain Green's function from the ambient noise cross-correlation function. *The Journal of the Acoustical Society of America* **118**(6): 3524-3531.
- Sabra, K. G., Roux, P., et al. (2005d).** Using ocean ambient noise for array self-localization and self-synchronization. *IEEE Journal of Oceanic Engineering* **30**(2): 338-347.
- Shapiro, N. M., Campillo, M., et al. (2005).** Highresolution surface-wave tomography from ambient seismic noise. *Science* **29** 1615-1617.
- Shapiro, N. M., and Campillo, M. (2004).** Emergence of broadband Rayleigh waves from correlations of the ambient seismic noise. *Geophys. Res. Lett.* **31**(L07614).
- Shukla, S., Bulusu, N., et el. (2004).** Cane toad monitoring in Kakadu National Park using wireless sensor networks. In *Proceedings of the Asia Pacific Advanced Network Conference (APAN)*.
- Shwe, Y. W., and Liang, Y. C. (2009).** Smart Dust Sensor Network with Piezoelectric Energy Harvesting. *The 6th International Conference on Information Technology and Applications (ICITA 2009)*. Hanoi, Vietnam.
- Sicignano, D., Tardioli, D., et al. (2010).** RT-WMP in Underground Voice Communication. *ICWCUCA 2010* Val-d'Or -Québec-Canada.
- Siderius, M., Harrison, C.H., Porter, M.B. (2006).** A passive fathometer technique for imaging seabed layering using ambient noise. *J. Acoust. Soc. Am.*, vol. 120(3), pp. 1315–1323.
- Simplot-Ryl, D., Stojmenovic, I., et al. (2006).** A hybrid randomized protocol for RFID tag identification. *Sensor Review* **26**: 147-154.
- Sirovich, L., Casti, A., et al. (2011).** An Introduction to MATLAB<sup>TM</sup>. *Center for Scientific Computing and Visualization*.
- Smith, S. W. (1999).** Chapter 2: Statistics, Probability and Noise. *The Scientist and Engineer's Guide to Digital Signal Processing*. San Diego, CA, California Technical Publishing
- Snieder, R. (2007).** Extracting the Green's function of attenuating heterogeneous acoustic media from uncorrelated waves. *The Journal of the Acoustical Society of America* **121**(5): 2637-2643.

- Snieder, R. (2004).** Extracting the green's function from the correlation of coda waves: A derivation based on stationary phase. *Physical Review E* **69**(4): 046610- (046611-046618).
- Soreide, N. N., Woody, C.E., et al. (2004).** Overview of ocean based buoys and drifters: Present applications and future needs. *16th International Conference on Interactive Information and Processing Systems (IIPS) for Meteorology, Oceanography, and Hydrology*, Long Beach, CA, USA.
- Sozer, E. M., Stojanovic, M., et al. (2000).** Underwater acoustic networks. *IEEE Journal of Oceanic Engineering* **25**(1): 72-83.
- Stojanovic, M. (2006a).** On the relationship between capacity and distance in an underwater acoustic communication channel. *WUWNet'06*, Los Angeles, California, USA.
- Stojanovic, M. (2006b).** Underwater Wireless Communications: Current Achievements and Research Challenges. *Newsletter* IEEE Oceanic Engineering Society.
- Stuntebeck, E. P., Pompili, D., et al. (2006).** Wireless underground sensor networks using commodity terrestrial motes. *2nd IEEE Workshop on Wireless Mesh Networks, 2006 (WiMesh 2006)*.
- Swamy, R. K., Murty, K. S. R., et al. (2007).** Determining number of speakers from multispeaker speech signals using excitation source information. *IEEE Signal Process. Lett.* **14**(7): 481.
- Syed, A. A. (2009).** Understanding and Exploiting the Acoustic Propagation Delay in Underwater Sensor Networks. *Faculty of the Graduate School*. Los Angeles, CA, University Of Southern California. **PhD**.
- Urlick, R. J. (1986).** Ambient Noise in the Sea. *Peninsula publishing*.
- Urlick, R. J. (1983).** Principles of Underwater Sound. *McGraw-Hill*.
- Varma, K. (2002).** Time-Delay-Estimate Based Direction-of-Arrival Estimation for Speech in Reverberant Environments. *Department of Electrical and Computer Engineering*. Blacksburg, VA Virginia Polytechnic Institute and State University. **MSc**.
- Venkitasubramaniam, P., Adireddy, S., et al. (2004).** Sensor networks with mobile access: optimal random access and coding. *IEEE Journal on Selected Areas in Communications* **22**(6): 1058-1068.
- Vladimirova, T., and Sidibeh, K. (2008).** WLAN for Earth Observation Satellite Formations in LEO. In *Proceedings of the 2008 Bio-inspired, Learning and*

- Intelligent Systems for Security (BLISS '08)*. IEEE Computer Society, Washington, DC, USA, 119-124.
- Vogt, H. (2002a)**. Efficient object identification with passive RFID tags. *Lecture Notes in Computer Science* **2414**.
- Vogt, H. (2002b)**. Efficient Object Identification with Passive RFID Tags. *Pervasive Computing*: 98-113.
- Vogt, H. (2002c)**. Multiple object identification with passive RFID tags. *IEEE International Conference on Systems, Man and Cybernetics*. **3**.
- Wang, X., Xie, G., et al. (2007)**. Estimation Algorithm of Identifying Object Number in Passive RFID System. *Second Workshop on Digital Media and its Application in Museum & Heritage*.
- Wang, Y. H. (1993)**. On the number of successes in independent trials. *Statistica Sinica* **3**: 295-312.
- Wapenaar, K. (2004)**. Retrieving the Elastodynamic Green's Function of an Arbitrary Inhomogeneous Medium by Cross Correlation. *Physical Review Letters* **93**(25): 254301.
- Weaver, R. L. (2008)**. Ward identities and the retrieval of Green's functions in the correlations of a diffuse field. *Wave Motion* **45**(5): 596-604.
- Weaver, R. L., and Lobkis, O. I. (2005a)**. Fluctuations in diffuse field--field correlations and the emergence of the Green's function in open systems. *The Journal of the Acoustical Society of America* **117**(6): 3432-3439.
- Weaver, R. L., and Lobkis, O. I. (2005b)**. The mean and variance of diffuse field correlations in finite bodies. *The Journal of the Acoustical Society of America* **118**(6): 3447-3456.
- Weaver, R. L., and Lobkis, O. I. (2004)**. Diffuse fields in open systems and the emergence of the Green's function (L). *The Journal of the Acoustical Society of America* **116**(5): 2731-2734.
- Weaver, R. L., and Lobkis, O. I. (2003)**. Elastic wave thermal fluctuations, ultrasonic waveforms by correlation of thermal phonons. *The Journal of the Acoustical Society of America* **113**(5): 2611-2621.
- Weaver, R. L., and Lobkis, O. I. (2002)**. On the emergence of the Green's function in the correlations of a diffuse field: pulse-echo using thermal phonons. *Ultrasonics* **40**(1-8): 435-439.

- Weaver**, R. L., and Lobkis, O. I. (2001). On the emergence of the Green's function in the correlations of a diffuse field. *J. Acoust. Soc. Am.* **110** 3011-3017.
- Wenli**, L., Deshi, L., et al. (2008). Architecture of Underwater Acoustic Sensor Networks: A Survey. *First International Conference on Intelligent Networks and Intelligent Systems, 2008 (ICINIS '08)*.
- Wills**, J., Ye, W., et el. (2006). Low Power Acoustic Modem for Dense Underwater Sensor Networks. *WUWNet'06*, Los Angeles, California, USA.
- Yang**, X., Ong, K., et al. (2002). Design of a Wireless Sensor Network for Long-term, In-Situ Monitoring of an Aqueous Environment. *Sensors* **2**(11): 455-472.